Sensor-based characterization of anthropogenic material systems: Developing characterization methods and novel applications for optimizing the mechanical recycling of lightweight packaging waste

From the Faculty of Georesources and Materials Engineering of the RWTH Aachen University

to obtain the academic degree of

Doctor of Engineering Science

approved thesis

submitted by

Nils Kroell, M. Sc.

Advisors:

Univ.-Prof. Dr. rer. nat. Kathrin Britta Greiff

Univ.-Prof. Dr. mont. Roland Pomberger

Date of the oral examination: 01.12.2023

Imprint

D82 (Diss. RWTH Aachen University, 2023)

Please cite as:
Kroell, Nils (2023). *Sensor-based characterization of anthropogenic material systems: Devel- oping characterization methods and novel applications for optimizing the mechanical recycling of lightweight packaging waste* (Doctoral thesis). RWTH Aachen University. Aachen, Department of Anthropogenic Material Cycles. https://doi.org/10.18154/RWTH-2023-11638

This cumulative dissertation contains seven pre-published peer-reviewed journal articles:

- Kroell, N., Chen, X., Greiff, K., & Feil, A. (2022). Optical sensors and machine learning algorithms in sensor-based material flow characterization for mechanical recycling processes: A systematic literature review. *Waste Management*, *149*, 259–290. https://doi.org/10.1016/j.wasman.2022.05.015
- Kroell, N. (2021). imea: A Python package for extracting 2D and 3D shape measurements from images. *Journal of Open Source Software*, *6*(60), 3091. https://doi.org/10.21105/joss.03091
- Kroell, N., Chen, X., Maghmoumi, A., Koenig, M., Feil, A., & Greiff, K. (2021). Sensor-based particle mass prediction of lightweight packaging waste using machine learning algorithms. *Waste Management*, *136*, 253–265. https://doi.org/10.1016/j.wasman.2021.10.017
- Kroell, N., Chen, X., Küppers, B., Lorenzo, J., Maghmoumi, A., Schlaak, M., Thor, E., Nordmann, C., & Greiff, K. (2023). Near-infrared-based determination of mass-based material flow compositions in mechanical recycling of post-consumer plastics: Technical feasibility enables novel applications. *Resources, Conservation and Recycling*, *191*, 106873. https://doi.org/10.1016/j.resconrec.2023.106873
- Kroell, N., Chen, X., Maghmoumi, A., Lorenzo, J., Schlaak, M., Nordmann, C., Küppers, B., Thor, E., & Greiff, K. (2023). NIR-MFCO dataset: Near-infrared-based false-color images of post-consumer plastics at different material flow compositions and material flow presentations. *Data in brief*, *48*, 109054. https://doi.org/10.1016/j.dib.2023.109054
- Kroell, N., Chen, X., Küppers, B., Schlögl, S., Feil, A., & Greiff, K. (2024). Near-infrared-based quality control of plastic pre-concentrates in lightweight-packaging waste sorting plants. *Resources, Conservation and Recycling*, *201*, 107256. https://doi.org/10.1016/j.resconrec.2023.107256
- Kroell, N., Maghmoumi, A., Dietl, T., Chen, X., Küppers, B., Scherling, T., Feil, A., & Greiff, K. (2024). Towards digital twins of waste sorting plants: Developing data-driven process models of industrial-scale sensor-based sorting units by combining machine learning with near-infrared-based process monitoring. *Resources, Conservation and Recycling*, *200*, 107257. https://doi.org/10.1016/j.resconrec.2023.107257

Acknowledgement

This dissertation evolved between September 2020 and August 2023 during my time as a scientific employee and research group leader at the Department of Anthropogenic Material Cycles (ANTS) at RWTH Aachen University. I extend my deepest gratitude to all who have supported me throughout this enriching journey.

I would like to express my special gratitude to Univ.-Prof. Dr. rer. nat. Kathrin Greiff, whose guidance, trust, and academic freedom were crucial in shaping my dissertation. Likewise, I would like to thank Univ.-Prof. Dipl.-Ing. Dr. mont. Roland Pomberger for his keen interest in my research and his valuable co-supervision. My sincere thanks go to Univ.-Prof. Dr.-Ing. Peter Quicker for chairing the examination committee.

This dissertation is based on seven publications emerging from the *EsKorte* and *ReVise* research projects. I am very grateful for the collaborative spirit and insightful feedback from my co-authors Dr.-Ing. Xiaozheng Chen, Univ.-Prof. Dr. rer. nat. Kathrin Greiff, Abtin Maghmoumi, Dr. mont. Bastian Küppers, Dr.-Ing. Alexander Feil, Julius Lorenzo, Matthias Schlaak, Christian Nordmann, Eric Thor, Morgane Koenig, Sabine Schlögl, Tobias Dietl, and Tabea Scherling.

My appreciation extends to the project partners of the *ReVise* (STADLER Anlagenbau GmbH, Hündgen Entsorgungs GmbH & Co. KG) and *EsKorte* project (Chair of Waste Processing Technology and Waste Management of Montanuniversitaet Leoben, EVK DI Kerschhaggl GmbH, Siemens AG Austria, Siemens Advanta, Brantner Environment Group GmbH) for the fruitful and invaluable cooperation. In particular, I would like to thank STADLER Anlagenbau GmbH for the generous provision of technical infrastructure such as near-infrared sensors, the technical center in Slovenia and access to multiple sorting plants as well as their technical expertise and support, without which I would not have been able to conduct my research on an industrial scale. Thanks a lot to Christian Hündgen and Frank Arleth of Hündgen Entsorgungs GmbH & Co. KG for providing light packaging waste samples and access to their sorting plant.

I acknowledge the funding of the research projects *ReVise* (grant number 033R341), *EsKorte* (grant number 16KN080621) and *PROBE* (grant number 877341) by the German Federal Ministry of Education and Research, the Austrian Research Promotion Agency, and the German Federal Ministry for Economic Affairs and Energy, respectively, without which this dissertation would not have been possible. The responsibility for the content of this dissertation, of course, remains mine.

I would like to thank all current and former student assistants at ANTS for their extensive support. In particular, I am especially grateful to Abtin Maghmoumi, Matthias Schlaak, Morgane Koenig, Peter Bardenheuer, Paula Schönfelder, Lara Bergfelder, and Christian de Ridder for their support in literature research, practical investigations and data pre-processing. Many thanks to

Torsten Fleischer, Elias Pfund, Dr. mont. Juan Carlos Hernández Parrodi, Dr. mont. Bastian Küppers, Alena Spies, and Johanna Beaupoil for their support with the integration of various sensor systems in sorting plants and data acquisition.

Thanks a lot to all my current and former colleagues from ANTS for the enjoyable collaboration; the supportive and inspiring work environment; and the valuable exchanges during the doctoral seminars, trial presentations, and beyond. Many thanks to Dr.-Ing. Alexander Feil and Dr.-Ing. Karoline Raulf for always supporting me with their experience and expertise. I extend my sincere gratitude to Angelika Müller for her unwavering administrative support and daily dedication, which has been invaluable to our team. Thanks a lot to Christoph Plum and the joint mechanical workshop of the Division of Mineral Resources and Raw Materials Engineering for their support in the construction and implementation of the experimental setups.

A heartfelt thank you to my family, especially my parents, Silke and Volker Kröll and my sister, Ina Kröll, and who always believed in me and supported me extensively through this journey and beyond. A special thanks to my friends and the Debattierclub Aachen e. V. for the wonderful hours we spent together.

In this last paragraph, I would like to express my deepest gratitude to my beloved partner, Dr.-Ing. Xiaozheng Chen. You accompanied my dissertation from the first idea to the final submission through all the ups and downs and always gave me incomparable support. Without you, I would not have been able to complete my dissertation this successful. I am infinitely grateful for your support in both my professional and private life.

Aachen, December 2023

Nils Kroell, M. Sc.

Declaration on publications

PhD-relevant publications

This dissertation is composed of seven peer-reviewed journal publications (Table 1).

Table 1. PhD-relevant publications.

ID	Publication
A	**Kroell, N.**, Chen, X., Greiff, K., & Feil, A. (2022). Optical sensors and machine learning algorithms in sensor-based material flow characterization for mechanical recycling processes: A systematic literature review. *Waste Management*, *149*, 259–290. https://doi.org/10.1016/j.wasman.2022.05.015
B	**Kroell, N.** (2021). imea: A Python package for extracting 2D and 3D shape measurements from images. *Journal of Open Source Software*, *6*(60), 3091. https://doi.org/10.21105/joss.03091
C	**Kroell, N.**, Chen, X., Maghmoumi, A., Koenig, M., Feil, A., & Greiff, K. (2021). Sensor-based particle mass prediction of lightweight packaging waste using machine learning algorithms. *Waste Management*, *136*, 253–265. https://doi.org/10.1016/j.wasman.2021.10.017
D	**Kroell, N.**, Chen, X., Küppers, B., Lorenzo, J., Maghmoumi, A., Schlaak, M., Thor, E., Nordmann, C., & Greiff, K. (2023). Near-infrared-based determination of mass-based material flow compositions in mechanical recycling of post-consumer plastics: Technical feasibility enables novel applications. *Resources, Conservation and Recycling*, *191*, 106873. https://doi.org/10.1016/j.resconrec.2023.106873
E	**Kroell, N.**, Chen, X., Maghmoumi, A., Lorenzo, J., Schlaak, M., Nordmann, C., Küppers, B., Thor, E., & Greiff, K. (2023). NIR-MFCO dataset: Near-infrared-based false-color images of post-consumer plastics at different material flow compositions and material flow presentations. *Data in brief*, *48*, 109054. https://doi.org/10.1016/j.dib.2023.109054
F	**Kroell, N.**, Chen, X., Küppers, B., Schlögl, S., Feil, A., & Greiff, K. (2024). Near-infrared-based quality control of plastic pre-concentrates in lightweight-packaging waste sorting plants. *Resources, Conservation and Recycling*, *201*, 107256. https://doi.org/10.1016/j.resconrec.2023.107256
G	**Kroell, N.**, Maghmoumi, A., Dietl, T., Chen, X., Küppers, B., Scherling, T., Feil, A., & Greiff, K. (2024). Towards digital twins of waste sorting plants: Developing data-driven process models of industrial-scale sensor-based sorting units by combining machine learning with near-infrared-based process monitoring. *Resources, Conservation and Recycling*, *200*, 107257. https://doi.org/10.1016/j.resconrec.2023.107257

Contributions of PhD candidate

As shown in Table 2, in all seven publications, I have extensively contributed to the conducted research from the conceptualization of the research questions and aims, over the development of a comprehensive research methodology, carrying out and/or supervising practical investigations, curating and analyzing obtained datasets, developing software and visualizations, writing and revising the manuscript, to coordination of the overall project and supervision of student assistants and thesis students. Furthermore, I contributed to the acquisition of research funding for five of seven publications.

Table 2. PhD candidate contributions according to the *Contributor Roles Taxonomy* (Brand et al., 2015). ✓ contribution, - no contribution, * not applicable.

Contributor Role	**Publication**						
	A	**B**	**C**	**D**	**E**	**F**	**G**
Conceptualization	✓	✓	✓	✓	✓	✓	✓
Methodology	✓	✓	✓	✓	✓	✓	✓
Software	✓	✓	✓	✓	✓	✓	✓
Validation	✓	✓	✓	✓	✓	✓	✓
Formal analysis	✓	*	✓	✓	*	✓	✓
Investigation	✓	✓	✓	✓	✓	✓	✓
Resources	-	-	-	-	-	-	-
Data Curation	✓	*	✓	✓	✓	✓	✓
Writing - Original Draft	✓	✓	✓	✓	✓	✓	✓
Writing - Review & Editing	✓	✓	✓	✓	✓	✓	✓
Visualization	✓	✓	✓	✓	✓	✓	✓
Supervision	-	-	-	✓	✓	✓	✓
Project administration	✓	✓	✓	✓	✓	✓	✓
Funding acquisition	✓	-	-	✓	✓	✓	✓

Further publications by PhD candidate

Besides the seven first-author publications comprised in this dissertation, I have been actively contributing to the sensor technology and data science in mechanical recycling research field, resulting in 21 additional publications (= 28 publications in total). The additional publications comprise five first-author publications and 16 co-author publications (twelve as second author):

- Wu, X., **Kroell**, **N.**, & Greiff, K. (2023). Deep learning-based instance segmentation on 3D laser triangulation data for inline monitoring of particle size distributions in construction and demolition waste recycling [under review]. *Resources, Conservation and Recycling*
- **Kroell**, **N.**, Chen, X., Feil, A., & Greiff, K. (2023). Sensortechnik in der Sortierung und Aufbereitung von Kunststoffverpackungen - Potenziale und Grenzen. In S. Flamme (Ed.),

18. Kreislaufwirtschaftstage

- Chen, X., **Kroell**, **N.**, Hofmann, B., Schlögl, S., & Greiff, K. (2023). Improving drum sieve performance in lightweight packaging waste recycling by automatic parameter adjustment through 3D laser triangulation-based process monitoring. *Resources, Conservation and Recycling*, *192*, 106924. https://doi.org/10.1016/j.resconrec.2023.106924

- Chen, X., **Kroell**, **N.**, Althaus, M., Pretz, T., Pomberger, R., & Greiff, K. (2023). Enabling mechanical recycling of plastic bottles with shrink sleeves through near-infrared spectroscopy and machine learning algorithms. *Resources, Conservation and Recycling*, *188*, 106719. https://doi.org/10.1016/j.resconrec.2022.106719

- Chen, X., **Kroell**, **N.**, Feil, A., & Greiff, K. (2023). Sensor-based sorting. In C. Meskers, E. Worrell, & M. A. Reuter (Eds.), *Handbook of recycling*. Elsevier

- Schlögl, S., Kamleitner, J., **Kroell**, **N.**, Chen, X., & Aldrian, A. (2023). Developing a Prediction Model in a Lightweight Packaging Waste Sorting Plant using Sensor-based Sorting Data combined with Data of External Near-infrared and LiDAR Sensors [under review]. *Waste management & research*

- Greiff, K., Wotruba, H., Feil, A., **Kroell**, **N.**, Chen, X., Gürsel, D., & Merz, V. (Eds.). (2022). *9th Sensor-Based Sorting & Control 2022*. Shaker. https://doi.org/10.2370/9783844085457

- **Kroell**, **N.**, Dietl, T., Maghmoumi, A., Chen, X., Küppers, B., Feil, A., & Greiff, K. (2022). Assessment of sensor-based sorting performance for lightweight packaging waste through sensor-based material flow monitoring: Concept and preliminary results. In K. Greiff, H. Wotruba, A. Feil, **N. Kroell**, X. Chen, D. Gürsel, & V. Merz (Eds.), *9th Sensor-Based Sorting & Control 2022*. Shaker

- **Kroell**, **N.**, Schönfelder, P., Chen, X., Johnen, K., Feil, A., & Greiff, K. (2022). Sensorbasierte Vorhersage von Korngrößenverteilungen durch Machine Learning Modelle auf Basis von 3D-Lasertriangulationsmessungen. In Deutsche Gesellschaft für Abfallwirtschaft e.V. (Ed.), *11. DGAW-Wissenschaftskongress Abfall- und Ressourcenwirtschaft*. innsbruck university press

- **Kroell**, **N.**, Chen, X., Nordmann, C., Pfund, E., Lorenzo, J., Dietl, T., Maghmoumi, A., Küppers, B., Feil, A., & Greiff, K. (2022). Optimierte Sortierung von Leichtverpackungsabfällen durch ein intelligentes Stoffstrommanagement. In R. Pomberger, J. Adam, M. Altendorfer, T. Bouvier-Schwarz, P. Haslauer, L. Kandlbauer, K. Khodier, G. Koinig, N. Kuhn, T. Lasch, N. Mhaddolkar, T. Nigl, B. Rutrecht, R. Sarc, T. Sattler, S. Schlögl, H. Stipanovic, A. Tischberger-Aldrian, & S. Viczek (Eds.), *Vorträge-Konferenzband zur 16.*

Recy & DepoTech-Konferenz (pp. 347–352). Abfallverwertungstechnik & Abfallwirtschaft Eigenverlag

- Küppers, B., Schlögl, S., **Kroell**, **N.**, & Radkohl, V. (2022). Relevance and challenges of plant control in the pre-processing stage for enhanced sorting performance. In K. Greiff, H. Wotruba, A. Feil, **N. Kroell**, X. Chen, D. Gürsel, & V. Merz (Eds.), *9th Sensor-Based Sorting & Control 2022* (pp. 17–33). Shaker

- Schlögl, S., Kamleitner, J., **Kroell**, **N.**, & Chen, X. (2022). Implementierung von Sensor-based Material flow Monitoring in einer Kunststoffsortieranlage. In R. Pomberger, J. Adam, M. Altendorfer, T. Bouvier-Schwarz, P. Haslauer, L. Kandlbauer, K. Khodier, G. Koinig, N. Kuhn, T. Lasch, N. Mhaddolkar, T. Nigl, B. Rutrecht, R. Sarc, T. Sattler, S. Schlögl, H. Stipanovic, A. Tischberger-Aldrian, & S. Viczek (Eds.), *Vorträge-Konferenzband zur 16. Recy & DepoTech-Konferenz*. Abfallverwertungstechnik & Abfallwirtschaft Eigenverlag

- Chen, X., **Kroell**, **N.**, Li, K., Feil, A., & Pretz, T. (2021). Influences of bioplastic polylactic acid on near-infrared-based sorting of conventional plastic. *Waste management & research*, *39*(9), 1210–1213. https://doi.org/10.1177/0734242X211003969

- Chen, X., **Kroell**, **N.**, Wickel, J., & Feil, A. (2021). Determining the composition of post-consumer flexible multilayer plastic packaging with near-infrared spectroscopy. *Waste Management*, *123*, 33–41. https://doi.org/10.1016/j.wasman.2021.01.015

- Chen, X., **Kroell**, **N.**, Dietl, T., Feil, A., & Greiff, K. (2021). Influence of long-term natural degradation processes on near-infrared spectra and sorting of post-consumer plastics. *Waste Management*, *136*, 213–218. https://doi.org/10.1016/j.wasman.2021.10.006

- Feil, A., **Kroell**, **N.**, Pretz, T., & Greiff, K. (2021). Anforderungen an eine effiziente technologische Behandlung von Post-Consumer Verpackungsmaterialien in Sortieranlagen: Möglichkeiten und Grenzen. *Müll und Abfall*, *21*(7), 362–370. https://doi.org/10.37307/j.1863-9763.2021.07.04

- **Kroell**, **N.**, Johnen, K., Chen, X., & Feil, A. (2021). Fine metal-rich waste stream characterization based on RGB data: Comparison between feature-based and deep learning classification methods. In J. Beyerer & T. Längle (Eds.), *OCM 2021 - Optical Characterization of Materials: Conference Proceedings*. KIT Scientific Publishing

- Parrodi, J. C. H., **Kroell**, **N.**, Chen, X., Dietl, T., Pfund, E., Küppers, B., & Nordmann, C. (2021). Nahinfrarot-basierte Stoffstromüberwachung von Bau- und Abbruchabfällen. In S. Thiel, E. Thomé-Kozmiensky, D. Senk, H. Wotruba, H. Antrekowitsch, & R. Pomberger (Eds.), *Mineralische Nebenprodukte und Abfälle* (pp. 92–111). Thomé-Kozmiensky Verlag GmbH

- Johnen, K., **Kroell**, **N.**, & Feil, A. (2020). Entwicklung einer Methodik zur Wertstoffgehaltsbestimmung von feinkörnigen Abfällen. In R. Pomberger, J. Adam, A. Aldrian, M. Altendorfer, A. Curtis, T. Dobra, K. Friedrich, L. Kandlbauer, K. E. Lorber, S. Möllnitz, T. Nigl, R. Sarc, T. Sattler, S. Viczek, D. Vollprecht, T. Weißenbach, & M. Wellacher (Eds.), *Recy & DepoTech 2020*. Abfallverwertungstechnik & Abfallwirtschaft Eigenverlag

- Johnen, K., & **Kroell**, **N.** (2020). Quantitative Klemmkornbestimmung mittels Bildauswertung am Beispiel der Siebung von Abfallfeinfraktionen. In Deutsche Gesellschaft für Abfallwirtschaft e.V. (Ed.), *10. DGAW-Wissenschaftskongress Abfall- und Ressourcenwirtschaft*. innsbruck university press

- Chen, X., **Kroell**, **N.**, Feil, A., & Pretz, T. (2020). Determination of the composition of multilayer plastic packaging with nir spectroscopy. *Detritus*, (13), 62–66. https://doi.org/10.31025/2611-4135/2020.14027

Future readers will find an up-to-date list of my publications on *ResearchGate*[1] or *Google Scholar*[2].

[1] https://www.researchgate.net/profile/Nils-Kroell
[2] https://scholar.google.com/citations?user=ecsw9RcAAAAJ&hl=de

Abstract

Mechanical recycling of post-consumer plastic packaging is characterized by a high lack of transparency due to the high effort of manual material flow characterization. As a consequence, optimizing collection processes in a targeted manner as well as adaptively designing and operating sorting and processing plants are often not possible, and confidence in secondary raw materials is often missing. This dissertation demonstrates how sensor technology in mechanical recycling can evolve from a sorting technology towards a key technology for enabling value-chain-wide transparency, and what optimization potentials can be derived from this enabled transparency.

In the first part of the dissertation, a systematic literature review was conducted, which introduces a unified terminology, provides a comprehensive overview of the current state of research and identifies ten essential future research potentials. In the second part, novel characterization methods for extracting mass-based material flow compositions from area/volume-based sensor data were developed. Machine learning models were successfully trained to determine binary compositions of plastic flakes and post-consumer plastic packaging with a measurement uncertainty of 1.2 vol% and 2.4 wt%, respectively, across different material flow presentations and compositions using near-infrared (NIR) sensors.

Based on the developed characterization methods, two novel sensor technology applications were demonstrated at industrial scale in the third part. First, a sensor-based quality monitoring of plastic pre-concentrates from sorting plants was developed using inline NIR sensors. The results showed that for a PET tray fraction as an example, sensor-based quality control of mass-based product purities is possible with a measurement uncertainity of 0.31 wt%. In comparison with state-of-the-art sampling-based quality analyses, it was shown that more than 350 kg of a 600 kg PET tray pre-concentrate bale would need to be analyzed manually to achieve a comparable measurement accuracy. Second, inline NIR sensors were used for sensor-based process monitoring of an industrial sensor-based sorting (SBS) unit. Using artificial neural networks, the process data was used to develop a process model that can predict the sorting behavior of the SBS unit across different sorting scenarios with a mean absolute error of 3.0%.

In summary, the dissertation demonstrates the promising potentials of sensor technology in optimizing the circular economy. Based on the generated transparency, future process improvements can be implemented in individual process stages and across value chains, thus increasing the quantity and quality of recycled materials and the resulting ecological and economic benefits.

Zusammenfassung

Das mechanische Recycling von Post-Consumer Kunststoffverpackungen ist durch den hohen Aufwand einer manuellen Stoffstromcharakterisierung von einer weitgehend fehlenden Transparenz geprägt. Aufgrund dieser fehlenden Transparenz können Sammelprozesse häufig nicht zielgerichtet optimiert werden, Sortier- und Aufbereitungsanlagen nicht adaptiv auf schwankende Inputstoffströme ausgelegt werden und es fehlt oftmals an Vertrauen in Sekundärrohstoffe. Die vorliegende Dissertation zeigt auf, wie sich Sensortechnik im mechanischen Recycling von einer Sortiertechnologie hin zu einer Schlüsseltechnologie zur Ermöglichung von Transparenz weiterentwickeln kann und welche Optimierungspotenziale sich daraus ableiten lassen.

Im ersten Teil der Dissertation wurde hierzu ein systematisches Literaturreview durchgeführt, welches eine vereinheitlichte Terminologie einführt, einen fundierten Überblick über den aktuellen Forschungsstand gibt und daraus zehn zukünftige Forschungspotenziale aufgedeckt. Im zweiten Teil wurden neuartige Charakterisierungsmethoden zur Extraktion massenbasierter Stoffstromzusammensetzungen aus flächen-/volumenbasierter Sensordaten entwickelt. Hierbei gelang es, Machine Learning Modelle zur trainieren, mit denen sich binäre Zusammensetzungen von Kunststoffflakes und Post-Consumer Kunststoffverpackungen mit einer Messunsicherheit von respektive 1,2 vol% und 2,4 Ma.-% über verschiedene Stoffstrompräsentationen und -zusammensetzungen hinweg mittels Nahinfrarot (NIR)-Sensoren bestimmen lassen.

Basierend auf den entwickelten Charakterisierungsmethoden wurden im dritten Teil zwei innovative Sensortechnik-Anwendungen im industriellen Maßstab demonstriert. Erstens wurde ein sensorbasiertes Qualitätsmonitoring für Kunststoffvorkonzentrate aus Sortieranlagen mittels Inline-NIR-Sensoren entwickelt. Hierbei wurde am Beispiel einer PET-Tray Fraktion gezeigt, dass es möglich ist, massenbasierte Produktreinheiten sensorbasiert mit einer Messunsicherheit von 0,31 Ma.-% zu bestimmen. Im Abgleich mit probenahmebasierten Qualitätsanalysen nach Stand der Technik zeigte sich, dass mehr als 350 kg eines 600 kg PET Tray Vorkonzentratballens manuell hätten analysiert werden müssen, um eine vergleichbare Messgenauigkeit zu erzielen. Zweitens wurden Inline-NIR-Sensoren zum sensorbasierten Prozessmonitoring eines industriellen Sensorsortierers eingesetzt. Mittels künstlicher neuronaler Netze wurde hieraus ein Prozessmodell entwickelt, das das Sortierverhalten des Sensorsortierers über verschiedene Sortierszenarien hinweg mit einem mittleren absoluten Fehler von 3,0 % vorhersagen kann.

Zusammenfassend demonstriert die Dissertation vielversprechende Potenziale von Sensortechnik zur Optimierung der Kreislaufwirtschaft. Auf Basis der erzeugten Transparenz können zukünftig Prozessverbesserungen in einzelnen Wertschöpfungsstufen sowie wertschöpfungskettenübergreifend implementiert und damit die Menge und Qualität im Kreislauf geführter Materialien und daraus erzielte ökologische und ökonomische Vorteile gesteigert werden.

Contents

List of Figures

List of Tables

List of Abbreviations

3DLT	3D laser triangulation
AI	artificial intelligence
CNN	convolutional neural network
CE	Circular Economy
EU	European Union
HDPE	high-density polyethylene
LiDAR	light detection and ranging
LWP	lightweight packaging
MAE	mean absolute error
ML	machine learning
MFC	material flow characteristic
MFCO	material flow composition
MQC	manual quality control
NIR	near-infrared
PET	polyethylene terephthalate
RFID	radio-frequency identification
RQ	research question
SBMC	sensor-based material flow characterization
SBMM	sensor-based material flow monitoring
SBPC	sensor-based process control
SBPM	sensor-based process monitoring
SBQC	sensor-based quality control
SBS	sensor-based sorting
SLR	systematic literature review
TC	transfer coefficient
VIS	visible

1 Introduction

1.1 Motivation

Despite inhabiting only a single planet, humanity currently exhausts the resources equivalent to more than 1.7 earths (Lin et al., 2023). Accelerating climate change (IPCC, 2023), continuing biodiversity losses (Dirzo et al., 2014; WWF, 2020), and increasing pollution of terrestrial and marine ecosystems (Horton et al., 2017; Jambeck et al., 2015; Prata et al., 2020) are already painting a drastic picture of future consequences of a life beyond our planetary boundaries (O'Neill et al., 2018; Rockström et al., 2023; Rockström et al., 2009; Steffen et al., 2015). To ensure a habitable planet for current and future generations, transitioning the world to sustainable development has thus a global priority and necessity (UN General Assembly, 2015).

A significant factor propelling these environmental impacts is the extraction and processing of natural resources, currently contributing to about 50% of global greenhouse gas emissions and more than 90% of water and biodiversity stress (IRP, 2019). Global material extraction has tripled from about 27 billion tons in 1970 to about 92 billion tons in 2017 (IRP, 2019) and may more than double by 2050 (IRP, 2017).

The Circular Economy (CE) proposes a solution to these pressing issues, seeking to decouple economic growth and societal well-being from the environmental impacts of resource utilization, by extending the life cycle of products, materials, and resources as long as possible and fostering a sustainable, low-carbon, resource-efficient, and competitive economy (European Commission, 2020). Effectively implementing CE requires the interplay of various R-strategies (Kirchherr et al., 2017; Kirchherr et al., 2023).

One of these R-strategies is *recycling*, which aims to transform unwanted waste into demanded secondary raw materials (Pretz et al., 2020). In 2020, the European Union (EU) 27+3 alone generated approximately 776.3 million tons (Eurostat, 2023) of waste (excluding major mineral wastes) – presenting a vast opportunity to reclaim secondary raw materials and realize the associated environmental benefits of primary raw material substitution (Schwarz et al., 2021; Zhang et al., 2023).

However, global resource demand is currently still heavily dependent on primary resource extraction. Presently, the world is estimated to be just 7.2 wt% circular (Circle Economy, 2023), and even the EU, despite being recognized as a CE pioneer (European Commission, 2019, 2020), sourced only a mere 12.7 wt% of its raw material supply from secondary resources in 2021 (Eurostat, 2023). Significant improvements in current material cycles and value chains are thus necessary to increase both the quantity and quality of recovered secondary raw materials (European Commission, 2020; European Parliament and Council, 2018).

1.2 Optimization potentials in recycling: Lack of transparency

Modern recycling systems of post-consumer, mixed waste streams consist of several stages (Figure 1.1). After their use-phase, materials declared as *waste* are collected depending on country-specific collection schemes. Sorting plants pre-treat and sort the collected waste streams into material and/or color-specific pre-concentrates. Pre-concentrates as well as material streams from mono-collection are then further processed into secondary raw materials by processing plants. The generated secondary raw materials can then substitute primary raw materials during production processes and thereby re-enter the material cycle. (Feil & Pretz, 2020)

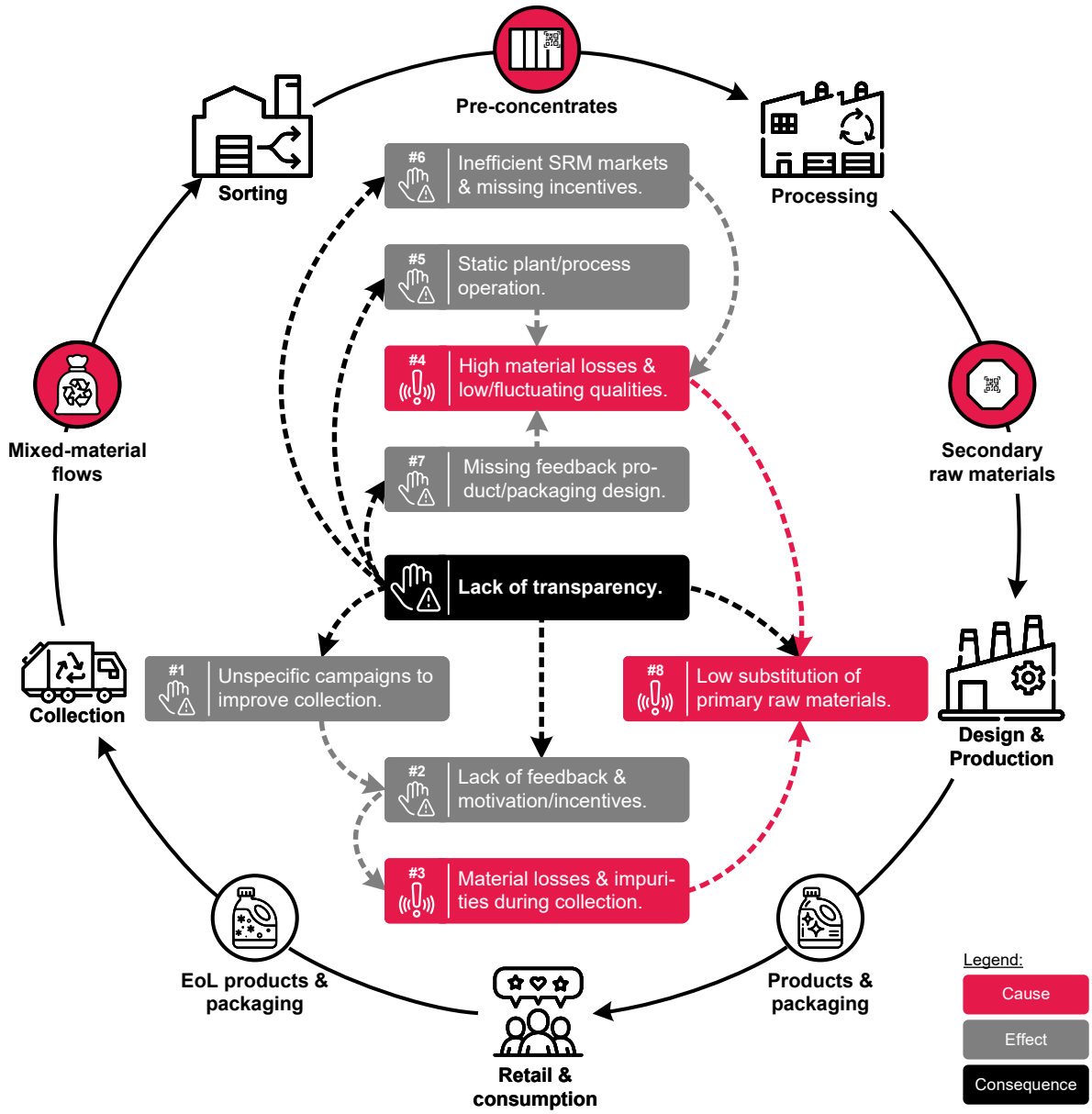

Figure 1.1. Simplified elements of modern recycling systems for post-consumer, mixed waste streams based on (Feil et al., 2021) and negative influences of a lack of transparency on material circulation; SRM: secondary raw material; *#i* references for Section 1.2.

Especially the collection, sorting, and processing stages are subject to a considerable *lack of transparency* regarding up-to-date material flow characteristics, which significantly hampers the overall material circulation (Figure 1.1):

- During *waste collection*, region-specific material flow compositions and impurity contents are often unknown, such that public campaigns to improve the quality of separate collection can often only be carried out in a general and unspecific manner (#1 in Figure 1.1) and citizens often lack feedback or incentives on effective separate collection (#2) (Initiative Mülltrennung wirkt, 2021). Both effects lead to material losses as residual waste towards energy recovery (Kuchta & Picuno, 2020) or high impurity contents in the collected waste streams, which hamper subsequent sorting processes and lead to material losses towards energy recovery (#3, #4) (Brune & Feil, 2020; Nigl et al., 2021; Wieczorek, 2017).
- Due to lacking up-to-date material flow information, *sorting and processing plants* are mostly operated at static process parameters (#5), which, in combination with fluctuating material flow properties, can lead to considerable material and/or quality losses (#4) (Küppers et al., 2022).
- A lack of transparency regarding produced pre-concentrate and recyclate qualities leads to *inefficient secondary raw material markets* and a *lack of incentives* (#6) for plant operators to further improve secondary raw material qualities (#4) (Knappe et al., 2021).
- Due to the lack of up-to-date material flow information from the collection, sorting, and processing stages, product and packaging designers often lack (real-time) *feedback on real-world sortability and recyclability* of end-of-life products and packaging (cf. Pomberger, 2021). Consequently, products and packaging are not always optimally sortable and recyclable, leading to avoidable material losses and/or low pre-concentrate/secondary raw material qualities (#4).
- Due to the accumulated losses from collection, sorting, and processing stages (Picuno et al., 2021), only a small amount of secondary raw materials is made available (cf. Section 1.1), which, together with fluctuating or insufficient secondary raw material qualities (cf. #3), hampers *large-scale substitution of primary raw materials* (#8).

A major reason for the prevailing lack of transparency in the recycling sector is that material flow characteristics so far had to be determined mostly manually via sampling and manual sorting analyses or laboratory measurements (e.g., European Committee for Standardization, 2005, 2006; Länderarbeitsgemeinschaft Abfall, 2001), cf. Figure 1.2b. This procedure is (i) personnel- and cost-intensive (Borowski, 2018), (ii) highly dependent on the sampling quality (Khodier et al., 2020), and (iii) characterized by a considerable time delay between sampling and available results (Flamme & Krämer, 2015). Consequently, manual material flow characterization is often carried out infrequently, resulting in the prevailing lack of transparency (Borowski, 2018).

1.3 A new key role for sensor technology

A solution to these problems by providing more transparency could lie in *sensor technology*. While optical sensors have been so far mainly been used for sensor-based sorting (SBS) (cf. Figure 1.2c) in the recycling industry, sensor technology could evolve into a new role: In the future, sensors could not only be applied for SBS but be transformed into a key technology for bringing transparency into recycling value chains and thereby unlocking novel optimization potentials for implementing the CE (Figure 1.2d). This new perspective and the methods for the implementation of it will be referred to as *sensor-based material flow characterization* (SBMC).

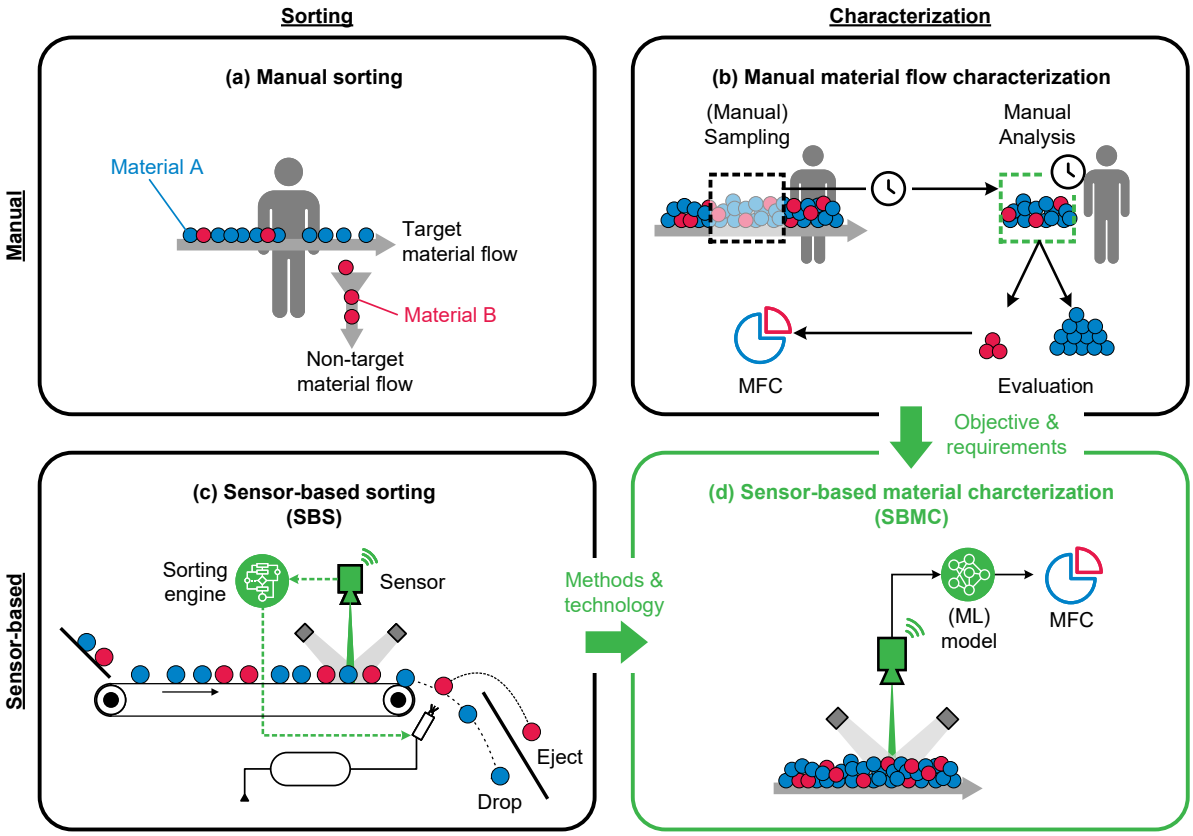

Figure 1.2. Manual and sensor-based characterization and sorting technologies; MFC: material flow characteristic; ML: machine learning.

SBMC has the potential to help to solve existing problems of manual material flow characterization, as the characterization happens (i) automatically, (ii) 24/7, (iii) inline, and (iv) in nearly real-time (Kroell, Chen, Greiff, et al., 2022). Based on the transparency acquired by SBMC in recycling value chains, novel applications such as sensor-based quality and process monitoring, adaptive process control of sorting and processing plants, or modeling of recycling chains via digital process twins could be enabled. These novel SBMC applications could help to significantly advance CE through higher-quality secondary raw materials and lower material losses.

1.4 Research gap, aim, and overarching research questions

While sensor technology for SBS has been state-of-the-art for several years across various material flows (Gundupalli et al., 2017), the use of sensor technology for further SBMC applications such as sensor-based quality or process monitoring has been scarcely investigated so far (Kroell, Chen, Greiff, et al., 2022). It is therefore currently largely unclear if and how sensor technology can be applied to characterize material flows outside of SBS applications, and if and how novel SBMC applications can be implemented based on developed characterization methods at industrial scales. To close this research gap and demonstrate that the aforementioned potentials are not only theoretically imaginable but also technical feasible, this dissertation aims at proving the following hypothesis:

> *In addition to state-of-the-art sensor-based sorting, it is technical feasible to use sensor technology for the inline characterization of post-consumer material flows with industrial-relevant accuracies and at industrial scales. Based on the extracted material flow characteristics, novel SBMC applications can make the value-chain-wide material circulation more transparent and efficient.*

To prove this hypothesis, three overarching research questions (RQs) need to be positively answered:

RQ I. *State of research:* Which existing research findings can be used, and which research gaps have to be filled to enable an inline SBMC of post-consumer waste streams?

RQ II. *Characterization methods:* How can the open research gaps from RQ I be closed and thus the sensor-based inline characterization of post-consumer material flows regarding their mass-based material flow compositions be enabled?

RQ III. *Applications:* Can the developed characterization methods from RQ II be translated into novel, industrial-scale SBMC applications to enhance CE?

To answer RQ I, a general overview on sensor technology applications in mechanical recycling should be given. Then, RQ II and RQ III should be answered based on practical case studies of *lightweight packaging waste* (LWP). Due to the high heterogeneity and complexity (e.g., influences of packaging design, post-consumer effects, missing bulk properties, high and complex impurity contents [Feil et al., 2021]), LWP waste is excellently suited as a transfer platform to other material flows. Once the stated hypothesis is proven for the case study of LWP, the generated insights can be transferred to other waste streams in future work, as discussed in Chapter 5.

1.5 Dissertation structure

To answer the overarching RQs and prove the stated hypothesis, the dissertation is structured into six chapters (Figure 1.3). Following the introduction (Chapter 1), first, Chapter 2 will aim at identifying research gaps that hamper the technical feasibility of inline-SBMC of post-consumer waste streams (RQ I) based on a systematic literature review (Publication A).

Second, two characterization approaches are developed in Chapter 3 for the sensor-based characterization of LWP waste streams regarding their mass-based material flow composition (RQ II). In a first particle-level approach, a novel Python package for the automatic extraction of particle features from sensor data (*imea*) is developed (Publication B), based on which a machine learning (ML)-based approach for the particle mass prediction from sensor data is created (Publication C). In a second material-flow-level approach, regression approaches are applied to directly predict mass-based material flow compositions from sensor data (Publication D), and the underlying dataset is made available to other SBMC researchers (Publication E).

Third, the developed characterization methods are applied to the industrial-scale demonstration of two novel SBMC applications in Chapter 4 (RQ III): In Publication F, an inline sensor-based quality control of pre-concentrates in LWP sorting plants is developed. In Publication G, a data-driven process model of an industrial-scale SBS unit is developed and its potentials for digital twins of sorting plants are discussed. Obtained insights are then synthesized in Chapter 5 to verify or falsify the stated hypothesis, before a final conclusion is drawn in Chapter 6.

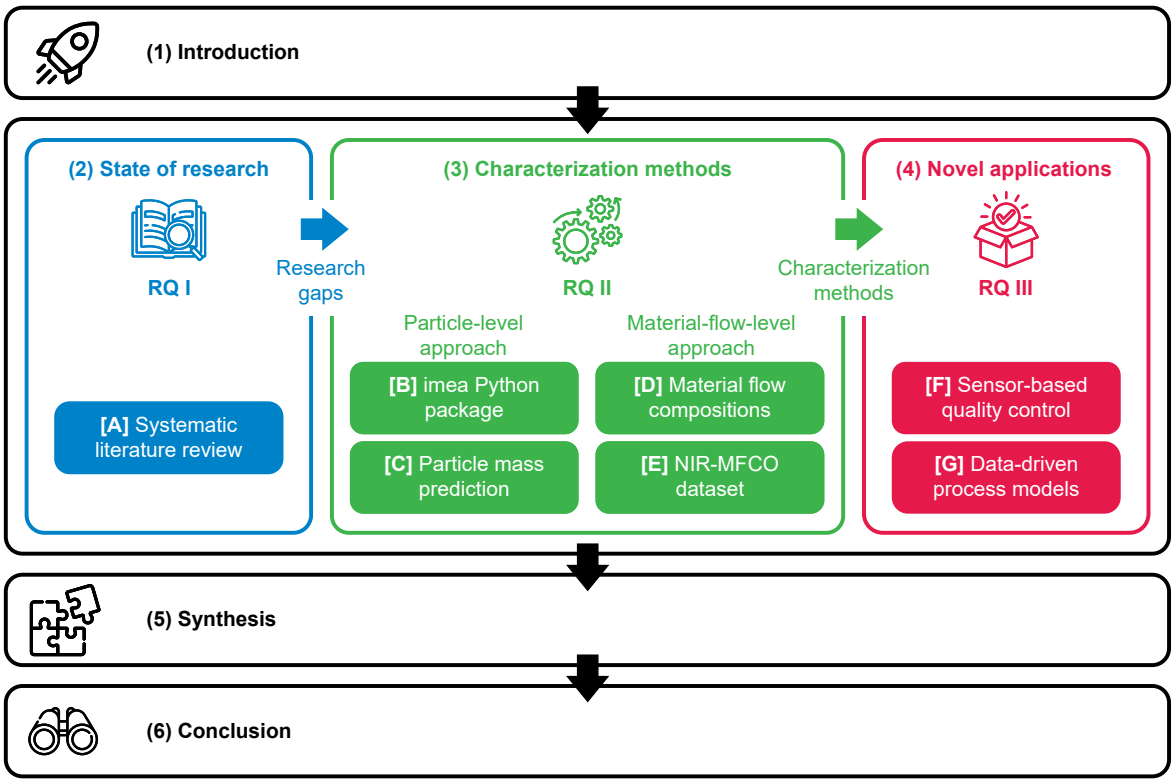

Figure 1.3. Dissertation structure; (*i*): chapters, [*i*]: publications according to Table 1.

2 State of research

To answer RQ I, Section 2.1 presents an systematic literature review (SLR) on sensor technology applications in mechanical recycling. The SLR aims to identify essential research gaps and summarize existing research findings for inline SBMC of post-consumer material flows. The identified research gaps and findings create the conceptual basis for developing characterization methods (RQ II) in Chapter 3 and verifying the dissertation hypothesis.

2.1 Publication A: Systematic literature review

> **Kroell, N.**, Chen, X., Greiff, K., & Feil, A. (2022). Optical sensors and machine learning algorithms in sensor-based material flow characterization for mechanical recycling processes: A systematic literature review. *Waste Management*, *149*, 259–290. https://doi.org/10.1016/j.wasman.2022.05.015

The SLR comprises the evidence of 267 investigations from 198 peer-reviewed journal articles on optical sensor applications in mechanical recycling (Figure 2.1). One of the core findings of the SLR was that so far research on sensor technology applications in mechanical recycling is scattered across different disciplines and often not received as a homogeneous and coherent research field. An essential reason for this is the lack of a consistent SBMC terminology, which hinders effective communication across different disciplines. Therefore, a unified SBMC terminology was developed in the SLR firstly, based on which a holistic overview of existing SBMC research was given. Based on this overview, ten future research potentials were identified to further advance SBMC research. Five of these future research potentials are especially relevant to prove the hypothesis of this dissertation and are thus addressed in Chapter 3 and Chapter 4.

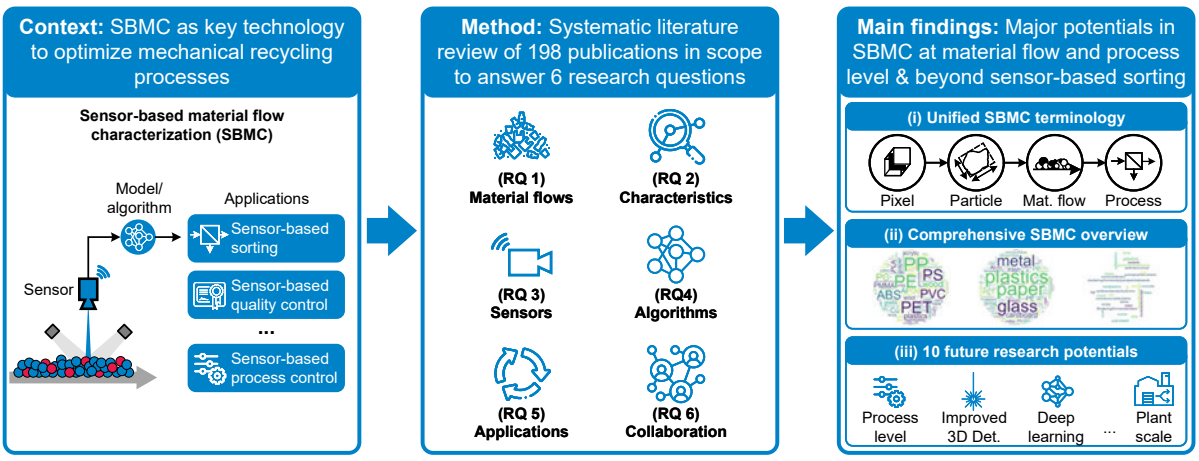

Figure 2.1. Graphical abstract Publication A; RQ: research questions.

Waste Management 149 (2022) 259–290

Contents lists available at ScienceDirect

Waste Management

journal homepage: www.elsevier.com/locate/wasman

Optical sensors and machine learning algorithms in sensor-based material flow characterization for mechanical recycling processes: A systematic literature review

Nils Kroell *, Xiaozheng Chen, Kathrin Greiff, Alexander Feil

Department of Anthropogenic Material Cycles, RWTH Aachen University, Germany

ARTICLE INFO

Keywords:
Sensor-based material flow characterization
Sensor-based sorting
Mechanical recycling
Optical sensors
Machine learning
Digitalization

ABSTRACT

Digital technologies hold enormous potential for improving the performance of future-generation sorting and processing plants; however, this potential remains largely untapped. Improved sensor-based material flow characterization (SBMC) methods could enable new sensor applications such as adaptive plant control, improved sensor-based sorting (SBS), and more far-reaching data utilizations along the value chain. This review aims to expedite research on SBMC by (i) providing a comprehensive overview of existing SBMC publications, (ii) summarizing existing SBMC methods, and (iii) identifying future research potentials in SBMC. By conducting a systematic literature search covering the period 2000 – 2021, we identified 198 peer-reviewed journal articles on SBMC applications based on optical sensors and machine learning algorithms for dry-mechanical recycling of non-hazardous waste. The review shows that SBMC has received increasing attention in recent years, with more than half of the reviewed publications published between 2019 and 2021. While applications were initially focused solely on SBS, the last decade has seen a trend toward new applications, including sensor-based material flow monitoring, quality control, and process monitoring/control. However, SBMC at the material flow and process level remains largely unexplored, and significant potential exists in upscaling investigations from laboratory to plant scale. Future research will benefit from a broader application of deep learning methods, increased use of low-cost sensors and new sensor technologies, and the use of data streams from existing SBS equipment. These advancements could significantly improve the performance of future-generation sorting and processing plants, keep more materials in closed loops, and help paving the way towards circular economy.

Abbreviations: 1D, One-dimensional; 3DLT, 3D laser triangulation; ABS, Acrylonitrile butadiene styrene; Al, Aluminum; ANN, Artificial neural network; ASR, Automotive shredder residue; Au, Gold; BC, Beverage carton; BN, Bayesian network; CBR, Case based reasoning; CDW, Construction and demolition waste; CNN, Convolutional neural network; CRF, Conditional random field; CT, Complementary troubleshooting; Cu, Copper; CuZn, Brass; CVA, Canonical variate analysis; DBC, Dissimilarity-based classifier; DT, Decision tree; ELV, End-of-life vehicles; eMFC, Extensive MFC; F, False; Fe, Iron; Fuzzy, Fuzzy based algorithm; GA, Genetic algorithm; GMM, Gaussian mixture models; GPC, Gaussian process classifier; HD, High-density; HIPS, High Impact PS; HSI, Hyperspectral imaging; ICA, Independent component analysis; iMFC, Intensive MFC; IR, Infrared; kNN, k nearest neighbors; LD, Low-density; LDA, Linear discriminant analysis; LEMAP, Laplacian Eigenmaps; LIBS, Laser-induced breakdown spectroscopy; LIDAR, Light detection and ranging; LIF, Laser-induced fluorescence; Linear, Linear regression; LWP, Lightweight packaging waste; MAE, Mean absolute error; MAP, Maximum a posteriori estimation; MCW, Mixed commercial waste; MFC, Material flow characteristic; MIR, Mid-infrared; ML, Machine learning; MLR, Multinomial logistic regression; MSW, Mixed solid waste; N, Negative; NC, Nearest centroid; Ni, Nickel; NIR, Near-infrared; P, Positive; PA, Polyamide; PBT, Polybutylene terephthalate; PC, Polycarbonate; PCA, Principal component analysis; PE, Polyethylene; PET, Polyethylene terephthalate; PLS, Partial least squares; PMMA, Polymethylmethacrylate; POM, Polyoxymethylene; PP, Polypropylene; PPC, Paper, paperboard, and cardboard; PPS, Polyphenylene sulfide; PS, Polystyrene; PSD, Particle size distribution; PVC, Polyvinylchloride; PVDF, Polyvinyliden fluoride; QA, Quality assessment; QDA, Quadratic discriminant analysis; RAMAN, Raman spectroscopy; RDA, Resemblance discriminate analysis; RF, Random forest; RGB, Red green blue; RMSE, Root mean square error; RQ, Research question; SAM, Spectral angle mapper; SBMC, sensor-based material flow characterization; SBMM, sensor-based material flow monitoring; SBPC, Sensor-based process control; SBPM, Sensor-based process monitoring; SBPM/C, SBPM or SBPC; SBQC, Sensor-based quality control; SBR, Styrene-butadiene rubber; SBS, sensor-based sorting; SCC, Spectral cross-correlation; SIMCA, Soft independent modelling by class analogy; SOM, Self-organized map; SVD, Singular value decomposition; SVM, Support vector machine; T, True; TEEE, Thermoplastic elastomer-ether-ester; THz, Terahertz; TPE, Thermoplastic elastomers; TPU, Thermoplastic polyurethane; TRL, Technological readiness level; UV, Ultraviolet; VIS, Visible; ViT, Vision transformer; VNIR, VIS-NIR; WEEE, Waste from electrical and electronic equipment.

* Corresponding author at: Department of Anthropogenic Material Cycles, RWTH Aachen University, Wuellnerstr. 2, D-52062 Aachen, Germany.
E-mail address: nils.kroell@ants.rwth-aachen.de (N. Kroell).

https://doi.org/10.1016/j.wasman.2022.05.015
Received 20 February 2022; Received in revised form 17 April 2022; Accepted 17 May 2022
Available online 24 June 2022

1. Introduction

Global material extraction has more than tripled from approximately 27 billion tons in 1970 to approximately 92 billion tons in 2017 (IRP, 2019), and may more than double by 2050 (IRP, 2017). The extraction and processing of natural resources make up approximately 50% of total greenhouse gas emissions and account for more than 90% of water stress and biodiversity loss (IRP, 2019). Accelerating climate change (IPCC, 2021) and biodiversity loss (Dirzo et al., 2014; WWF, 2020) indicate the urgency and critical importance of transitioning the world to sustainable development within current planetary boundaries (O'Neill et al., 2018; Rockström et al., 2009).

In the interests of sustainable development, the circular economy concept aims to reduce, alternatively reuse, recycle, and recover materials in production, distribution, and consumption processes (Kirchherr et al., 2017). Moving towards a circular economy requires streamlined efforts of all stakeholders along the value chain. For example, products have to be designed with a focus on durability, reusability, upgradability, and reparability; packaging materials have to be designed for reuse and recyclability. For products and packaging whose lifespan cannot be further extended ("end-of-life"), high-quality recycling should keep valuable materials in closed material loops as long as possible (European Commission, 2020).

In 2018, about 808.9 million tons of waste were generated in the EU-27 (excluding major mineral wastes) (Eurostat, 2021a), of which 38.1 wt % was fed into recycling processes (Eurostat, 2020). After recycling, secondary raw materials can—if their quality is sufficient—substitute primary raw materials, and achieve significant environmental benefits because primary raw material extraction is avoided, and secondary raw materials often have significantly lower environmental footprints (Astrup et al., 2009; Bajpai, 2014; Grimes et al., 2008; Shen et al., 2010; Simion et al., 2013).

Nevertheless, the current material supply in the EU is still largely dependent on primary resources, and as of 2018, only 12.2 wt% of used materials have come from secondary resources (Eurostat, 2021b). Therefore, significant improvements along the value chain are needed to increase the substitution of primary raw materials (IRP, 2019).

Increasing the performance of the future-generation of mechanical recycling processes would largely contribute to this goal through (i) recovering a higher amount of secondary raw materials from existing waste flows and (ii) producing secondary raw materials in higher quality to enable a high-value substitution of primary raw materials.

1.1. Concepts for increased performance of future-generation mechanical recycling processes

Mechanical recycling of valuable materials from wastes into secondary raw materials comprises two stages: First, in the pre-enrichment stage, *sorting plants* sort mixed wastes into preconcentrates (e.g., polypropylene [PP] plastic bales). Second, in the refinement stage, *processing plants* refine preconcentrates into secondary raw materials (e.g., PP recyclates). Whereby material flows from mono-collection (e.g., PET bottles from deposit return systems) can be directly passed on to the refinement stage.

Recently, several publications have argued that integrating *digital technologies* in mechanical recycling processes will increase their performance (Khodier et al., 2019; Sarc et al., 2019; Vrancken et al., 2017) and enhance circular economy in general (Antikainen et al., 2018; Berg et al., 2020; Hannan et al., 2015; Hedberg and Šipka, 2020; Hedberg et al., 2019; European Commission, 2020). More specifically, great potential is seen in increased exploitation of sensor technology in future-generation sorting and processing plants (Curtis et al., 2021; Feil et al., 2019; Khodier et al., 2019; Sarc et al., 2019; Serranti et al., 2011; Vrancken et al., 2017).

First, advanced sensors and characterization algorithms could increase sorting performance and enable new sorting possibilities in sensor-based sorting (SBS), thus improving the quality and quantity of recovered secondary raw materials. Second, an automated and adaptive process control could significantly improve the overall performance of future-generation sorting and processing plants. A key prerequisite for this is the availability of real-time material flow characteristics (MFCs) as a decision-making basis for an intelligent process control algorithm. The process control algorithm could then adapt remotely controllable actuators to maximize a given goal function (Khodier et al., 2019), e.g., to optimize the ecological or economic performance of the plant. Third, sensor-based material flow data could be used further along the value chain to improve material circulation in general; for example, by using sensor data from sorting plants for improved waste collection or sensor data from processing plants for optimized secondary raw material use in production.

Despite these promising advantages and applications, past reviews have concluded that digitization in waste management is "still in [its] infancy" (Sarc et al., 2019, p. 479) or "in an early phase" (Berg et al., 2020, p. 2). In particular, more far-reaching applications of sensor technology beyond SBS remain largely unexploited.

1.2. Key technology: Sensor-based material flow characterization

A fundamental prerequisite to improve or enable the applications mentioned above is a precise characterization of anthropogenic material flows: While SBS processes separate material flows mainly based on accurate classification decisions at the particle level, adaptive process control and further applications require precise MFCs at the material flow level. The present paper focuses on predicting characteristics of anthropogenic material flows with sensor technology and machine learning (ML) algorithms—a process we refer to as *sensor-based material flow characterization* (SBMC).

Scientific literature has so far reviewed applications of sensor technology in waste management for waste segregation (Hannan et al., 2015), recovery and production of solid recovered fuels (Vrancken et al., 2017), identification and sorting of plastics (Araujo-Andrade et al., 2021), SBS (Gundupalli et al., 2017a), digitalization in general (Sarc et al., 2019), and applications of ML algorithms for waste management (Abdallah et al., 2020; Ni et al., 2021; Xia et al., 2021b). However, a systematic review of SBMC has yet to be conducted in the context of high-value material recycling.

1.3. Aim and scope

This paper aims to expedite future research on SBMC by (i) providing a comprehensive overview of existing publications on SBMC, (ii) summarizing existing methods for SBMC, and (iii) indicating future research potentials in SBMC.

The first emphasis of this review is on *non-destructive optical sensors*, as previous reviews have highlighted their suitability for SBMC (Vrancken et al., 2017). Compared to other sensors, optical sensors are advantageous for large-scale integration in sorting and processing plants because of their lower investment and operating costs and lower health risks compared with other sensors such as X-ray detection or laser-induced breakdown spectroscopy (LIBS)[1] (Sarc et al., 2019; Vrancken et al., 2017).

The second emphasis is on *ML algorithms,* which enable automatic extraction of MFCs from the acquired sensor data (Sarc et al., 2019; Vrancken et al., 2017). Compared to traditional algorithms, ML algorithms are not required to be explicitly programmed but can instead learn prediction patterns from given training data (Marsland, 2014).

During conducting the review at hand, we noticed that there is no consistent terminology used in SBMC and that research in SBMC is

[1] Readers interested in LIBS applications may find interest in the reviews of Noll et al. (2018) and Legnaioli et al. (2020).

dispersed widely and is often not perceived as a homogeneous research field. Based on our review findings, we will thus firstly propose a unified SBMC terminology in Section 2 before we elaborate on our review method (Section 3), present and discuss obtained results (Section 4), indicate possible future research directions (Section 5), and draw final conclusions (Section 6).

2. Background and terminology

SBMC describes digitally capturing material flows with sensors and applying algorithms to extract MFCs from the acquired sensor data. As SBS (based on particle characteristics) has been applied and investigated for decades and is focused on pixel- or particle-based material classes, we focus here on process-relevant MFCs defined in Section 2.1. Section 2.2 then determines how optical sensors can digitally capture material flows, and Section 2.3 elaborates on applying algorithms to extract process-relevant MFCs from sensor data.

2.1. Process-relevant MFCs

This paper defines a material flow as a material, or a mix of materials, which is regularly transported from position *A* to position *B*. Material transportation can be achieved either with continuous conveyors (e.g., belt conveyors) or non-continuous conveyors (e.g., wheel loaders) (Griemert and Römisch, 2020). In modern sorting and processing plants, material flows are almost exclusively transported on continuous conveyors because of their higher efficiency and lower costs (Griemert and Römisch, 2020). Thus, material flows on continuous conveyors are especially relevant for SBMC applications (Sarc et al., 2019).

In the context of SBMC, we propose to divide MFCs into *extensive* and *intensive* MFCs. The magnitude of extensive characteristics (e.g., mass or volume) depends on the size of a system; however, the magnitude of intensive characteristics (e.g., material composition or bulk density) is independent of a system's size (Cohen and Mills, 2007; Tolman, 1917).

2.1.1. Extensive MFCs

Two extensive MFCs (eMFCs) of high practical relevance exist: the mass flow rate $\dot{m}$ (Eq. (1)), which is the flow of mass m per unit of time t through a process line; and the volume flow $\dot{V}$ (Eq. (2)), which is the flow of volume V per unit of time t through a process line (Ghasem and Henda, 2012).

$$\dot{m} = \frac{dm}{dt} \tag{1}$$

$$\dot{V} = \frac{dV}{dt} \tag{2}$$

While the mass flow of any closed system is constant over time (law of conservation of mass) (Whitaker, 1975), volume flows might change over time, e.g., because of changing bulk densities (Curtis and Sarc, 2021; Feil et al., 2019). Volume flows are therefore only of limited suitability for process evaluation; mass flows, on the other hand, cannot be measured directly with optical sensors.

2.1.2. Intensive MFCs

While process-relevant eMFCs are usually limited to mass and volume flows, several intensive MFCs (iMFCs) have been proposed. For example, Christensen (2011) identifies (i) *physical iMFCs* (material composition, particle size distribution [PSD], moisture content, densities), (ii) *chemical iMFCs* (pH and alkalinity, organic matter, inorganics, calorific value, heating value), and (iii) *performance iMFCs* (compressibility, aqueous leachability of substances, biological degradability [respiration tests], biochemical methane potential).

In addition, Vrancken et al. (2017) list nine so-called *critical quality attributes* in the context of material recovery and solid recovered fuel production: problematic objects, PSDs, calorific value, ash content, moisture, composition, biogenic carbon, biochemical methane potential, and contaminants.

Another group of iMFCs describes the *material flow presentation*. These presentation iMFCs include, e.g., the fluctuations of volume flows (Curtis et al., 2021; Feil et al., 2019) and occupation densities (Küppers et al., 2021; Küppers et al., 2020), as both strongly influence the (sensor-based) sorting performance (Kroell et al., 2022).

Based on the available literature, we propose to structure MFCs into two groups, namely eMFCs and iMFCs, as well as four subgroups of iMFCs, as shown in Table 1. This listing is not exhaustive, as additional iMFCs are likely to be proposed for future applications.

2.1.3. MFCs of high practical relevance for mechanical recycling processes

As the scope of this review does not extend to reviewing research on all MFCs, we focus on MFCs of high practical relevance for mechanical recycling processes and the research vision described in Section 1.1. We have already identified two relevant eMFCs in Section 2.1.1: mass and volume flows. To identify iMFCs with high practical relevance, we will investigate iMFCs used in two major applications of (currently manual) material flow characterization: (i) technical process assessment and (ii) quality control of generated pre-concentrates.

2.1.3.1. iMFCs in technical process assessment. Sorting and processing plants comprise a sequence of mechanical unit operations. For each mechanical unit operation (sorting, sieving, or comminution), one or more *indicators* are used to assess the process performance. Each indicator is calculated on the basis of one or multiple MFCs. MFCs used in these indicators are thus likely to be of high importance for future SBMC applications.

Sorting processes are assessed on the basis of the two indicators *purity* (c_w) and *yield* (R_w) (Feil et al., 2016). Purity (Eq. (3)) describes the mass fraction of valuable material ($\dot{m}_{w,i}$) in a material flow ($\dot{m}_i$). Yield (Eq. (4)) describes how much valuable material of the input material flow of a process ($\dot{m}_{w,\,input}$) is transferred to the desired output material flow ($\dot{m}_{w,output}$).

$$c_{w,i} = \frac{\dot{m}_{w,i}}{\dot{m}_i} \tag{3}$$

$$R_w = \frac{\dot{m}_{w,\,output}}{\dot{m}_{w,\,input}} = \frac{\dot{m}_{output} * c_{w,\,output}}{\dot{m}_{input} * c_{w,\,input}} \tag{4}$$

Sieving processes are assessed on the basis of the screening efficiency η_s, which is the ratio of fines (index f) in the input material flow ($\dot{m}_{input}$) that is transferred into the fine fraction ($\dot{m}_{FF}$) (Eq. (5)) (Schmidt et al., 2006).

Table 1
Grouping of MFCs in eMFCs and iMFCs.

Group	Subgroup	Examples
eMFCs	–	Mass flow
		Volume flow
iMFCs	Physical iMFCs	Material composition
		PSD
		Moisture content
		Densities
	Chemical iMFCs	pH and alkalinity
		Organic matter
		Inorganics
		Calorific value
	Performance iMFCs	Heating value
		Compressibility
		Aqueous leachability of substances
		Biological degradability
		Biochemical methane potential
	Presentation iMFCs	Occupation density
		Particle singling
		Particle distances
		Fluctuations of iMFCs

$$\eta_s = \frac{\dot{m}_{f,\,FF}}{\dot{m}_{f,\,input}} = \frac{\dot{m}_{FF} * c_{f,\,FF}}{\dot{m}_{input} * c_{f,\,input}} \quad (5)$$

Comminution processes are assessed by comparing the PSD of the output material flow with those of the input material flow, e.g., through the *reduction ratio* (Eq. (6)), where *d* is a measure for the PSD (Wills and Finch, 2016).

$$n_c = \frac{d_{output}}{d_{input}} \quad (6)$$

Notably, all presented indicators (Eq. (3) – Eq. (6)) are based on the iMFCs *material flow composition* and *PSD*, therefore being relevant iMFCs for technical process assessment.

2.1.3.2. iMFCs in quality control. For quality control, slightly varying standards and guidelines exist across different countries. Table 2 shows that, for example, in Germany, quality control standards for secondary raw materials most frequently focus on *material flow composition* (100.0%), *PSDs* (66.7%), and *moisture content* (44.4%).

Based on these findings, subsequent sections will primarily focus on the material (flow) composition and PSD. A comprehensive overview of existing publications on sensor-based moisture content determination is given by Vrancken et al. (2017).

2.2. Optical sensors for material flow characterization

Optical sensors cover the wavelength range between 100 nm and 1 mm, which includes the ultraviolet (UV; 100 nm – 380 nm), visible (VIS; 380 nm – 780 nm), and infrared (IR; 780 nm – 1 mm) region (DIN 5031-7, 1984). For SBMC applications, various sensors are available that can be integrated into sorting and processing plants.

Table 2
Considered MFC in quality control standards and guidelines in Germany.

Material flow	Addressed MFC			
	Material composition	PSD	Moisture	Other MFCs
Plastics[1]	✓	–	–	–
Glass[2]	✓	✓	✓	–
Non-ferrous metal scrap[3]	✓	✓	✓[(a)]	Origin, condition (corrosion)[(a)]
Steel scrap[4]	✓	✓	–	Bulk density
Aggregates[5]	✓	✓	–	pH content, electrical conductivity
Paper[6]	✓	–	✓	Age[(b)]
WEEE[(c), 7]	✓	–	–	–
Textiles[8]	✓	✓[(b)]	–	Water retention, hydrophobic/ hydrophilic
Compost[9]	✓	✓	✓	rotting degree
Percentage covered	**100.0%**	**66.7%**	**44.4%**	**≤ 11.1%**

[(a)] for some fractions;
[(b)] fiber length and morphology;
[(c)] waste of electrical and electronic equipment.
[1] (Der Grüne Punkt, 2021),
[2] (Bundesverband Glasindustrie e. V., 2014),
[3] (Verein Deutscher Metallhändler e. V., 1988),
[4] (Bundesvereinigung Deutscher Stahlrecycling- und Entsorgungsunternehmen e. V., 1995),
[5] (TL Gestein-StB 04, 2007),
[6] (DIN EN 643, 2014),
[7] (ElektroG, 2015),
[8] (Bartl et al., 2011),
[9] (Bundesgütegemeinschaft Kompost e. V., 2021a, 2021b, 2021c).

2.2.1. Available optical sensors for SBMC

Optical sensors have been developed and applied to characterize materials across the UV, VIS, and IR regions (Beel, 2017; Flamme and Krämer, 2015; Küppers and Pomberger, 2017). Depending on the selected wavelength range and sensor arrangement (reflective or transmissive measurements), different material characteristics can be derived from the acquired sensor data. Despite the different wavelengths addressed, almost all currently applied sensors follow the same measuring principle: (i) an emitter emits electromagnetic radiation that interacts with the material to be characterized; (ii) a detector detects the reflected or transmitted radiation; (iii) an algorithm analyzes the captured sensor data to characterize the material (Chen et al., 2021a).

Table 3 presents optical sensors suitable for measuring material characteristics for each spatial measuring point (*pixel*). In the VIS range, two types of sensors are commonly used: RGB-sensors (VIS-RGB), which capture the intensity at three different color channels (red [R], green [G], and blue [B]) and hyperspectral imaging (HSI) sensors, which measure the intensity at more than 100 different wavelength bins (VIS-HSI). In addition, sensors that cover (parts of) the VIS and near-infrared (NIR) range (VNIR) are available. Aside from measuring these pixel-based characteristics, most optical sensors can generate a spatial representation (image) of the recorded area (Jähne, 2005), which can be further analyzed at the particle or material flow level (cf. Section 2.3.1).

2.2.2. Integration of sensors in sorting and processing plants

Sensors can be integrated at different positions in sorting and processing plants with the goal of characterizing material flows or monitoring (sub)processes. According to Kessler (2012), process-analytical methods can be classified as *offline*, *atline*, *online,* and *inline*. For all four methods, the taxonomy is defined by the process proximity of the analyzer in use (Kessler, 2012): (i) *Offline* analytics involve sampling the material flow and transporting the sample, e.g., to a laboratory, where the sample is analyzed. The obtained results are only available with a considerable time delay. (ii) *Atline* analytics are characterized by a reduced time delay, as the analysis occurs in close proximity to the process. (iii) *Online* analytics automatically analyze a part of the material flow through a bypass. (iv) *Inline* analytics measure the entire material flow, thus avoiding potential sampling errors. Real-time SBMC required for the applications outlined in Section 1.1 can only be achieved by online and inline methods, discussed in subsequent sections.

2.3. Sensor-data analysis for SBMC applications

As most material and material flow characteristics cannot be directly measured with available sensors, suitable algorithms are often necessary to extract MFCs of interest (Sun, 2009). The necessary data analysis can be performed at different *investigation levels*, depending on the application and characteristic of interest.

2.3.1. SBMC investigation levels

Sensor data analysis for SBMC can be performed at four investigation levels:

Pixel level. The information of a pixel is represented as a one-dimensional (1D) array containing a numeric value for each channel. For example, the 1D array of each pixel can represent measured heights (one channel), RGB colors (three channels), or NIR/VIS spectra (> 100 channels). In pixel-based analysis, the information of each pixel is considered independently. Characteristics extracted at pixel level include, e.g., material classes (per pixel) or heights.

Particle level. Multiple, connected pixels can represent individual particles. In particle-based analysis, the information from multiple pixels representing a particle is combined. Furthermore, new particle-based features such as particle sizes and shapes often characterize individual particles. Characteristics extracted at the particle level include, e.g., material classes (per particle) or particle sizes.

Material flow level. A material flow consists of multiple particles. In

Table 3
Available non-destructive, optical sensors for SBMC.

Sensor technology		Wavelength range [nm]		Working principle	Pixel-based extractable characteristics	Surface technology	Reference
		from	to				
LIF	Laser-induced fluorescence	100[(a)]	380[(a)]	Fluorescence	Chemical composition	✓	(Küch and Gaastra, 2014)
VIS	Visual	380	780	Reflection, absorption	Color	✓[(b)]	(Beyerer et al., 2016)
RAMAN	Raman spectroscopy	380[(a)]	780[(a)]	Raman effect	Chemical composition	✓	(Smith and Dent, 2019)
3DLT	3D laser triangulation	–	–	Reflection + triangulation	Height	✓	(Beyerer et al., 2016)
NIR	Near-infrared spectroscopy	780	2,500	Reflection, absorption	Chemical composition	✓[(c)]	(Ozaki et al., 2021)
MIR	Mid-infrared spectroscopy	2,500	25,000	Reflection, absorption	Chemical composition	✓[(c)]	(Sun, 2009)
THz	Terahertz	10^4	10^6	Transmission	Chemical composition	–	(Maul and Nagel, 2014)

[(a)] LIF uses monochromatic excitation; the numerical values indicate typical application areas;
[(b)] for transparent objects, transmissive measurements are also possible;
[(c)] limited penetration depth.

material-flow-based analysis, the characteristics of multiple particles or pixels are combined to extract MFCs. Characteristics extracted at the material flow level include, e.g., material compositions, PSDs, or volume flows.

Process level. A process involves two or more material flows. In process-based analysis, several material flows and their relationships (e.g., input and output material flow) are combined to characterize or assess a process. Characteristics extracted at the process level include, e.g., the indicators *yield*, *screening efficiency*, and *reduction ratio* (cf. Section 2.1.3.1).

Characteristics from lower investigation levels (e.g., pixel or particle level) are needed to extract characteristics at higher investigation levels (e.g., material flow or process level). Taking the determination of screening efficiency (Eq. (5)) at the process level as an example, the sensor-based assessment may involve four steps: First, pixels may be segmented into foreground and background (*pixel level*). Second, particle sizes and masses of the identified particles may be predicted (*particle level*). Third, particle sizes and masses may be combined into PSDs (*material flow level*). Fourth, PSDs and screen underflow and overflow quantities may be combined to compute the screening efficiency (*process level*). The extracted characteristics at different investigation levels can then be utilized in applications such as automatic quality control (material flow level) or adaptive process control (process level). Fig. 1 summarizes the four SBMC investigation levels and their hierarchical interplay. It is important to note that investigation levels can be skipped in specific cases; for example, characteristics from the pixel level can be directly aggregated at the material flow level (see dotted lines in Fig. 1).

2.3.2. Machine learning algorithms

Many tasks in sensor-data analysis for SBMC applications involve predicting an unknown characteristic (e.g., material class) from known sensor data (e.g., NIR spectra). In ML terminology, the unknown characteristic is called *target variable y*, and the known sensor data is called *input variable X* (Hastie et al., 2009c). In such prediction problems, the goal is to develop a mathematical *model* that predicts the target variable *y* from the input variable *X* as accurately as possible.

Supervised ML algorithms can solve such prediction tasks without being explicitly programmed by *learning* relationships between *X* and *y* from labeled training data, i.e., known input variables *and* known target variables (Marsland, 2014). Trained ML models can then predict unknown target variables from known input variables (Bishop, 2006).

Two types of supervised ML problems can be distinguished. First, in *classification* problems, the target variable is discrete. Common applications with classification problems are, e.g., the prediction of material classes (e.g., "PET", "PE", "PP") or color classes (e.g., "red", "green", "blue") from sensor data. Second, in *regression* problems, the target variable is continuous. Common applications with regression problems are, e.g., the prediction of material compositions [%], particle sizes

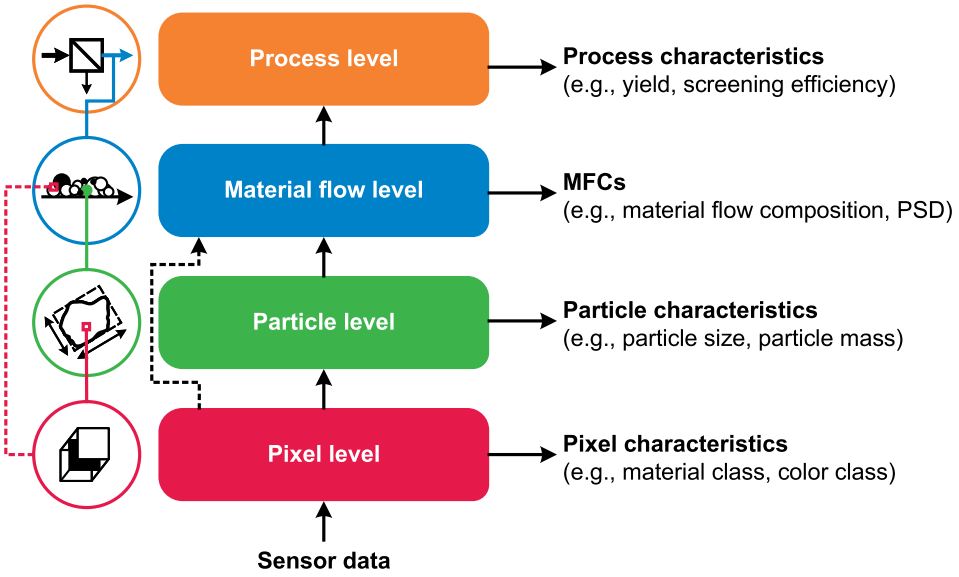

Fig. 1. SBMC investigation levels.

[mm], or moisture contents [%]. (Rebala et al., 2019).

Different metrics can be used to evaluate the performance of supervised ML algorithms. For this evaluation, a labeled dataset is divided into training and test data. ML algorithms are trained on the training dataset, and predictions of the trained algorithms based on the input variables of the test set are compared with the ground truth, i.e., the known target variables of the test dataset, to determine the prediction accuracy. (Kubat, 2017).

2.3.2.1. Classification metrics. In binary classification problems, y can have two values: "positive" (P) and "negative" (N). True (T) and false (F) predictions can then be visualized in a 2x2 *confusion matrix* (Eq. (7)) (Marsland, 2014).

$$\text{Confusion matrix}: \begin{bmatrix} TP & FP \\ FN & TN \end{bmatrix} \tag{7}$$

Based on the confusion matrix, common classification metrics can be calculated, including *accuracy* (Eq. (8)), *precision* (Eq. (9)), *recall* (Eq. (10)), and *F1-score* (Eq. (11)).

$$accuracy = \frac{\#TP + \#TN}{\#TP + \#FP + \#TN + \#FN} \tag{8}$$

$$precision = \frac{\#TP}{\#TP + \#FP} \tag{9}$$

$$recall = \frac{\#TP}{\#TP + \#FN} \tag{10}$$

$$F1 - score = 2 \bullet \frac{precision \bullet recall}{precision + recall} \tag{11}$$

Multi-class classification problems (> 2 classes) can be reformulated as a combination of binary classification problems. Calculated binary metrics can then be aggregated in terms of *macro-* or *micro-averages*. For macro-averages, all classes are weighted equally; for micro-averages, classes are weighted by the number of instances of each class. (Kubat, 2017).

2.3.2.2. Regression metrics. Regression metrics compare true target variables y_i with their corresponding predictions $\widehat{y}_i$. Common metrics for regression problems are the R^2-score (Eq. (12)), the mean absolute error (*MAE*) (Eq. (13)), and the root mean square error (*RMSE*) (Eq. (14)). Accurate predictions are indicated both by low *MAE* and *RMSE* values and R^2-scores close to 1. (Fahrmeir et al., 2009; Willmott and Matsuura, 2005).

$$R^2 = \frac{\sum_{i=1}^{n}(\widehat{y}_i - \overline{y})^2}{\sum_{i=1}^{n}(y_i - \overline{y})^2}, \text{ with } \overline{y} = \frac{\sum_{i=1}^{n} y_i}{n} \tag{12}$$

$$MAE = \frac{1}{n}\sum_{i=1}^{n}|\widehat{y}_i - y_i| \tag{13}$$

$$RMSE = \sqrt{\frac{1}{n}\sum_{i=1}^{n}(\widehat{y}_i - y_i)^2} \tag{14}$$

3. Material and methods

To achieve the research objectives outlined in Section 1.3, we conducted a systematic literature review. Systematic literature reviews are a method for identifying, evaluating and interpreting all available research relevant to a particular set of research questions (Kitchenham, 2007).

Based on the systematic literature review guidelines of Kitchenham (2007), the following steps were taken to conduct the review: formulation of research questions (Section 3.1), development of a search strategy (Section 3.2), selection of relevant publications (Section 3.3), quality assessment of selected publications (Section 3.4), and data extraction (Section 3.5).

3.1. Research questions

To achieve the research objectives outlined in Section 1.3, the following six research questions (RQs) have been formulated:

RQ 1. Which *material flows* and *material classes* have been investigated so far, and which material flows have been addressed most frequently?

RQ 2. The prediction of which *characteristics* has been investigated and which *investigation levels* have been targeted?

RQ 3. Which optical *sensors* have been applied for which tasks?

RQ 4. Which *ML algorithms* have been applied and which prediction accuracies have been achieved?

RQ 5. Which *applications* are envisioned based on SBMC methods, and at which *scales* have the investigations occurred?

RQ 6. How *interconnected* is SBMC research, and how is the research of different SBMC aspects interlinked?

3.2. Search strategy

Firstly, an initial literature set was compiled from prior known publications and initial searches. Then, based on the initial literature set, multiple search strings were developed, tested, and iteratively optimized for the full review. Furthermore, systematic forward and backward searches were applied to extend the obtained literature set.

3.2.1. Search strings

The developed search strings (Table 4) targeted different sensor applications (sorting, quality control, characterization, monitoring, process control), methods (classification/discrimination), and MFCs (material composition, PSD; cf. Section 2.1.3). Depending on the relevance for the target, the individual search words either target for the title (*TITLE*) or the title, abstract, and keywords (*TITLE-ABS-KEY*). Using Boolean operators (*AND*, *OR*) and wildcard operators (*) ensured that different spellings and synonyms were considered. All search strings were adapted to the database-specific syntax (Table 4 shows the syntax for Scopus as an example).

3.2.2. Databases

All search strings were applied to three large, multidisciplinary bibliographic databases of three different providers to minimize potential biases through database selection and identify as many relevant publications as possible. The three selected databases were Scopus (Scopus., 2021), Web of Science (Clarivate, 2021), and Google Scholar (Google LLC, 2021). All search strings were applied in October 2021.

3.2.3. Forward and backward searches

To identify relevant publications that might not be covered by the search strings (cf. Table 4), all references of the selected publications (*backward search*) as well as citations of those publications (*forward search*) were included in the review and underwent the selection process (Section 3.3). In this way, the review relies not only on the developed search strategy but also utilizes the extensive literature searches of each of the included publications and overcomes possible limitations of the developed search strings.

3.3. Selection criteria and procedures

3.3.1. Inclusion criteria

Of interest for our review are publications on in- or online applications of optical sensor technologies for material flows in dry-mechanical recycling processes of non-hazardous wastes. We considered peer-reviewed journal articles in the English language published in the time

Table 4
Developed and applied search strings for the systematic literature review; Abbr.: Abbreviation.

Abbr.	Target	Search string
Q	Quality control	*TITLE-ABS-KEY*(quality *AND* (product *OR* assess* *OR* analys* *OR* control* *OR* monitor* *OR* assurance)) *AND TITLE*((waste *OR* recyc* *OR* recover* *OR* "post-consumer" *OR* "post-industrial") *AND* (sensor* *OR* *spectr* *OR* imag*))
C	Characterization	*TITLE-ABS-KEY*(characteri*) *AND TITLE*((waste *OR* recyc* *OR* recover* *OR* "post-consumer" *OR* "post-industrial") *AND* (sensor* *OR* *spectr* *OR* imag*))
M	Monitoring	*TITLE-ABS-KEY*(monitor*) *AND TITLE*((waste *OR* recyc* *OR* recover* *OR* "post-consumer" *OR* "post-industrial") *AND* (sensor* *OR* *spectr* *OR* imag*))
P	Process control	*TITLE-ABS-KEY*("process control" *OR* real*time *OR* on*line *OR* in*line) *AND TITLE*(waste *OR* recyc* *OR* "post-consumer" *OR* "post-industrial")
S	SBS	*TITLE-ABS-KEY*((sensor*based *OR* automatic) *AND* (sort* *OR* separat*)) *AND TITLE*(waste *OR* recyc* *OR* "post-consumer" *OR* "post-industrial")
D	Classification/ discrimination	*TITLE-ABS-KEY*(classif* *OR* discrimi*) *AND TITLE*((waste *OR* recyc* *OR* recover* *OR* "post-consumer" *OR* "post-industrial") *AND* (sensor* *OR* *spectr* *OR* imag*))
CO	Composition	*TITLE-ABS-KEY*(content *OR* composition *OR* purity) *AND TITLE*((waste *OR* recyc* *OR* recover* *OR* "post-consumer" *OR* "post-industrial") *AND* (sensor* *OR* *spectr* *OR* imag*))
PS	PSD	*TITLE-ABS-KEY*((particle *OR* grain) *AND* (size *OR* distribution)) *AND TITLE*((waste *OR* recyc* *OR* recover* *OR* "post-consumer" *OR* "post-industrial") *AND* (sensor* *OR* *spectr* *OR* imag*))

range from 2000 to 2021. The scope was limited to peer-reviewed journal articles to ensure a high quality of included manuscripts (Xiao and Watson, 2019) and maximum transparency of the search and selection process (Kraus et al., 2020). The timeframe 2000 – 2021 was chosen as related reviews indicated that most publications on sensor technologies in the waste management sector had been published from 2012 onwards (Sarc et al., 2019), and far older publications are often less relevant due to advancements in sensor technologies and ML algorithms in recent years (Vrancken et al., 2017; Xia et al., 2021b).

3.3.2. Exclusion criteria

Publications on hazardous wastes, biological or chemical treatment of wastes, liquid or gaseous wastes (e.g., wastewater or sludges), and mining wastes were not considered as these applications address significantly other MFCs compared to those relevant for mechanical recycling processes (cf. Section 2.1). Similarly, (pre-)treatment of wastes for thermal processes, including solid recovered fuel production, are not considered, which have been partly reviewed by Vrancken et al. (2017). Publications using virgin materials were only considered if an intended application for mechanical recycling is outlined in the abstract or title.

Non-sensor-based characterization methods and methods that cannot be directly applied to inline or online characterization are not considered as they are not suitable for inline SBMC in sorting and processing plants (see Section 2). Such methods include (semi-)manual methods, non-inline laboratory measurements (e.g., microscopes), sensors that strictly require a 1D singulation of the material flow, or manual positioning (e.g., handheld devices).

Furthermore, applications of sensors at the waste segregation or collection level were excluded, as the material presented to the sensor units in these applications differ from online and inline applications in sorting and processing plants (e.g., 1D singulation and material presentation), cf. Section 2.2.2. Applications of sensors for waste segregation and collection have, among others, been reviewed by Hannan et al. (2015).

3.3.3. Selection process

For publications identified by the search strategy (cf. Section 3.2), a multi-stage selection process (cf. Fig. 2) was conducted. Firstly, the titles of all search results were screened, and publications not meeting the selection criteria were excluded. Secondly, the abstract and keywords of all non-excluded publications were checked, and publications not meeting the selection criteria were further excluded. Thirdly, full copies of all non-excluded publications were obtained and checked against the inclusion and exclusion criteria. In case of uncertainty, a copy was sent to a second reviewer and discussed within the review team.

Due to the full-text search and lack of filters in Google Scholar, we observed a large number of hits for each search string (17,400 – 19,400 hits per search string, 144,500 hits in total). As Google Scholar sorts the search results by relevance and screening all 144,500 titles was practically infeasible, we limited the title screening in Google Scholar to the first 300, i.e., the most relevant, results. The limit of 300 publications was chosen because (i) we did not find additional publications in our scope after screening the first 200 search results, and (ii) we observed a similar number of hits for Web of Science and Scopus with the title and abstract specific search terms (cf. Fig. 2).

3.3.4. Included and excluded publications

In total, $n = 11{,}607$ publications were found by applying the eight search strings. $n = 10{,}720$ publications were excluded during title screening. From the remaining $n = 887$ publications, $n = 377$ publications were excluded during abstract screening. After removing $n = 309$ duplicates (publications that match multiple search strings), a total of $n = 201$ publications were selected for review. Unfortunately, $n = 4$ of these $n = 201$ publications were unavailable, despite all efforts devoted (search all available databases, search journal/publisher page, contact corresponding authors directly via ResearchGate and e-mail). $n = 108$ publications were considered out of scope during the full review. Applying the forward and backward searches revealed another $n = 217$ publications after abstract and title screening, of which $n = 113$ met the selection criteria after full review and were included in the review. The final dataset obtained $n = 198$ publications, as summarized in Fig. 2.

3.4. Quality assessment

For each publication, a quality assessment (QA) was performed by answering the following four QA questions for each included publication:

QA 1. Is the publication an original research article (i.e., did the publication conduct an experiment or propose a new method/concept)? *Yes (1 P), No (0 P).*

QA 2. Did the publication reference related work and contextualize the findings within existing research? *Yes (1 P), Partly (0.5 P), No (0 P).*

QA 3. Are the applied methods clearly described (e.g., applied sensor (s), measurement settings, applied preprocessing techniques and ML algorithms)? *Yes (1 P), Partly (0.5 P), No (0 P).*

QA 4. Are the results clearly described and discussed (e.g., quantitative assessment of achieved prediction results)? *Yes (1 P), Partly (0.5 P), No (0 P).*

Extensive pre-review discussion ensured a consistent calibration of all reviewers. Uncertainties and edge cases were discussed and jointly decided within the review team. By summing up the scores of all four QA questions, an overall QA score was obtained. The final review considered publications with overall QA scores greater than 3.

3.5. Data extraction

To answer the research questions, a data extraction form was developed (Table 5), based on which the relevant data was extracted.

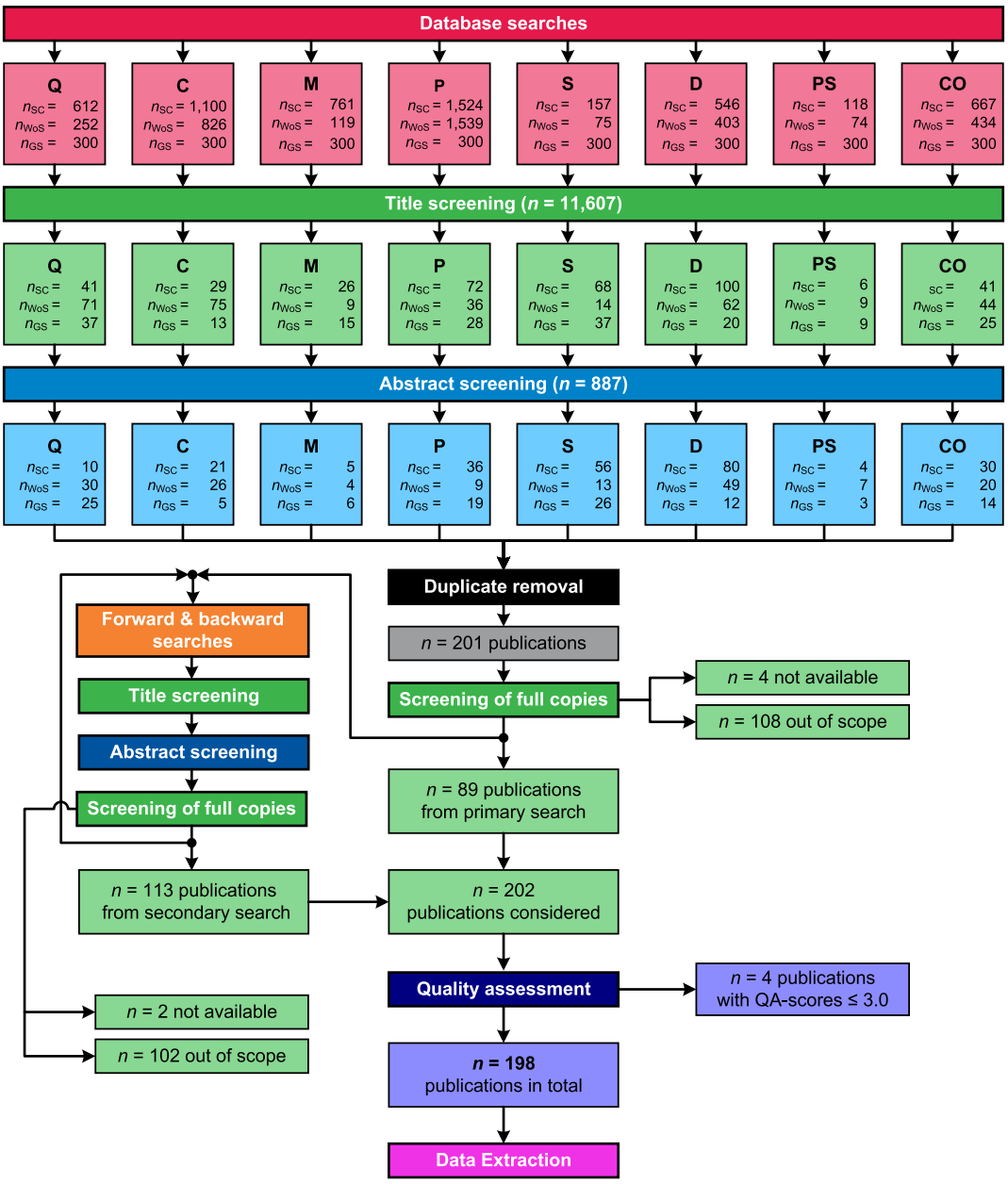

Fig. 2. Included and excluded publications. SC: Scopus, WoS: Web of Science, GS: Google Scholar; Q, C, M, P, S, D, PS, CO: search string abbreviations introduced in Table 4.

For each publication, a unique identifier was used to connect the extracted data to the bibliometric *meta*-information. Data extraction was performed by one reviewer and checked by a second reviewer. Ambiguities or discrepancies during data extraction were discussed within the review team.

As some authors published two or more independent investigations in one publication, while others split such results into multiple publications, a potential weighting bias could occur in subsequent data analysis. Furthermore, combining multiple independent investigations into one publication complicates data extraction and analysis. To minimize such biases and ensure a sophisticated data analysis, we decided to split up publications containing multiple independent experiments into separate *investigations* during data extraction and assess them independently from each other during data analysis (Section 4). Thus, one publication can contain one or multiple investigations. Examples of such publications include, e.g., publications that reported a series of investigations for different sensors, material flows, or scales (e.g., laboratory experiments followed by scale-up to industrial level) in independent experiments.

4. Results and discussion

After data extraction, the final obtained dataset contains $n = 267$ investigations from $n = 198$ publications. As a reference for the reader, we summarize all publications sorted by applied sensors and investigated material flows in Table 6. As shown in Fig. 3a, the number of reported investigations increases super-linear from $n = 2$ investigations in 2000 to $n = 65$ investigations in 2021. More than half of all investigations (155 of 267, 58.1%) were published between 2019 and 2021.

4.1. Material flows and classes

In total, $n = 17$ different material flows were studied by the

Table 5
Description of the developed data extraction form for the systematic literature review.

Field	Description
Sensor	Type of applied sensor, including multi-sensors (cf. Table 3).
Investigated materials	List of investigated materials (e.g., ["PET", "PE", "PP"]).
Material flow	Material flow from which the investigated sample originated (e.g., WEEE or MSW).
Virgin samples	Whether virgin materials were used as sample material (see Section 3.3.1).
Investigation method	Used investigation method (e.g., spectra description, classification, sensor-based sorting, material flow monitoring).
Investigation level	Whether the investigation was applied at the pixel, particle, material flow, or process level (cf. Section 2.3.1).
Investigation scale	Measure for scale and technological readiness level (TRL) (International Organization for Standardization, 2013) of the investigated technology: *concept*: formulation of (unproven) concepts (TRL 0–2), *lab scale*: basic research and laboratory-scale prototypes (TRL 2–4), *industrial-scale*: research at an industrial scale or industrial-scale prototypes (TRL 5–8), *plant scale*: investigations in plant scale (TRL 6–9).
Applied ML algorithm(s)	List of applied ML algorithms (excluding non-ML algorithms and static [preprocessing] algorithms).
Best ML algorithm	Best performing ML algorithm (highest *score* on test data).
Score type	Type of score (e.g., accuracy, F1-score, R^2-score; cf. Section 2.3.2).
Score	Score value on test data (aggregated as macro-average; cf. Section 2.3.2.1).
Intended application(s)	List of intended applications from the publication.
Quality assessment	Answers to QA questions, upon which the QA score is calculated (cf. Section 3.4).

investigations in our dataset. Table 7 summarizes the investigated material flows and introduces their abbreviations.

4.1.1. Investigated material flows

As shown in Table 7, about a third of all investigations focused on plastics (32.6%), followed by WEEE (11.2%), and CDW (10.1%). SBMC on public datasets such as *TrashNet* (Yang and Thung, 2016) and *Huawei garbage classification challenge cup* (Huawei, 2019) was examined by only 16 of 267 investigations (6.0%); the majority of researchers generated the sensor data for the investigation itself.

As shown in Fig. 3a, the focus of the investigations in our dataset has shifted over time. For example, while investigations on publicly available *datasets* started in 2019 and doubled or more since then, no new investigations on the material flow *paper* have been reported in our dataset since 2015. To quantify which material flows have gained or lost relative importance, we calculated for each material flow its relative frequency among (a) all investigations in the last five years (2016 – 2021) and (b) the years before (2000 – 2016). By comparing both relative frequencies, we observe that investigations on *datasets* (+9.8 percentage points [pp] increase in relative frequency), *plastics* (+5.2 pp) and *waste* in general (+5.2 pp) have gained relative frequency, while investigations on *paper* (-13.3 pp), *ASR/ELV* (-8.0 pp), and *CDW* (-6.3 pp) have lost relative frequency.

4.1.2. Investigated material classes

In total, 594 unique material classes (including subgroups such as high-density (HD)- and low-density (LD)-PE) and 321 unique material groups (after summarizing material classes to material groups, e.g., summarizing LDPE and HDPE to PE) have been reported. By analyzing the correlation (simultaneous occurrence) between the 20 most frequently studied material classes in Fig. 3b, we identify two groups of investigations.

The first group focuses on the classification of different polymers. Here, the classification often takes place on the pixel level and based on NIR data. The focus of the first group is often on plastic waste streams or plastics in other material flows (e.g., LWP or WEEE). Material classes frequently investigated by this group are also among the most frequently investigated pixel-level material classes (PP, PE, PET, PS, and PVC), see Fig. 3c.

The second group focuses on the discrimination of more general waste classes. Here, the classification often takes place at the particle level and with deep learning classification models on VIS-RGB data, e.g., from public datasets. Material classes frequently investigated by this group are also among the most frequently investigated particle-level material classes (plastics, paper, glass, metal, and cardboard), which correspond to the material classes of *TrashNet* (Yang and Thung, 2016), see Fig. 3d.

In contrast to the pixel and particle level, significantly less material groups are mentioned at the material flow level (Fig. 3e), which is likely caused by the few investigations published so far (see Section 4.2.1).

4.2. Characteristics and investigation levels

Fig. 4 summarizes the investigated characteristics and investigation levels by investigations in our dataset.

4.2.1. Investigation levels

As shown in Fig. 4a, investigations in our dataset have so far focused almost exclusively at the pixel and particle level with 123 (46.1%) and 133 of 267 (49.8%) investigations, respectively. Only $n = 11$ (4.1%) investigations addressed the material flow level, and we identified no investigations at the process level (cf. Section 2.3.1). For all three investigation levels, the number of investigations increases super-linear over time (Fig. 4a). Applying the trend analysis of Section 4.1.1 (2000 – 2015 vs. 2016 – 2021) shows a relative increase of investigations at the particle (+5.9 pp) and material flow (+3.4 pp) level compared to a relative decrease of investigations at the pixel level (-9.3 pp).

We assume two main reasons can explain the large discrepancy between the number of investigations at the pixel and particle vs. the material flow level. First, precise predictions at the pixel and particle level are often needed as a basis for investigations at the material flow level (cf. Section 2.3.1 and Fig. 1); thus, investigations at the pixel and particle level need to be conducted first. Second, pixel- and particle-based analysis finds a broader application than material flow-based analysis: As elaborated in Section 2, industrial applications in the past three decades have primarily focused on SBS (Feil et al., 2021), which requires pixel- and particle-based material classification, while other SBMC applications at material flow level have only emerged in recent years (see Section 4.4).

While the increased share of material flow-based investigations might indicate an increased research interest in SBMC applications beyond SBS, the increased share of particle-based investigations is likely caused by an increased application of deep learning classification algorithms in recent years (see Section 4.4.1), which are often directly applied to images (LeCun et al., 2015), i.e., particles (Kroell et al., 2021b).

4.2.2. Investigated characteristics

Investigations in our dataset almost exclusively focused on iMFCs. eMFCs have in our dataset only been investigated by Feil et al. (2019) and Curtis et al. (2021) in terms of volume flows and we identified no investigations on the determination of mass flows in our dataset.

Regarding iMFCs, investigations have so far mostly focused on material classification (207 of 264 investigations, 78.4%). Despite the practical relevance of PSDs derived in Section 2.1.3, only $n = 3$ investigations studied the determination of particle sizes at the particle (Hoffmann Sampaio et al., 2021; Kandlbauer et al., 2021) and material flow level (Di Maria et al., 2016).

As shown in Fig. 4c, the variety of investigated characteristics has

Table 6
Overview of the 198 publications in scope of the review arranged by applied sensors (columns) and addressed material flows (rows).

	VIS-RGB	VIS-HSI	VNIR-HSI	NIR	MIR	FTIR	thermal	RAMAN	THz	3DLT	multi-sensor
ASR/ELV	(Chen et al., 2021b; Li et al., 2021b; Wang et al., 2019a)	–	(Barnabé et al., 2015; Serranti et al., 2011)	(Barnabé et al., 2015; Serranti et al., 2011; Zhao and Chen, 2015)	–	–	–	–	–	(Koyanaka et al., 2013; Koyanaka and Kobayashi, 2010)	(Barnabé et al., 2015)
CDW	(Anding et al., 2013; Chen et al., 2021a; Davis et al., 2021; Di Maria et al., 2016; Gokyuu et al., 2011; Hoffmann Sampaio et al., 2021; Hoong et al., 2020; Lu et al., 2022a; Zhuang et al., 2019)	–	(Serranti et al., 2011)	(Bonifazi et al., 2018b, 2017, 2015; de Groot et al., 2002, 2001; Ku et al., 2021; Luciani et al., 2015; Serranti et al., 2015b; Serranti et al., 2012a, 2011; Trotta et al., 2021; Vegas et al., 2015; Xiao et al., 2020; Xiao et al., 2019a, Xiao et al., 2019b)	–	–	–	–	–	(Ku et al., 2021; Xiao et al., 2020)	(Ku et al., 2021; Xiao et al., 2020)
LWP	(Kroell, 2021)	–	–	(Chen et al., 2021f; Chen et al., 2021c; Chen et al., 2021e; Chen et al., 2020; Curtis et al., 2021)	–	–	–	–	–	(Feil et al., 2019; Kroell, 2021)	(Kroell, 2021)
MCW	(Kandlbauer et al., 2021)	–	–	(Curtis et al., 2021; Möllnitz et al., 2021)	–	–	–	–	–	(Curtis et al., 2021)	–
MSW	(Bobulski et al., 2021; Kiyokawa et al., 2021; Li and Chen, 2020; Mustaffa et al., 2019; Yu et al., 2020; Zhang et al., 2019)	–	–	(Hryb, 2015; Hu et al., 2013; Möllnitz et al., 2021; Serranti et al., 2015; Serranti et al., 2012b; Zheng et al., 2018)	(Rozenstein et al., 2017)	–	(Gundupalli et al., 2017b)	–	–	(Feil et al., 2019)	–
WEEE	(Hayashi et al., 2019; Lu et al., 2022b)	Picón et al., 2012; Picón et al., 2009)	(Barnabé et al., 2015; Candiani et al., 2017)	(Barnabé et al., 2015; Beigbeder et al., 2013; Bonifazi et al., 2020a; Bonifazi et al., 2020b, 2020c; Candiani et al., 2017; Palmieri et al., 2014; Wu et al., 2020)	(Jacquin et al., 2021; Signoret et al., 2020a; Signoret et al., 2020b; Signoret et al., 2019a, 2019b)	(Protopapa et al., 2021; Taurino et al., 2010)	(Gundupalli et al., 2018)	(Protopapa et al., 2021)	–	–	(Barnabé et al., 2015; Candiani et al., 2017)
Glass	(Krcmarik et al., 2019)	–	(Bonifazi and Serranti, 2006)	(Bonifazi and Serranti, 2006)	(Serranti et al., 2006)	(Farcomeni et al., 2008)	–	(de Groot et al., 2002)	–	–	(Bonifazi and Serranti, 2006)

(*continued on next page*)

Table 6 (*continued*)

	VIS-RGB	VIS-HSI	VNIR-HSI	NIR	MIR	FTIR	thermal	RAMAN	THz	3DLT	multi-sensor
Landfill	–	–	–	(Küppers et al., 2019b)	–	–	–	–	–	–	–
Metals	(Díaz-Romero et al., 2021)	–	–	–	–	–	–	–	–	(Díaz-Romero et al., 2021)	(Díaz-Romero et al., 2021)
Paper	(Rahman et al., 2015; Rahman et al., 2012a; Rahman et al., 2012b; Rahman et al., 2011; Rahman et al., 2010; Rahman et al., 2009; Shan et al., 2014)	(Ramasubramanian et al., 2005)	–	(Borel et al., 2007; Tatzer et al., 2005)	–	–	–	–	–	–	–
Plastics	(Fang et al., 2021; Küppers et al., 2020; Özkan et al., 2015; Peršak et al., 2020; Ramli et al., 2008; Scavino et al., 2009a; Scavino et al., 2009b; Tachwali et al., 2007; Tan et al., 2021; Wang et al., 2019b; Zulkifley et al., 2014)	(Arenas-Vivo et al., 2017; Kuřitka et al., 2020; Rafi Ahmad, 2000; Safavi et al., 2010; Woidasky et al., 2020)	(Brunner et al., 2015; Fomin et al., 2017; Fomin and Kargel, 2019; Gruber et al., 2019; Gruber et al., 2018; Maris et al., 2012; Serranti et al., 2010; Serranti and Bonifazi, 2010)	(Alassali et al., 2018; Barcala et al., 2004; Bonifazi et al., 2021; Bonifazi et al., 2018a; Calvini et al., 2018; Cucuzza et al., 2021; Duan and Li, 2021; Galdón-Navarro et al., 2018; Kulcke et al., 2003; Küppers et al., 2021; Küppers et al., 2019c; Küppers et al., 2019a; Leitner et al., 2003; Li et al., 2019; Michel et al., 2020; Moroni et al., 2015; Moroni and Mei, 2020; Pieszczek, l., Daszykowski, M., , 2019; Serranti and Bonifazi, 2010; Tachwali et al., 2007; Ulrici et al., 2013; van Engelshoven et al., 2019; Vázquez-Guardado et al., 2015; Wahab et al., 2006; Xia et al., 2021a; Yang et al., 2020; Zhu et al., 2019)	(Becker et al., 2017; Kassouf et al., 2014; Signoret et al., 2020a,2019a ; Vázquez-Guardado et al., 2015; Zinchik et al., 2021)	(Bae et al., 2019; da Silva and Wiebeck, 2017; Jiang et al., 2021; Michel et al., 2020; Roh et al., 2018; Serranti and Bonifazi, 2010)	–	(Bae et al., 2019; da Silva and Wiebeck, 2017; Roh et al., 2017; Roh and Oh, 2016; Serranti and Bonifazi, 2010)	(Küter et al., 2018)	–	(Serranti and Bonifazi, 2010; Tachwali et al., 2007)
Textile	(Furferi and Governi, 2008; Zhou et al., 2021)	(Furferi and Governi, 2008)	(Blanch-Perez-del-Notario et al., 2019)	(Cura et al., 2021; Li et al., 2021a; Liu et al., 2020; Mäkelä et al., 2020; Zhou et al., 2019)	–	(Riba et al., 2020)	–	–	–	–	–
Waste	(Altikat et al., 2022; Chen et al., 2021g; Fatovatikhah et al., 2021; Gondal et al., 2021; Guo et al., 2021; Kumar et al., 2021;	–	–	(Serranti et al., 2011)	–	–	–	–	–	–	–

(*continued on next page*)

Table 6 (*continued*)

	VIS-RGB	VIS-HSI	VNIR-HSI	NIR	MIR	FTIR	thermal	RAMAN	**THz**	**3DLT**	**multi-sensor**
	Liang and Gu, 2021; Ma et al., 2020; Masand et al., 2021; Pieper et al., 2018; Salmador et al., 2008; Toğaçar et al., 2020; Vo et al., 2019; Wang et al., 2020; Zhang et al., 2021; Zheng and Gu, 2021)										
Wood	–	–	(Kobori et al., 2008)	(Jin et al., 2020; Kobori et al., 2017; Kobori et al., 2008; Mauruschat et al., 2016; So et al., 2004; Tsuchikawa et al., 2003; Tsuchikawa and Yamato, 2003)	–	–	–	–	–	–	(Kobori et al., 2008)
Dataset	(Adedeji and Wang, 2019; Ahmad et al., 2020; Fu et al., 2021; Huang et al., 2021; Huang et al., 2020; Mao et al., 2021; Masand et al., 2021; Melinte et al., 2020; Patrizi et al., 2021; Qin et al., 2021; Rajak et al., 2020; Shi et al., 2021; Vo et al., 2019; Zhang et al., 2021; Zheng and Gu, 2021)	–	–	–	–	–	–	–	–	–	–
Virgin	(Maier et al., 2019; Rybarczyk et al., 2020)	–	–	–	–	–	–	–	–	–	–
None	(Ata et al., 2005; Maier et al., 2021)	–	–	–	–	–	–	–	–	(Mattone et al., 2000)	–

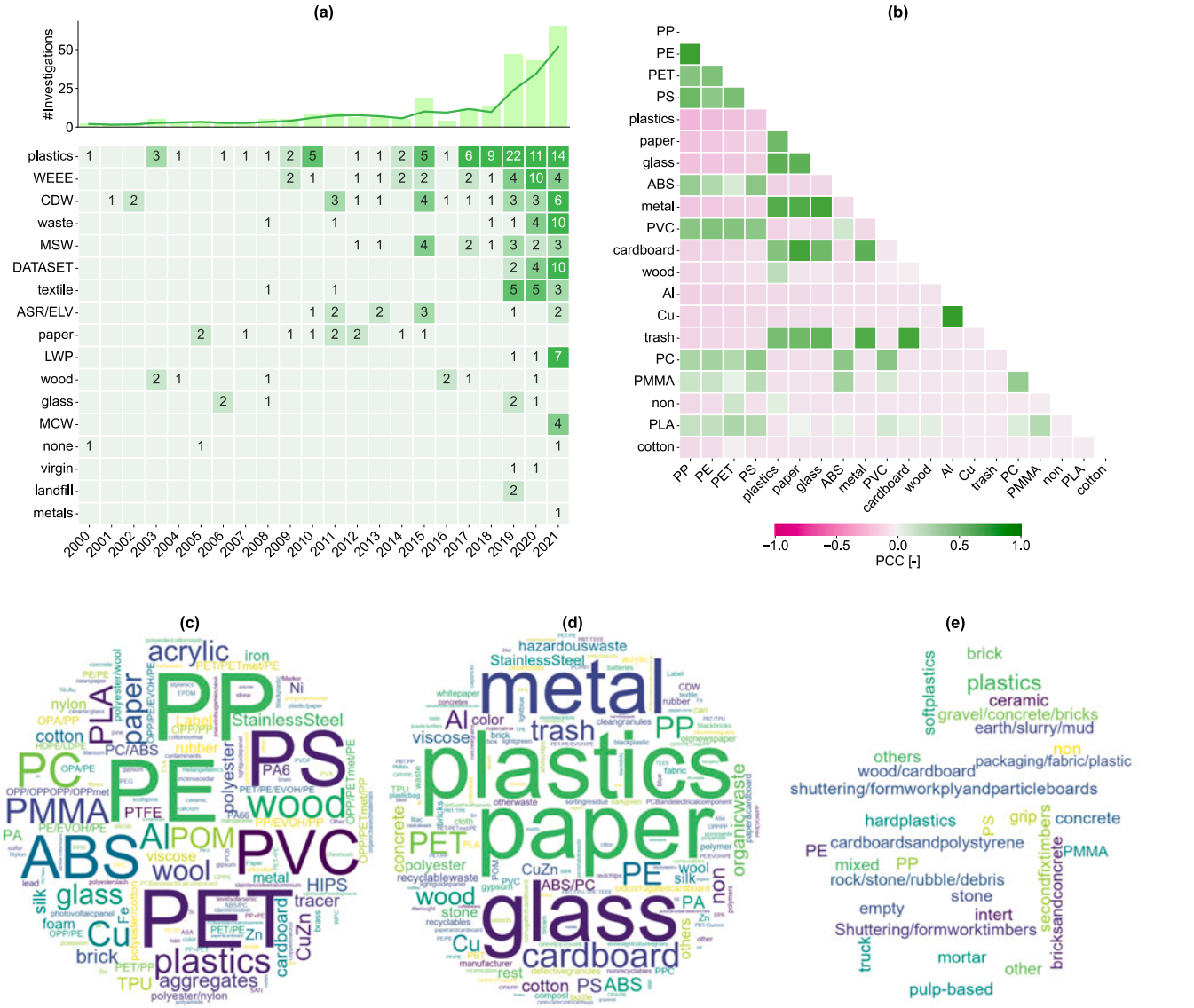

Fig. 3. Material flows and material classes. (a) Material flows and total investigations per year; (b) correlation between the 20 most frequent (top 20) material classes; (c-e) word clouds (Mueller et al., 2018) of investigated material classes (font size proportional to frequency) on the (c) pixel, (d) particle and (e) material flow investigation level. ABS: Acrylonitrile butadiene styrene, HIPS: High Impact PS, PA: Polyamide, PBT: Polybutylene terephthalate, PC: Polycarbonate, PE: Polyethylene, PET: Polyethylenterephthalate, PMMA: Polymethylmethacrylate, POM: Polyoxymethylene, PP: Polypropylene, PPS: Polyphenylene sulfide, PS: Polystyrene, PVC: Polyvinylchloride, PVDF: Polyvinylidenfluoride, SBR: Styrene-butadiene rubber, TEEE: Thermoplastic elastomer-ether-ester, TPE: Thermoplastic elastomers, TPU: Thermoplastic polyurethane, TPU: Thermoplastic polyurethanes; BC: Beverage carton, PPC: Paper, paperboard and cardboard; Al: Aluminium, Au: Gold, Cu: Copper, CuZn: Brass, Fe: Iron, Ni: Nickel.

expanded over time, especially over the last five years. Until 2015, researchers in our dataset have focused on a total of six different characteristics: material identification, i.e., the determination of *material classes* (since 2001), *material compositions* (since 2004), and *material flow compositions* (since 2011); the identification of *tracers* (since 2000) and *colors* (since 2005); and image *segmentation* (since 2000). Starting in 2016, newer publications widened the scope of investigated characteristics subsequently to *PSDs* (Di Maria et al., 2016), *presentation iMFCs* (Pieper et al., 2018), mechanical properties (*melt viscosity* and *tensile strength*) (van Engelshoven et al., 2019), *sub material classes* (van Engelshoven et al., 2019), *volume flows* (Feil et al., 2019), *particle sizes* (Kandlbauer et al., 2021), *particle masses* (Kroell et al., 2021a), and *grasping parameters* (Ku et al., 2021).

When comparing the relative frequency between characteristics for material and color identification (*material class*, *material composition*, *material flow composition*, *color class*) and all other characteristics in 2000 – 2015 vs. 2016 – 2021 (cf. Section 4.1.1), we observe a relative decrease of investigations on material and color classification (-9.1 pp) and a simultaneous increase of investigations on other characteristics (+9.1 pp).

A likely explanation of the large share of material (as well as color and tracer) classification investigations in our dataset is the outstanding importance of material and color classification for SBS, to which much research has been devoted in recent years (Gundupalli et al., 2017a). In contrast, the expansion of the addressed characteristics and the higher relative shares of other characteristics indicates a more widened use of sensor data for advanced SBS and other SBMC applications.

4.2.2.1. Investigated characteristics at different investigation levels. As shown in Fig. 4b, the investigated characteristics differ per investigation level. Publications in our dataset have so far reported four groups of characteristics (see braces in Fig. 4b): (i) purely pixel-based, (ii) pixel- or particle-based, (iii) purely particle-based, and (iv) purely material-flow-

Table 7
Overview on investigated material flows.

Material flow	Abbreviation	#Investigations	%
Plastics	–	87	32.6%
Waste from electrical and electronic equipment	WEEE	30	11.2%
Construction and demolition waste	CDW	27	10.1%
Waste (not further specified)		18	6.7%
Mixed solid waste	MSW	17	6.4%
Dataset	–	16	6.0%
Textile	–	15	5.6%
Automotive shredder residue/end-of-life vehicles	ASR/ELV	11	4.1%
Paper	–	11	4.1%
Lightweight packaging waste	LWP	9	3.4%
Wood	–	8	3.0%
Glass	–	6	2.2%
Mixed commercial waste	MCW	4	1.5%
None (no material flow addressed)	–	3	1.1%
Landfill	–	2	0.7%
Virgin test material	–	2	0.7%
Metals	–	1	0.4%
	Σ	267	100.0%

based characteristics.

4.2.2.2. Investigated characteristics for different material flows. While material classification has been investigated for all identified material flows (except for *virgin* and *none*), many other characteristics have so far been investigated for only few material flows (Fig. 4d). For example, the prediction of particle sizes and PSDs has only been researched for CDW and MCW (Di Maria et al., 2016; Hoffmann Sampaio et al., 2021; Kandlbauer et al., 2021); particle mass prediction has only been studied for LWP waste (Kroell et al., 2021a); mechanical material properties have only been predicted for plastics (van Engelshoven et al., 2019) in our dataset. The highest number of unique characteristics have been investigated for plastics (8 of 16 characteristics, 50.0%).

4.3. Sensors

As shown in Fig. 5, ten different optical sensors were applied in total: NIR, VIS-RGB, VNIR-HSI, MIR, 3DLT, Fourier-transform infrared spectroscopy (FTIR), VIS-HSI, RAMAN, THz, and thermal sensors, with the VIS-NIR range being addressed most frequently (234 of 282 mentioned sensors, 83.0%). Comparing the relative frequency of sensors from 2000 – 2015 and 2016 – 2021 (cf. Section 4.1.1) shows that especially VIS-RGB sensors have been increasingly applied in recent years (+14.6 pp).

Fig. 5a shows that within the theoretical wavelength ranges of each sensor (cf. Table 3), sensors in the investigations were operated at specific wavelength ranges to varying extents: For example, NIR sensors theoretically covering the wavelength range from 780 nm to 2500 nm, have increasingly been applied in between 1000 nm and 1700 nm, which results from the high market share of sensors in a lower wavelength range but at the same time sufficient distinct spectra of commonly applied materials.

Multi-sensors offer the possibility of combining advantages and compensating disadvantages of different sensors; however, only 15 of 267 (5.6%) investigations in our dataset applied multi-sensors. One reason for this may be the increased technical effort required to merge the data from multiple sensors (early or late sensor fusion). The 15 multi-sensor investigations have so far focused on the combination of NIR, VNIR, 3DLT, and VIS-RGB sensors.

4.3.1. Applied sensors for different characteristics

The 16 different characteristics presented in Section 4.2 can be abstracted into three distinct tasks: (i) material identification, (ii)

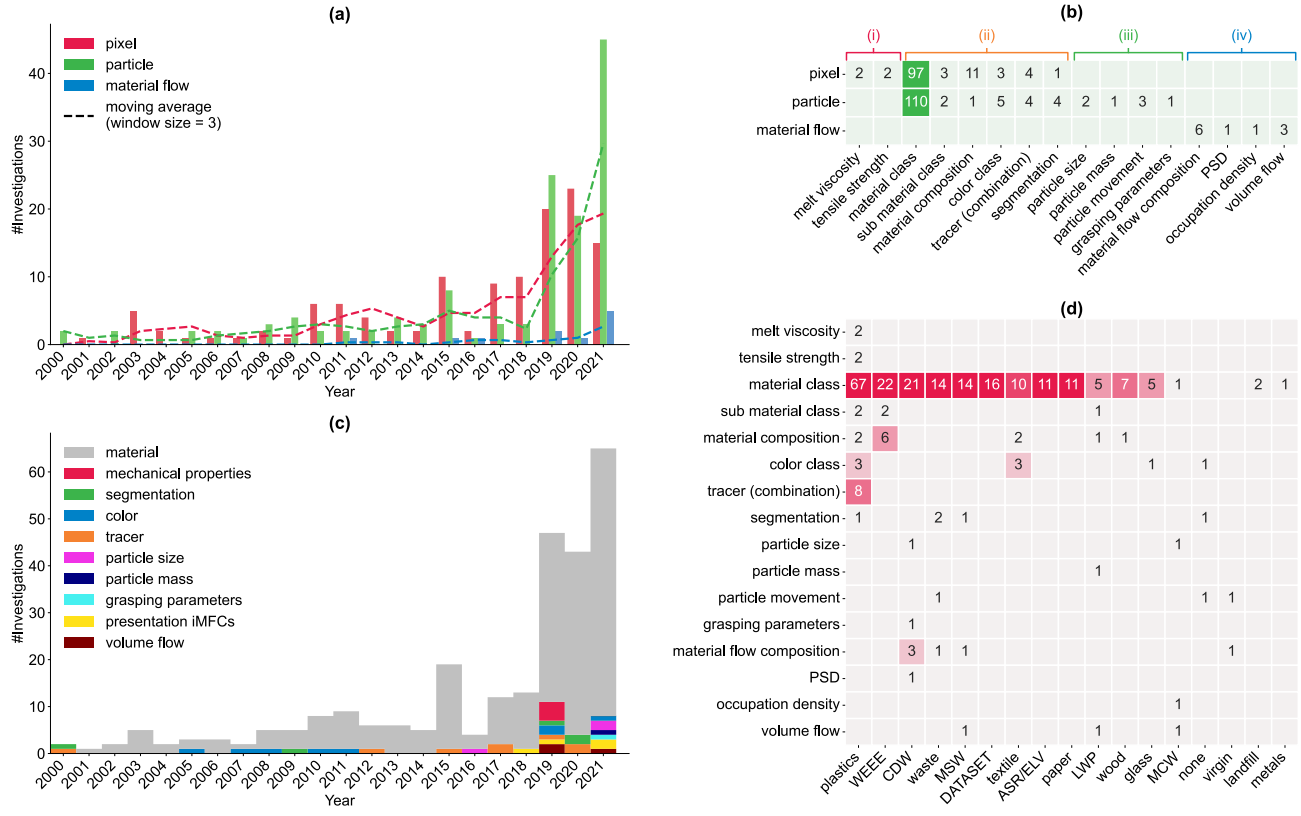

Fig. 4. Characteristics and investigation levels. (a) Investigation levels per year; (b) investigated characteristics per material flow, (i) purely pixel-based, (ii) pixel- or particle-based, (iii) purely particle-based, (iv) purely material-flow-based characteristics; (c) investigated characteristics (aggregated) per year; (d) investigation levels per material flows (see Table 7 for abbreviated material flows).

Fig. 5. Sensors. (a) Addressed wavelength ranges (kernel density estimation), (i) full optical wavelength range (100 nm – 1 mm) in logarithmic scale*, (ii) zoom in on VIS-NIR range; (b-f) investigated sensors per (b) investigation level, (c) year, (d) characteristic, (e) material classes (top 20), and (f) material flow. *two THz-investigations from (Küter et al., 2018) focus on the lower THz range (84 GHz to 96 GHz) and are not shown in [a] for better readability.

segmentation and measurement, and (iii) prediction of material properties.

4.3.1.1. Material identification. Material identification can be performed at the pixel, particle and material flow level. At the **pixel level**, predominantly sensors in the IR range (NIR, MIR, and FTIR) have been applied (Fig. 5b). Especially for common plastics and other IR-active materials, NIR-based material classification has been developed to such an extent that classification accuracies of more than 99% have been achieved in many applications (e.g., Duan and Li, 2021; Jin et al., 2020; Li et al., 2021a; Palmieri et al., 2014; Zheng et al., 2018).

Partly for this reason, research interest has shifted to newer classification applications in the NIR wavelength range in recent years. Examples for such new applications are the discrimination of LDPE and HDPE (Bonifazi et al., 2018a), increasing classification depths (e.g., packaging types) (van Engelshoven et al., 2019), investigations of mixed NIR spectra such as multilayer plastics (Chen et al., 2021f; Chen et al., 2020), classification of new materials such as bioplastics (e.g., Chen et al., 2021e; Moroni and Mei, 2020), and investigation and prediction of aging or degradation processes based on NIR spectra (e.g., Chen et al., 2021c; Chen et al., 2021e).

In addition to NIR, fundamental vibrations in the MIR range open new sensor-based characterization opportunities. Besides an early study by Serranti et al. (2006) focusing an the detection of ceramic glass contaminants with MIR, investigations on MIR have been increasingly conducted since 2014 (Fig. 5c). In contrast to NIR, most MIR

investigations (10 of 13, 76.9%) are limited to a pure description of the spectra data and classifications based on MIR has so far only been reported by Kassouf et al. (2014), Jacquin et al. (2021), and Zinchik et al. (2021) with classification accuracies between 92% and 100%. The low share of classification investigations based on MIR might be attributed to the lower technological maturity of MIR compared to NIR. Furthermore, MIR investigations to date have focused almost exclusively on plastic identification with the exception of the aforementioned investigation by Serranti et al. (2006) (detection of ceramic glass contaminants) and an investigation by Rozenstein et al. (2017) (PET, PE, PVC, PP, PLA, PS, cardboard, paper, and wood). Moreover, the focus of MIR investigations is often on technical polymers or carbon black plastics (cf. Table 6), for which the classification based on NIR can be difficult or even technical impossible. In addition, advanced material characterization (e.g., investigation of aging effects) represents an application field of MIR (Signoret et al., 2020b).

In contrast to the pixel level, VIS-RGB and 3DLT sensors are particularly used at the **particle level** (cf. Fig. 5b). Two main reasons for the increased application of VIS-RGB sensors at the particle level are (i) the low investment cost compared to other sensors and (ii) the possibility of transferring RGB-based deep learning algorithms (especially CNNs) from other research fields (e.g., autonomous driving) to the waste management sector. 3DLT sensors, in contrast, can measure the 3D shape of particles, which can be used as a feature for the prediction algorithm (e.g., Koyanaka et al., 2013; Koyanaka and Kobayashi, 2010; Mattone et al., 2000). Another way to identify materials at the particle level is to aggregate pixel-based classification results for example by majority voting (argmax) or the use of number of pixel-based classifications as a particle-based classification feature (e.g., Bonifazi et al., 2021; Chen et al., 2021f). This occurs mainly for sensors in IR range and VIS sensors; for example, Chen et al. (2021f) has defined a threshold (70%) of correct pixel-based classification share as a correct particle prediction.

Like the particle level, classification results from different sensors of the pixel and particle level can be aggregated at the **material flow level** (e.g., Curtis et al., 2021; Serranti et al., 2015). Alternatively, direct predictions can be made at the material flow level, which have been investigated so far with CNNs based on VIS-RGB data by Lu et al. (2022a) and Davis et al. (2021).

4.3.1.2. Segmentation and measurement. A second task involves the 2D or 3D measurement of particles and material flows. The starting point for all 2D measurements are *binary images* that divide the sensor data into foreground and background at the **pixel level**. Depending on the sensor used, the segmentation can be based on different features, e.g., color or brightness from VIS-RGB data (e.g., Maier et al., 2021), intensity or dynamics of NIR spectra (e.g., Curtis et al., 2021), or height information from 3DLT sensors (e.g., Kroell et al., 2021a). Starting point for all three-dimensional measurements are 3D heightmaps, for example from 3DLT data.

At the **particle level**, binary images (2D) or heightmaps (3D) can be used to localize or measure individual particles. The localization of particles is of high relevance for SBS processes, in order to sort individual particles using coordinate-precise air pressure bursts (e.g., Maier et al., 2021; Pieper et al., 2018) or with mechanical grippers (e.g., Ku et al., 2021; Xiao et al., 2020). In addition, 2D and 3D particle dimensions form the basis for predicting other particle properties such as particle size (Kandlbauer et al., 2021) and particle mass (Kroell et al., 2021a) or can be an (additional) input for material classification (see Section 4.3.1.1).

Table 8
Overview of investigated ML algorithms.

Abbr.	Algorithm	#Investigated	#In best	Reference
PCA	Principal component analysis	73	24	(Karhunen, 1998)
CNN	Convolutional neural network	47	42	(Lecun et al., 1998)
PLS	Partial least squares	46	37	(Wold et al., 1989)
kNN	k nearest neighbors	36	20	(Altman, 1992)
SVM	Support vector machine	32	17	(Cristianini and Shawe-Taylor, 2013)
LDA	Linear discriminant analysis	28	13	(Tharwat et al., 2017)
ANN	Artificial neural network	25	13	(Wang, 2003)
DT	Decision tree	12	2	(Grajski et al., 1986)
QDA	Quadratic discriminant analysis	10	3	(Hastie et al., 2009b)
RF	Random forest	9	5	(Breiman, 2001)
Fuzzy	Fuzzy based algorithm	7	5	(Perfilieva, 2006)
SAM	Spectral angle mapper	5	2	(Kruse et al., 1993)
SIMCA	Soft independent modelling by class analogy	5	2	(Wold and Sjöström, 1977)
GMM	Gaussian mixture models	4	0	(Figueiredo and Jain, 2002)
CVA	Canonical variate analysis	3	0	(Tofallis, 1999)
SCC	Spectral cross-correlation	2	2	(Koenig, 1999)
GA	Genetic algorithm	2	1	(Holland, 1992)
BN	Bayesian network	2	0	(Holmes and Jain, 2008)
CBR	Case based reasoning	1	1	(Chen et al., 2008)
CRF	Conditional random field	1	1	(Lafferty et al., 2001)
CT	Complementary troubleshooting	1	1	(Xiao et al., 2019a)
DBC	Dissimilarity-based classifier	1	1	(Pekalska and Duin, 2000)
ICA	Independent component analysis	1	1	(Hyvärinen and Oja, 2000)
MAP	Maximum a posteriori estimation	1	1	(Gauvain and Lee, 1994)
ViT	Vision transformer	1	1	(Dosovitskiy et al., 2020)
DNA computing	–	1	0	(Adleman, 1998)
GPC	Gaussian process classifier	1	0	(Rasmussen and Williams, 2008)
LEMAP	Laplacian Eigenmaps	1	0	(Belkin and Niyogi, 2002)
Linear	Linear regression	1	0	(Fahrmeir et al., 2013)
MLR	Multinomial logistic regression	1	0	(Hosmer and Lemeshow, 2000)
NC	Nearest centroid	1	0	(Hastie et al., 2009a)
RDA	Resemblance discriminate analysis	1	0	(Koch, 2014)
SOM	Self-organized map	1	0	(Kohonen, 1998)
SVD	Singular value decomposition	1	0	(Boardman, 1989)
	Σ	368	199	

At the **material flow level**, 2D binary images can be used to quantify material flows in terms of area flows or occupation densities (e.g., Curtis et al., 2021; Küppers et al., 2021; Küppers et al., 2020); whereas 3D(LT) measurements allow the determination of volume flows (Curtis et al., 2021; Feil et al., 2019).

4.3.1.3. Prediction of material properties. Since material properties such as mechanical properties or material colors are usually not influenced by particle shapes or sizes, these can be measured directly at the **pixel level**. In our dataset, mechanical properties such as melt viscosity and tensile strength have so far only been predicted based on NIR data for plastics by van Engelshoven et al. (2019).

Information on color classes is (obviously) extracted in the VIS wavelength range (Fig. 5d). The $n = 8$ investigations on color classification in our dataset, predominantly applied VIS-RGB sensors (6 of 8 investigations, 75.0%), but also VIS-HSI have been applied (2 of 8 investigations, 25.0%). Among the $n = 8$ color classification investigations, $n = 5$ investigations (62.5%) conducted classifications at the **particle level** to reduce the influence of, e.g., labels, colored bottle caps, or contaminates (Ata et al., 2005; Krcmarik et al., 2019; Tachwali et al., 2007; Wang et al., 2019b; Zhou et al., 2021).

4.3.2. Applied sensors for different material flows and classes

Fig. 5e shows the application of optical sensors for different material classes. As introduced in Section 4.1.2, two groups can be identified: Sensors in the IR range (especially NIR) are often applied to plastics (e.g., PP, PET, PE, PS), while VIS-RGB sensors find increased applications for the broader material classes (glass, paper, metal, cardboard, trash) of *TrashNet* (Yang and Thung, 2016).

Regarding material flows (Fig. 5f), two effects play a role: First, for material identification (Section 4.3.1.1), the application of different sensors follows their suitability for identifying different material classes, e.g., NIR sensors are often applied for material flows that contain higher amounts of polymers (e.g., plastics, LWP, and WEEE), while VIS-RGB sensors are often applied for broader material identification (e.g., *TrashNet*) or classification of different paper grades (e.g., "old corrugated cardboard", "old newsprint", or "white paper"), mainly by optical characteristics (Rahman et al., 2014). Second, for characteristics based on segmentation and measurements (Section 4.3.1.2) the characterization is independent from the contained material classes. For these characteristics, VIS-RGB or 3DLT are often used due to their low investment cost or their ability to perform 3D measurements, respectively. Fig. 5f shows a superposition of both effects: While NIR sensors are mainly used for plastic-rich material flows, other sensors (e.g. VIS-RGB and 3DLT) find a wide range of material flow applications. The selection of sensors is therefore not necessarily based at the material flow itself, but rather on the characteristics and material classes of interest, as well as the suitability of the respective sensors for their combination.

4.4. ML algorithms

In our dataset, 204 of 267 (76.4%) investigations studied ML algorithms to extract characteristics from the acquired sensor data. For 188 of 204 (92.2%) investigations, details on the studied ML algorithm(s) were given, which are the focus of this section (hereinafter referred to as *ML investigations*).

Table 8 summarizes the 34 unique ML algorithms investigated by ML investigations in our dataset, introduces their abbreviations, and gives reference to further details for each ML algorithm. In addition, four investigations developed *custom* ML algorithms, i.e., ML algorithms that were developed for the investigation itself (Di Maria et al., 2016; Koyanaka and Kobayashi, 2010; Li et al., 2019; Zhang et al., 2019). Among all investigated ML algorithms, PCA ($n = 73$ investigations), CNN ($n = 47$), PLS ($n = 46$), kNN ($n = 36$), and SVM ($n = 32$) were studied most often.

Furthermore, 45 of 319 (14.1%) studied algorithms were ensembles of multiple algorithms (e.g., PCA + PLS). Most ensembles composed two algorithms (42 of 45 ensembles, 93.3%) and combined PCA as a preprocessing step with other ML algorithms (37 of 45, 82.2%).

Fig. 6 gives an overview of ML algorithms investigated more than once. As shown in Fig. 6a, the frequency at which different ML algorithms were applied has changed over the years. While some algorithms (e.g., ANN and LDA) have been studied since the early 2000s, other algorithms (e.g., SVM and RF) have been investigated since 2013. Especially for CNNs, which were studied since 2018 by investigations in our datasets, a steep increase in the number of investigations (2.5-fold increase or more per year) can be observed.

4.4.1. Investigated ML algorithms for different prediction tasks

Each prediction task can be broken down into (i) a sensor that defines the input to the ML algorithm, as well as (ii) an investigation level and (iii) a characteristic that define the model output.

4.4.1.1. Investigated ML algorithms for different sensors. As shown in Fig. 6c, most ML algorithms have been applied to data from various sensors. However, while CNN (37 of 43 CNN investigations, 86.0%), kNN (15 of 34, 44.1%), and SVM (14 of 28, 50.0%) algorithms were most frequently applied to data from VIS-RGB sensors, PCA (38 of 53, 71.7%) and PLS (40 of 45, 88.9%) algorithms were most frequently applied to NIR data, which might be traced back to their dimensionality reduction capability for highly correlated spectral data.

4.4.1.2. Investigated ML algorithms for different investigation levels. From 34 unique ML algorithms, 23 and 25 algorithms have been investigated on the pixel and particle level, respectively (see Fig. 6b). Since PCA and PLS are capable of dimensionality reduction, they have been often applied on the pixel level (48 of 58 [82.8%] and 39 of 45 investigations [86.7%], respectively), e.g., to process high-dimensional data from hyperspectral sensors such as NIR sensors. In contrast, CNNs have found increased application on the particle level (39 of 46, 84.8%) due to their suitability for image classification. On the material flow level, researchers have so far applied CNNs (Davis et al., 2021; Lu et al., 2022a), ensembles of CNNs and SVMs (Chen et al., 2021a), and custom algorithms (Di Maria et al., 2016).

4.4.1.3. Investigated ML algorithms for different characteristics. Although most ML algorithms are suitable for a wide range of predictions (Marsland, 2014), Fig. 6d shows that most algorithms have so far been applied to material classification, which can be attributed to the high number of material classification investigations (cf. Section 4.2). Besides material identification, ML algorithms have only been investigated in occasional case studies for other characteristics. In fact, of $n = 288$ possible algorithm-characteristic combinations, only $n = 46$ (16.0%) have been investigated.

4.4.2. ML prediction scores

In total, 167 of 188 (88.8%) ML investigations in our dataset reported the achieved test score of the best-performing ML algorithm. As depicted in Fig. 6f, the reported test scores range from 49.1% to 100.0%. 133 of 167 (79.6%) ML investigations report test scores of 90% or higher. On average, higher best test scores are reported on the pixel level (mean: 95.4%) compared to the particle level (mean: 91.3%). Only three investigations reported test scores on the material flow level (68.4% – 94.0%), which do not allow further statements due to the small sample size.

When analyzing the development of test scores over time (Fig. 6e), for both the pixel ($p = 0.048$) and particle level ($p = 0.015$), a slight increase of the reported test scores can be observed. At the pixel level, reported test scores increased about 0.21% per year; at the particle level, test scores increased steeper with about 0.41% per year.

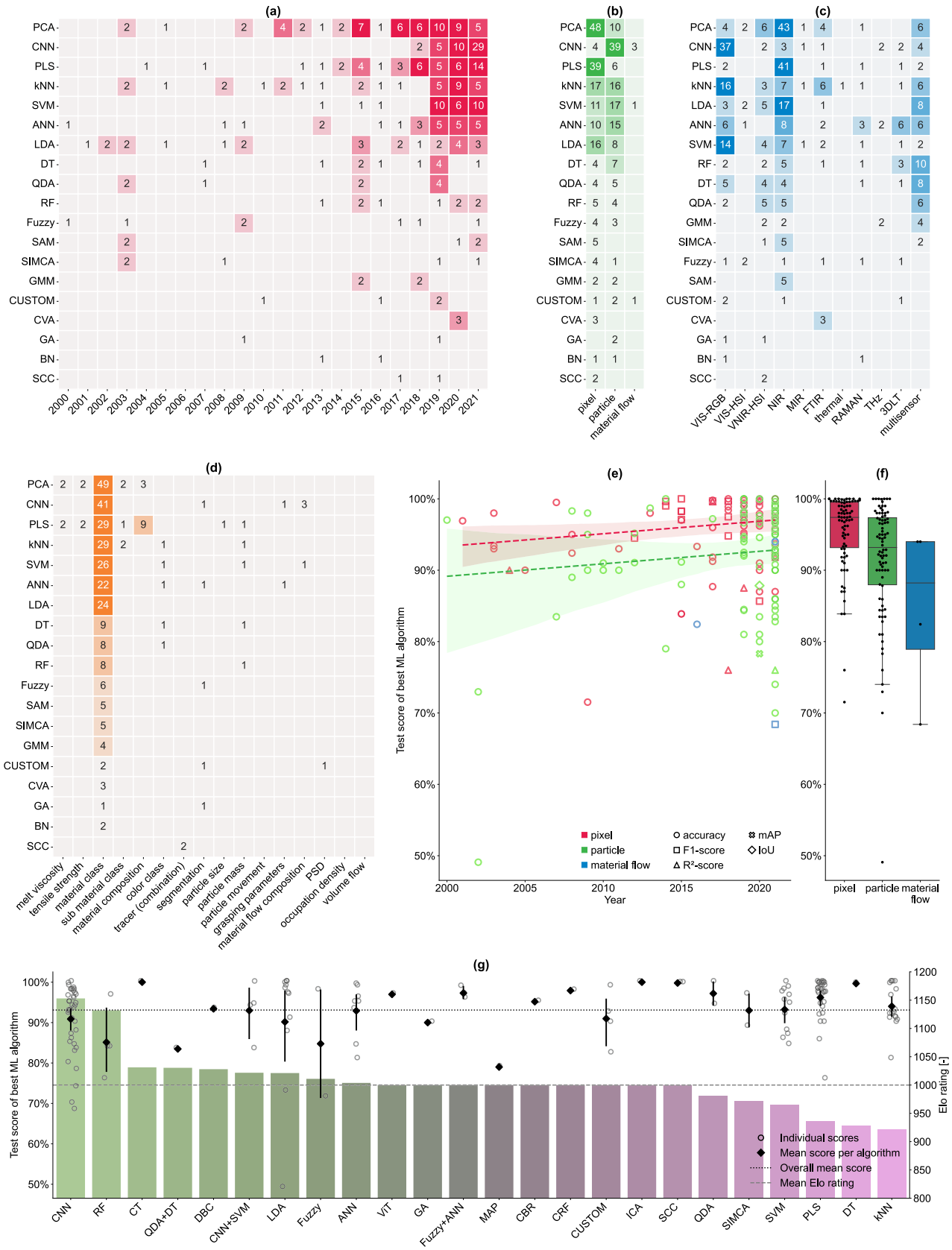

Fig. 6. Investigated ML algorithms* (a) per year, (b) per investigation level, (c) per sensor, and (d) per characteristic; (e) test scores of best-performing ML algorithms per year and investigation level; (f) test scores per investigation level; (g) Elo rating and test scores of best-performing ML algorithm combinations per investigation. *for better readability, only ML algorithms investigated more than once are depicted (see Table 8 for frequency and abbreviations).

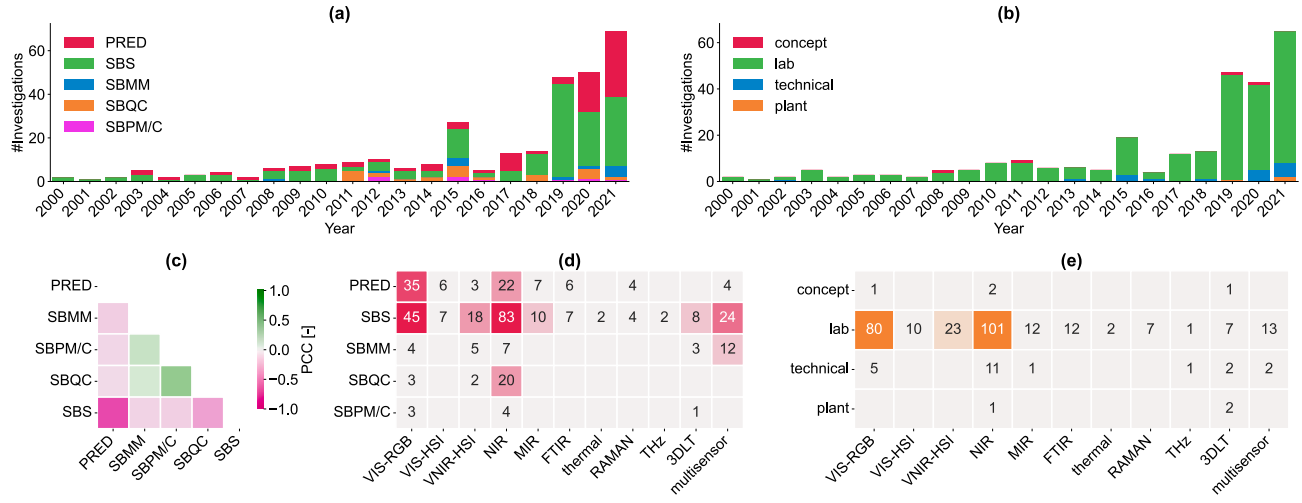

Fig. 7. Applications and investigation scales. (a) Applications per year; (b) investigation scales per year; (c) correlation (simultaneous occurrence) between different applications; (d) applications for different sensors; (e) investigation scales per sensor. PCC: Pearson correlation coefficient.

However, these results must be interpreted with great caution as several biases could distort the reported test scores. For example, (i) researchers are incentivized to publish only sufficient test scores (publication bias); (ii) most predictions are based on different datasets and are therefore only comparable to a very limited extent (if at all); (iii) different types of test scores (e.g., accuracy and R^2-score) cannot be directly compared; and (iv) different investigations may use different implementations and hyperparameter settings.

From 34 investigated ML algorithms, 22 algorithms of the were reported once or more as the best-performing ML algorithm or as part of a best-performing ML ensemble (cf. Table 8). Among the best-performing ML algorithms, CNN ($n = 42$), PLS ($n = 37$), PCA ($n = 24$), kNN ($n = 20$), and SVM ($n = 17$) algorithms were most often reported.

However, the frequency at which ML algorithms are reported as the best performing ML algorithms is not sufficient to draw conclusions about the suitability of different ML algorithms for SBMC. First, ML algorithms studied more often have a higher probability of being the best-performing ML algorithm (cf. Table 8). Second, ML algorithms, which are less often compared to other ML algorithms, have a higher probability of being reported as the best-performing ML algorithm.

To overcome these limitations, we propose an alternative method to assess the suitability of different ML algorithms for SBMC: The Elo rating system (Elo, 2008), which is a method to calculate relative skill levels of different players that is used in zero-sum games such as chess and football.

In our Elo implementation, we model each investigation as pairwise *matches* between the tested ML algorithms and the best-performing ML algorithm within each investigation. All algorithms start with an initial Elo rating of 1,000. After each match, the winning algorithm takes points from the losing algorithm, and both Elo ratings are updated. The transferred points after each match are based on the difference between both Elo ratings, which makes the rating system self-correcting. If a higher-rated algorithm wins a match against a lower-rated algorithm, fewer points will be transferred compared to a match in which a lower-rated algorithm wins against a higher-rated algorithm since a win in the first case is more likely than in the second case (Elo, 2008). Therefore, ML algorithms of higher suitability will achieve higher Elo ratings than algorithms of lower suitability.

Fig. 6g summarizes the Elo ratings and the achieved test scores of the 25 different ML algorithms (ensembles) that were reported as best-performing ML algorithms (ensembles) by the investigations in our dataset (excluding PCA[2]). As a result, we observe high Elo ratings for CNN (Elo-score: 1153.1, 14 [matches won]: 1 [match lost]) and RF (1132.0, 17:4). In contrast, low Elo ratings are observed for PLS (935.8, 0:5), DT (928.0, 3:9), and kNN (922.4, 7:14).

In conclusion, the calculated Elo ratings indicate a high suitability of CNN and RF algorithms for SBMC and confirm the observed outperformance of CNN in comparison to other traditional ML algorithms observed in other research fields. However, these results must be interpreted with great caution, as outlined above and in Section 4.7.

4.5. Applications and investigation scales

Fig. 7 summarizes the envisioned applications by investigations in our dataset and the scales at which the investigations were conducted.

4.5.1. Envisioned applications

In total, we identified six different applications envisioned by the publications in our dataset. Table 9 defines the envisioned applications and introduces their abbreviations.

As shown in Fig. 7a, SBS applications have been mentioned since the beginning of the period under review (2000 – 2021) and by the majority of investigations (cf. Table 9). Starting in 2003, the first investigations on PRED applications were published followed by SBMM (2008), SBQC (2011), and SBPM/C applications (2012). When comparing the relative share of applications mentioned between 2011 – 2021 (last ten years) and 2000 – 2011 (cf. Section 4.1.1), we observe that SBMC research has been expanding from SBS applications (-18.6 pp) towards SBQC (+9.7 pp), PRED (+3.6 pp), SBPM/C (+3.1 pp), and SBMM (+2.3 pp) in recent years.

Fig. 7c indicates that the identified applications can be clustered into three groups: (i) SBS; (ii) PRED; and (iii) SBMM, SBQC, and SBPM/C.

[2] Note that we chose to exclude the PCA algorithm from our Elo evaluation because PCA is commonly used for explanatory data analysis or preprocessing (high frequency among investigated ML algorithms), but has less application in final model prediction (low frequency among the best-performing ML algorithms), which would systematically bias the Elo evaluation towards other algorithms.

Table 9
Overview and definition of envisioned applications by the publications in our dataset; *SBPC or SBMM*.

Abbr.	Name	Description	Target level	Example	#Mentions	Mention share
PRED	Prediction	Prediction of material or material flow characteristics from sensor measurements.	Pixel, particle, material flow	Classification of polymers based on NIR spectra.	81	30.3%
SBS	Sensor-based sorting	Particle-wise sorting of material flows based on predicted characteristics from sensor measurements through actuators.	Particle	Sorting PET bottles out of LWP waste.	174	65.2%
SBMM	Sensor-based material flow monitoring	Sensor-based measurement of MFCs through SBMC over a period of time and evaluation of measured MFCs or comparison with a target or reference value.	Material flow	Sensor-based monitoring of the input material composition in a sorting plant.	13	4.9%
SBQC	Sensor-based quality control	Comparison of MFCs acquired through SBMC with predefined quality criteria.	Material flow	Sensor-based monitoring of the purity of preconcentrates in a sorting plant.	25	9.4%
SBPM	Sensor-based process monitoring	Monitoring of characteristics or indicators acquired through SBMC at the process level.	Process	Sensor-based monitoring the screening efficiency of a drum screen.	8*	3.0%*
SBPC	Sensor-based process control	Adjustment of actuators based on characteristics or indicators through SBMC at the process level.	Process	Setting the shaft speed of a pre-shredder based on the measured output volume flow.	8*	3.0%*

* During data extraction, we observed that it is difficult to identify if authors intended an SBPM or SBPC application (since both applications require similar technological prerequisites), which we thus unified to SBPM or SBPC (abbreviated as SBPM/C) in the following.

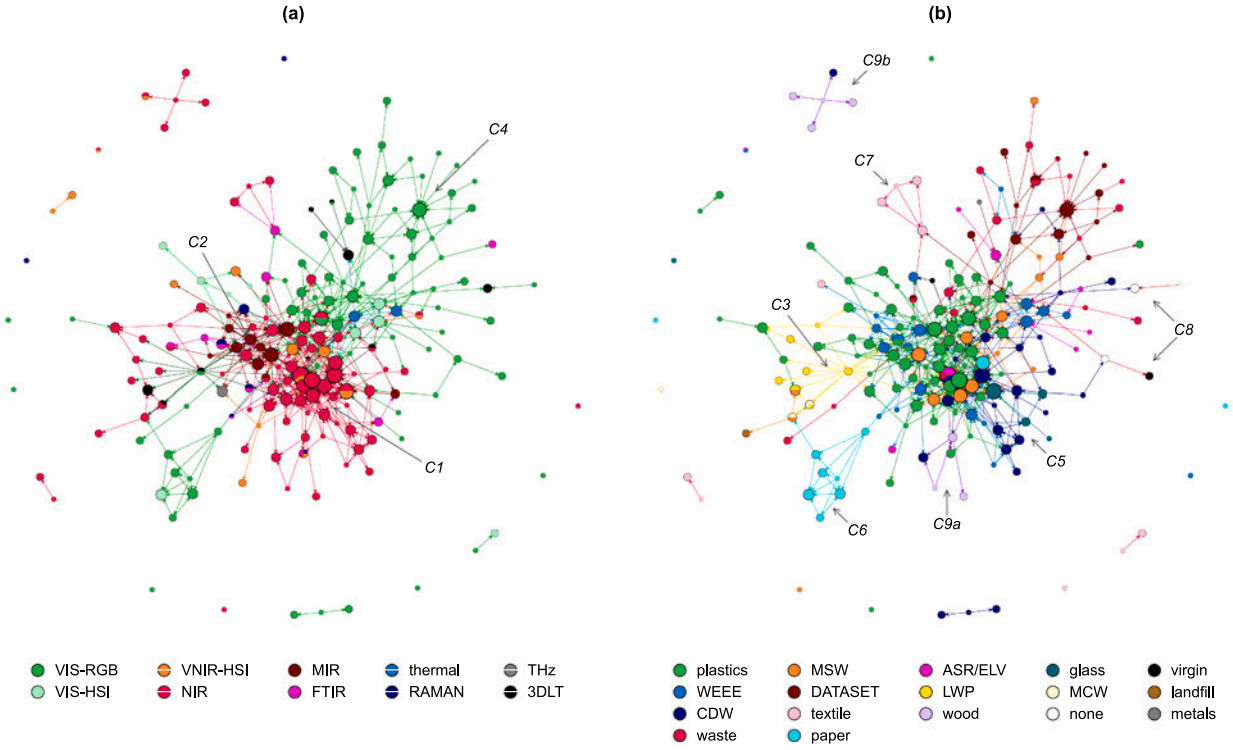

Fig. 8. Citation network between the 198 publications in our dataset colored by (a) applied sensors and (b) addressed material flows. Vertices: publications, edges: citations, pie: relative frequency of respective among a publication, vertex size: #citations among the 198 publications in our dataset.

While applications that require data analysis on the material flow level (SBMM, SBQC, or SBPM/C) are positively correlated with each other, SBS and PRED applications tend to be envisioned independently, which might be traced back to different researchers targeting for different applications.

As shown in Fig. 7d, the envisioned applications differ significantly in terms of investigated sensors. While NIR-sensors find more frequent applications in SBS ($n = 83$ mentions on NIR vs. $n = 45$ mentions on VIS-RGB [1.84:1]), VIS-RGB sensors are more frequently investigated for PRED applications ($n = 22$ mentions on NIR vs. $n = 35$ mentions on VIS-

RGB [0.63:1]).

4.5.2. Investigation scales

As shown in Fig. 7b, most investigations in our dataset were conducted on laboratory scale (242 of 267 investigations, 90.6%), followed by investigations on technical (n = 18, 6.7%) and plant scale (n = 3, 1.1%). In addition, n = 4 investigations (1.5%) were classified as novel concepts (Feil et al., 2019; Salmador et al., 2008; Serranti et al., 2011; Wu et al., 2020).

Besides an early investigation by de Groot et al. (2002), investigations on a technical scale in our dataset have been reported frequently since 2013 (Beigbeder et al., 2013). Comparing the relative shares of different investigation scales between 2000 – 2015 and 2016 – 2021 (cf. Section 4.1.1) shows an increasing trend towards higher TRL levels in recent years: While the relative frequency of concepts (-2.1 pp) and investigations on lab-scale (-4.1 pp) decreased, more investigations were published on a technical (+4.7 pp) and plant scale (+1.4 pp).

As shown in Fig. 7e, all ten optical sensors in our dataset have been studied extensively on the laboratory scale. On a technical scale, however, the investigated sensors in our dataset reduces to NIR (n = 11), VIS-RGB (n = 5 investigations), 3DLT (n = 2), MIR (n = 1), THz (n = 1), and multi-sensors (n = 2). Moreover, investigated sensors at the plant level are currently limited to NIR (Curtis et al., 2021) and 3DLT (Curtis et al., 2021; Feil et al., 2019).

In summary, we observe that most reviewed investigations have taken place at the laboratory scale, which can be explained mainly by the type of reviewed literature (peer-reviewed journal articles). However, researchers have made significant efforts towards upscaling to plant scale. While SBS with many sensors is already state-of-the-art (Chen et al., 2021d; Gundupalli et al., 2017a; Sarc et al., 2019), SBMC methods rapidly evolve towards plant scale maturity. So far, NIR and 3DLT have been proven to be suitable for SBMM at plant scale (Curtis and Sarc, 2021; Feil et al., 2019).

4.6. Collaboration and networks

To determine how interconnected research on SBMC is (RQ 6), we evaluate two types of connections in the following subsections: Citation networks (Section 4.6.1) and co-authorship networks (Section 4.6.2). Both connections will be visualized as graphs. In the citation network, the modeled graph consists of publications (vertices) and citations (edges) between them. In the co-authorship network, the modeled graph consists of authors (vertices) and co-authorships (edges) between them.

For visualizing both graphs, we will determine the vertex positions through the force-based graph drawing algorithm of Hu (2005), implemented in *graph-tool* (Peixoto, 2014). In force-based graph drawing, the edges are modeled as mechanical springs that pull connected vertices together, while repulsive electrical forces of the vertices push vertices away from each other. Vertex positions are initialized randomly and then iteratively updated to minimize the system's energy until an equilibrium is reached. In this way, more connected vertices are closer together in the final graph than other vertices, enabling us to identify relationships between different publications and authors visually.

4.6.1. Citation networks

Fig. 8 shows the resulting citation network of the 198 publications in our dataset. To interpret the resulting graph, all vertices (publications) are visualized as pie charts with the different sensors (Fig. 8a) and material flows (Fig. 8b) of the underlying investigations defining their color and share (e.g., a publication containing one NIR and one VIS-RGB investigation would result in a 50% NIR and 50% VIS-RGB pie).

In total, we identified n = 497 citations among the 198 publications in our dataset. On average, publications in our dataset cited/got cited from n = 2.5 other publications from our dataset. The three most cited vertices within our dataset are Serranti et al. (2011) [n = 23], Ulrici et al. (2013) [n = 18], and Serranti et al. (2012a) [n = 17].

The majority of publications (174 of 198, 87.9%) belong to a large subgraph (shown in the center of Fig. 8a and b), which contains 98.2%

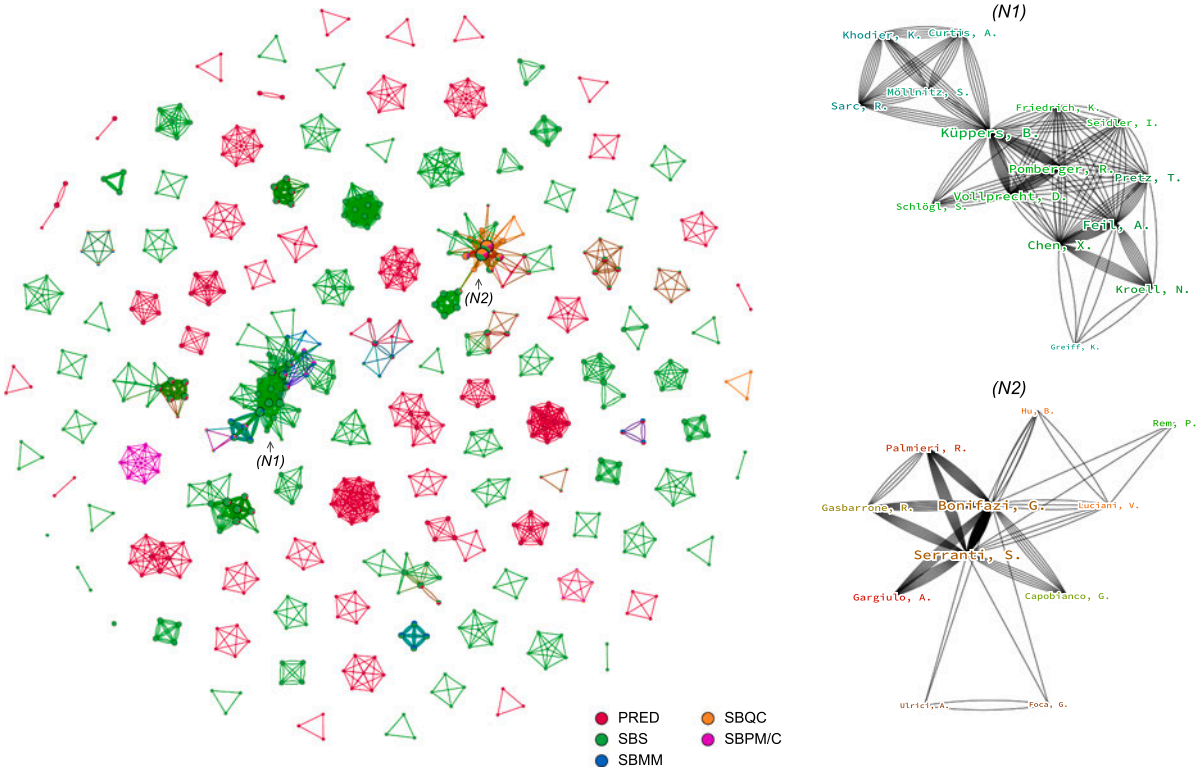

Fig. 9. Co-Authorship Network of the 611 authors from 198 publications in our dataset. (N1) largest and (N2) second-largest co-authorship subnet (for clarity, only authors with two or more total publications are shown in N1 and N2).

($n = 488$) of all citations. When we calculate the shortest paths between all publications within this subgraph (considering both citations and references), we observe that it takes, on average, 2.7 intermediate publications to reach any target publication from any source publication (min: 0, median: 3, maximum: 7), which indicates a strong interconnection of this subgraph. In contrast, we identify 15 subgraphs isolated from the main subgraph containing between $n = 1$ and $n = 5$ publications each (shown at the borders of Fig. 8).

When analyzing both colored citation graphs, we observe that publications with similar sensors (Fig. 8a) or material flows (Fig. 8b) often cite each other and are thus located closer to each other. Five broader clusters can be identified that are closely connected to the main citation network: publications that focus on the material flows plastics and MSW and apply NIR sensors (*C1*), publications on plastics and WEEE with MIR sensors (*C2*), NIR publications on LWP (*C3*), VIS-RGB publications on public available datasets or waste classification in general (*C4*), and mostly NIR publications on CDW and glass (*C5*). In contrast, publications on paper based on VIS sensors (*C6*), NIR and FTIR publications on textile (*C7*), material-independent publications (*C8*), and investigations on wood (*C9a*, *C9b*) are less connected to the main citation subgraph.

In accordance with the findings of Section 4.3, we see that the (main) citation network is largely dominated by two research communities focusing (a) on the application of NIR (and MIR) sensors for a more nuanced identification of (mostly) plastics (*C1*, *C2*) and (b) the application of CNNs for more general waste classification especially on public datasets.

4.6.2. Co-authorship networks

Fig. 9 shows the co-authorship graph, in which vertices are colored based on the envisioned applications. In total, the co-authorship graph contains $n = 611$ different authors (vertices) and $n = 2{,}472$ co-authorships (edges). In contrast, to the citation network, the co-authorships network is significantly less connected with $n = 111$ co-authorship networks in total, ranging from $n = 1$ to $n = 33$ authors per group (mean: $n = 5.5$).

As shown in Fig. 9, the largest co-authorship network (*N1*) in our dataset contains a total of $n = 33$ authors (for clarity, only authors with two or more total publications are shown in the detailed views of Fig. 9), which can be traced back to researchers from the RWTH Aachen University (Germany) and Montanuniversitaet Leoben (Austria). Fig. 9.N2 shows the second-largest co-authorship network (*N2*) with $n = 28$ authors, which can be traced back to researchers from the Sapienza University of Rome (Italy).

In summary, two main conclusions can be drawn from Section 4.6. First, individual co-authorship networks are often focused on a limited number of applications. Second, despite extensive citation within our dataset (Fig. 8), research collaboration often ends at the boundaries of single or a few universities or research groups (Fig. 9). Therefore, research across university and research group boundaries has likely the potential to provide new impulses for SBMC research. Readers may find related researchers by the overview given in Table 6.

4.7. Limitations

Despite all efforts devoted, this study has three major limitations. First, as the review has focused on peer-reviewed journal articles in the English language, non-peer-reviewed publications such as conference proceedings and non-english literature have not been included, which may add systematic errors to the obtained findings. For example, most recent findings from conference publications as well as industrial research results are not represented in the review, which may result in an underestimation of the state-of-research or reached TRL levels. Here, a systematic literature review on non-peer-reviewed and/or non-English language literature could complement the present study.

Second, the focus of this review was on dry-mechanical recycling of non-hazardous waste streams. However, it is likely that sensor-based characterization methods already exist for virgin materials or hazardous wastes that could be transferred to the waste management sector. Here, an additional review focusing on transfer from other industries (with more advanced levels of digitalization) could be of great value.

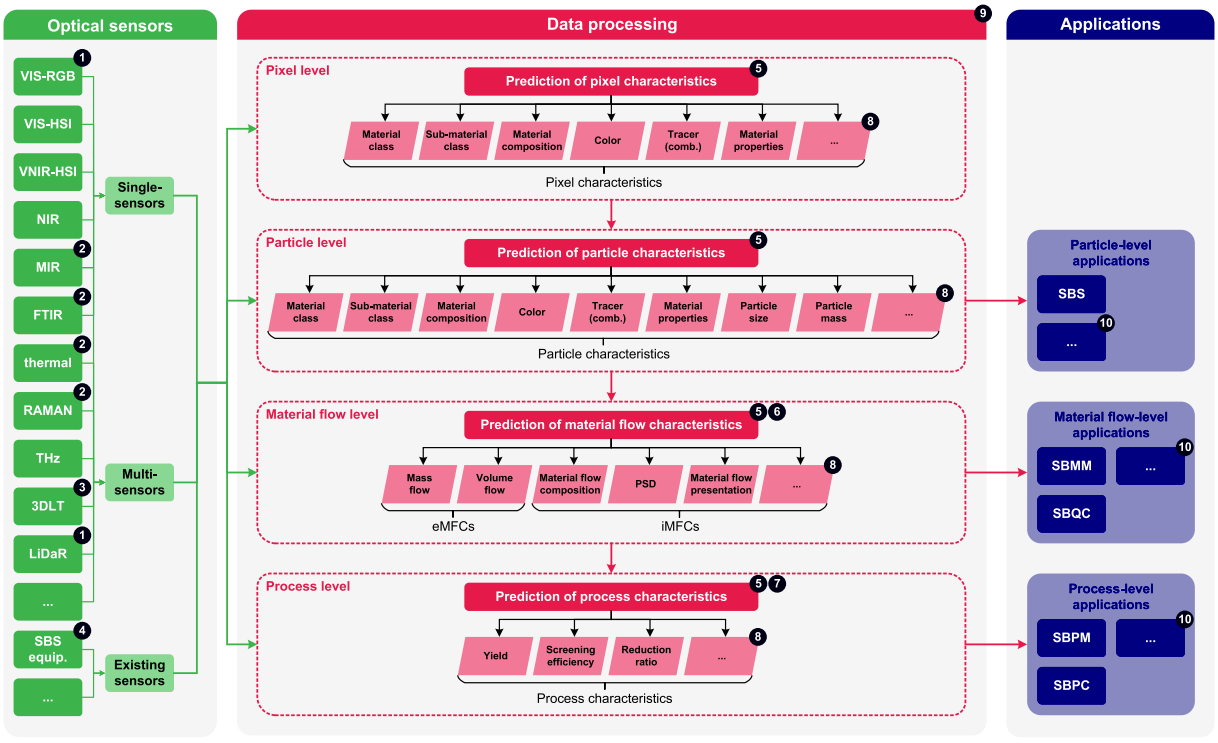

Fig. 10. SBMC data processing pipeline and future research potentials. Research potentials 1–10 (in circles): Future research potentials as outlined in Section 5 (Research potential *i* corresponds to Section 5.*i*).

Third, although our ML algorithm comparison based on Elo ratings ensures that only algorithms on the same datasets and for the same tasks are compared, several effects could still distort the comparison. (i) The fact that each investigation makes a pre-selection of algorithms to be investigated could lead to systematic biases, e.g., a better performing algorithm might exist but was not considered in the respective study. (ii) The Elo rating does not consider how large the prediction difference is between individual algorithms. Especially in the case of very small differences, random effects (e.g., splitting of training and test data) can impact on the comparison. (iii) The algorithm comparison may be affected by different implementations or hyperparameter optimizations among the respective investigations. (iv) It should be noted that our Elo implementation compares ML algorithms across different prediction tasks within our dataset and does not , e.g., differenciate between classification and regression tasks. Thus, it is still possible that despite an overall low Elo rating, certain algorithms are better suited for certain tasks than algorithms with overall higher Elo ratings. Therefore, our evaluations only provide evidence for particularly well-suited SBMC algorithms, but do not replace a direct algorithm comparison in primary studies.

5. Future research potentials

Based on the obtained overview of existing SBMC publications and existing SBMC methods in Section 4, several future research potentials can be derived. In Fig. 10, we integrate the insights from Section 4 into an SBMC data processing pipeline that illustrates how data from different sensors can be used to extract characteristics at different investigation levels and what applications emerge from these characteristics. Using the framework provided by Fig. 10, we identify $n = 10$ future research opportunities, which we discuss in more detail in the following subsections (one potential per section; Section 5.*i* referrers to research potential *i* in Fig. 10).

5.1. Utilizing low-cost sensors

Modern sorting plants often produce ten or more output material flows; several dozen material flows are often conveyed between individual separation units inside the plant. To realize the research vision of automated and adaptive process control in next-generation sorting plants (Section 1.1), it is likely that a significant part of these material flows has to be monitored by SBMC methods in the future to obtain a full picture of the process state and enable a precise process control for optimal sorting results. Many existing sensor technologies have rather high unit costs, making exhaustive process monitoring economically unfeasible.

Possible strategies to reduce these investments costs comprise (i) the use of existing sensors (see Section 5.4), (ii) positioning additional sensors at strategically useful locations, and (iii) reducing the investments cost per sensor. Regarding reducing the investment cost of sensors for eMFCs (especially volume flows), we see large potential in light detection and ranging (LIDAR) sensors, which could measure volume flows at a significantly lower cost compared to state-of-the-art 3DLT sensors (Nordmann and Pfund, 2020). Regarding iMFCs, we see great potential in VIS-RGB sensors, which could substitute 3DLT sensors where 2D particle measurements are sufficient (e.g., Kandlbauer et al., 2021) or other sensors when combined with advanced ML algorithms such as CNNs (e.g., Chen et al., 2021a; Davis et al., 2021; Lu et al., 2022a).

5.2. Upscaling and utilization of emerging sensor technologies

In addition, potential improvements could be achieved by further upscaling emerging optical sensor technologies such as THz and MIR, which have proven to solve intractable problems such as sorting carbon-black plastics in the past (e.g., Küter et al., 2018; Rozenstein et al., 2017; Signoret et al., 2020a, Signoret et al., 2019a, Signoret et al., 2019b). For example, a more detailed characterization with MIR sensors could enable the identification of specific plastic additives, the prediction of application-specific material properties of post-consumer recyclates (van Engelshoven et al., 2019), or quantify aging effects (Signoret et al., 2020b), which can be challenging in the NIR range (e.g., Chen et al., 2021c).

These predicted characteristics could be utilized in advanced SBS and SBQC and contribute to higher-quality material recycling (e.g., additives like flame retardants could damage the quality of the plastic recyclate). As these emerging sensor technologies have so far predominantly been applied to plastics, the extension to other use cases such as the discrimination of different waste wood categories, a more nuanced paper sorting, or SBS in CDW recycling could contribute further to an improved material circulation.

5.3. Improvement of 3D(LT) detection

As discussed in Section 4.3.1, 3D sensors are of great value for measuring volume flows (3DLT and LIDAR) and individual particles (3DLT) in SBMC. However, many problems in applying 3DLT sensors for SBMC are still under-researched. For example, many post-consumer material flows contain transparent materials such as PET bottles or glass, which can only be detected to a limited extent using 3DLT because the laser beam (depending on transparency and surface contamination) penetrates the transparent material and cannot be measured at the particle's surface. Regarding volumetric flow measurement, 3DLT and LIDAR sensors often overestimate or underestimate the volumetric flow through cavities or overshadowing, respectively, or it is unclear how the "true" volumetric flow is even defined in such cases.

5.4. Utilization of existing sensor equipment and data streams

As mentioned under Section 5.1, there is great potential in using existing sensor data in sorting plants. Many modern sorting plants contain several SBS units. Since the material flow on the acceleration belts/chutes of existing SBS equipment is presented as a singled monolayer, and the existing sensors classify the material flow, either way, the use of sensor data from existing SBS units offers great potential for material flow monitoring. SBS manufacturers are already recording this data and making it available to their customers (e.g., TOMRA Systems ASA., 2022a). However, challenges in this area are mainly of a technical and organizational nature. Since the data is primarily used for SBS, material flow information (e.g., area-related material flow compositions) is usually stored in an aggregated form and cannot be evaluated and used in more detail for other SBMC applications. In addition, sensor data often have material-specific weights, and individual reference spectra are stored for the sorting recipe, which can be very different if they are saved desirably for, e.g., SBMM applications. Besides, recipes often change over time (due to SBS unit maintenance), complicating the data analysis. A simple technical solution would be to split the sensor data stream into an SBS and an SBMM data stream immediately after acquisition so that the sensor data can be analyzed at high resolution without affecting the actual sorting task (and vice versa).

5.5. Open-access datasets and further utilization of deep learning methods

CNNs have so far achieved impressive classification results on VIS-RGB datasets of post-consumer wastes (e.g., *TrashNet* [Yang and Thung, 2016] and *Huawei garbage classification challenge cup* [Huawei, 2019]; see Section 4.4.2). However, the public datasets available are quite different from the reality in many industrial sorting plants. For example, in sorting plants, particles usually must be identified on (dirty) conveyor belts, whereas the particles in, e.g., *TrashNet* were created in front of mostly homogeneous, white, and clean backgrounds. In addition, waste collection and preconditioning particles in sorting plants are

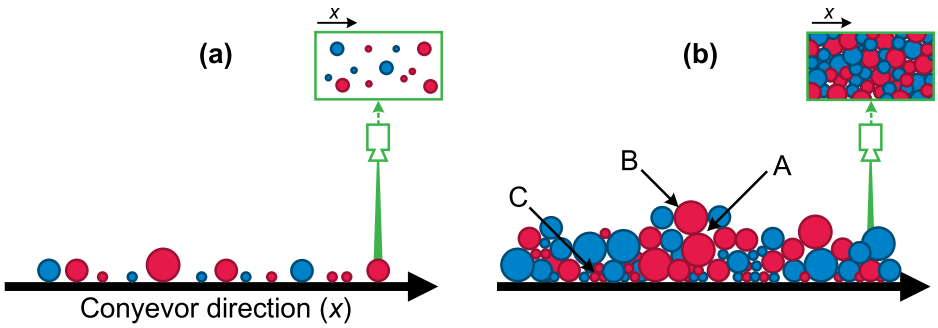

Fig. 11. Presentation of material flows as (a) singled monolayer and (b) multilayered bulks to SBMC sensors. A. hallow spaces, B. large particles aggregate on top, C. smaller particles accumulate on the bottom.

often covered with dust, ash, or dirt, exist as agglomerates with other materials, or are often heavily deformed or partially damaged by waste collection or preconditioning processes. Additionally, modern sorting plants often sort according to other and more nuanced material classes than the ones used in *TrashNet*.

ML researchers could largely profit from open-access datasets of post-consumer or post-industrial waste closer to real-world sorting plants' reality. Open access could help exploit datasets once generated through elaborate labeling more intensively by many researchers. For example, Lu et al. (2022a) report that it took $n = 10$ annotators "a month of hard work" (Lu et al., 2022a, p. 4) to label their dataset of $n = 5{,}022$ images for semantic segmentation, yet, the dataset has only been investigated by the authors themselves.

Furthermore, CNNs could be applied to predict other characteristics such as particle sizes and masses, as stated earlier (Kroell et al., 2021a). To date, the prediction of particle sizes and masses has been mostly conducted on manually engineered particle features (e.g., Kroell, 2021), which might not be optimal for the given prediction task. Here, CNNs could be of great value since the extracted features are learned by the model itself and might thus be adapted better to the specific prediction task. Since CNNs can be trained on any type of data array, CNNs could be applied to other types of sensor data at the pixel and particle level. First investigations following this approach have already presented promising results (e.g., Gruber et al., 2019; Jiang et al., 2021; Liu et al., 2020; Xia et al., 2021a; Zinchik et al., 2021). Especially transfer learning techniques (Alom et al., 2019) could help to utilize existing CNNs models for SBMC applications.

5.6. Development and demonstration of sensor-based characterization methods at the material flow level

As discussed in Section 4.2, characteristics have so far been predicted only occasionally at the material flow level. Several research gaps need to be overcome to enable a reliable extraction of iMFCs.

First, all existing optical sensors create area- or volume-based measurements. As elaborated detailed in (Kroell et al., 2021a), most applications in waste management require mass-based MFCs. Therefore, a transformation of the area- or volume-based sensor measurements into mass-based MFCs is necessary, which so far has been researched only briefly for a limited set of material flows (Krämer, 2017; Kroell et al., 2021a; Serranti et al., 2015; Weissenbach and Sarc, 2022; Weissenbach and Sarc, 2021).

Second, outside SBS units, material flows in sorting and processing plants are often not transported as a singled monolayer (Fig. 11a) but as multilayered bulks (Fig. 11b) with materials touching or overlapping each other. When particle-based characteristics (e.g., PSDs) shall be determined in such an unfavorable material flow presentation, adapted segmentation algorithms need to be developed first. Here, we see great potential in the application of semantic instance segmentation algorithms based on deep learning such as U-Net (Ronneberger et al., 2015), Mask R-CNN (He et al., 2017) and DeepLabv3+ (Chen et al., 2018). Pixel-based derivable characteristics such as the material flow composition can be derived by analyzing the surface of the investigated material bulk (e.g., Curtis and Sarc, 2021). However, segregation errors, e.g., through granular convection ("Brazil nut effect") (Rosato and Prinz, 1987) (Fig. 11b) or different material densities, might result in high uncertainties when only considering the bulk surface. Here, extensive research is required to understand and quantify these effects on SBMC at the material flow level.

Third, little research has been conducted regarding the measurement of volume flows (see Section 5.3) and the transformation of volume to mass flows (Curtis and Sarc, 2021). Likewise, significant research gaps exist in the prediction of PSDs on conveyor belts (cf. Section 4.2).

Fourth, there is no consensus at which time intervals SBMM data should be aggregated or smoothed and how material flow fluctuations should be quantified best (Curtis et al., 2021; Feil et al., 2019). While there are rather clear prediction metrics on the pixel and particle level (see Section 2.3.2), first investigations on the targeting on a prediction of iMFCs show that there are yet no clear metrics to assess the prediction performance on the material flow level (e.g., Kandlbauer et al., 2021).

5.7. Development and demonstration of sensor-based characterization methods at the process level

As discussed in Section 4.2.1, we have not identified peer-reviewed investigations on the process level yet. However, such investigations would be of high value since they would enable SBPM or even SBPC in nearly real-time. From our initial experience (Kroell et al., 2022), it appears that SBPM is technically feasible, and the prediction accuracy depends especially on the prediction at the material flow level. Compared to other investigation levels, the challenge at the process level is that several sensors have to be used simultaneously as process evaluation usually consists of at least two different material flows (see Section 2.1.3). Once a precise characterization of the material flow level is possible, the process assessment can be performed relatively straightforward, e.g., based on the indicators presented in Section 2.1.3. We assume that case studies on performance assessments on the process level for mechanical unit operations frequently applied in sorting and processing plants would be of great value for a better process understanding. These insights could be helpful, for example, regarding the parameterization or modeling of individual unit operations or entire sorting or processing plants.

5.8. Extraction of new characteristics

Besides the characteristics listed in Section 2.1 and Section 4.2, new characteristics could be envisioned that could help to improve material circulation further. For example, differentiating food and non-food packaging through VIS-RGB data and CNNs could greatly value advanced SBS and SBQC. Furthermore, as mentioned in Section 5.2, MIR

or NIR sensors combined with CNNs could be used to classify more nuanced material classes (van Engelshoven et al., 2019) or, e.g., additives or hazardous substances in plastics. Especially the detection of application-orientated interfering substances through deep learning could be of great value for improving the quality of produced preconcentrates and secondary raw materials as, e.g., demonstrated by the detection of PE cartages in PE preconcentrates (STEINERT GmbH, 2020; TOMRA Systems ASA, 2022b) or waste wood sorting (TOMRA Systems ASA, 2022b).

5.9. Upscaling to plant scale

As shown in Section 4.5.2, most investigations in our dataset have so far been conducted on a laboratory or technical scale. Subsequent upscaling is necessary to reach higher TRL levels and bring the investigations from laboratories into applications that generate actual ecological benefits. Despite a higher number of unknowns, there is high potential in investigations at plant scale, since only under real-world conditions, unexpected challenges such as dust, vibrations, interfering substances, blockages, material overlay, and surface adhesions occur (Parrodi et al., 2021), which need to be overcome to reach higher TRL levels.

5.10. Development of new business models around SBMC

In addition to the long-term use of the material flow data obtained by SBMC for automatic and adaptive process control (see Section 1.1), new business models could contribute to increased material circulation along the way.

Downstream of a sorting plant, material flow data of preconcentrates could be utilized in processing plants to adapt, e.g., process parameters to different input compositions. Based on the measured material flow characteristics, SBQC and dynamic pricing models for preconcentrates could be possible. Improved SBS and an in-depth knowledge of material flows could help produce higher quality secondary raw materials for demanding applications.

Upstream of a sorting plant, input material flow data could be used to optimize waste collection and recycling-friendly production. For example, input material flow data could be used to monitor separate waste collection in different collection areas, e.g., to make public campaigns for separate waste collection more effective. In addition, material flow data could help to evaluate the recyclability of different products or packaging and provide feedback to product designers or to assess the environmental performance of individual products more accurately.

Ultimately, SBMC methods could contribute to greater transparency of mechanical recycling processes and the anthropogenic material cycles in which they are embedded. Currently, this transparency is largely lacking due to time-consuming and costly plant assessment and sorting analysis. SBMC methods can help to close this data gap, leading to more transparency and a better decision-making basis.

6. Conclusions

Focusing on optical sensors and machine learning algorithms for sensor-based material flow characterization in dry-mechanical recycling of non-hazardous wastes, this article systematically reviewed 267 investigations from 198 peer-reviewed journal publications published between January 2000 and October 2021.

The review demonstrates that applications of optical sensors and machine learning algorithms have received increased attention in recent years, with more than half of the investigations published in 2019 – 2021. The reviewed investigations addressed various material flows, especially plastics. Whereas most investigations presented analysis of sensor data at the pixel or particle level, less than 5% of all investigations conducted analyses at the material flow level, and we identified no investigations at the process level.

We identified ten different sensors among the wavelength range under review (100 nm and 1 mm), with the visible to near-infrared range being studied most often. While investigations with VIS-RGB sensors often focused on identifying broader material classes with CNNs, NIR and MIR sensors were most often used for plastic classification at the pixel level.

In the reviewed publications, a total of 34 different ML algorithms have been investigated to predict characteristics from sensor data, with PCA, CNN, and PLS being applied the most. CNNs in particular have been increasingly applied since 2018: the number of CNN investigations in our dataset doubled or more each year and became the most frequently applied machine algorithm in our dataset by 2021. A comparison of the reported test scores of different ML algorithms based on Elo ratings indicates that the predictive performance of CNN and RF models might be higher than that of other ML algorithms. While applications initially focused on only sensor-based sorting, a trend has emerged toward new applications including sensor-based material flow monitoring, quality control, and process monitoring/control over the past 10 years.

Our literature review revealed significant research gaps in the field of sensor-based material flow characterization demonstrating that little research has been conducted at the material flow and process level. In particular, research has yet to focus on the conversion of area-based sensor data into mass-based material flow characteristics as well as the prediction of material flow characteristics in the case of overlapping material flow presentation (multilayered bulks). Furthermore, more than 90% of all investigations were conducted on laboratory scale, with considerable upscaling potential. Future research can especially focus on further applications of deep learning methods, on advanced exploitation of low-cost sensor systems such as VIS-RGB, and on a broader application of new sensor technologies (e.g., MIR and THz) for new and more nuanced material characteristics.

The combination of increasingly better and cheaper optical sensors with advanced data analysis methods such as deep learning will probably make it possible to characterize material flows with sufficient accuracy at plant scale in the next few years. Together with developments in remotely controllable actuators and intelligent process control algorithms, next-generation sorting and processing plants could not only sort and process materials better, but also provide valuable material flow information for the entire value chain. In conjunction with other circular economy strategies, these developments could significantly close anthropogenic material cycles and help to transition the world toward sustainable development.

Funding

This work was supported by the German Federal Ministry of Education and Research (BMBF) within the program “Resource-efficient circular economy - plastics recycling technologies (KuRT)” under the project ReVise (grant no. 033R341).

CRediT authorship contribution statement

Nils Kroell: Conceptualization, Methodology, Software, Validation, Formal analysis, Investigation, Data curation, Writing – original draft, Writing – review & editing, Visualization, Project administration, Funding acquisition. **Xiaozheng Chen:** Methodology, Validation, Investigation, Data curation, Writing – review & editing, Funding acquisition. **Kathrin Greiff:** Supervision, Writing – review & editing, Funding acquisition. **Alexander Feil:** Supervision, Writing – review & editing, Funding acquisition.

Declaration of Competing Interest

The authors declare that they have no known competing financial interests or personal relationships that could have appeared to influence

the work reported in this paper.

References

Abdallah, M., Abu Talib, M., Feroz, S., Nasir, Q., Abdalla, H., Mahfood, B., 2020. Artificial intelligence applications in solid waste management: A systematic research review. Waste management (New York N.Y.) 109, 231–246. https://doi.org/10.1016/j.wasman.2020.04.057.

Adedeji, O., Wang, Z., 2019. Intelligent Waste Classification System Using Deep Learning Convolutional Neural Network. Procedia Manufacturing 35, 607–612. https://doi.org/10.1016/j.promfg.2019.05.086.

Adleman, L.M., 1998. Computing with DNA. Sci Am 279, 54–61. https://doi.org/10.1038/scientificamerican0898-54.

Ahmad, K., Khan, K., Al-Fuqaha, A., 2020. Intelligent Fusion of Deep Features for Improved Waste Classification. IEEE Access 8, 96495–96504. https://doi.org/10.1109/ACCESS.2020.2995681.

Alassali, A., Fiore, S., Kuchta, K., 2018. Assessment of plastic waste materials degradation through near infrared spectroscopy. Waste management (New York N.Y.) 82, 71–81. https://doi.org/10.1016/j.wasman.2018.10.010.

Alom, M.Z., Taha, T.M., Yakopcic, C., Westberg, S., Sidike, P., Nasrin, M.S., Hasan, M., van Essen, B.C., Awwal, A.A.S., Asari, V.K., 2019. A State-of-the-Art Survey on Deep Learning Theory and Architectures. Electronics 8, 292. https://doi.org/10.3390/electronics8030292.

Altikat, A., Gulbe, A., Altikat, S., 2022. Intelligent solid waste classification using deep convolutional neural networks. International Journal of Environmental Science and Technology 19 (3), 1285–1292.

Altman, N.S., 1992. An Introduction to Kernel and Nearest-Neighbor Nonparametric Regression. The American Statistician 46, 175–185. https://doi.org/10.1080/00031305.1992.10475879.

Anding, K., Garten, D., Linß, E., 2013. Application of intelligent image processing in the construction material industry. ACTA IMEKO 2, 61–73. https://doi.org/10.21014/acta_imeko.v2i1.100.

Antikainen, M., Uusitalo, T., Kivikytö-Reponen, P., 2018. Digitalisation as an Enabler of Circular Economy. Procedia CIRP 73, 45–49. https://doi.org/10.1016/j.procir.2018.04.027.

Araujo-Andrade, C., Bugnicourt, E., Philippet, L., Rodriguez-Turienzo, L., Nettleton, D., Hoffmann, L., Schlummer, M., 2021. Review on the photonic techniques suitable for automatic monitoring of the composition of multi-materials wastes in view of their posterior recycling. Waste management & research : the journal of the International Solid Wastes and Public Cleansing Association, ISWA 39, 631–651. https://doi.org/10.1177/0734242X21997908.

Arenas-Vivo, A., Beltrán, F.R., Alcázar, V., de La Orden, M.U., Martinez Urreaga, J., 2017. Fluorescence labeling of high density polyethylene for identification and separation of selected containers in plastics waste streams. Comparison of thermal and photochemical stability of different fluorescent tracers. Materials Today Communications 12, 125–132. https://doi.org/10.1016/j.mtcomm.2017.07.008.

Astrup, T., Fruergaard, T., Christensen, T.H., 2009. Recycling of plastic: accounting of greenhouse gases and global warming contributions. Waste management & research : the journal of the International Solid Wastes and Public Cleansing Association, ISWA 27, 763–772. https://doi.org/10.1177/0734242X09345868.

Ata, A.A., Rafeek, A., Yusof, H., 2005. Sensory-Based Colour Sorting Automated Robotic Cell. Journal of Intelligent and Robotic Systems 43, 99–110. https://doi.org/10.1007/s10846-005-3895-0.

Bae, J.-S., Oh, S.-K., Pedrycz, W., Fu, Z., 2019. Design of fuzzy radial basis function neural network classifier based on information data preprocessing for recycling black plastic wastes: comparative studies of ATR FT-IR and Raman spectroscopy. Applied Intelligence 49, 929–949. https://doi.org/10.1007/s10489-018-1300-5.

Bajpai, P., 2014. Recycling and deinking of recovered paper. Elsevier, Amsterdam, Boston, Heidelberg, p. 304.

Barcala, J.M., Luis Fernandez, J., Zabala Alberdi, J., Jiménez, J., Lázaro, J.C., Navarrete, J.J., Oller, J.C., 2004. Identification of plastics using wavelets and quaternion numbers. Measurement Science and Technology 15, 371–376. https://doi.org/10.1088/0957-0233/15/2/009.

Barnabé, P., Dislaire, G., Leroy, S., Pirard, E., 2015. Design and calibration of a two-camera (visible to near-infrared and short-wave infrared) hyperspectral acquisition system for the characterization of metallic alloys from the recycling industry. J. Electron. Imaging 24 (6), 061115.

Bartl, A., Haner, S., Pico, D., Marini, I., Kasser-Heil, G., Slanovc, J., 2011. Wissenschaftliche Untersuchungen zur stofflichen Verwertung der textilen Restfraktion durch mechanische Verfahrensschritte und Entwicklung eines geschlossenen Gesamtkreislaufes. Berichte aus Energie- und Umweltforschung, 35 pp. https://nachhaltigwirtschaften.at/resources/fdz_pdf/endbericht_1106_stoffliche_verwertung.pdf?m=1469660210&.

Becker, W., Sachsenheimer, K., Klemenz, M., 2017. Detection of Black Plastics in the Middle Infrared Spectrum (MIR) Using Photon Up-Conversion Technique for Polymer Recycling Purposes. Polymers 9, 435. https://doi.org/10.3390/polym9090435.

Beel, H., 2017. Sortierung von schwarzen Kunststoffen nach ihrer Polymerklasse mit Hyperspectral-Imaging-Technologie. In: Thomé-Kozmiensky, K.J., Thiel, S., Thomé-Kozmiensky, E., Goldmann, D. (Eds.), Recycling und Rohstoffe. TK-Vlg, Nietwerder, pp. 175–191.

Beigbeder, J., Perrin, D., Mascaro, J.-F., Lopez-Cuesta, J.-M., 2013. Study of the physico-chemical properties of recycled polymers from waste electrical and electronic equipment (WEEE) sorted by high resolution near infrared devices. Resources, Conservation and Recycling 78, 105–114. https://doi.org/10.1016/j.resconrec.2013.07.006.

Belkin, M., Niyogi, P., 2002. Laplacian Eigenmaps and Spectral Techniques for Embedding and Clustering, in: Advances in Neural Information Processing Systems. MIT Press.

Berg, H., Sebestyén, J., Bendix, P., Le Blevennec, K., Vrancken, K., 2020. Digital waste management ETC/WMGE 2020/4. European Environment Agency, 72 pp.

Beyerer, J., Puente León, F., Frese, C., 2016. Machine Vision. Springer Berlin Heidelberg, Berlin, Heidelberg, 802 pp.

Bishop, C.M., 2006. Pattern recognition and machine learning. Springer, New York, NY, 738 pp.

Blanch-Perez-del-Notario, C., Saeys, W., Lambrechts, A., 2019. Hyperspectral imaging for textile sorting in the visible–near infrared range. Journal of Spectral. Imaging a17. https://doi.org/10.1255/jsi.2019.a17.

Boardman, J.W., 1989. Inversion Of Imaging Spectrometry Data Using Singular Value Decomposition, in: 12th Canadian Symposium on Remote Sensing Geoscience and Remote Sensing Symposium. 12th Canadian Symposium on Remote Sensing Geoscience and Remote Sensing Symposium, Vancouver, Canada. IEEE, pp. 2069–2072.

Bobulski, J., Kubanek, M., 2021. Deep Learning for Plastic Waste Classification System. Applied Computational Intelligence and Soft Computing 2021, 6626948. 10.1155/2021/6626948.

Bonifazi, G., Capobianco, G., Serranti, S., 2018a. A hierarchical classification approach for recognition of low-density (LDPE) and high-density polyethylene (HDPE) in mixed plastic waste based on short-wave infrared (SWIR) hyperspectral imaging. Spectrochimica acta. Part A, Molecular and biomolecular spectroscopy 198, 115–122. https://doi.org/10.1016/j.saa.2018.03.006.

Bonifazi, G., Fiore, L., Hennebert, P., Serranti, S., 2020a. DEVELOPMENT OF A SELECTION SYSTEM BASED ON HYPERSPECTRAL IMAGING FOR PLASTIC WASTE WITH BROMINATED FLAME RETARDANTS. Environ. Eng. Manag. J. 19 (10), 1755–1763.

Bonifazi, G., Gasbarrone, R., Palmieri, R., Serranti, S., 2020b. Hierarchical modelling for recycling-oriented classification of shredded spent flat monitor products based on hyperspectral imaging. Detritus 13, 122–130. https://doi.org/10.31025/2611-4135/2020.14031.

Bonifazi, G., Gasbarrone, R., Palmieri, R., Serranti, S., 2020c. Near infrared hyperspectral imaging-based approach for end-of-life flat monitors recycling. at -. Automatisierungstechnik 68, 265–276. https://doi.org/10.1515/auto-2019-0058.

Bonifazi, G., Gasbarrone, R., Serranti, S., 2021. Detecting contaminants in post-consumer plastic packaging waste by a nir hyperspectral imaging-based cascade detection approach. Detritus 15, 94–106. https://doi.org/10.31025/2611-4135/2021.14086.

Bonifazi, G., Palmieri, R., Serranti, S., 2015. Hyperspectral imaging applied to end-of-life (EOL) concrete recycling. tm -. Technisches Messen 82, 616–624. https://doi.org/10.1515/teme-2015-0044.

Bonifazi, G., Palmieri, R., Serranti, S., 2017. Concrete drill core characterization finalized to optimal dismantling and aggregates recovery. Waste management (New York N.Y.) 60, 301–310. https://doi.org/10.1016/j.wasman.2016.10.008.

Bonifazi, G., Palmieri, R., Serranti, S., 2018b. Evaluation of attached mortar on recycled concrete aggregates by hyperspectral imaging. Construction and Building Materials 169, 835–842. https://doi.org/10.1016/j.conbuildmat.2018.03.048.

Bonifazi, G., Serranti, S., 2006. Imaging spectroscopy based strategies for ceramic glass contaminants removal in glass recycling. Waste management (New York N.Y.) 26, 627–639. https://doi.org/10.1016/j.wasman.2005.06.004.

Borel, P., Sabater, J., Tourtollet, G.E.P., Cochaux, A., Veiga, J., 2007. Using NIR spectrometry for direct control of recovered papers. Palpu Chongi Gisul/Journal of Korea Technical Association of the Pulp and Paper Industry 39, 58–63.

Breiman, L., 2001. Random Forests. Machine Learning 45, 5–32. https://doi.org/10.1023/A:1010933404324.

Brunner, S., Fomin, P., Kargel, C., 2015. Automated sorting of polymer flakes: fluorescence labeling and development of a measurement system prototype. Waste management (New York N.Y.) 38, 49–60.

Bundesvereinigung Deutscher Stahlrecycling- und Entsorgungsunternehmen e. V., 1995. “Europäische Stahlschrottsortenliste”.

Bundesverband Glasindustrie e. V., 2014. Leitlinie “Qualitätsanforderungen an Glasscherben zum Einsatz in der Behälterglasindustrie”. Standardblatt T 120.

Calvini, R., Orlandi, G., Foca, G., Ulrici, A., 2018. Development of a classification algorithm for efficient handling of multiple classes in sorting systems based on hyperspectral imaging. Journal of Spectral. Imaging a13. https://doi.org/10.1255/jsi.2018.a13.

Candiani, G., Picone, N., Pompilio, L., Pepe, M., Colledani, M., 2017. Characterization of Fine Metal Particles Derived from Shredded WEEE Using a Hyperspectral Image System: Preliminary Results. Sensors (Basel, Switzerland) 17, 1117. https://doi.org/10.3390/s17051117.

Chen, J., Lu, W., Xue, F., 2021a. “Looking beneath the surface”: A visual-physical feature hybrid approach for unattended gauging of construction waste composition. Journal of environmental management 286, 112233. https://doi.org/10.1016/j.jenvman.2021.112233.

Chen, L.-C., Zhu, Y., Papandreou, G., Schroff, F., Adam, H., 2018. Encoder-Decoder with Atrous Separable Convolution for Semantic Image Segmentation. https://arxiv.org/pdf/1802.02611.

Chen, S., Hu, Z., Wang, C., Pang, Q., Hua, L., 2021b. Research on the process of small sample non-ferrous metal recognition and separation based on deep learning. Waste management (New York N.Y.) 126, 266–273. https://doi.org/10.1016/j.wasman.2021.03.019.

Chen, S.H., Jakeman, A.J., Norton, J.P., 2008. Artificial Intelligence techniques: An introduction to their use for modelling environmental systems. Mathematics and

Computers in Simulation 78, 379–400. https://doi.org/10.1016/j.matcom.2008.01.028.
Chen, X., Kroell, N., Dietl, T., Feil, A., Greiff, K., 2021c. Influence of long-term natural degradation processes on near-infrared spectra and sorting of post-consumer plastics. Waste management (New York N.Y.) 136, 213–218. https://doi.org/10.1016/j.wasman.2021.10.006.
Chen, X., Kroell, N., Feil, A., Greiff, K., 2021d. Sensor-based sorting [UNDER REVIEW]. In: Reuter, M. (Ed.), Handbook of Recycling, 2nd ed. Elsevier.
Chen, X., Kroell, N., Feil, A., Pretz, T., 2020. Determination of the composition of multilayer plastic packaging with nir spectroscopy. Detritus 62–66.
Chen, X., Kroell, N., Li, K.e., Feil, A., Pretz, T., 2021e. Influences of bioplastic polylactic acid on near-infrared-based sorting of conventional plastic. Waste Manag Res 39 (9), 1210–1213.
Chen, X., Kroell, N., Wickel, J., Feil, A., 2021f. Determining the composition of post-consumer flexible multilayer plastic packaging with near-infrared spectroscopy. Waste management (New York N.Y.) 123, 33–41. https://doi.org/10.1016/j.wasman.2021.01.015.
Chen, Y., Sun, J., Bi, S., Meng, C., Guo, F., 2021g. Multi-objective solid waste classification and identification model based on transfer learning method. Journal of Material Cycles and Waste Management 23, 2179–2191. https://doi.org/10.1007/s10163-021-01283-8.
Christensen, T.H. (Ed.), 2011. Solid waste technology & management. Wiley, Chichester, p. 1026.
Clarivate, 2021. Web of Science. webofscience.
Cohen, E.R., Mills, I., 2007. Quantities, units and symbols in physical chemistry, 3rd ed. RSC Publ, Cambridge, p. 233.
2a. Connect to possibilities with TOMRA Insight. https://content.tomra.com/insight.
Cristianini, N., Shawe-Taylor, J., 2013. An Introduction to Support Vector Machines and Other Kernel-based Learning Methods. Cambridge University Press.
Cucuzza, P., Serranti, S., Bonifazi, G., Capobianco, G., 2021. Effective Recycling Solutions for the Production of High-Quality PET Flakes Based on Hyperspectral Imaging and Variable Selection. Journal of imaging 7, 181. https://doi.org/10.3390/jimaging7090181.
Cura, K., Rintala, N., Kamppuri, T., Saarimäki, E., Heikkilä, P., 2021. Textile Recognition and Sorting for Recycling at an Automated Line Using Near Infrared Spectroscopy. Recycling 6, 11. https://doi.org/10.3390/recycling6010011.
Curtis, A., Küppers, B., Möllnitz, S., Khodier, K., Sarc, R., 2021. Real time material flow monitoring in mechanical waste processing and the relevance of fluctuations. Waste management (New York N.Y.) 120, 687–697. https://doi.org/10.1016/j.wasman.2020.10.037.
Curtis, A., Sarc, R., 2021. Real-time monitoring of volume flow, mass flow and shredder power consumption in mixed solid waste processing. Waste management (New York N.Y.) 131, 41–49. https://doi.org/10.1016/j.wasman.2021.05.024.
da Silva, D.J., Wiebeck, H., 2017. Using PLS, iPLS and siPLS linear regressions to determine the composition of LDPE/HDPE blends: A comparison between confocal Raman and ATR-FTIR spectroscopies. Vibrational Spectroscopy 92, 259–266. https://doi.org/10.1016/j.vibspec.2017.08.009.
Davis, P., Aziz, F., Newaz, M.T., Sher, W., Simon, L., 2021. The classification of construction waste material using a deep convolutional neural network. Automation in Construction 122, 103481. https://doi.org/10.1016/j.autcon.2020.103481.
de Groot, P.J., Postma, G.J., Melssen, W.J., Buydens, L.M., 2001. Influence of Wavelength Selection and Data Preprocessing on Near-Infrared-Based Classification of Demolition Waste. Applied spectroscopy 55, 173–181. https://doi.org/10.1366/0003702011951470.
de Groot, P.J., Postma, G.J., Melssen, W.J., Buydens, L.M., 2002. Validation of remote, on-line, near-infrared measurements for the classification of demolition waste. Analytica Chimica Acta 453, 117–124. https://doi.org/10.1016/S0003-2670(01)01508-2.
Der Grüne Punkt, 2021. Specifications. https://www.gruener-punkt.de/en/downloads (accessed 12 July 2021).
Deutsches Institut für Normung e. V., 1984. Strahlungsphysik im optischen Bereich und Lichttechnik: Benennung der Wellenlängenbereiche (accessed 20 July 2021), 2 pp.
Di Maria, F., Bianconi, F., Micale, C., Baglioni, S., Marionni, M., 2016. Quality assessment for recycling aggregates from construction and demolition waste: An image-based approach for particle size estimation. Waste management (New York N.Y.) 48, 344–352.
Díaz-Romero, D., Sterkens, W., van den Eynde, S., Goedemé, T., Dewulf, W., Peeters, J., 2021. Deep learning computer vision for the separation of Cast- and Wrought-Aluminum scrap. Resources, Conservation and Recycling 172, 105685. https://doi.org/10.1016/j.resconrec.2021.105685.
Dirzo, R., Young, H.S., Galetti, M., Ceballos, G., Isaac, N.J.B., Collen, B., 2014. Defaunation in the Anthropocene. Science (New York N.Y.) 345, 401–406. https://doi.org/10.1126/science.1251817.
DIN EN 643, 2014. Papier, Karton und Pappe – Europäische Liste der Altpapier-Standardsorten. Deutsches Institut für Normung e. V. Beuth Verlag GmbH. Berlin.
Dosovitskiy, A., Beyer, L., Kolesnikov, A., Weissenborn, D., Zhai, X., Unterthiner, T., Dehghani, M., Minderer, M., Heigold, G., Gelly, S., Uszkoreit, J., Houlsby, N., 2020. An Image is Worth 16x16 Words: Transformers for Image Recognition at Scale. https://arxiv.org/pdf/2010.11929.
Duan, Q., Li, J., 2021. Classification of Common Household Plastic Wastes Combining Multiple Methods Based on Near-Infrared Spectroscopy. Acs Es&T Engineering 1, 1065–1073. https://doi.org/10.1021/acsestengg.0c00183.
Elo, A.E., 2008. The rating of chessplayers, past and present, 2nd ed. Ishi Press International, Bronx, NY, 208 pp.
ElektroG, 2015. Gesetz über das Inverkehrbringen, die Rücknahme und die umweltverträgliche Entsorgung von Elektro-. und Elektronikgeräten.
European Commission, 2020. Circular Economy Action Plan: For a cleaner and more competitive Europe, 28 pp. https://ec.europa.eu/environment/circular-economy/pdf/new_circular_economy_action_plan.pdf (accessed 3 March 2021).
Eurostat, 2021b. Circular material use rate. http://appsso.eurostat.ec.europa.eu/nui/show.do?dataset=env_ac_cur&lang=en (accessed 3 March 2021).
Eurostat, 2021a. Generation of waste by waste category, hazardousness and NACE Rev. 2 activity. https://appsso.eurostat.ec.europa.eu/nui/show.do?dataset=env_wasgen&lang=en (accessed 3 March 2021).
Eurostat, 2020. Waste statistics. https://ec.europa.eu/eurostat/statistics-explained/index.php/Waste_statistics (accessed 3 March 2021).
Fahrmeir, L., Kneib, T., Lang, S., 2009. Regression: Modelle, Methoden und Anwendungen, 2nd ed. Springer, Berlin, 501 pp.
Fahrmeir, L., Kneib, T., Lang, S., Marx, B., 2013. Regression: Models, methods and applications. Springer, Berlin, Heidelberg, p. 698.
Fang, H., Cao, J., Cai, L., Zhou, T., Wang, M., 2021. The recognition of plastic bottle using linear multi hierarchical SVM classifier. Journal of Intelligent & Fuzzy Systems 40, 11509–11522. https://doi.org/10.3233/JIFS-202729.
Farcomeni, A., Serranti, S., Bonifazi, G., 2008. Non-parametric analysis of infrared spectra for recognition of glass and glass ceramic fragments in recycling plants. Waste management (New York N.Y.) 28, 557–564. https://doi.org/10.1016/j.wasman.2007.01.019.
Fatovatikhah, F., Ahmedy, I., Noor, R.M., Kolandaisamy, R., Sabri, A.Q.M., Othman, F., Noor, N.M., 2021. A hybrid flood waste classification model using 3D-wavelet transform and support vector machines techniques. Journal of Ambient Intelligence and Humanized Computing. https://doi.org/10.1007/s12652-020-02674-9.
Feil, A., Coskun, E., Bosling, M., Kaufeld, S., Pretz, T., 2019. Improvement of the recycling of plastics in lightweight packaging treatment plants by a process control concept. Waste management & research : the journal of the International Solid Wastes and Public Cleansing Association, ISWA 37, 120–126. https://doi.org/10.1177/0734242X19826372.
Feil, A., Kroell, N., Pretz, T., Greiff, K., 2021. Anforderungen an eine effiziente technologische Behandlung von Post-Consumer Verpackungsmaterialien in Sortieranlagen. Müll und Abfall 21, 362–370. https://doi.org/10.37307/j.1863-9763.2021.07.04.
Feil, A., van Thoden Velzen, E.U., Jansen, M., Vitz, P., Go, N., Pretz, T., 2016. Technical assessment of processing plants as exemplified by the sorting of beverage cartons from lightweight packaging wastes. Waste management (New York N.Y.) 48, 95–105. https://doi.org/10.1016/j.wasman.2015.10.023.
Figueiredo, M., Jain, A.K., 2002. Unsupervised learning of finite mixture models. IEEE Trans. Pattern Anal. Mach. Intell. 24, 381–396. https://doi.org/10.1109/34.990138.
Flamme, S., Krämer, P., 2015. Erhöhung der Ressourceneffizienz durch Echtzeitanalytik. In: Thomé-Kozmiensky, K.J. (Ed.), Recycling und Rohstoffe. TK-Verl, Neuruppin, pp. 629–643.
Fomin, P., Kargel, C., 2019. Performance Evaluation of a Time-Gated Fluorescence Spectroscopy Measurement System for the Classification and Recycling of Plastics. Applied spectroscopy 73, 610–622. https://doi.org/10.1177/0003702819831278.
Fomin, P., Zhelondz, D., Kargel, C., 2017. Optimized Time-Gated Fluorescence Spectroscopy for the Classification and Recycling of Fluorescently Labeled Plastics. Applied spectroscopy 71, 919–928. https://doi.org/10.1177/0003702816664104.
Fu, B., Li, S., Wei, J., Li, Q., Wang, Q., Tu, J., 2021. A Novel Intelligent Garbage Classification System Based on Deep Learning and an Embedded Linux System. IEEE Access 9, 131134–131146. https://doi.org/10.1109/ACCESS.2021.3114496.
Furferi, R., Governi, L., 2008. The recycling of wool clothes: an artificial neural network colour classification tool. The International Journal of Advanced Manufacturing Technology 37, 722–731. https://doi.org/10.1007/s00170-007-1011-2.
2b. GAIN Intelligence. https://solutions.tomra.com/en/gain-deep-learning (accessed 6 February 2).
Galdón-Navarro, B., Prats-Montalbán, J.M., Cubero, S., Blasco, J., Ferrer, A., 2018. Comparison of latent variable-based and artificial intelligence methods for impurity detection in PET recycling from NIR hyperspectral images. Journal of Chemometrics 32, 2980. https://doi.org/10.1002/cem.2980.
Gauvain, J.-L., Lee, C.-H., 1994. Maximum a posteriori estimation for multivariate Gaussian mixture observations of Markov chains. IEEE Trans. Speech Audio Process. 2, 291–298. https://doi.org/10.1109/89.279278.
Ghasem, N., Henda, R., 2012. Principles of Chemical Engineering Processes. CRC Press, Boca Raton, p. 394.
Gokyuu, T., Nakamura, S., Ueno, T., Nakamura, M., Inoue, D., Yanagihara, Y., 2011. Sorting System for Recycling of Construction Byproducts with Bayes' Theorem-Based Robot Vision. Journal of Robotics and Mechatronics 23, 1066–1072. 10.20965/jrm.2011.p1066.
Gondal, A.U., Sadiq, M.I., Ali, T., Irfan, M., Shaf, A., Aamir, M., Shoaib, M., Glowacz, A., Tadeusiewicz, R., Kantoch, E., 2021. Real Time Multipurpose Smart Waste Classification Model for Efficient Recycling in Smart Cities Using Multilayer Convolutional Neural Network and Perceptron. Sensors (Basel, Switzerland) 21, 4916. https://doi.org/10.3390/s21144916.
1. Google Scholar. https://scholar.google.com/ (accessed 23 October 1).
Grajski, K.A., Breiman, L., Di Viana Prisco, G., Freeman, W.J., 1986. Classification of EEG spatial patterns with a tree-structured methodology: CART. IEEE transactions on biomedical engineering 33, 1076–1086. https://doi.org/10.1109/TBME.1986.325684.
0. Greater sorting reliability thanks to Artificial Intelligence-supported software and hardware upgrades. https://steinertglobal.com/news/news-in-detail/greater-sorting-reliability-thanks-to-artificial-intelligence-supported-software-and-hardware-upgrades/ (accessed 6 February 2).
Griemert, R., Römisch, P., 2020. Fördertechnik. Springer Fachmedien Wiesbaden, Wiesbaden, p. 386.

Grimes, S., Donaldson, J., Gomez, G.C., 2008. Report on the Environmental Benefits of Recycling, 51 pp. https://www.mgg-recycling.com/wp-content/uploads/2013/06/BIR_CO2_report.pdf (accessed 1 June 2020).
Gruber, F., Grählert, W., Wollmann, P., Kaskel, S., 2019. Classification of Black Plastics Waste Using Fluorescence Imaging and Machine Learning. Recycling 4, 40. https://doi.org/10.3390/recycling4040040.
Gruber, F., Wollmann, P., Grählert, W., Kaskel, S., 2018. Hyperspectral Imaging Using Laser Excitation for Fast Raman and Fluorescence Hyperspectral Imaging for Sorting and Quality Control Applications. Journal of imaging 4, 110. 10.3390/jimaging4100110.
Gundupalli, S.P., Hait, S., Thakur, A., 2017a. A review on automated sorting of source-separated municipal solid waste for recycling. Waste management (New York N.Y.), 56–74. https://doi.org/10.1016/j.wasman.2016.09.015.
Gundupalli, S.P., Hait, S., Thakur, A., 2017b. Multi-material classification of dry recyclables from municipal solid waste based on thermal imaging. Waste management (New York N.Y.) 70, 13–21. https://doi.org/10.1016/j.wasman.2017.09.019.
Gundupalli, S.P., Hait, S., Thakur, A., 2018. Classification of metallic and non-metallic fractions of e-waste using thermal imaging-based technique. Process Safety and Environmental Protection 118, 32–39. https://doi.org/10.1016/j.psep.2018.06.022.
Guo, D., Yang, Q., Zhang, Y.-D., Jiang, T., Yan, H., 2021. Classification of Domestic Refuse in Medical Institutions Based on Transfer Learning and Convolutional Neural Network. Computer Modeling in Engineering & Sciences 127, 599–620. 10.32604/cmes.2021.014119.
Hannan, M.A., Abdulla Al Mamun, M., Hussain, A., Basri, H., Begum, R.A., 2015. A review on technologies and their usage in solid waste monitoring and management systems: Issues and challenges. Waste management (New York, N.Y.) 43, 509–523. 10.1016/j.wasman.2015.05.033.
Hastie, T., Tibshirani, R., Friedman, J., 2009a. High-Dimensional Problems: p N. In: Hastie, T., Tibshirani, R., Friedman, J.H. (Eds.), The elements of statistical learning: Data mining, inference, and prediction. Springer, New York, pp. 649–698.
Hastie, T., Tibshirani, R., Friedman, J., 2009b. Linear Methods for Classification. In: Hastie, T., Tibshirani, R., Friedman, J.H. (Eds.), The elements of statistical learning: Data mining, inference, and prediction. Springer, New York, pp. 101–137.
Hastie, T., Tibshirani, R., Friedman, J.H., 2009c. The elements of statistical learning: Data mining, inference, and prediction. Springer, New York, p. 745.
Hayashi, N., Koyanaka, S., Oki, T., 2019. Constructing an automatic object-recognition algorithm using labeling information for efficient recycling of WEEE. Waste management (New York N.Y.) 88, 337–346. https://doi.org/10.1016/j.wasman.2019.03.065.
He, K., Gkioxari, G., Dollár, P., Girshick, R., 2017. Mask R-CNN. https://arxiv.org/pdf/1703.06870.
Hedberg, A., Šipka, S., 2020. The circular economy: Going digital, 120 pp. https://www.epc.eu/en/publications/The-circular-economy-Going-digital~30c848 (accessed 6 March 2021).
Hedberg, A., Šipka, S., Bjerkem, J., 2019. Creating a digital roadmap for a circular economy, 24 pp. https://wms.flexious.be/editor/plugins/imagemanager/content/2140/PDF/2019/pub_difital_roadmap_for_circular_economy.pdf (accessed 6 March 2021).
Hoffmann Sampaio, C., Ambrós, W.M., Cazacliu, B.G., Oliva Moncunill, J., Veras, M.M., Miltzarek, G.L., Silva, L.F.O., Kuerten, A.S., Liendo, M.A., 2021. Construction and Demolition Waste Recycling through Conventional Jig, Air Jig, and Sensor-Based Sorting: A Comparison. Minerals 11, 904. 10.3390/min11080904.
Holland, J.H., 1992. Genetic Algorithms: Computer programs that “evolve” in ways that resemble natural selection can solve complex problems even their creators do not fully understand. Scientific American, 66–73.
Holmes, D.E., Jain, L.C., 2008. Introduction to Bayesian Networks, in: Holmes, D.E. (Ed.), Innovations in Bayesian networks: Theory and applications, vol. 156. Springer, Berlin, Heidelberg, pp. 1–5.
Hosmer, D.W., Lemeshow, S., 2000. Multiple Logistic Regression. In: Hosmer, D.W., Lemeshow, S. (Eds.), Applied logistic regression, 2nd ed. Wiley, New York, pp. 31–46.
Hryb, W., 2015. Sorting Tests of Unsorted Municipal Solid Waste from Germany for a Selected Opto-Pneumatic Sorting Machine. Polish Journal of Environmental Studies 24, 99–105. https://doi.org/10.15244/pjoes/26387.
Hu, B., Serranti, S., Fraunholcz, N., Di Maio, F., Bonifazi, G., 2013. Recycling-oriented characterization of polyolefin packaging waste. Waste management (New York N.Y.) 33, 574–584. https://doi.org/10.1016/j.wasman.2012.11.018.
Hu, Y., 2005. Efficient and High Quality Force-Directed Graph. Mathematica Journal 10, 37–71.
Huang, G.-L., He, J., Xu, Z., Huang, G., 2020. A combination model based on transfer learning for waste classification. Concurrency and Computation: Practice and Experience 32, 5751. https://doi.org/10.1002/cpe.5751.
Huang, K., Lei, H., Jiao, Z., Zhong, Z., 2021. Recycling Waste Classification Using Vision Transformer on Portable Device. Sustainability 13, 11572. https://doi.org/10.3390/su132111572.
Huawei, 2019. garbage_classify: huawei garbage classification challenge cup. https://modelarts-competitions.obs.cn-north-1.myhuaweicloud.com/garbage_classify/dataset/garbage_classify.zip.
Hyvärinen, A., Oja, E., 2000. Independent component analysis: algorithms and applications. Neural Networks 13, 411–430. https://doi.org/10.1016/S0893-6080(00)00026-5.
International Organization for Standardization, 2013. Space systems — Definition of the Technology Readiness Levels (TRLs) and their criteria of assessment ISO 16290:2013 (E) (accessed 1 January 2022), 20 pp.
IPCC (Ed.), 2021. Climate Change 2021: The Physical Science Basis. Contribution of Working Group I to the Sixth Assessment Report of the Intergovernmental Panel on Climate Change.
IRP, 2019. Global Resources Outlook 2019: Natural Resources for the Future We Want. Oberle, B., Bringezu, S., Hatfeld-Dodds, S., Hellweg, S., Schandl, H., Clement, J., and Cabernard, L., Che, N., Chen, D., Droz-Georget , H., Ekins, P., Fischer-Kowalski, M., Flörke, M., Frank, S., Froemelt , A., Geschke, A., Haupt , M., Havlik, P., Hüfner, R., Lenzen, M., Lieber, M., Liu, B., Lu, Y., Lutter, S., Mehr , J., Miatto, A., Newth, D., Oberschelp , C., Obersteiner, M., Pfster, S., Piccoli, E., Schaldach, R., Schüngel, J., Sonderegger, T., Sudheshwar, A., Tanikawa, H., van der Voet, E., Walker, C., West, J., Wang, Z., Zhu, B. A Report of the International Resource Panel. United Nations Environment Programme. Nairobi, Kenya.
IRP, 2017. Assessing global resource use: A systems approach to resource efficiency and pollution reduction. Bringezu, S., Ramaswami, A., Schandl, H., O’Brien, M., Pelton, R., Acquatella, J., Ayuk, E., Chiu, A., Flanegin, R., Fry, J., Giljum, S., Hashimoto, S., Hellweg, S., Hosking, K., Hu, Y., Lenzen, M., Lieber, M., Lutter, S., Miatto, A., Singh Nagpure, A., Obersteiner, M., van Oers, L., Pfister, S., Pichler, P., Russell, A., Spini, L., Tanikawa, H., van der Voet, E., Weisz, H., West, J., Wiijkman, A., Zhu, B., Zivy, R. A Report of the International Resource Panel. United Nations Environment Programme. Nairobi, Kenya.
Jacquin, L., Imoussaten, A., Trousset, F., Perrin, D., Montmain, J., 2021. Control of waste fragment sorting process based on MIR imaging coupled with cautious classification. Resources, Conservation and Recycling 168, 105258. https://doi.org/10.1016/j.resconrec.2020.105258.
Jähne, B., 2005. Digital Image Processing, 1st ed. Springer-Verlag, s.l., p. 607
Jiang, S., Xu, Z., Kamran, M., Zinchik, S., Paheding, S., McDonald, A.G., Bar-Ziv, E., Zavala, V.M., 2021. Using ATR-FTIR spectra and convolutional neural networks for characterizing mixed plastic waste. Computers & Chemical Engineering 155, 107547. https://doi.org/10.1016/j.compchemeng.2021.107547.
Jin, H., Fan, W., Chen, H., Wang, Y., 2020. Anti-corrosion wood automatic sorting robot system based on near-infrared imaging technology. Journal of Mechanical Science and Technology 34, 3049–3055. https://doi.org/10.1007/s12206-020-0636-z.
Kandlbauer, L., Khodier, K., Ninevski, D., Sarc, R., 2021. Sensor-based Particle Size Determination of Shredded Mixed Commercial Waste based on two-dimensional Images. Waste management (New York N.Y.) 120, 784–794. https://doi.org/10.1016/j.wasman.2020.11.003.
Karhunen, J., 1998. Principal component neural networks ? Theory and applications. Pattern Analysis & Applic 1, 74–75. https://doi.org/10.1007/bf01238029.
Kassouf, A., Maalouly, J., Rutledge, D.N., Chebib, H., Ducruet, V., 2014. Rapid discrimination of plastic packaging materials using MIR spectroscopy coupled with independent components analysis (ICA). Waste management (New York N.Y.) 34, 2131–2138. https://doi.org/10.1016/j.wasman.2014.06.015.
Kessler, R.W., 2012. Prozessanalytik: Strategien und Fallbeispiele aus der industriellen Praxis. Wiley, Somerset, p. 755.
Khodier, K., Curtis, A., Sarc, R., Lehner, M., O’Leary, P., Pomberger, R., 2019. Smart solid waste processing plant: vision and pathway, in: ISWA world congress 2019, Bilbao, Spain. 07.10.2019-09.10.2019.
Kirchherr, J., Reike, D., Hekkert, M., 2017. Conceptualizing the circular economy: An analysis of 114 definitions. Resources, Conservation and Recycling 127, 221–232. https://doi.org/10.1016/j.resconrec.2017.09.005.
Kitchenham, B., 2007. Guidelines for performing Systematic Literature Reviews in Software Engineering. Version 2 (3), 65 pp.
Kiyokawa, T., Katayama, H., Tatsuta, Y., Takamatsu, J., Ogasawara, T., 2021. Robotic Waste Sorter With Agile Manipulation and Quickly Trainable Detector. IEEE Access 9, 124616–124631. https://doi.org/10.1109/ACCESS.2021.3110795.
Kobori, H., Higa, S., Tsuchikawa, S., Kojima, Y., Suzuki, S., 2017. Segregating wood wastes by repetitive principal component analysis of near infrared spectra. Journal of Near Infrared Spectroscopy 25, 180–187. https://doi.org/10.1177/0967033517714344.
Kobori, H., Yonenobu, H., Noma, J., Tsuchikawa, S., 2008. Discriminant Analyzing System for Wood Wastes Using A Visible-Near-Infrared Chemometric Imaging Technique. Applied spectroscopy 62, 854–859. https://doi.org/10.1366/000370208785284295.
Koch, I., 2014. Discriminant Analysis. In: Koch, I. (Ed.), Analysis of multivariate and high-dimensional data. Cambridge University Press, Cambridge, pp. 116–164.
Koenig, J.L., 1999. Experimental IR spectroscopy of polymers. Spectroscopy of Polymers. Elsevier 77–145.
Kohonen, T., 1998. The self-organizing map. Neurocomputing 21, 1–6. https://doi.org/10.1016/S0925-2312(98)00030-7.
Bundesgütegemeinschaft Kompost e. V., 2021a. Qualitätsanforderungen für Fertigkompost. https://www.kompost.de/guetesicherung/guetesicherung-kompost/produkte-/-anforderungen (accessed 12 July 2021).
Bundesgütegemeinschaft Kompost e. V., 2021b. Qualitätsanforderungen für Frischkompost. https://www.kompost.de/guetesicherung/guetesicherung-kompost/produkte-/-anforderungen (accessed 12 July 2021).
Bundesgütegemeinschaft Kompost e. V., 2021c. Qualitätsanforderungen für Substratkompost. https://www.kompost.de/guetesicherung/guetesicherung-kompost/produkte-/-anforderungen (accessed 12 July 2021).
Koyanaka, S., Kobayashi, K., 2010. Automatic sorting of lightweight metal scrap by sensing apparent density and three-dimensional shape. Resources, Conservation and Recycling 54, 571–578. https://doi.org/10.1016/j.resconrec.2009.10.014.
Koyanaka, S., Kobayashi, K., Yamamoto, Y., Kimura, M., Rokucho, K., 2013. Elemental analysis of lightweight metal scraps recovered by an automatic sorting technique combining a weight meter and a laser 3D shape-detection system. Resources Conservation and Recycling 75, 63–69. https://doi.org/10.1016/j.resconrec.2013.03.010.

Krämer, P., 2017. Entwicklung von Berechnungsmodellen zur Ermittlung relevanter Einflussgrößen auf die Genauigkeit von Systemen zur nahinfrarotgestützten Echtzeitanalytik von Ersatzbrennstoffen. Dissertation. Aachen.
Kraus, S., Breier, M., Dasí-Rodríguez, S., 2020. The art of crafting a systematic literature review in entrepreneurship research. Int Entrep Manag J 16, 1023–1042. https://doi.org/10.1007/s11365-020-00635-4.
Krcmarik, D., Petru, M., Masin, I., 2019. Increasing of Precision Technology of Glass Sorting Based on Very Fast Reconfigurable Image Processing. Manufacturing Technology 19, 431–438. https://doi.org/10.21062/ujep/309.2019/a/1213-2489/MT/19/3/431.
Kroell, N., 2021. imea: A Python package for extracting 2D and 3D shape measurements from images. JOSS 6, 3091. 10.21105/joss.03091.
Kroell, N., Chen, X., Maghmoumi, A., Koenig, M., Feil, A., Greiff, K., 2021a. Sensor-based particle mass prediction of lightweight packaging waste using machine learning algorithms. Waste management (New York N.Y.) 136, 253–265. https://doi.org/10.1016/j.wasman.2021.10.017.
Kroell, N., Dietl, T., Maghmoumi, A., Chen, X., Küppers, B., Feil, A., Greiff, K., 2022. Assessment of sensor-based sorting performance for lightweight packaging waste through sensor-based material flow monitoring: Concept and preliminary results, in: 9th Sensor-Based Sorting & Control 2022. Sensor-based Sorting and Control (SBSC) 2022, Aachen. 13.04.2022 - 14.04.2022. doi: 10.2370/9783844085457.
Kroell, N., Johnen, K., Chen, X., Feil, A., 2021b. Fine metal-rich waste stream characterization based on RGB data: Comparison between feature-based and deep learning classification methods. In: Beyerer, J., Längle, T. (Eds.), OCM 2021 - Optical Characterization of Materials: Conference Proceedings. KIT Scientific Publishing.
Kruse, F.A., Lefkoff, A.B., Boardman, J.W., Heidebrecht, K.B., Shapiro, A.T., Barloon, P. J., Goetz, A., 1993. The spectral image processing system (SIPS)—interactive visualization and analysis of imaging spectrometer data. Remote Sensing of Environment 44, 145–163. https://doi.org/10.1016/0034-4257(93)90013-N.
Ku, Y., Yang, J., Fang, H., Xiao, W., Zhuang, J., 2021. Deep learning of grasping detection for a robot used in sorting construction and demolition waste. Journal of Material Cycles and Waste Management 23, 84–95. https://doi.org/10.1007/s10163-020-01098-z.
Kubat, M., 2017. An introduction to machine learning. Springer, Cham, Switzerland, p. 348.
Küch, C., Gaastra, M., 2014. Principles of laser-induced fluorescence. In: Nienhaus, K. (Ed.), Sensor technologies: Impulses for the raw materials industry. Shaker, Aachen, pp. 64–73.
Kulcke, A., Gurschler, C., Spöck, G., Leitner, R., Kraft, M., 2003. On-Line classification of synthetic polymers using near infrared spectral imaging. Journal of Near Infrared Spectroscopy 11, 71–81. https://doi.org/10.1255/jnirs.355.
Kumar, S., Yadav, D., Gupta, H., Verma, O.P., Ansari, I.A., Ahn, C.W., 2021. A Novel YOLOv3 Algorithm-Based Deep Learning Approach for Waste Segregation: Towards Smart Waste Management. Electronics 10, 14. https://doi.org/10.3390/electronics10010014.
Küppers, B., Chen, X., Seidler, I., Friedrich, K., Raulf, K., Pretz, T., Feil, A., Pomberger, R., Vollprecht, D., 2019a. Influences and consequences of mechanical delabeling on PET recycling. Detritus Volume 06 - June 2019, 39–46. 10.31025/2611-4135/2019.13816.
Küppers, B., Hernández Parrodi, J.C., Garcia Lopez, C., Pomberger, R., Vollprecht, D., 2019b. Potential of sensor-based sorting in enhanced landfill mining. Detritus 08, 24–30. https://doi.org/10.31025/2611-4135/2019.13875.
Küppers, B., Pomberger, R., 2017. Entwicklungen in der sensorgestützten Sortiertechnik, in: Österreichische Abfallwirtschaftstagung 2017, Graz. 10.05.2017-12.05.2017.
Küppers, B., Schlögl, S., Friedrich, K., Lederle, L., Pichler, C., Freil, J., Pomberger, R., Vollprecht, D., 2021. Influence of material alterations and machine impairment on throughput related sensor-based sorting performance. Waste management & research : the journal of the International Solid Wastes and Public Cleansing Association, ISWA 39, 122–129. https://doi.org/10.1177/0734242X20936745.
Küppers, B., Schlögl, S., Oreski, G., Pomberger, R., Vollprecht, D., 2019c. Influence of surface roughness and surface moisture of plastics on sensor-based sorting in the near infrared range. Waste management & research : the journal of the International Solid Wastes and Public Cleansing Association, ISWA 37, 843–850. https://doi.org/10.1177/0734242X19855433.
Küppers, B., Seidler, I., Koinig, G.R., Pomberger, R., Vollprecht, D., 2020. Influence of throughput rate and input composition on sensor-based sorting efficiency // Volume 09 - March 2020. Detritus, 59–67. 10.31025/2611-4135/2020.13906.
Kuřitka, I., Sedlařík, V., Harea, D., Harea, E., Urbánek, P., Šloufová, I., Coufal, R., Zedník, J., 2020. Polymer Labelling with a Conjugated Polymer-Based Luminescence Probe for Recycling in the Circular Economy. Polymers 12, 1226. https://doi.org/10.3390/polym12061226.
Küter, A., Reible, S., Geibig, T., Nüßler, D., Pohl, N., 2018. THz imaging for recycling of black plastics. tm -. Technisches Messen 85, 191–201. https://doi.org/10.1515/teme-2017-0062.
Lafferty, J., McCallum, A., Pereira, F., 2001. Conditional Random Fields: Probabilistic Models for Segmenting and Labeling Sequence Dataand Labeling Sequence Dat. Proceedings of the 18th International Conference on Machine Learning.
Lau Hiu Hoong, J.D., Lux, J., Mahieux, P.-Y., Turcry, P., Aït-Mokhtar, A., 2020. Determination of the composition of recycled aggregates using a deep learning-based image analysis. Automation in Construction 116, 103204. 10.1016/j.autcon.2020.103204.
Lecun, Y., Bottou, L., Bengio, Y., Haffner, P., 1998. Gradient-based learning applied to document recognition. Proc. IEEE 86, 2278–2324. https://doi.org/10.1109/5.726791.
LeCun, Y., Bengio, Y., Hinton, G., 2015. Deep learning. Nature 521, 436–444. https://doi.org/10.1038/nature14539.
Legnaioli, S., Campanella, B., Poggialini, F., Pagnotta, S., Harith, M.A., Abdel-Salam, Z. A., Palleschi, V., 2020. Industrial applications of laser-induced breakdown spectroscopy: a review. Anal. Methods 12, 1014–1029. https://doi.org/10.1039/C9AY02728A.
Leitner, R., Mairer, H., Kercek, A., 2003. Real-time classification of polymers with NIR spectral imaging and blob analysis. Real-Time Imaging 9, 245–251. https://doi.org/10.1016/j.rti.2003.09.016.
Li, J., Li, C., Liao, Q., Xu, Z., 2019. Environmentally-friendly technology for rapid on-line recycling of acrylonitrile-butadiene-styrene, polystyrene and polypropylene using near-infrared spectroscopy. Journal of Cleaner Production 213, 838–844. https://doi.org/10.1016/j.jclepro.2018.12.160.
Li, S., Chen, L., 2020. Study on Waste Type Identification Method Based on Bird Flock Neural Network. Mathematical Problems in Engineering 2020, 9214350. https://doi.org/10.1155/2020/9214350.
Li, W., Wei, Z., Liu, Z., Du, Y., Zheng, J., Wang, H., Zhang, S., 2021a. Qualitative identification of waste textiles based on near-infrared spectroscopy and the back propagation artificial neural network. Textile Research Journal 91, 2459–2467. https://doi.org/10.1177/00405175211007516.
Li, Y., Qin, X., Zhang, Z., Dong, H., 2021b. A robust identification method for nonferrous metal scraps based on deep learning and superpixel optimization. Waste management & research : the journal of the International Solid Wastes and Public Cleansing Association, ISWA 39, 573–583. https://doi.org/10.1177/0734242X20987884.
Liang, S., Gu, Y., 2021. A deep convolutional neural network to simultaneously localize and recognize waste types in images. Waste management (New York N.Y.) 126, 247–257. https://doi.org/10.1016/j.wasman.2021.03.017.
Liu, Z., Li, W., Wei, Z., 2020. Qualitative classification of waste textiles based on near infrared spectroscopy and the convolutional network. Textile Research Journal 90, 1057–1066. https://doi.org/10.1177/0040517519886032.
Lu, W., Chen, J., Xue, F., 2022a. Using computer vision to recognize composition of construction waste mixtures: A semantic segmentation approach. Resources Conservation and Recycling 178, 106022. https://doi.org/10.1016/j.resconrec.2021.106022.
Lu, Y., Yang, B., Gao, Y., Xu, Z., 2022b. An automatic sorting system for electronic components detached from waste printed circuit boards. Waste management (New York N.Y.) 137, 1–8. https://doi.org/10.1016/j.wasman.2021.10.016.
Luciani, V., Bonifazi, G., Rem, P., Serranti, S., 2015. Upgrading of PVC rich wastes by magnetic density separation and hyperspectral imaging quality control. Waste management (New York N.Y.) 45, 118–125. https://doi.org/10.1016/j.wasman.2014.10.015.
Ma, W., Wang, X., Yu, J., 2020. A Lightweight Feature Fusion Single Shot Multibox Detector for Garbage Detection. IEEE Access 8, 188577–188586. https://doi.org/10.1109/ACCESS.2020.3031990.
Maier, G., Pfaff, F., Pieper, C., Gruna, R., Noack, B., Kruggel-Emden, H., Längle, T., Hanebeck, U.D., Wirtz, S., Scherer, V., Beyerer, J., 2021. Experimental Evaluation of a Novel Sensor-Based Sorting Approach Featuring Predictive Real-Time Multiobject Tracking. IEEE Transactions on Industrial Electronics 68, 1548–1559. https://doi.org/10.1109/TIE.2020.2970643.
Maier, G., Pfaff, F., Wagner, M., Pieper, C., Gruna, R., Noack, B., Kruggel-Emden, H., Längle, T., Hanebeck, U.D., Wirtz, S., Scherer, V., Beyerer, J., 2019. Real-time multitarget tracking for sensor-based sorting. Journal of Real-Time Image Processing 16, 2261–2272. https://doi.org/10.1007/s11554-017-0735-y.
Mäkelä, M., Rissanen, M., Sixta, H., 2020. Machine vision estimates the polyester content in recyclable waste textiles. Resources, Conservation and Recycling 161, 105007. https://doi.org/10.1016/j.resconrec.2020.105007.
Mao, W.-L., Chen, W.-C., Wang, C.-T., Lin, Y.-H., 2021. Recycling waste classification using optimized convolutional neural network. Resources, Conservation and Recycling 164, 105132. https://doi.org/10.1016/j.resconrec.2020.105132.
Maris, E., Aoussat, A., Naffrechoux, E., Froelich, D., 2012. Polymer tracer detection systems with UV fluorescence spectrometry to improve product recyclability. Minerals Engineering 29, 77–88. https://doi.org/10.1016/j.mineng.2011.09.016.
Marsland, S., 2014. Machine Learning: An Algorithmic Perspective, Second Edition, 2nd ed. CRC Press, Hoboken, p. 452.
Masand, A., Chauhan, S., Jangid, M., Kumar, R., Roy, S., 2021. ScrapNet: An Efficient Approach to Trash Classification. IEEE Access 9, 130947–130958. https://doi.org/10.1109/ACCESS.2021.3111230.
Mattone, R., Campagiorni, G., Galati, F., 2000. Sorting of items on a moving conveyor belt. Part 1: a technique for detecting and classifying objects. Robotics and Computer-Integrated Manufacturing 16, 73–80. https://doi.org/10.1016/S0736-5845(99)00040-X.
Maul, A., Nagel, M., 2014. Principles of terahertz technology. In: Nienhaus, K. (Ed.), Sensor technologies: Impulses for the raw materials industry. Shaker, Aachen, pp. 141–150.
Mauruschat, D., Plinke, B., Aderhold, J., Gunschera, J., Meinlschmidt, P., Salthammer, T., 2016. Application of near-infrared spectroscopy for the fast detection and sorting of wood–plastic composites and waste wood treated with wood preservatives. Wood Science and Technology 50, 313–331. https://doi.org/10.1007/s00226-015-0785-x.
Melinte, D.O., Travediu, A.-M., Dumitriu, D.N., 2020. Deep Convolutional Neural Networks Object Detector for Real-Time Waste Identification. Applied Sciences 10, 7301. https://doi.org/10.3390/app10207301.
Michel, A.P.M., Morrison, A.E., Preston, V.L., Marx, C.T., Colson, B.C., White, H.K., 2020. Rapid Identification of Marine Plastic Debris via Spectroscopic Techniques and Machine Learning Classifiers. Environmental science & technology 54, 10630–10637. https://doi.org/10.1021/acs.est.0c02099.

Möllnitz, S., Küppers, B., Curtis, A., Khodier, K., Sarc, R., 2021. Influence of pre-screening on down-stream processing for the production of plastic enriched fractions for recycling from mixed commercial and municipal waste. Waste management (New York N.Y.) 119, 365–373. https://doi.org/10.1016/j.wasman.2020.10.007.

Moroni, M., Mei, A., 2020. Characterization and Separation of Traditional and Bio-Plastics by Hyperspectral Devices. Applied Sciences 10, 2800. https://doi.org/10.3390/app10082800.

Moroni, M., Mei, A., Leonardi, A., Lupo, E., La Marca, F., 2015. PET and PVC Separation with Hyperspectral Imagery. Sensors (Basel, Switzerland) 15, 2205–2227. https://doi.org/10.3390/s150102205.

Mueller, A., Fillion-Robin, J.-C., Boidol, R., Tian, F., Nechifor, P., yoonsubKim, Peter, Rampin, R., Corvellec, M., Medina, J., Dai, Y., Petrushev, B., Langner, K.M., Hong, Alessio, Ozsvald, I., vkolmakov, Jones, T., Bailey, E., Rho, V., IgorAPM, Roy, D., May, C., foobuzz, Piyush, Seong, L.K., van Goey, J., Smith, J.S., Gus, Mai, F., 2018. Amueller/Word_Cloud: Wordcloud 1.5.0. Zenodo.

Mustaffa, M.R., Nasharuddin, N.A., Hussin, M., Nazri, N.I., Mohd, N., Zakaria, A.H., Zamri, N.N., Ahmad, E.A.N., 2019. Automated Recyclable Waste Classification using Multiple Shape-based Properties and Quadratic Discriminant. International Journal of Innovative Technology and Exploring Engineering 8, 270–274.

Ni, D., Xiao, Z., Lim, M.K., 2021. Machine learning in recycling business: an investigation of its practicality, benefits and future trends. Soft Comput 25, 7907–7927. https://doi.org/10.1007/s00500-021-05579-7.

Noll, R., Fricke-Begemann, C., Connemann, S., Meinhardt, C., Sturm, V., 2018. LIBS analyses for industrial applications – an overview of developments from 2014 to 2018. J. Anal. At. Spectrom. 33, 945–956. https://doi.org/10.1039/C8JA00076J.

Nordmann, C., Pfund, E., 2020. Beschreibung und Darstellung der Messmöglichkeiten für die Gleichmäßigkeit inhomogener Stoffströme, in: Conference proceedings of the 15th Recy & DepoTech conference. Recy & Depotech 2020, Montanuniversität Leoben, Österreich.

O'Neill, D.W., Fanning, A.L., Lamb, W.F., Steinberger, J.K., 2018. A good life for all within planetary boundaries. Nat Sustain 1, 88–95. https://doi.org/10.1038/s41893-018-0021-4.

Ozaki, Y., Huck, C., Tsuchikawa, S., Engelsen, S.B., 2021. Near-Infrared Spectroscopy: Theory, Spectral Analysis, Instrumentation, and Applications, 1st ed. Springer, Singapore, Springer Singapore; Imprint, p. 593.

Özkan, K., Ergin, S., Işık, Ş., Işıklı, I., 2015. A new classification scheme of plastic wastes based upon recycling labels. Waste management (New York, N.Y.) 35, 29–35. 10.1016/j.wasman.2014.09.030.

Palmieri, R., Bonifazi, G., Serranti, S., 2014. Recycling-oriented characterization of plastic frames and printed circuit boards from mobile phones by electronic and chemical imaging. Waste management (New York N.Y.) 34, 2120–2130. https://doi.org/10.1016/j.wasman.2014.06.003.

Parrodi, J.C.H., Kroell, N., Chen, X., Dietl, T., Pfund, E., Küppers, B., Nordmann, C., 2021. Nahinfrarot-basierte Stoffstromüberwachung von Bau- und Abbruchabfällen [Near-Infrared-Based Material Flow Monitoring of Construction and Demolition Waste]. In: Thiel, S., Thomé-Kozmiensky, E., Senk, D., Wotruba, H., Antrekowitsch, H., Pomberger, R. (Eds.), Mineralische Nebenprodukte und Abfälle: Aschen, Schlacken, Stäube und Baurestmassen. Thomé-Kozmiensky Verlag GmbH, Neuruppin, pp. 92–111.

Patrizi, A., Gambosi, G., Zanzotto, F.M., 2021. Data Augmentation Using Background Replacement for Automated Sorting of Littered Waste. Journal of imaging 7, 144. https://doi.org/10.3390/jimaging7080144.

Peixoto, T.P., 2014. The graph-tool python library. figshare. https://doi.org/10.6084/m9.figshare.1164194.

Pekalska, E., Duin, R., 2000. Classifiers for dissimilarity-based pattern recognition, in: Proceedings / 15th International Conference on Pattern Recognition: Barcelona, Spain, September 3 - 7, 2000. 15th International Conference on Pattern Recognition, Barcelona, Spain. 3-7 Sept 2000. IEEE Computer Society, Los Alamitos, Calif., pp. 12–16.

Perfilieva, I., 2006. Fuzzy transforms: Theory and applications. Fuzzy Sets and Systems 157, 993–1023. https://doi.org/10.1016/j.fss.2005.11.012.

Peršak, T., Viltužnik, B., Hernavs, J., Klančnik, S., 2020. Vision-Based Sorting Systems for Transparent Plastic Granulate. Applied Sciences 10, 4269. https://doi.org/10.3390/app10124269.

Picón, A., Ghita, O., Bereciartua, A., Echarzarra, J., Whelan, P.F., Iriondo, P.M., 2012. Real-time hyperspectral processing for automatic nonferrous material sorting. Journal of Electronic Imaging 21, 013018. https://doi.org/10.1117/1.JEI.21.1.013018.

Picón, A., Ghita, O., Whelan, P.F., Iriondo, P.M., 2009. Fuzzy Spectral and Spatial Feature Integration for Classification of Nonferrous Materials in Hyperspectral Data. IEEE Transactions on Industrial Informatics 5, 483–494. https://doi.org/10.1109/TII.2009.2031238.

Pieper, C., Pfaff, F., Maier, G., Kruggel-Emden, H., Wirtz, S., Noack, B., Gruna, R., Scherer, V., Hanebeck, U.D., Längle, T., Beyerer, J., 2018. Numerical modelling of an optical belt sorter using a DEM–CFD approach coupled with particle tracking and comparison with experiments. Powder Technology 340, 181–193. https://doi.org/10.1016/j.powtec.2018.09.003.

Pieszczek, l., Daszykowski, M., 2019. Improvement of recyclable plastic waste detection – A novel strategy for the construction of rigorous classifiers based on the hyperspectral images. Chemometrics and Intelligent Laboratory Systems 187, 28–40. 10.1016/j.chemolab.2019.02.009.

Protopapa, M.L., Burresi, E., Palmisano, M., Pesce, E., Schioppa, M., Capodieci, L., Penza, M., Della Sala, D., Vincenti, N., Accili, A., Campadello, L., 2021. Optical methods to identify end-of-life PV panel structure. Resources Conservation and Recycling 171, 105634. https://doi.org/10.1016/j.resconrec.2021.105634.

Qin, L.W., Ahmad, M., Ali, I., Mumtaz, R., Zaidi, S.M.H., Alshamrani, S.S., Raza, M.A., Tahir, M., 2021. Precision Measurement for Industry 4.0 Standards towards Solid Waste Classification through Enhanced Imaging Sensors and Deep Learning Model. Wireless Communications and Mobile Computing 2021, 9963999. 10.1155/2021/9963999.

Rafi Ahmad, S., 2000. Marking of products with fluorescent tracers in binary combinations for automatic identification and sorting. Assembly Automation 20, 58–65. https://doi.org/10.1108/01445150010311617.

Rahman, M.O., Hannan, M.A., Scavino, E., Hussain, A., Basri, H., 2009. An Efficient Paper Grade Identification Method for Automatic Recyclable Waste Paper Sorting. European Journal of Scientific Research 25, 96–103.

Rahman, M.O., Hussain, A., Basri, H., 2014. A critical review on waste paper sorting techniques. Int. J. Environ. Sci. Technol. 11, 551–564. https://doi.org/10.1007/s13762-013-0222-3.

Rahman, M.O., Hussain, A., Basri, N.E.A., Scavino, E., Basri, H., Hannan, M.A., 2012a. Chromaticity Based Waste Paper Grade Identification. International Arab Journal of Information Technology 9, 411–417.

Rahman, M.O., Hussain, A., Scavino, E., Basri, H., Hannan, M.A., 2011. Intelligent computer vision system for segregating recyclable waste papers. Expert Systems with Applications 38, 10398–10407. https://doi.org/10.1016/j.eswa.2011.02.112.

Rahman, M.O., Hussain, A., Scavino, E., Basri, N.E.A., Basri, H., Hannan, M.A., 2010. Waste Paper Grade Identification System using Window Features. Journal of Computational Information Systems 6, 2077–2091.

Rahman, M.O., Hussain, A., Scavino, E., Hannan, M.A., Basri, H., 2012b. Real-time waste paper grading using CBR approach. International journal of innovative computing, information & control 8, 471–488.

Rahman, M.O., Hussain, A., Scavino, E., Hannan, M.A., Basri, H., 2015. DNA computer based algorithm for recyclable waste paper segregation. Applied Soft Computing 31, 223–240. https://doi.org/10.1016/j.asoc.2015.02.042.

Rajak, A., Hasan, S., Mahmood, B., 2020. Automatic waste detection by deep learning and disposal system design. Journal of Environmental Engineering and Science 15, 38–44. https://doi.org/10.1680/jenes.19.00023.

Ramasubramanian, M.K., Venditti, R., Ammineni, C., Mallapragada, V., 2005. Optical Sensor for Noncontact Measurement of Lignin Content in High-Speed Moving Paper Surfaces. IEEE Sensors Journal 5, 1132–1139. https://doi.org/10.1109/JSEN.2005.851007.

Ramli, S., Mustafa, M.M., Hussain, A., Abdul Waha, D., 2008. Histogram of Intensity Feature Extraction for Automatic Plastic Bottle Recycling System Using Machine Vision. American Journal of Environmental Sciences 4, 583–588. https://doi.org/10.3844/ajessp.2008.583.588.

Rasmussen, C.E., Williams, C.K.I., 2008. Gaussian processes for machine learning, 3rd ed. MIT Press, Cambridge, Mass., p. 248

Rebala, G., Ravi, A., Churiwala, S., 2019. An introduction to machine learning. Springer, Cham, p. 263.

Riba, J.-R., Cantero, R., Canals, T., Puig, R., 2020. Circular economy of post-consumer textile waste: Classification through infrared spectroscopy. Journal of Cleaner Production 272, 123011. https://doi.org/10.1016/j.jclepro.2020.123011.

Rockström, J., Steffen, W., Noone, K., Persson, A., Chapin, F.S., Lambin, E.F., Lenton, T.M., Scheffer, M., Folke, C., Schellnhuber, H.J., Nykvist, B., de Wit, C.A., Hughes, T., van der Leeuw, S., Rodhe, H., Sörlin, S., Snyder, P.K., Costanza, R., Svedin, U., Falkenmark, M., Karlberg, L., Corell, R.W., Fabry, V.J., Hansen, J., Walker, B., Liverman, D., Richardson, K., Crutzen, P., Foley, J.A., 2009. A safe operating space for humanity. Nature 461, 472–475. https://doi.org/10.1038/461472a.

Roh, S.-B., Oh, S.-K., 2016. Identification of Plastic Wastes by Using Fuzzy Radial Basis Function Neural Networks Classifier with Conditional Fuzzy C-Means Clustering. Journal of Electrical Engineering and Technology 11, 1872–1879. https://doi.org/10.5370/JEET.2016.11.6.1872.

Roh, S.-B., Oh, S.-K., Park, E.-K., Choi, W.Z., 2017. Identification of black plastics realized with the aid of Raman spectroscopy and fuzzy radial basis function neural networks classifier. Journal of Material Cycles and Waste Management 19, 1093–1105. https://doi.org/10.1007/s10163-017-0620-6.

Roh, S.-B., Oh, S.-K., Pedrycz, W., 2018. Identification of Black Plastics Based on Fuzzy RBF Neural Networks: Focused on Data Preprocessing Techniques Through Fourier Transform Infrared Radiation. IEEE Transactions on Industrial Informatics 14, 1802–1813. https://doi.org/10.1109/TII.2017.2771254.

Ronneberger, O., Fischer, P., Brox, T., 2015. U-Net: Convolutional Networks for Biomedical Image Segmentation. https://arxiv.org/pdf/1505.04597.

Rosato, S., Prinz, S., 1987. Why the Brazil nuts are on top: Size segregation of particulate matter by shaking. Physical review letters 58, 1038–1040. https://doi.org/10.1103/physrevlett.58.1038.

Rozenstein, O., Puckrin, E., Adamowski, J., 2017. Development of a new approach based on midwave infrared spectroscopy for post-consumer black plastic waste sorting in the recycling industry. Waste management (New York N.Y.) 68, 38–44. https://doi.org/10.1016/j.wasman.2017.07.023.

Rybarczyk, D., Jędryczka, C., Regulski, R., Sędziak, D., Netter, K., Czarnecka-Komorowska, D., Barczewski, M., Barański, M., 2020. Assessment of the Electrostatic Separation Effectiveness of Plastic Waste Using a Vision System. Sensors (Basel, Switzerland) 20. https://doi.org/10.3390/s20247201.

Safavi, S.M., Masoumi, H., Mirian, S.S., Tabrizchi, M., 2010. Sorting of polypropylene resins by color in MSW using visible reflectance spectroscopy. Waste management (New York N.Y.) 30, 2216–2222. https://doi.org/10.1016/j.wasman.2010.06.023.

Salmador, A., Cid, J.P., Rodríguez Novelle, I., 2008. Intelligent Garbage Classifier. International Journal of Interactive Multimedia and Artificial Intelligence 31–36.

Sarc, R., Curtis, A., Kandlbauer, L., Khodier, K., Lorber, K.E., Pomberger, R., 2019. Digitalisation and intelligent robotics in value chain of circular economy oriented

waste management - A review. Waste management (New York N.Y.) 95, 476–492. https://doi.org/10.1016/j.wasman.2019.06.035.
Scavino, E., Wahab, D.A., Basri, H., Mustafa, M.M., Hussain, A., 2009a. A Genetic Algorithm for the Segmentation of Known Touching Objects. Journal of Computer Science 5, 711–716. https://doi.org/10.3844/jcssp.2009.711.716.
Scavino, E., Wahab, D.A., Hussain, A., Basri, H., Mustafa, M.M., 2009b. Application of automated image analysis to the identification and extraction of recyclable plastic bottles. Journal of Zhejiang University-SCIENCE A 10, 794–799. https://doi.org/10.1631/jzus.A0820788.
Schmidt, P., Körber, R., Coppers, M., 2006. Sieben und Siebmaschinen: Grundlagen und Anwendung. Wiley-VCH, Weinheim.
1. Scopus®: Expertly curated abstract & citation database. https://www.scopus.com/ (accessed 16 July 1).
Serranti, S., Bonifazi, G., 2010. Post-Consumer Polyolefins (PP-PE) Recognition by Combined Spectroscopic Sensing Techniques. The Open Waste Management Journal 3, 35–45. https://doi.org/10.2174/1876400201003010035.
Serranti, S., Bonifazi, G., Pohl, R., 2006. Spectral cullet classification in the mid-infrared field for ceramic glass contaminants detection. Waste management & research : the journal of the International Solid Wastes and Public Cleansing Association, ISWA 24, 48–59. https://doi.org/10.1177/0734242X06061017.
Serranti, S., Gargiulo, A., Bonifazi, G., 2010. The Utilization of Hyperspectral Imaging for Impurities Detection in Secondary Plastics. The Open Waste Management Journal 3, 56–70. https://doi.org/10.2174/1876400201003010056.
Serranti, S., Gargiulo, A., Bonifazi, G., 2011. Characterization of post-consumer polyolefin wastes by hyperspectral imaging for quality control in recycling processes. Waste management (New York N.Y.) 31, 2217–2227. https://doi.org/10.1016/j.wasman.2011.06.007.
Serranti, S., Gargiulo, A., Bonifazi, G., 2012a. Classification of polyolefins from building and construction waste using NIR hyperspectral imaging system. Resources, Conservation and Recycling 61, 52–58. https://doi.org/10.1016/j.resconrec.2012.01.007.
Serranti, S., Gargiulo, A., Bonifazi, G., 2012b. Hyperspectral imaging for process and quality control in recycling plants of polyolefin flakes. Journal of Near Infrared Spectroscopy 20, 573–581. https://doi.org/10.1255/jnirs.1016.
Serranti, S., Luciani, V., Bonifazi, G., Hu, B., Rem, P.C., 2015. An innovative recycling process to obtain pure polyethylene and polypropylene from household waste. Waste management (New York N.Y.) 35, 12–20. https://doi.org/10.1016/j.wasman.2014.10.017.
Serranti, S., Palmieri, R., Bonifazi, G., 2015b. Hyperspectral imaging applied to demolition waste recycling: innovative approach for product quality control. Journal of Electronic Imaging 24, 043003-1 bis 043003-9. 10.1117/1.JEI.24.4.043003.
Shan, D., Men, X., Xin, H., 2014. Sorting Batteries from Waste Paper Based on Invariant Moments and Fractal Dimension. Applied Mechanics and Materials 475–476, 792–797. https://doi.org/10.4028/www.scientific.net/AMM.475-476.792.
Shen, L., Worrell, E., Patel, M.K., 2010. Open-loop recycling: A LCA case study of PET bottle-to-fibre recycling. Resources, Conservation and Recycling 55, 34–52. https://doi.org/10.1016/j.resconrec.2010.06.014.
Shi, C., Tan, C., Wang, T., Wang, L., 2021. A Waste Classification Method Based on a Multilayer Hybrid Convolution Neural Network. Applied Sciences 11, 8572. https://doi.org/10.3390/app11188572.
Signoret, C., Caro-Bretelle, A.-S., Lopez-Cuesta, J.-M., Ienny, P., Perrin, D., 2019a. MIR spectral characterization of plastic to enable discrimination in an industrial recycling context: I. Specific case of styrenic polymers. Waste management (New York N.Y.) 95, 513–525. https://doi.org/10.1016/j.wasman.2019.05.050.
Signoret, C., Caro-Bretelle, A.-S., Lopez-Cuesta, J.-M., Ienny, P., Perrin, D., 2019b. MIR spectral characterization of plastic to enable discrimination in an industrial recycling context: II. Specific case of polyolefins. Waste management (New York N.Y.) 98, 160–172. https://doi.org/10.1016/j.wasman.2019.08.010.
Signoret, C., Caro-Bretelle, A.-S., Lopez-Cuesta, J.-M., Ienny, P., Perrin, D., 2020a. Alterations of plastics spectra in MIR and the potential impacts on identification towards recycling. Resources, Conservation and Recycling 161, 104980. https://doi.org/10.1016/j.resconrec.2020.104980.
Signoret, C., Edo, M., Caro-Bretelle, A.-S., Lopez-Cuesta, J.-M., Ienny, P., Perrin, D., 2020b. MIR spectral characterization of plastic to enable discrimination in an industrial recycling context: III. Anticipating impacts of ageing on identification. Waste management (New York N.Y.) 109, 51–64. https://doi.org/10.1016/j.wasman.2020.04.043.
Simion, I.M., Fortuna, M.E., Bonoli, A., Gavrilescu, M., 2013. Comparing environmental impacts of natural inert and recycled construction and demolition waste processing using LCA. Journal of Environmental Engineering and Landscape Management 21, 273–287. https://doi.org/10.3846/16486897.2013.852558.
Smith, E., Dent, G., 2019. Modern Raman spectroscopy: A practical approach. Wiley, Hoboken NJ, 1 online resource.
So, C.-L., Lebow, S.T., Groom, L.H., Rials, T.G., 2004. The application of near infrared (NIR) spectroscopy to inorganic preservative-treated wood. Wood and Fiber Science 36, 329–336.
Sun, D.-W., 2009. Infrared spectroscopy for food quality analysis and control, 1st ed. Elsevier Academic Press, Amsterdam, p. 424.
Tachwali, Y., Al-Assaf, Y., Al-Ali, A., 2007. Automatic multistage classification system for plastic bottles recycling. Resources, Conservation and Recycling 52, 266–285. https://doi.org/10.1016/j.resconrec.2007.03.008.
Tan, Z., Fei, Z., Zhao, B., Yang, J., Xu, X., Wang, Z., 2021. Identification for Recycling Polyethylene Terephthalate (PET) Plastic Bottles by Polarization Vision. IEEE Access 9, 27510–27517. https://doi.org/10.1109/ACCESS.2021.3050816.
Tatzer, P., Wolf, M., Panner, T., 2005. Industrial application for inline material sorting using hyperspectral imaging in the NIR range. Real-Time Imaging 11, 99–107. https://doi.org/10.1016/j.rti.2005.04.003.
Taurino, R., Pozzi, P., Zanasi, T., 2010. Facile characterization of polymer fractions from waste electrical and electronic equipment (WEEE) for mechanical recycling. Waste management (New York N.Y.) 30, 2601–2607. https://doi.org/10.1016/j.wasman.2010.07.014.
Tharwat, A., Gaber, T., Ibrahim, A., Hassanien, A.E., 2017. Linear discriminant analysis: A detailed tutorial. AIC 30, 169–190. https://doi.org/10.3233/AIC-170729.
Tofallis, C., 1999. Model Building with Multiple Dependent Variables and Constraints. J Royal Statistical Soc D 48, 371–378. https://doi.org/10.1111/1467-9884.00195.
Toğaçar, M., Ergen, B., Cömert, Z., 2020. Waste classification using AutoEncoder network with integrated feature selection method in convolutional neural network models. Measurement 153, 107459. https://doi.org/10.1016/j.measurement.2019.107459.
Tolman, R., 1917. The Measurable Quantities of Physics. The Physical Review 9, 237–253.
Trotta, O., Bonifazi, G., Capobianco, G., Serranti, S., 2021. Recycling-Oriented Characterization of Post-Earthquake Building Waste by Different Sensing Techniques. Journal of imaging 7, 182. https://doi.org/10.3390/jimaging7090182.
Tsuchikawa, S., Yamato, K., 2003. Discriminant analysis of wood-based materials with weathering damage by near infrared spectroscopy. Journal of Near Infrared Spectroscopy 11, 391–399. https://doi.org/10.1255/jnirs.390.
Tsuchikawa, S., Yamato, K., Inoue, K., 2003. Discriminant analysis of wood-based materials using near-infrared spectroscopy. Journal of Wood Science 49, 275–280. https://doi.org/10.1007/s10086-002-0471-0.
Ulrici, A., Serranti, S., Ferrari, C., Cesare, D., Foca, G., Bonifazi, G., 2013. Efficient chemometric strategies for PET–PLA discrimination in recycling plants using hyperspectral imaging. Chemometrics and Intelligent Laboratory Systems 122, 31–39. https://doi.org/10.1016/j.chemolab.2013.01.001.
van Engelshoven, Y., Wen, P., Bakker, M., Balkenende, R., Rem, P., 2019. An Innovative Route to Circular Rigid Plastics. Sustainability 11, 6284. https://doi.org/10.3390/su11226284.
Vázquez-Guardado, A., Money, M., McKinney, N., Chanda, D., 2015. Multi-spectral infrared spectroscopy for robust plastic identification. Applied optics 54, 7396–7405. https://doi.org/10.1364/AO.54.007396.
Vegas, I., Broos, K., Nielsen, P., Lambertz, O., Lisbona, A., 2015. Upgrading the quality of mixed recycled aggregates from construction and demolition waste by using near-infrared sorting technology. Construction and Building Materials 75, 121–128. https://doi.org/10.1016/j.conbuildmat.2014.09.109.
Verein Deutscher Metallhändler e. V., 1988. Usancen und Klassifizierungen des Metallhandels. http://www.metallhandel-online.com/downloads/usancen_2012.pdf.
Vo, A.H., Le Son, H., Vo, M.T., Le, T., 2019. A Novel Framework for Trash Classification Using Deep Transfer Learning. IEEE Access 7, 178631–178639. https://doi.org/10.1109/ACCESS.2019.2959033.
Vrancken, C., Longhurst, P.J., Wagland, S.T., 2017. Critical review of real-time methods for solid waste characterisation: Informing material recovery and fuel production. Waste management (New York N.Y.) 61, 40–57. https://doi.org/10.1016/j.wasman.2017.01.019.
Wahab, D.A., Hussain, A., Scavino, E., Mustafa, M.M., Basri, H., 2006. Development of a Prototype Automated Sorting System for Plastic Recycling. American Journal of Applied Sciences 3, 1924–1928. https://doi.org/10.3844/ajassp.2006.1924.1928.
Wang, C., Hu, Z., Pang, Q., Hua, L., 2019a. Research on the classification algorithm and operation parameters optimization of the system for separating non-ferrous metals from end-of-life vehicles based on machine vision. Waste management (New York N.Y.) 100, 10–17. https://doi.org/10.1016/j.wasman.2019.08.043.
Wang, S.-C., 2003. Artificial Neural Network. In: Wang, S.-.-C. (Ed.), Interdisciplinary Computing in Java Programming. Springer, Boston, MA, pp. 81–100.
Wang, T., Cai, Y., Liang, L., Ye, D., 2020. A Multi-Level Approach to Waste Object Segmentation. Sensors (Basel, Switzerland) 20, 3816. https://doi.org/10.3390/s20143816.
Wang, Z., Peng, B., Huang, Y., Sun, G., 2019b. Classification for plastic bottles recycling based on image recognition. Waste management (New York N.Y.) 88, 170–181. https://doi.org/10.1016/j.wasman.2019.03.032.
TL Gestein-StB 04, 2007. "Technical Delivery Terms for Aggregates in Road Construction". Forschungsgesellschaft für Straßen- und Verkehrswesen e.V.
Weissenbach, T., Sarc, R., 2021. Investigation of particle-specific characteristics of non-hazardous, fine shredded mixed waste. Waste management (New York N.Y.) 119, 162–171. https://doi.org/10.1016/j.wasman.2020.09.033.
Weissenbach, T., Sarc, R., 2022. Particle-specific characterisation of non-hazardous, coarse-shredded mixed waste for real-time quality assurance. Journal of environmental management 301, 113878. https://doi.org/10.1016/j.jenvman.2021.113878.
Whitaker, R.D., 1975. An historical note on the conservation of mass. J. Chem. Educ. 52, 658. https://doi.org/10.1021/ed052p658.
Willmott, C.J., Matsuura, K., 2005. Advantages of the mean absolute error (MAE) over the root mean square error (RMSE) in assessing average model performance. Climate Research 30, 79–82. https://doi.org/10.3354/cr030079.
Wills, B.A., Finch, J.A., 2016. Comminution. In: Wills, B.A., Finch, J.A. (Eds.), Wills' mineral processing technology: An introduction to the practical aspects of ore treatment and mineral recovery. Butterworth-Heinemann is an imprint of Elsevier, Amsterdam, pp. 109–122.
Woidasky, J., Sander, I., Schau, A., Moesslein, J., Wendler, P., Wacker, D., Gao, G., Kirchenbauer, D., Kumar, V., Busko, D., Howard, I.A., Richards, B.S., Turshatov, A., Wiethoff, S., Lang-Koetz, C., 2020. Inorganic fluorescent marker materials for

identification of post-consumer plastic packaging. Resources, Conservation and Recycling 161, 104976. https://doi.org/10.1016/j.resconrec.2020.104976.
Wold, S., Kettaneh-Wold, N., Skagerberg, B., 1989. Nonlinear PLS modeling. Chemometrics and Intelligent Laboratory Systems 7, 53–65. https://doi.org/10.1016/0169-7439(89)80111-X.
Wold, S., Sjöström, M., 1977. SIMCA: A Method for Analyzing Chemical Data in Terms of Similarity and Analogy, in: Kowalski, B.R. (Ed.), Chemometrics: theory and application: A symposium sponsored by the Division of Computers in Chemistry at the 172nd Meeting of the American Chemical Society, San Fancisco, Calif., Sept. 2, 1976, vol. 52. AMERICAN CHEMICAL SOCIETY, Washington, DC, pp. 243–282.
Wu, X., Li, J., Yao, L., Xu, Z., 2020. Auto-sorting commonly recovered plastics from waste household appliances and electronics using near-infrared spectroscopy. Journal of Cleaner Production 246, 118732. https://doi.org/10.1016/j.jclepro.2019.118732.
WWF, 2020. Living Planet Report 2020 - Bending the curve of biodiversity loss. Gland, Switzerland, p. 83.
Xia, J., Huang, Y., Li, Q., Xiong, Y., Min, S., 2021a. Convolutional neural network with near-infrared spectroscopy for plastic discrimination. Environmental Chemistry Letters 19, 3547–3555. https://doi.org/10.1007/s10311-021-01240-9.
Xia, W., Jiang, Y., Chen, X., Zhao, R., 2021b. Application of machine learning algorithms in municipal solid waste management: A mini review. Waste Manag Res 734242X211033716. https://doi.org/10.1177/0734242X211033716.
Xiao, W., Yang, J., Fang, H., Zhuang, J., Ku, Y., 2019a. A robust classification algorithm for separation of construction waste using NIR hyperspectral system. Waste management (New York N.Y.) 90, 1–9. https://doi.org/10.1016/j.wasman.2019.04.036.
Xiao, W., Yang, J., Fang, H., Zhuang, J., Ku, Y., 2019b. Development of online classification system for construction waste based on industrial camera and hyperspectral camera. PloS one 14, e0208706. https://doi.org/10.1371/journal.pone.0208706.
Xiao, W., Yang, J., Fang, H., Zhuang, J., Ku, Y., Zhang, X., 2020. Development of an automatic sorting robot for construction and demolition waste. Clean Technologies and Environmental Policy 22, 1829–1841. https://doi.org/10.1007/s10098-020-01922-y.
Xiao, Y., Watson, M., 2019. Guidance on Conducting a Systematic Literature Review. Journal of Planning Education and Research 39, 93–112. https://doi.org/10.1177/0739456X17723971.
Yang, M., Thung, G., 2016. Classification of Trash for Recyclability Status.
Yang, Y., Zhang, X., Yin, J., Yu, X., 2020. Rapid and Nondestructive On-Site Classification Method for Consumer-Grade Plastics Based on Portable NIR Spectrometer and Machine Learning. Journal of Spectroscopy 2020, 6631234. https://doi.org/10.1155/2020/6631234.
Yu, Y., Zou, S., Yin, K., 2020. A novel detection fusion network for solid waste sorting. International Journal of Advanced Robotic Systems 17. https://doi.org/10.1177/1729881420941779.
Zhang, J., Qiu, Y., Chen, J., Guo, J., Chen, J., Chen, S., 2019. Three dimensional object segmentation based on spatial adaptive projection for solid waste. Neurocomputing 328, 122–134. https://doi.org/10.1016/j.neucom.2018.03.079.
Zhang, Q., Yang, Q., Zhang, X., Bao, Q., Su, J., Liu, X., 2021. Waste image classification based on transfer learning and convolutional neural network. Waste management (New York N.Y.) 135, 150–157. https://doi.org/10.1016/j.wasman.2021.08.038.
Zhao, Q., Chen, M., 2015. Characterization of Automobile Plastics by Principal Component Analysis and Near-Infrared Spectroscopy. Analytical Letters 48, 301–307. https://doi.org/10.1080/00032719.2014.942910.
Zheng, H., Gu, Y., 2021. EnCNN-UPMWS: Waste Classification by a CNN Ensemble Using the UPM Weighting Strategy. Electronics 10, 427. https://doi.org/10.3390/electronics10040427.
Zheng, Y., Bai, J., Xu, J., Li, X., Zhang, Y., 2018. A discrimination model in waste plastics sorting using NIR hyperspectral imaging system. Waste management (New York N.Y.) 72, 87–98. https://doi.org/10.1016/j.wasman.2017.10.015.
Zhou, C., Han, G., Via, B.K., Song, Y., Gao, S., Jiang, W., 2019. Rapid identification of fibers from different waste fabrics using the near-infrared spectroscopy technique. Textile Research Journal 89, 3610–3616. https://doi.org/10.1177/0040517518817043.
Zhou, J., Zou, X., Wong, W.K., 2021. Computer vision-based color sorting for waste textile recycling. International Journal of Clothing Science and Technology ahead-of-print. https://doi.org/10.1108/ijcst-12-2019-0190.
Zhu, S., Chen, H., Wang, M., Guo, X., Lei, Y., Jin, G., 2019. Plastic solid waste identification system based on near infrared spectroscopy in combination with support vector machine. Advanced Industrial and Engineering Polymer Research 2, 77–81. https://doi.org/10.1016/j.aiepr.2019.04.001.
Zhuang, J., Yang, J., Fang, H., Xiao, W., Ku, Y., 2019. Recognition of Concrete and Gray Brick Based on Color and Texture Features. Journal of Testing and Evaluation 47, 3224–3237. https://doi.org/10.1520/JTE20180523.
Zinchik, S., Jiang, S., Friis, S., Long, F., Høgstedt, L., Zavala, V.M., Bar-Ziv, E., 2021. Accurate Characterization of Mixed Plastic Waste Using Machine Learning and Fast Infrared Spectroscopy. ACS Sustainable Chemistry & Engineering 9, 14143–14151. https://doi.org/10.1021/acssuschemeng.1c04281.
Zulkifley, M.A., Mustafa, M.M., Hussain, A., Mustapha, A., Ramli, S., 2014. Robust identification of polyethylene terephthalate (PET) plastics through Bayesian decision. PloS one 9, e114518. https://doi.org/10.1371/journal.pone.0114518.

3 Characterization methods

To answer RQ II, Chapter 3 aims to develop characterization methods for determining mass-based material flow compositions of post-consumer LWP material flows. By closing essential research gaps and utilizing existing research findings from Chapter 2, these characterization methods can enable novel SBMC applications (RQ III) in Chapter 4. As shown by Publication A (Section 2.1), a major challenge for SBMC applications is the determination of mass-based material flow compositions from pixel- or volume-based sensor data. In Chapter 3, two complementary approaches are pursued in this respect. In a particle-level approach (Sections 3.1 and 3.2), individual particle mass predictions are investigated, based on which pixel- or volume-based sensor data can be transformed into mass-based material flow compositions. In a material-flow-level approach (Sections 3.3 and 3.4), a direct transformation of pixel data to mass-based material flow compositions using data aggregation and regression models is investigated.

3.1 Publication B: imea

> **Kroell, N.** (2021). imea: A Python package for extracting 2D and 3D shape measurements from images. *Journal of Open Source Software*, *6*(60), 3091. https://doi.org/10.21105/joss.03091

The first essential step of the particle-level approach is the extraction of particle measurements from sensor data for subsequent particle mass prediction (Section 3.2). While a large number of particle descriptors has been proposed in scientific and technical literature (Deutsches Institut für Normung e. V., 2012; Pabst & Gregorova, 2007; Pahl et al., 1973a, 1973b, 1973c; Steuer, 2010), only a fraction of these are available in current software packages (e.g., *scikit-image* [van der Walt et al., 2014] or *opencv* [Itseez, 2015]). To close this gap and enable the development of particle mass prediction models in Publication C (Section 3.2), the *imea* Python package (Figure 3.1) was developed to automatically extract particle measurements from sensor data.

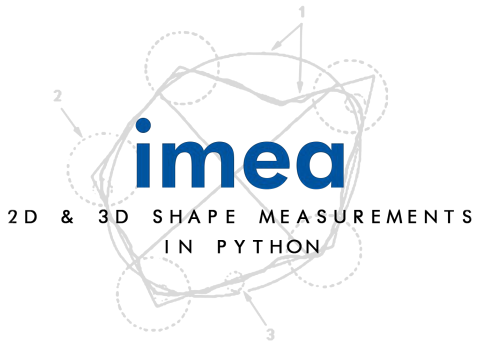

Figure 3.1. Graphical abstract Publication B.

The Journal of Open Source Software

imea: A Python package for extracting 2D and 3D shape measurements from images

Nils Kroell[1]

1 Department of Anthropogenic Material Cycles, RWTH Aachen University, Aachen, Germany

DOI: 10.21105/joss.03091

Software

- Review
- Repository
- Archive

Editor: Monica Bobra

Reviewers:

- @Atif-Anwer
- @tuelwer

Submitted: 27 February 2021
Published: 06 April 2021

Summary

Quantitative measurement of 2D and 3D shapes from images is used in many research fields, for example, chemistry (Lau et al., 2013), mineral engineering (Andersson et al., 2012), medicine (Nguyen & Rangayyan, 2005), biology (Smith et al., 1996), and environmental engineering (Kandlbauer et al., 2021; Weissenbach & Sarc, 2021). In the past, a variety of shape measurements have been proposed in the scientific literature and as technical norms (DIN ISO 9276-6, 2012; Pabst & Gregorova, 2007; Pahl et al., 1973a, 1973b, 1973c; Steuer, 2010).

`imea` is an open source Python package for extracting 2D and 3D shape measurements from images. The current version of `imea` enables the extraction of 53 different 2D shape measurements, covering *macrodescriptors* such as minimal bounding boxes (Steuer, 2010), *mesodescriptors* such as the numbers of erosion to erase a binary image (DIN ISO 9276-6, 2012), *microdescriptors* such as the fractal dimension (DIN ISO 9276-6, 2012), as well as *statistical lengths* like Feret, Martin or Nassenstein diameters (Pahl et al., 1973a), as shown by the exemplary selection in Figure 1. Furthermore, 13 different 3D shape measurements ranging from volume (Pahl et al., 1973a) and minimal 3D bounding boxes (Steuer, 2010) to 3D Feret diameters and maximum dimensions (Steuer, 2010) can be extracted.

Both 2D shapes, represented as 2D binary images, as well as 3D shapes, represented as grayscale images where the grayvalue of each pixel represents its height, can be analyzed automatically with a single function call. Extracted shape measurements are returned as a *pandas* dataframe (McKinney, 2010), and by specifying the spatial resolution of inserted images, results are automatically converted into metric units for further quantitative analysis.

Statement of need

Only a minority of 2D and 3D shape measurements proposed in the scientific literature and as technical norms are available in existing open source packages for image processing, such as *scikit-image* (van der Walt et al., 2014) and *OpenCV* (Itseez, 2015). In the past, unavailable shape measurements had to be implemented manually by individual researchers or could not be used at all. Moreover, the utilization of different existing packages for shape measurement extraction requires switching between different coordinate systems and data formats. Both cases create unnecessary "reinventing the wheel" and may induce potential calculation errors.

`imea` solves this problem by simplifying the extraction of 2D and 3D shape measurements from images into a single function call. Researchers can focus on the analysis and utilization of extracted shape measurements, while the shape measurement extraction is handled by `imea`. A computationally efficient implementation of underlying algorithms makes even complicated shape measurements available to a wide variety of researchers from different fields.

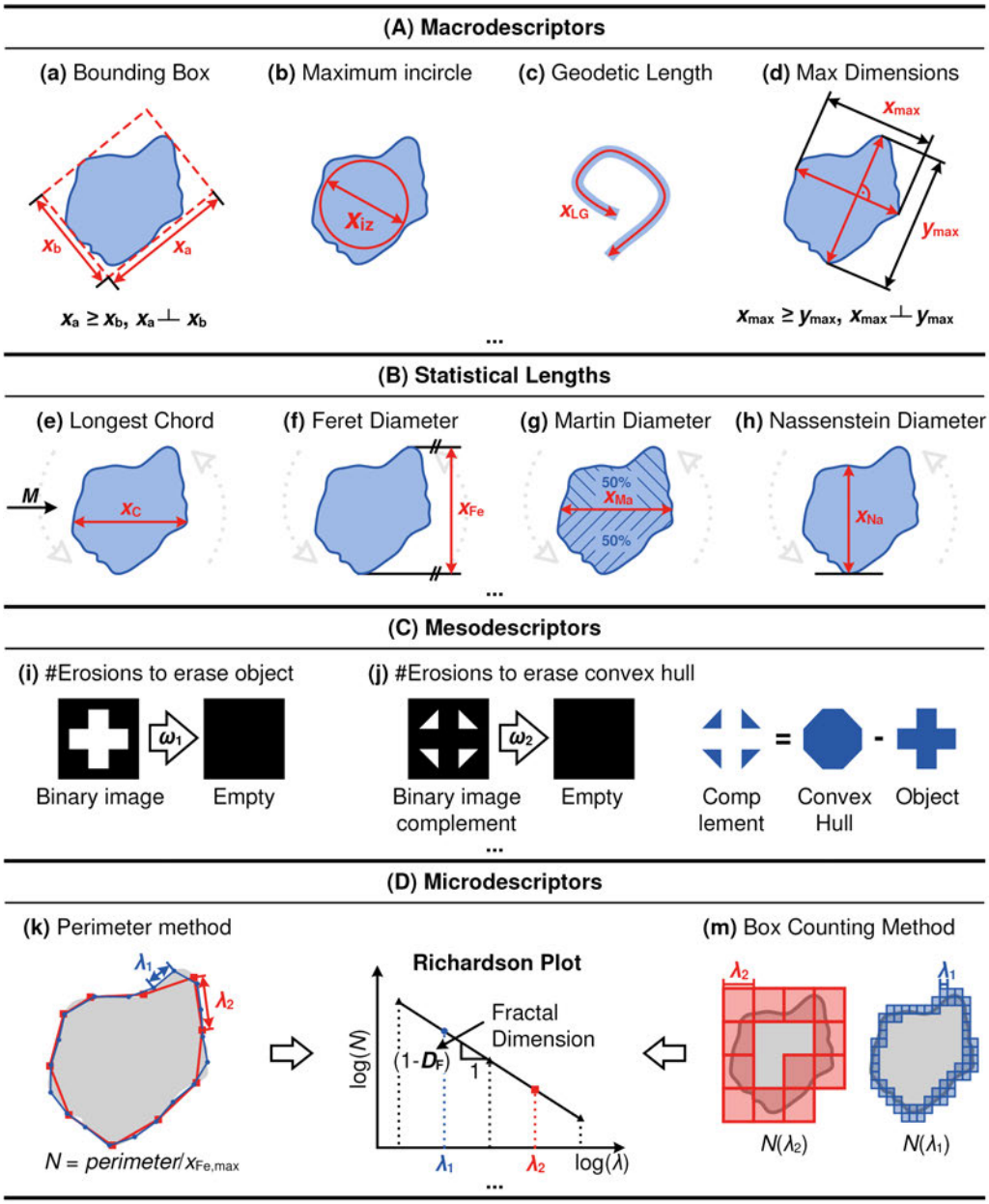

Figure 1: Exemplary selection of 2-dimensional shape measurements available in `imea`.

Acknowledgements

The development of `imea` was funded by the German Federal Ministry for Economic Affairs and Energy within the "Central Innovation Programme for small and medium-sized enterprises (SMEs)" under the project PROBE (grant no. 16KN080621) and the Austrian Research Promotion Agency within the programme "Production of the Future" under the project EsKorte (grant no. 877341).

References

Andersson, T., Thurley, M. J., & Carlson, J. E. (2012). A machine vision system for estimation of size distributions by weight of limestone particles. *Minerals Engineering*, *25*(1), 38–46. https://doi.org/10.1016/j.mineng.2011.10.001

DIN ISO 9276-6. (2012). *Darstellung der Ergebnisse von Partikelgrößenanalysen: Teil 6: Deskriptive und quantitative Darstellung der Form und Morphologie von Partikeln*. Deutsches Institut für Normung e.V. Beuth Verlag.

Itseez. (2015). *Open source computer vision library*. https://github.com/opencv/opencv.

Kandlbauer, L., Khodier, K., Ninevski, D., & Sarc, R. (2021). Sensor-based Particle Size Determination of Shredded Mixed Commercial Waste based on two-dimensional Images. *Waste Management*, *120*, 784–794. https://doi.org/10.1016/j.wasman.2020.11.003

Lau, Y. M., Deen, N. G., & Kuipers, J. A. M. (2013). Development of an image measurement technique for size distribution in dense bubbly flows. *Chemical Engineering Science*, *94*, 20–29. https://doi.org/10.1016/j.ces.2013.02.043

McKinney, Wes. (2010). Data Structures for Statistical Computing in Python. In Stéfan van der Walt & Jarrod Millman (Eds.), *Proceedings of the 9th Python in Science Conference* (pp. 56–61). https://doi.org/10.25080/Majora-92bf1922-00a

Nguyen, T. M., & Rangayyan, R. M. (2005). Shape analysis of breast masses in mammograms via the fractal dimension. *2005 IEEE Engineering in Medicine and Biology 27th Annual Conference*, 3210–3213. https://doi.org/10.1109/IEMBS.2005.1617159

Pabst, W., & Gregorova, E. (2007). *Characterization of particles and particle systems*. ICT: Prague.

Pahl, M., Schädel, G., & Rumpf, H. (1973a). Zusammenstellung von Teilchenformbeschreibungsmethoden: 1. Teil. *Aufbereitungstechnik*, *14*(5), 257–264.

Pahl, M., Schädel, G., & Rumpf, H. (1973b). Zusammenstellung von Teilchenformbeschreibungsmethoden: 2. Teil. *Aufbereitungstechnik*, *14*(10), 672–683.

Pahl, M., Schädel, G., & Rumpf, H. (1973c). Zusammenstellung von Teilchenformbeschreibungsmethoden: 3. Teil. *Aufbereitungstechnik*, *14*(11), 759–764.

Smith, T. G., Lange, G. D., & Marks, W. B. (1996). Fractal methods and results in cellular morphology — dimensions, lacunarity and multifractals. *Journal of Neuroscience Methods*, *69*(2), 123–136. https://doi.org/10.1016/s0165-0270(96)00080-5

Steuer, M. (2010). Serial classification. *AT Mineral Processing English Edition*, *51*(1), 2–8.

van der Walt, S., Schönberger, J. L., Nunez-Iglesias, J., Boulogne, F., Warner, J. D., Yager, N., Gouillart, E., & Yu, T. (2014). scikit-image: image processing in Python. *PeerJ*, *2*, e453. https://doi.org/10.7717/peerj.453

Weissenbach, T., & Sarc, R. (2021). Investigation of particle-specific characteristics of non-hazardous, fine shredded mixed waste. *Waste Management*, *119*, 162–171. https://doi.org/10.1016/j.wasman.2020.09.033

3.2 Publication C: Sensor-based particle mass prediction

> **Kroell**, **N.**, Chen, X., Maghmoumi, A., Koenig, M., Feil, A., & Greiff, K. (2021). Sensor-based particle mass prediction of lightweight packaging waste using machine learning algorithms. *Waste Management*, *136*, 253–265. https://doi.org/10.1016/j.wasman.2021.10.017

Based on particle descriptors extracted with the *imea* package (Publication B [Section 3.1]), a sensor-based particle mass prediction using ML based on 3D laser triangulation (3DLT) data is investigated in Publication C (Figure 3.2). The main motivation of Publication C was transferring sensor data to recycling-industry-relevant reference unit: As shown in Publication A, the material class of LWP particles can already be classified very precisely with, e.g., near-infrared (NIR) and state-of-the-art classification models on the acceleration bands on SBS units. However, the information is always only available on an area basis [a%] (e.g., with NIR sensors) or on a volume basis [vol%] (e.g., with 3DLT sensors), whereas material characterization in the recycling industry is always wanted mass-based [wt%] (cf. future research potential 6 in Publication A [Section 2.1]). Since individual particle masses cannot be measured inline, the goal of Publication C was to develop an ML model that can predict the mass of individual particles from area- or volume-based sensor data. By combining the existing classification models and the newly developed mass prediction model, mass-based material flow characteristics (MFCs) can be derived from the area- or volume-based sensor data. The sensor technology used here is 3DLT, since it can be used to simulate both 2D (e.g., NIR) and 3D sensors, and 3DLT sensors are already in large-scale use in SBS (e.g., STEINERT GmbH, 2023; TOMRA Systems ASA, 2023).

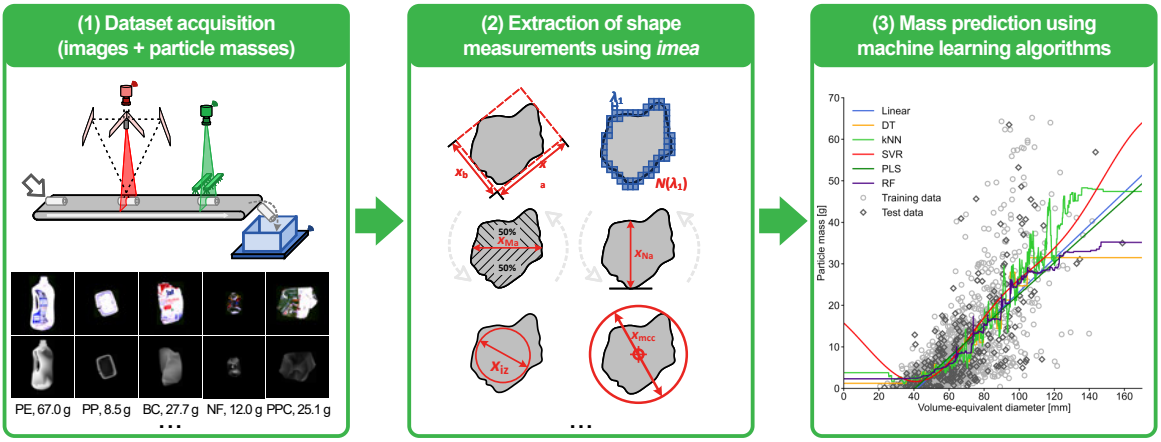

Figure 3.2. Graphical abstract Publication C.

Waste Management 136 (2021) 253–265

Contents lists available at ScienceDirect

Waste Management

journal homepage: www.elsevier.com/locate/wasman

Sensor-based particle mass prediction of lightweight packaging waste using machine learning algorithms

Nils Kroell *, Xiaozheng Chen, Abtin Maghmoumi, Morgane Koenig, Alexander Feil, Kathrin Greiff

Department of Anthropogenic Material Cycles, RWTH Aachen University, Germany

ARTICLE INFO

Keywords:
Sensor-based material flow characterization
Particle mass prediction
Lightweight packaging waste
3D laser triangulation
Machine learning
Shape measurements

ABSTRACT

Sensor-based material flow characterization (SBMC) promises to improve the performance of future-generation sorting plants by enabling new applications like automatic quality monitoring or process control. Prerequisite for this is the derivation of mass-based material flow characteristics from pixel-based sensor data, which requires known individual particle masses. Since particle masses cannot be measured inline, the prediction of particle masses of lightweight packaging (LWP) waste using machine learning (ML) algorithms is investigated. Five LWP material classes were sampled, preprocessed, and scanned on a custom-made test rig, resulting in a dataset containing 3D laser triangulation (3DLT) images, RGB images, and corresponding masses of $n = 3{,}830$ particles. Based on 66 extracted shape measurements, six ML models were trained for particle mass prediction (PMP). Their performance was compared with two state-of-the-art reference models using (i) material-specific mean particle masses and (ii) grammages. Obtained particle masses showed a high variation and significant differences between material classes and particle size classes. After feature selection, both reference models achieving R^2-scores of (i) 0.422 ± 0.121 and (ii) 0.533 ± 0.224 were outperformed by all investigated ML models. A random forest regressor with an R^2-score of 0.763 ± 0.091 and a normalized mean absolute error of 0.243 ± 0.050 achieved the most accurate PMP. In contrast to studies on primary raw materials, PMP of LWP waste is challenging due to influences of packaging design and post-consumer disposal behavior. ML algorithms are a promising approach for PMP that outperform state-of-the-art methods by 43% higher R^2-scores.

1. Introduction

1.1. Plastic packaging

In 2018, Europeans generated about 89.5 Mt/a of packaging waste (Eurostat, 2021). Among all packaging wastes, plastic packaging has occupied about 19 wt% (17.2 Mt/a) in 2018 and has risen from about 29.1 kg per capita in 2009 to about 33.5 kg per capita in 2018 (Eurostat, 2021). Member states of the European Union have developed collection and recycling systems for different packaging wastes with the aim of (a) avoiding unwanted leakage of packaging wastes into the environment, (b) reducing/avoiding landfill volumes, and (c) recycling of contained valuable materials to achieve environmental benefits (European Union, 2018; Ragaert et al., 2017); e.g., in terms of energy savings (Perugini et al., 2005) and reduced greenhouse gas emissions (Astrup et al., 2009).

Germany alone produced about 5.35 Mt/a of post-consumer plastic wastes in 2019; 59 wt% (3.16 Mt/a) of which was collected as lightweight packaging (LWP) waste together with metal and composite packaging materials (Conversio Market & Strategy GmbH, 2020). LWP waste is initially sorted by LWP sorting plants into material-specific preconcentrates and a remaining sorting residue (Feil and Pretz, 2020). Preconcentrates are then further refined into secondary raw materials by specialized recycling plants and re-enter the anthropogenic material cycle (Feil and Pretz, 2020).

Abbreviations: 3DLT, 3D laser triangulation; BC, beverage carton; CNN, convolutional neural network; DT, decision tree regressor; kNN, k-nearest neighbor regressor; LWP, lightweight packaging; MFC, material flow characteristic; ML, machine Learning; NF, non-ferrous metals; NIR, near-infrared; PCA, principal component analysis; PCC, Pearson correlation coefficient; PE, polyethylene; PLS, partial least squares; PMP, particle mass prediction; PP, polypropylene; PPC, paper and cardboard; PSC, particle size class; PSD, particle size distribution; RF, random forest regressor; RM, reference model; RQ, research question; SBMC, sensor-based material flow characterization; SCC, Spearman correlation coefficient; SRF, solid recovered fuel; SVR, support vector regressor.

* Corresponding author at: Department of Anthropogenic Material Cycles, RWTH Aachen University, Wüllnerstr. 2, D-52062 Aachen, Germany.
E-mail address: nils.kroell@ants.rwth-aachen.de (N. Kroell).

https://doi.org/10.1016/j.wasman.2021.10.017
Received 3 July 2021; Received in revised form 29 September 2021; Accepted 11 October 2021
Available online 26 October 2021

Despite all efforts devoted in the past, the current performance of plastic recycling remains unsatisfactory: From about 5.35 Mt/a collected post-consumer plastic waste in Germany, only about 19 wt% (1.02 Mt/a) could be converted into recyclates, and only about 8 wt% (0.43 Mt/a) was used to substitute virgin plastics (Conversio Market & Strategy GmbH, 2020). To increase the substitution of primary raw materials and the accompanying environmental benefits, substantial improvements of LWP sorting plants are necessary.

1.2. Concepts for future generation sorting plants

Scientific studies have proposed several improvements for LWP sorting plants in recent years. Suggested improvements range from optimized pre-conditioning (Küppers et al., 2019; Möllnitz et al., 2021) and material flow management (Feil et al., 2019); to the application of new sensor technologies such as mid-infrared (Rozenstein et al., 2017; Signoret et al., 2019a, 2019b), terra-hertz imaging (Küter et al., 2018), or laser-induced breakdown spectroscopy (Junjuri and Gundawar, 2020); the extension classification algorithms to new packaging materials such as bioplastics (Chen et al., 2021a; Moroni and Mei, 2020) or multilayer plastic packaging (Chen et al., 2021b; Chen et al., 2020); to new discharge principles such as robotic sorters (Chen et al., 2019; Lapusan et al., 2018; Papadakis et al., 2020).

Especially an integration and utilization of advanced sensors for automated process control and increased plant performance is shared as a research goal by many scientists (Curtis et al., 2021; Feil et al., 2019; Khodier et al., 2019; Sarc et al., 2019; Serranti et al., 2011; Vrancken et al., 2017). In the context of sensor-based material flow characterization (SBMC), suitable algorithms could extract process-relevant material flow characteristics (MFCs) from integrated sensors and existing sensor-based sorting equipment. Monitoring, e.g., volume flows, material compositions, and particle size distributions inline and in real-time with SBMC methods, would enable new applications such as (i) automatic quality control of product fractions, e.g., for quality-dependent price models or product quality certification; (ii) automatic process monitoring, e.g., to detect process anomalies and increase plant uptime; (iii) automatic inline-characterization of input streams, e.g., to monitor separate segregation efficiencies of different waste collection regions to inform the public or optimize public campaigns for improved separate collection; and (iv) gaining new process insights for improved design and development of future sorting plants.

However, the high innovation potential of SBMC methods stands in contrast to many unaddressed research problems that inhibit their implementation. One of the most critical problems, the conversion of pixel-based sensor measurements into mass-based MFCs, is addressed in this study.

1.3. Sensor-based particle mass prediction: from pixel to mass

Accurate conversion from pixel-based measurements to mass-based MFCs is of utmost importance for SBMC applications as acquired sensor images are represented in pixels. However, nearly all applications require MFCs related to masses, as the following examples show: (i) Product specifications for preconcentrates from LWP sorting plants define minimum purities in terms of *mass percentages* (Der Grüne Punkt, 2018). (ii) Process performance is assessed by *mass-based* indicators such as purity, yield, and recovery (Feil et al., 2016). (iii) According to (DIN EN 15415-1, 2011), particle size distributions are based on *particle masses*. (iv) The throughput of sorting machines and plants is evaluated in *tones per hour* (Küppers et al., 2020a; Küppers et al., 2020b).

To precisely extract mass-based MFCs from sensor images, it is essential to know the mass of the smallest elements in a material flow – particles. As an inline measurement of individual particle masses is technically infeasible in industrial-scale sorting plants, particle masses must be determined indirectly from other measurements. One approach is to predict individual particle masses from captured sensor images based on a reference dataset and corresponding machine learning (ML) algorithms which we summarize in the following as sensor-based particle mass prediction (PMP). In PMP, algorithms are trained on a reference dataset that contains particle images or other particle measurements and their corresponding masses, which can be acquired by weighting individual particles of a reference sample offline.

A key advantage of this approach is its independence from the type of applied sensors, as long as the applied sensors can represent the particles in sufficient spatial resolution in terms of a 2D binary image or a 3D heightmap. 2D binary images can, for example, be derived from hyperspectral, multispectral, RGB, or gray value images by segmenting the image into foreground (particles) and background (conveyor surface). Typical sensors already used in LWP sorting plants and can produce such images are, e.g., RGB cameras or near-infrared (NIR) sensors (Pellenc ST SAS, 2021; STEINERT GmbH, 2021; TOMRA Sorting GmbH, 2021). High-resolution 3D heightmaps can, for example, be obtained by 3D laser triangulation (3DLT) sensors which are already applied in industrial-scale sensor-based sorting (STEINERT GmbH, 2021; TOMRA Sorting GmbH, 2021) and waste management research (Feil et al., 2019).

Despite the utmost importance for SBMC applications (cf. Section 1.2), models for PMP have yet only been developed in the primary raw material industry (cf. Section 1.4), which cannot be directly transferred to post-consumer waste streams, as fundamental model assumptions such as (i) constant material densities, (ii) the absence of large hollow spaces, and (iii) limited shape complexity are violated. PMP of LWP waste seems especially challenging due to various packaging designs and post-consumer influences, e.g., folding or compression of packages during waste collection.

The aim of this study is thus to investigate the technical feasibility of sensor-based PMP for LWP wastes with frequently applied sensors in LWP sorting plants. The following research questions (RQs) shall be answered:

RQ 1: How much do particle masses of LWP wastes vary between different material and particle size classes? Which factors influence the distribution of particle masses and particle-specific grammages?

RQ 2: Which shape measurements are suitable for predicting particle masses? How significantly do they correlate?

RQ 3: How precisely can particle masses for LWP wastes be predicted? Which ML models achieve the most accurate prediction results, and how is the performance compared to state-of-the-art methods (e.g., mean particle weights or grammages)?

1.4. Related work

Prediction of particle masses from images has been researched in the primary raw material industry to convert number-based particle size distributions (PSDs) determined from images into mass-based PSDs, which requires a prediction of individual particle masses. In contrast, sensor-based PMP in waste management is still at an early stage.

1.4.1. Applications in the primary raw material industry

Existing studies have implemented PMPs by using mean particle masses per particle size class, predicting particle volumes with regression models, and estimating particle volumes by geometric bodies:

Andersson et al. (2012) presented a machine vision system for estimating mass-based PSDs for limestone. For weight transformation, a total of $n = 1{,}912$ particle weights was acquired. Across six trials, mass-based PSDs could be predicted with R^2 scores between 0.921 and 0.992 (mean: 0.965).

Zhang et al. (2012), Banta et al. (2003), and Vallebuona et al. (2003) investigated the prediction of particle volumes and masses from 2D images. After extracting several shape descriptors from 2D binary images, regression models were applied to establish a relationship between measured shape descriptors and mean particle heights or particle volumes. Based on the assumption of a constant material density, the

determined particle volumes were converted into particle masses with the achieved R^2-scores summarized in Table 1. Zhang (2015) classified coal particles based on color and texture features into seven density classes using a support vector machine. Using the predicted densities and the mass model from Zhang et al. (2012), mass-based density distributions were obtained.

Igathinathane and Ulusoy (2012) predicted volumes of coal particles in the particle size range from 0.038 mm to 1.7 mm. After determining particle lengths and widths from 2D binary images, the particle volume was approximated by the volume of a rotational ellipsoid with equal dimensions.

1.4.2. Applications in waste management

We are aware of four studies that partly address PMP for anthropogenic waste streams:

Krämer (2017) studied the distribution of particle weights, projection areas, and grammages in the context of solid recovered fuel (SRF) quality control. By investigating the distribution of $n = 3{,}171$ particles, it was found that both particle masses and projection areas follow a log-normal distribution.

Weissenbach and Sarc (2021) followed a similar approach and found log-normal distributions of projection areas and particle masses for $n =$ 12,100 particles from fine-shredded SRF (10 mm – 30 mm). In addition, a correlation between projection areas and particle masses was found with a Pearson correlation coefficient (*PCC*) of 0.57 on logarithmized data and a Spearman correlation coefficient (*SCC*) of 0.53 on the original data.

Kroell et al. (2021) created two datasets of particles from fine metal-rich waste streams containing RGB images and individual particle masses of $n = 12{,}480$ and $n = 19{,}498$ instances. The work already published describes the classification process (assigning material classes to the particles based on RGB images). Results of PMP from the captured RGB images are planned to be published in the near future.

Serranti et al. (2015) investigated the characterization of post-consumer polyolefin wastes with hyperspectral imaging for future quality control applications. To transform the pixel-based classification results into mass-based material compositions, they determined the mass of PE/PP-mixtures by multiplying projection areas with manually determined mean particle grammages.

While Krämer (2015), Weissenbach and Sarc (2021), and Kroell et al. (2021) created datasets that are necessary for PMP, the prediction of individual particle masses based on the acquired data has not been investigated. Serranti et al. (2015) used manually determined mean particle grammages for transforming area-based into mass-based compositions but did not investigate mass prediction on a particle level nor report prediction accuracies. To our best knowledge, *sensor-based PMP of anthropogenic waste streams* remains an open research gap that we will address in subsequent sections.

2. Material and methods

Firstly, LWP materials were sampled from an LWP sorting plant and preprocessed for subsequent acquisition steps to create a reference dataset for model training and evaluation. Secondly, samples were scanned particle by particle on a custom-made test rig. Thirdly, acquired sensor data was preprocessed to extract individual particles' features for subsequent model training and evaluation. Different models were then compared regarding their performance in predicting individual particle masses based on the acquired dataset.

Table 1
R^2 test scores of existing studies on particle volume and particle mass prediction using regression models; *excluding feature combinations.

Study	Material	Particle size [mm]	#Features*	#Instances	R^2-Score [–]
(Vallebuona et al., 2003)	Rocks	6–75	6	3,570	0.78
(Banta et al., 2003)	Limestone	4.75–25	4	1,900	0.91
(Zhang et al., 2012)	Coal	3–50	4	496	0.99

2.1. Sampling campaign and sample preparation

A sampling campaign was conducted in December 2020 at the LWP sorting plant Hündgen Entsorgungs GmbH & Co. KG (Swisttal, Germany). To investigate the PMP for a variety of different materials, the following five different material fractions were sampled: polyethylene (PE), polypropylene (PP), beverage cartons (BC), paper and cardboard (PPC), and non-ferrous metals (NF).

Each material fraction was sampled from the respective product fraction at the end of the sorting process. To ensure maximum representativity during sampling, the full material flow was sampled from a continuously falling waste stream according to LAGA PN 98 (2001). For each material fraction, a total volume of approx. 500 L was collected.

To avoid individual particle weight changes during the investigation, e.g., due to water evaporation, all samples were dried according to DIN EN 15934 (2012) for 48 h in a drying chamber at a temperature of 85 °C until weight constancy. After drying, all material classes were screened into four particle size fractions (0 mm – 60 mm, 60 mm – 120 mm, 120 mm – 240 mm, and > 240 mm) on a polygonal drum sieve with a diameter of 1.5 m, a length of 1 m and an angular velocity of 0.82 s^{-1} for a screen duration of 120 s. The sieve was operated in batch mode with a filling level of 10 vol% for maximum sieving efficiency (Feil and Pretz, 2017). Subsequent steps focused on the particle size classes 60 mm – 120 mm (PSC I) and 120 mm – 240 mm (PSC II), as these (a) accounted for $\gg$ 80 wt% of the investigated material flows and (b) are the target fractions of the sorting plant.

Dried and sieved fractions were then manually sorted based on recycling codes printed on the packages to generate pure fractions for building the reference dataset. For particles without recycling codes or if recycling codes could not be identified clearly, an NIR sensor was used for validation, described in detail in (Chen et al., 2021a). To maximize the number of acquired particles and dataset representativity, impurities in one material fraction were added to the corresponding correct material fraction. For example, if a BC particle was found in the PPC fraction, it was added to the BC fraction for data acquisition.

2.2. Test rig and data acquisition

Mass prediction models need a dataset of particle images and corresponding masses. Prior studies (Krämer, 2017; Weissenbach and Sarc, 2021) have solved this problem by using a photo box to acquire images and a separate digital balance to acquire weights. This approach has two main limitations. First, it is only suitable for area sensors (e.g., RGB cameras), while frequently applied sensors in sensor-based waste sorting (e.g., NIR or 3DLT) work as line scan sensors. Second, separately acquiring images and weights induces a potential error in matching images and particle masses. For example, Weissenbach and Sarc (2021) reported several mismatches or recording errors during an outlier analysis which had to be corrected or eliminated manually afterward.

To overcome these limitations, we propose a new test rig design that solves both problems, enables the data acquisition in an automated manner, and applies to all inline and area sensors. The developed test rig is shown in Fig. 1 and described in detail below.

2.2.1. Feeding

Particles were dispended on the conveyor belt one after another at a rate of approx. 7.5 s/particle to achieve a one-dimensional singulation on the conveyor belt for accurate mass determination. The black conveyor belt was 385 mm wide and had a belt speed of $v_{belt} = 0.15$ m/s.

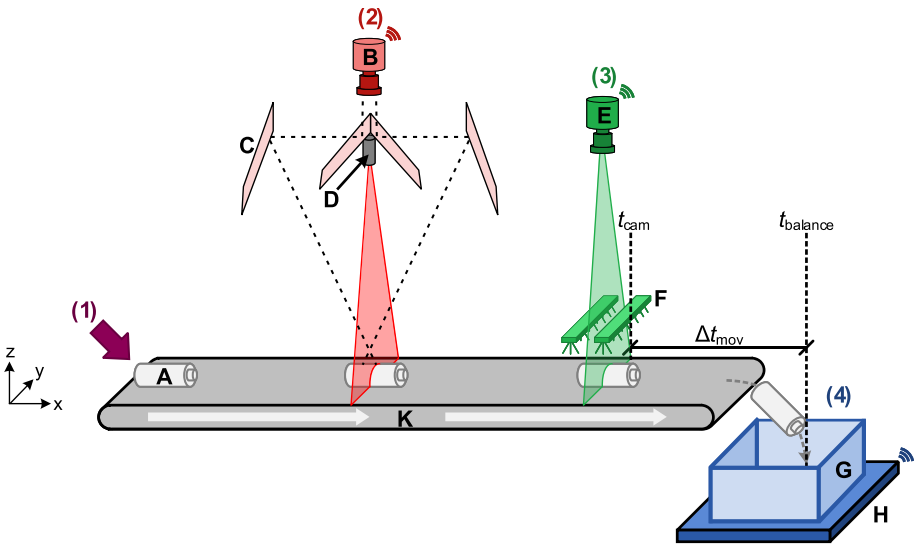

Fig. 1. Schematic sketch of the custom-made test rig for data acquisition; (1) Feeding, (2) 3D image acquisition, (3) RGB image acquisition, (4) weighing; A. particle, B. 3DLT camera, C. mirror, D. line laser, E. RGB camera, F. LED lighting, G. collecting vessel, H. digital balance, K. conveyor belt; *t*: time.

2.2.2. 3D image acquisition

A custom-made 3DLT measurement setup firstly recorded the 3D shape of a particle. A laser line was projected on the conveyor/particle surface and detected by a 3D camera (Automation Technology C3-1280-CL [Bad Oldesloe, Germany]) from two sides ("front" and "back") via a mirror setup (cf. Fig. 1-C). After merging and calibrating both camera views (cf. Section 2.3), the resulting 3D images had a spatial resolution of 0.331 mm per pixel in *x*- and *y*-direction and 0.758 mm per gray value in *z*-direction.

2.2.3. RGB image acquisition

Particles were then captured by an RGB line scan camera (IDS Imaging Development Systems UI-5240CP-C-HQ [Obersulm, Germany]). At the left and right side of the camera, three LED stripes each illuminate particles uniformly across the belt width as they pass through the camera capturing area (cf. Fig. 1-F). After preprocessing, the resulting RGB images had a spatial resolution of 0.286 mm per pixel.

2.2.4. Weighting

Particles fell into a collecting vessel on a digital weight balance (KERN & Sohn DS 30 K0.1L [Balingen, Germany]) with a precision of ± 0.1 g. The current weight from the balance was recorded every 125 ms for particle mass extraction in subsequent processing steps.

2.3. Dataset generation

The dataset was obtained by preprocessing and extracting images and particle masses as outlined below. Afterward, the dataset was manually examined, and outliers were removed for subsequent PMP.

2.3.1. Image preprocessing

3D images of the front and back recordings were preprocessed by (i) subtracting the background (conveyor surface) from both recordings, (ii) rescaling the images in *x*-direction to achieve "square" pixels ($dx = dy$), and (iii) transforming gray values representing the height in *z*-direction into metric values by applying a calibration function determined from a reference recording (calibration cylinders with $d = 60$ mm diameter at different heights $h_i \in \{10\,\text{mm}, 20\,\text{mm}, 30\,\text{mm}, \ldots, 120\,\text{mm}\}$). After initial preprocessing, front and back images are merged by taking the maximum value from both camera views to remove shading effects typical for 3DLT recordings. Similarly, RGB images were rescaled in *x*-direction to ensure "square" pixels ($dx = dy$).

2.3.2. Image extraction

Image sections showing the particles were extracted separately from both 3DLT and RGB images by (i) segmenting the image using thresholding (maximum intensity of R, G, or B channel > 0.12), (ii) improving the segmentation result with morphological filters, and (iii) extracting the image section based on found bounding boxes. Image preprocessing and extraction algorithms were implemented in *Python* 3.8 in a *scikit-image* v0.18.1 (van der Walt et al., 2014) and *NumPy* v1.20.0 (Harris et al., 2020) framework. Examples of extracted RGB and 3DLT images are shown in Fig. 3.

2.3.3. Particle mass extraction

Based on the timestamps of the RGB recordings, the timestamp t_{cam} showing a particle has passed the RGB camera is determined. After adding (i) the transportation time Δt_{mov} of a particle from the RGB camera to the collecting vessel incl. falling time (cf. Fig. 2), and (ii) an additional buffer time Δt_{buffer} until the weight display of the balance is stable, the displayed weight of the balance was automatically extracted at the calculated timepoint $t_{readout}$ (Eq. (1)).

$$t_{readout} = t_{cam} + \Delta t_{mov} + \Delta t_{buffer} \quad (1)$$

To make the mass extraction more robust, $n = 8$ data points were extracted in the interval $t_{readout} \pm 500$ms and the median of these eight data points were used for subsequent processing. Individual particle masses were extracted by differentiating the resulting cumulative particle mass distribution, as illustrated in Fig. 2.

2.3.4. Manual quality control and outlier removal

After automatically processing the acquired images, all recordings were manually checked to ensure the highest possible data quality. As black objects (e.g., black PE washing agent bottles) could not be appropriately segmented from the black conveyor belt (e.g., only brighter labels could be detected), they were manually removed from the dataset.

During data analysis, a few outliers that do not represent typical LWP objects were identified. Examples of non-representative objects include, e.g., filled plastic bottles, heavy non-packaging NF particles, and packaging materials containing interfering substances. These outliers massively disturbed model training due to overfitting and model evaluation due to the significant influence of individual outliers on the performance metrics (high particle masses). Such outliers have been removed with the interquartile range method (Vinutha et al., 2018) to

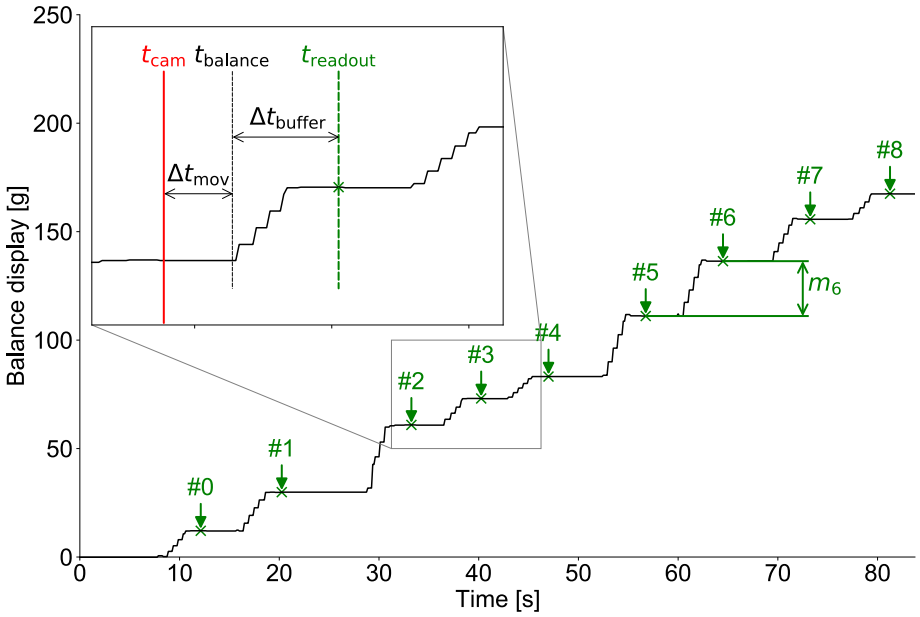

Fig. 2. Extraction of individual particle masses from the read-out balance weights; m_i: mass of particle i, t: time.

achieve high dataset representativity and enable sophisticated model training and evaluation. In total, 105 particles (59 PE, 8 PP, 10 BC, 18 PPC, and 10 NF particles; 2.7% of the overall dataset) were removed as outliers to obtain the final dataset. An exemplary selection of RGB and 3DLT images in the final dataset is shown in Fig. 3.

2.4. Feature extraction

In order to predict individual particle masses from sensor images, particle features were extracted from the images. In this study, two types of features are considered: Material classes and shape measurements.

2.4.1. Material classes

In addition to the size and shapes of particles (Section 2.4.2), particle masses are influenced by contained materials and their densities (Baur et al., 2013). Material classes of LWP particles can be determined with high accuracy by state-of-the-art NIR spectroscopy (Pellenc ST SAS, 2021; STEINERT GmbH, 2021; TOMRA Sorting GmbH, 2021) and are thus also available for inline SBMC applications and PMP. Consequently, the material class of each particle was encoded as a one-hot vector and added as a feature to the reference dataset for PMP.

2.4.2. Shape measurements

2D and 3D shape measurements were extracted from the calibrated 3D images of individual particles. For this purpose, the *imea* Python package v0.3.2 (Kroell, 2021) was used, which allows the extraction of 53 different 2D and 13 different 3D shape measurements from the acquired 3D images. Extracted shape measurements with a short description are summarized in Table 2. Besides, the PSC of each particle was recorded during data acquisition. Recorded PSCs were used for exploratory data analysis and visualization purposes, but not as a feature for model training, as they cannot be (directly) determined from sensor measurements.

2.5. Mass prediction models

PMP can be transferred to a regression problem. This paper uses regression models to predict a particle's mass (=model output) based on a feature vector containing the corresponding material class (encoded as one-hot-vector) and selected shape measurements (=model input).

2.5.1. Model implementation and training

As we present the first study on ML-based PMP for anthropogenic material flows, no prior experience is available on how different ML algorithms perform on this specific task. Furthermore, as stated by the *No Free Lunch Theorem* (Wolpert, 1996), there is no *a priori* best ML model for any prediction problem. Thus, we investigated six different ML algorithms in this first-of-a-kind study for PMP, with each of them using different modeling techniques (Hastie et al., 2009; Kubat, 2017). The investigated algorithms are summarized in Table 3, including the used model implementation from *scikit-learn* v0.24.1 (Pedregosa et al., 2011) and reference to further information about each model.

Since the shape dimensions extracted with *imea* (Kroell, 2021) are already in metric units, additional scaling or further preprocessing were omitted to avoid possible information losses. For each regression model, a systematic hyperparameter optimization (GridSearchCV) was performed using a 5-fold cross-validation.

2.5.2. Reference models

The trained regression models were then compared with two reference models (RMs). RM1 follows the mean particle mass approach of Andersson et al. (2012). For each material class, its mean particle mass was calculated from the training set, based on which the individual particle mass is predicted. Training of RM2 is based on the mean grammage of each material class by dividing the sum of all masses in this material class by all corresponding projection areas, as demonstrated by (Serranti et al., 2015). Accordingly, the mass prediction of an individual particle was calculated by multiplying its projection area by the mean grammage of its matching material class.

2.5.3. Model evaluation

After manual quality control and outlier removal (cf. Section 2.3.4), the obtained dataset was randomly split into a training dataset and a test dataset with a training-test-split-ratio of 80%:20%. Firstly, algorithms were trained on the training dataset. Secondly, the model performance was evaluated on the test dataset by comparing the model predictions (i.e., the predicted particle masses) with the ground truth (i.e., the known particle masses) using the R^2-*score* and *normalized mean absolute error* (*nMAE*) (Devore, 2012; Willmott and Matsuura, 2005). The *nMAE* describes the normalized differences between true mass and predicted mass of individual particles. Accurate predictions are indicated by low *nMAE* values, while the closer R^2 is to 1, the better the model prediction

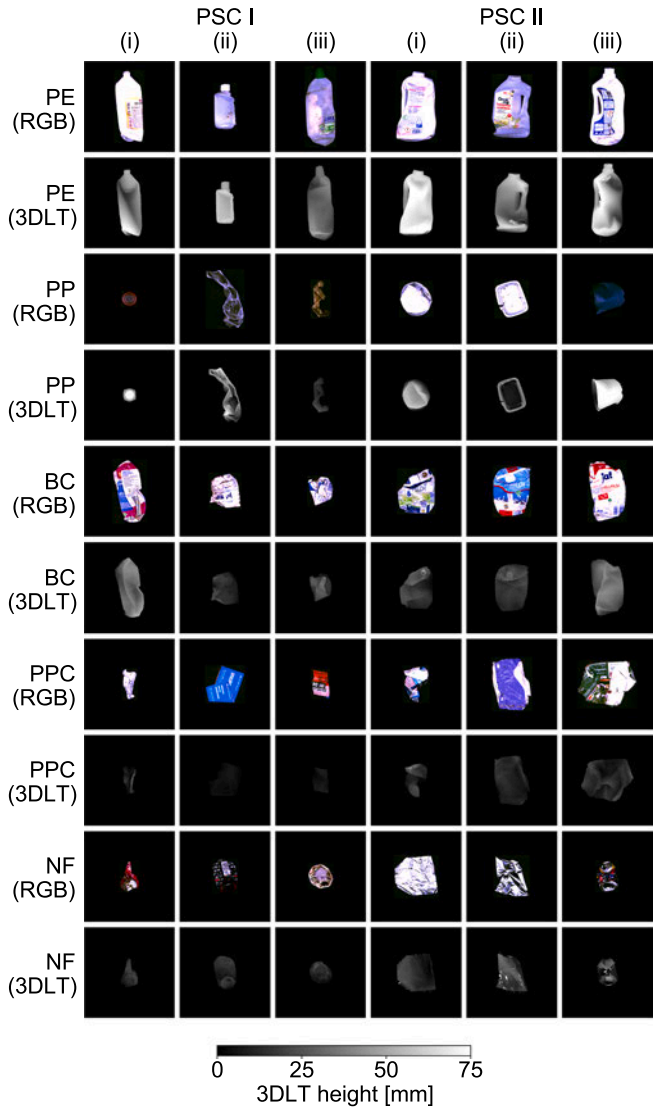

Fig. 3. Randomly selected example images in the acquired dataset; RGB: RGB image, 3DLT: Image from 3D laser triangulation.

is.

3. Results and discussion

The obtained LWP dataset contains n = 3,830 instances in total (Table 4). Due to the material-specific PSDs and particle volumes, the number of instances varies strongly between different material classes. Overall, more instances are contained in PSC I (n = 2,820) compared to PSC II (n = 1,010).

3.1. Distribution of particle masses, grammages, and densities

Particle masses of the n = 3,830 analyzed LWP particles (excluding outliers, cf. Section 2.3.4) range from 0.1 g to 65.4 g. The distribution of particle masses, grammages, and densities differs considerably between material and particle size classes.

3.1.1. Particle mass distribution across different material classes

As shown in Fig. 4a, particle masses vary significantly between the five investigated material classes with a p-value of p = 0.00, making the material class an important feature when predicting individual particle masses. Moreover, material-specific packaging designs strongly

Table 2
Extracted shape measurements using imea (Kroell, 2021).

Variable	Description	Unit
2D shape measurements (extracted from 2D binary image)		
perimeter	Perimeter	mm
convex_perimeter	Perimeter of the convex hull	mm
area_projection	Projection area	mm^2
area_filled	Filled projection area	mm^2
area_convex	Area of the convex hull	mm^2
major_axis_length, minor_axis_length	Major and minor axis length of the Legendre ellipse of inertia	mm
diameter_max_inclosing_circle	Diameter of maximum incircle of the projection area	mm
diameter_min_enclosing_circle	Diameter of minimum circumference of the projection area	mm
diameter_circumscribing_circle	Diameter of circumcircle with same center as particle contour and maximum area, which touches the particle contour from the inside	mm
diameter_inscribing_circle	Diameter of circumcircle with same center as particle contour and minimum area, which touches the particle contour from the outside	mm
diameter_equal_area	Diameter of a circle of equal projection area	mm
diameter_equal_perimeter	Diameter of a circle of equal perimeter	mm
x_max	Maximum longest chord	mm
y_max	Longest chord orthogonal to *y_max*	mm
length_min_bb, width_min_bb	Width and length of minimal 2D bounding box	mm
geodeticlength	Geodetic length	mm
thickness	Thickness according to (DIN ISO 9276-6, 2012)	mm
n_erosions	Number of pixel erosions to completely erase the silhouette of a particle in the binary image	px
n_erosions_complement	Number of pixel erosions to completely erase the complement between convex hull and object	px
fractal_dimension_boxcounting_method	Fractal dimension determined by the box-counting method	–
fractal_dimension_perimeter_method	Fractal dimension determined by the perimeter method according to (DIN ISO 9276-6, 2012) (evenly structured gait)	–
feret_{max, min, median, mean, mode, std}	Maximum, minimum, median, mean, mode, and standard deviation of Feret diameters	mm
martin_{max, min, median, mean, mode, std}	Maximum, minimum, median, mean, mode, and standard deviation of Martin diameters	mm
nassenstein_{max, min, median, mean, mode, std}	Maximum, minimum, median, mean, mode, and standard deviation of Nassenstein diameters	mm
maxchords_{max, min, median, mean, mode, std}	Maximum, minimum, median, mean, mode, and standard deviation of max chords (max chord = max of all chords for one particle rotation)	mm
allchords_{max, min, median, mean, mode, std}	Maximum, minimum, median, mean, mode, and standard deviation of all chords for all rotations	mm
3D shape measurements (extracted from 3D heightmap)		
volume	Volume	mm^3
volume_convexhull	Volume of convex hull	mm^3
surface_area	Surface area (determined by convex hull)	mm^2
diameter_volume_equivalent	Diameter of a volume-equivalent sphere	mm
diameter_surfacearea_equivalent		mm

(*continued on next page*)

Table 2 (*continued*)

Variable	Description	Unit
	Diameter of a sphere with the same surface area	
width_3d_bb, *length_3d_bb*, *height_3d_bb*	Width, length and height of minimal 3D bounding box (*width_3d_bb* ≤ *length_3d_bb*)	mm
feret_3d_{max, min}	Maximum and minimum 3D Feret diameter	mm
x_max_3d	Maximum particle dimension (equal to *feret_3d_max*)	mm
y_max_3d	Mean particle dimension (*y_max_3d* ≥ *x_max_3d*, *y_max_3d* orthogonal to *x_max_3d*)	mm
z_max_3d	Minimum particle dimension (*z_max_3d* ≤ *y_max_3d*, *z_max_3d* orthogonal to *y_max_3d* and *x_max_3d*)	mm

Table 3
Investigated regression models for PMP.

Abbreviation	Model	Implementation in *scikit-learn* (Pedregosa et al., 2011)	Reference
Linear	Linear regression	*linear_model.LinearRegression*	(Fahrmeir, 2013)
DT	Decision tree regressor	*tree.DecisionTreeRegressor*	(Grajski et al., 1986)
kNN	*k*-nearest neighbor regressor	*neighbors.KNeighborsRegressor*	(Altman, 1992)
SVR	Support vector regressor	*svm.SVR*	(Chang and Lin, 2011)
PLS	Partial least squares	*cross_decomposition.PLSRegression*	(Wold, 2005)
RF	Random forest regressor	*ensemble.RandomForestRegressor*	(Breiman, 2001)

Table 4
Number of instances *n* in the generated LWP dataset.

	PSC I		PSC II		∑	
	n	%	*n*	%	*n*	%
PE	203	7,2%	33	3,3%	236	6,2%
PP	259	9,2%	78	7,7%	337	8,8%
BC	769	27,3%	548	54,3%	1,317	34,4%
PPC	1,113	39,5%	317	31,4%	1,430	37,3%
NF	476	16,9%	34	3,4%	510	13,3%
∑	2,820	100,0%	1,010	100,0%	3,830	100,0%

influence mass distributions, and underlying raw material densities are of minor importance. For example, PE and PP have similar raw material densities (0.94 g cm^{-3} – 0.965 g cm^{-3} and 0.84 g cm^{-3} – 0.91 g cm^{-3}, respectively [Wypych, 2012]). However, PE particles found in the sampled LWP streams were, on average, more than twice as heavy as PP particles (30.2 g vs. 10.3 g in PSC I and 50.8 g vs. 24.6 g in PSC II, respectively), which can be traced back to different packaging applications of both polymers: While large and thus relatively heavier packages like detergent bottles and plastic containers are more frequently made of PE, smaller and lighter packages like yogurt or margarine cups are more frequently made of PP.

3.1.2. Particle mass distribution across different particle sizes classes

PE, PP, BC, and PPC particles from PSC II have significantly higher particle masses than PSC I ($p = 0.00$), and a correlation between particle masses and their projection area can be observed (cf. Fig. 4b and Section 3.2). In contrast, NF particles show similar particle masses ($p = 0.48$) in PSC I (12.55 g) and PSC II (11.27 g), despite particles of PSC II being larger (Fig. 4b). The possible reason is the accumulation of specific lighter 2D packaging like aluminum foils in PSC II, compared to heavier 3D packaging like aluminum cans or cat food containers in PSC I (Fig. 4c).

3.1.3. Grammages and densities

For the material classes PE, PP, BC, and NF, a decrease of grammages (particle mass divided by projection area) and 3DLT densities (particle mass divided by 3DLT volume) for larger particle sizes can be observed (Fig. 4b and c). Lower grammages and 3DLT densities for larger particle sizes can be explained by a lower ratio of packaging material to hollow spaces for larger packages. In contrast, the grammage of PPC particles increases with the particle size from 7.44 g dm^{-2} (PSC I) to 10.07 g dm^{-2} (PSC II) ($p = 0.00$). This effect is most likely explained by a higher share of cardboards in PSC II with higher grammages compared to thinner paper particles in PSC I. As PPC particles have fewer hollow spaces compared to other investigated material classes, their 3DLT densities are similar ($p = 0.55$) in PSC I (54.52 g dm^{-3}) and PSC II (56.12 g dm^{-3}).

3.2. Correlation and feature importance of shape measurements

After identifying material classes as a relevant feature for PMP in Section 3.1, relevant shape measurements for PMP are identified in the following section. Furthermore, their relative feature importance will be studied to extract optimal feature sets for subsequent PMP in Section 3.3.

3.2.1. Correlation between shape measurements and particle masses

Fig. 5a shows the correlation between each of the 66 shape measurements (Kroell, 2021) and particle masses determined by the *PCC* (Pearson, 1895) and *SCC* (Spearman, 1961). Interpreting the *SCC* according to Mukaka (2012), several shape measurements show high ($n = 2$), moderate ($n = 37$), or low ($n = 18$) positive correlation coefficients, which are thus suitable for PMP. The correlation of $n = 7$ features is negligible, and $n = 2$ features correlate negatively with the particle mass (cf. Fig. 5a).

Over all material classes, the *volume-equivalent diameter* (*SCC* = 0.71, *PCC* = 0.70) and the *3DLT volume* (*SCC* = 0.71, *PCC* = 0.65) show the highest correlation with the corresponding particle masses. The correlation between the 2D projection area and the particle mass for the LWP dataset is with an *SCC* of 0.64, slightly higher than the *SCC* of 0.53 reported by Weissenbach and Sarc (2021) for fine shredded mixed waste.

In accordance with Section 3.1.1, considerable differences can be observed between different material classes. Over all shape measurements, PE particles ($SCC_{mean} = 0.74$) show the highest correlation, followed by PPC (0.47), PP (0.46), and BC (0.41). NF particles show low correlation values (0.15), probably due to the high variation of particle weights for different 2D and 3D packaging types, as described in Section 3.1.

3.2.2. Feature importance

As shown for an exemplary shape measurement selection in Fig. 5b, most shape measurements correlate strongly with each other. For example, an *SCC* of 0.83 can be observed between the 2D surface area and the 3DLT volume. Moreover, different statistical lengths correlate significantly with each other with *SCC* values between 0.69 and 0.95.

Applying a principal component analysis (PCA) supports this finding, as 94.8% of the variance can be explained by one principal component (*pc0*) (Fig. 5c) and all positive correlating shape measurements contribute to *pc0* (Fig. 5a). The high correlation between shape measurements (Fig. 5b) and the high explained variance of *pc0* (Fig. 5c) lead to the question if a combination of multiple shape measurements in terms of *pc0* can improve the correlation between extracted features (*pc0*) and particle masses and thus PMP. However, analyzing the relation between *pc0* and corresponding particle masses (Fig. 5d) did not reveal improved correlation values (*SCC* = 0.63, *PCC* = 0.51). For the

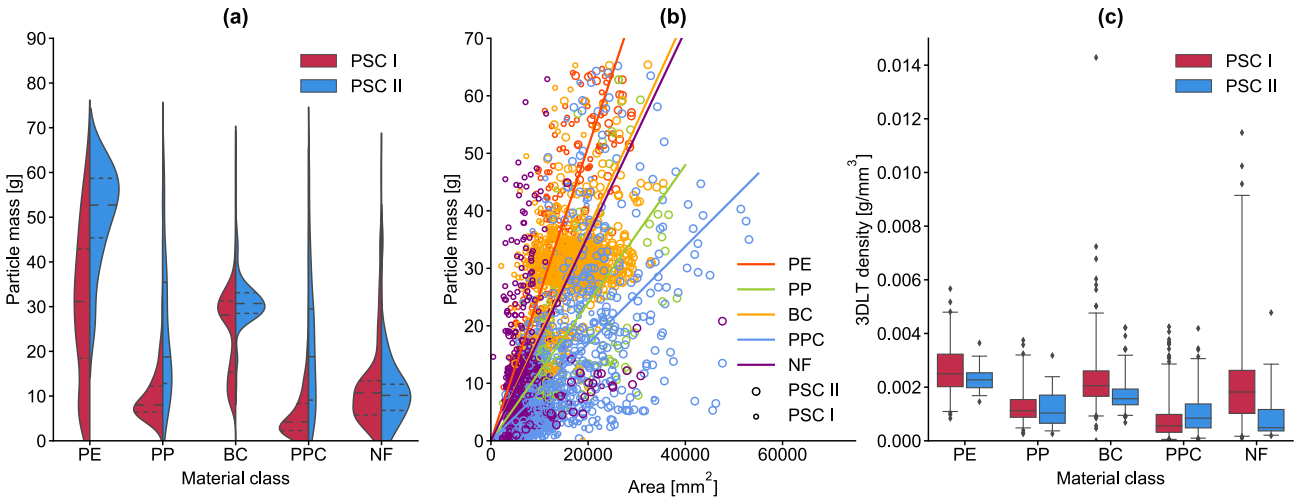

Fig. 4. Distribution of particle masses, grammages, and densities in the obtained dataset. (a) Distribution of particle masses by material and particle size class; (b) relation between particle masses and projection area; (c) distribution of 3DLT densities by material and particle size class; box: 25% and 75% percentile, whisker: 1% and 99% percentile, middle line: median.

investigated dataset, PMP based on individual shape measurements is thus an advantageous approach compared to using principal components as features.

3.3. Comparison of PMP models

3.3.1. Feature selection

Due to the high correlation between shape measurements described in Section 3.2.2, selecting a subset of features for training PMP models could be suitable for reducing computational costs or improving model performance (Marsland, 2015). However, manual feature selection may introduce subjective biases, and testing *all* possible feature combinations ($n = 7.38 \cdot 10^{19}$) is practically infeasible.

To address this problem, we sorted the 66 shape measurements in descending order by the *SCC* values (cf. Fig. 5a) and obtained 66 feature sets by including the first n features for the n-th data set, respectively. A systematic hyperparameter optimization was then performed for each feature combination and model, resulting in a total of $n = 690{,}030$ trained models.

3.3.2. Performance evaluation of PMP models

The achieved *nMAE* values (mean over five cross-validations) of the hyperparameter-optimized models for each feature set are shown in Fig. 6a. Best-performing PMP models over all feature sets and their hyperparameters are summarized in Table 5.

Given an appropriate feature set, both reference models were outperformed by all ML models with *nMAE* values between 0.303 ± 0.061 (SVR) and 0.243 ± 0.050 (RF), see Fig. 6a. Over all feature sets, the best PMP was achieved with random forests models followed by decision trees (Fig. 6a). Since random forests are an ensemble of decision trees, this suggests that the hierarchical decision structure and feature selection mechanism of decision trees may be advantageous for PMP. The overall best found PMP model is a random forest regression model based on 40 shape measurements achieving an *nMAE* of 0.243 ± 0.050 and an R^2-score of 0.763 ± 0.091.

Looking closer at Fig. 6a, two groups of ML models can be identified: For the SVR and kNN-models, best predictions were achieved with a low number of features ($n = 1$ for kNN and $n = 2$ for SVR), and adding new features decreased the kNN and SVR model performance. For other ML models (linear regression, DT, RF, and PLS), the prediction accuracy increases with added features. A possible explanation for this could be that DT, RF, and PLS models can suppress irrelevant features (Hastie et al., 2009; Marsland, 2015) and benefit from more (potentially relevant) features. As other algorithms (e.g., kNN) are less capable of suppressing irrelevant features, their prediction performance may thus have decreased due to higher noise in the training data or higher feature dimensionality (Kubat, 2017).

Furthermore, the prediction accuracy of the best-performing models reaches a saturation after about three to six included features, and most ML models did not benefit from larger feature vectors. An explanation for this could be the strong correlation and similarity between different shape measurements (cf. Fig. 5b).

Selecting an optimal feature set is crucial for real-time SBMC applications in order to (a) meet time limits in real-time applications (#PMPs per second) and (b) ensure precise model predictions. Different feature selection algorithms that could help to identify optimal feature sets for real-time SBMC applications have been proposed in the scientific literature (Karagiannopoulos et al., 2007). To reach a given time limit, not only the computational costs for model predictions but also the extraction of shape measurements as features from the 3DLT images should be considered. For example, while some shape measurements can be extracted relatively efficiently (e.g., projection areas), other shape measurements require computational intensive operations (e.g., multiple image rotations to calculate statistical lengths).

3.3.3. Learning curves and validation

Studying the predictions of the best-performing PMP models in more detail (Fig. 6b) shows that the masses of PE particles were most challenging to predict. As the prediction accuracy is both influenced by the training set size (Table 4) and feature correlation (Fig. 5), it cannot be identified how both factors interact with each other. For instance, PE particles are the least frequent material class in the LWP dataset ($n = 236$ PE instances of $n = 3{,}830$ instances in total; Table 4) but showed the highest correlation with the particle mass (Fig. 5).

To study the influence of the dataset size independent from material-specific influences, we artificially limited the training set size by training the best-performing models (Table 5) with random subsets of the original training dataset. As expected, the model performance increases with the number of training instances given to the algorithms (Fig. 6c), and typical learning curves (Mukherjee et al., 2003) can be observed. While the reference models converge quickly after a few hundred training instances, most ML algorithms converge significantly later after a few thousand training instances. Moreover, the learning curves of different ML algorithms vary significantly. For example, increasing the training set size from $n = 100$ instances to $n = 3{,}000$ instances for the SVR model results in a reduction of *nMAE* from 0.356 to 0.302 (-15%) compared to a

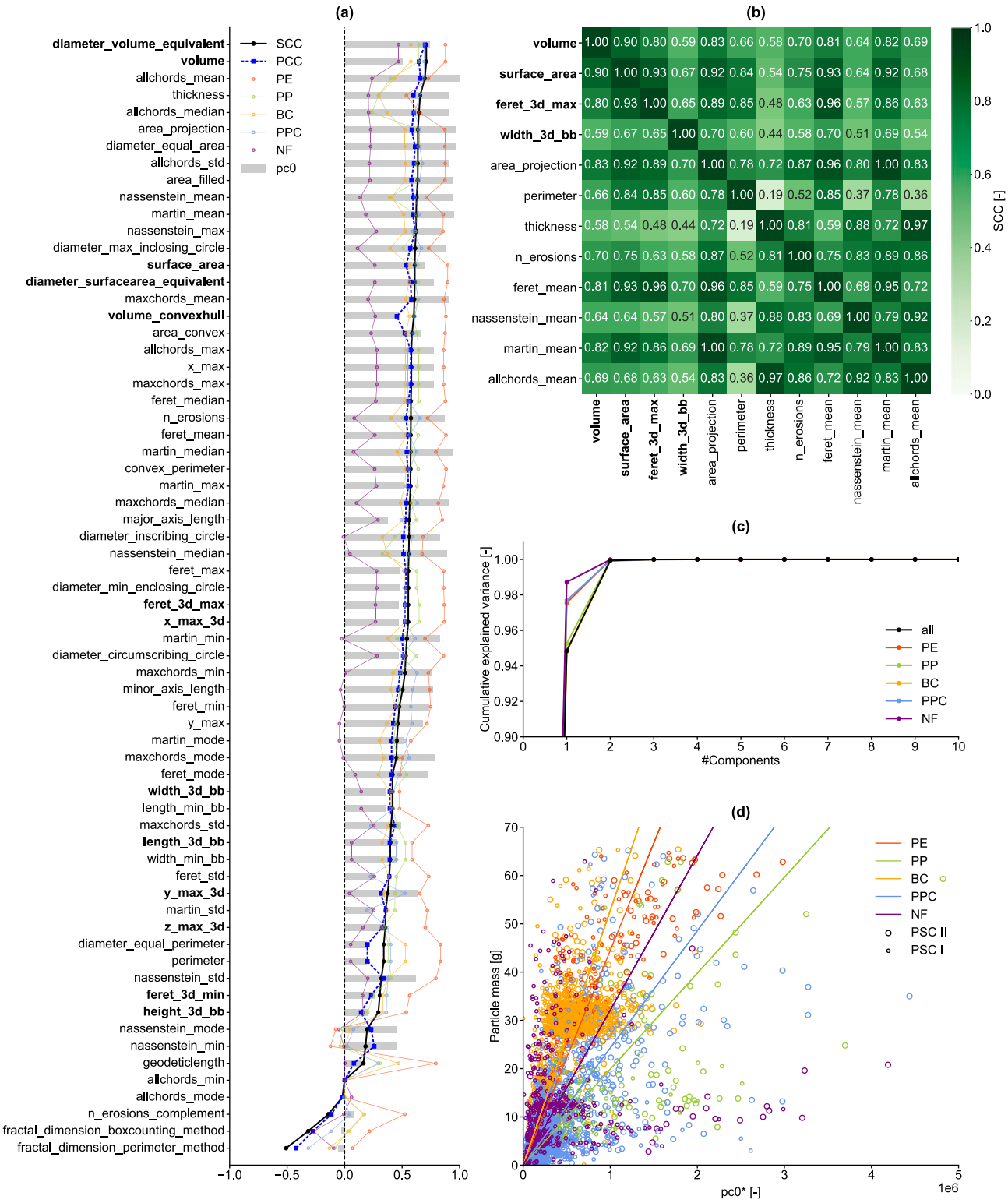

Fig. 5. Feature importance of shape measurements and correlation with particle masses. (a) Correlation between shape measurements and particle masses and components of first principal component (*pc0*); (b) correlation between selected shape measurements; (c) cumulative explained variance through PCA; (d) visualization of *pc0* and corresponding particle masses; * *pc0* is shifted to positive values for visualization purposes; bold font-weight: 3D shape measurements, normal font-weight: 2D shape measurements.

reduction from 0.403 to 0.260 (-35%) for the DT model. Extrapolating the results from Fig. 6c suggests that the model performance may be increased further by extending the LWP dataset, i.e., adding more training instances.

An exemplary plot of the resulting regression functions in Fig. 6d shows that all six ML models can generate reasonable PMP. For visualization purposes, the hyperparameter-optimized models are shown for one feature (volume-equivalent diameter) and one material class (PPC). The high variation of particle masses for similar shape measurements illustrates the challenge of accurate PMP for LWP wastes.

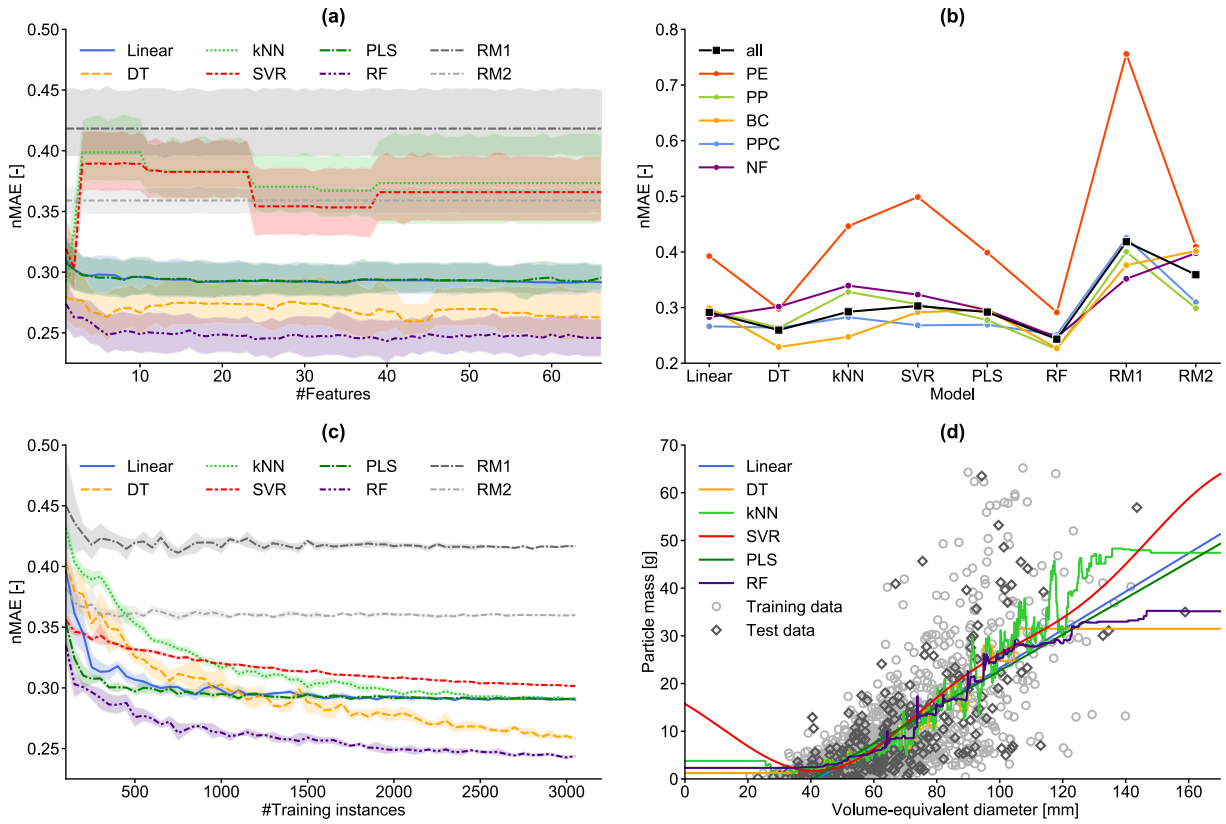

Fig. 6. Comparison of PMP models. (a) Prediction accuracy (*nMAE*) of hyperparameter-optimized PMP models with respect to the number of given features (in ascending *SCC*-order according to Fig. 5a); (b) mean *nMAE* of best-performing PMP models per material class; (c) prediction accuracy (*nMAE*) of best performing PMP models with respect to the number of given training instances; (d) regression functions of different hyperparameter-optimized PMP models for predicting particle masses based on material classes (one-hot-vector) and best correlating shape measurement (volume-equivalent diameter) exemplary shown for the material class PPC; colored regions: 95% confidence interval.

Table 5
Best found PMP models after systematic hyperparameter optimization and feature selection (cf. Fig. 5a); *not listed hyperparameters are default values of *scikit-learn* v0.24.1 (Pedregosa et al., 2011).

Model	*nMAE* [–]	R^2 [–]	#Features	Hyperparameters*
RF	0.243 ± 0.050	0.763 ± 0.091	40	*max_depth* = 10 *min_samples_leaf* = 2 *n_estimators* = 110
DT	0.260 ± 0.038	0.722 ± 0.051	43	*max_depth* = 6 *min_samples_leaf* = 17
Linear	0.291 ± 0.039	0.724 ± 0.064	35	–
PLS	0.292 ± 0.043	0.718 ± 0.069	17	*n_components* = 19
kNN	0.292 ± 0.069	0.682 ± 0.101	1	*n_neighbors* = 15
SVR	0.303 ± 0.061	0.654 ± 0.074	2	*C* = 50.0 *epsilon* = 0.333
RM2	0.359 ± 0.032	0.533 ± 0.224	1	–
RM1	0.418 ± 0.084	0.422 ± 0.121	0	–

3.4. Discussion

3.4.1. Comparison with reference models

Comparing our best-performing ML model with the two state-of-the-art approaches (RM1 and RM2) in Fig. 7, it can be seen that the RF model achieves significantly better predictions compared to RM1 and RM2. Predicting material-specific mean particle mass (RM1) achieved *nMAE* values of 0.418 ± 0.084 and R^2 scores of 0.422 ± 0.121. As shown in Fig. 7a, the high variance of particle weights and shape measurements in the LWP dataset can only insufficiently be modeled by RM1.

Using mean, material-specific grammages (RM2), the prediction accuracies are improved (*nMAE* = 0.359 ± 0.032, R^2 = 0.533 ± 0.224) as different particle sizes (modeled by the 2D projection area) can be considered (Fig. 7b). Nevertheless, the model still gets confused by varying grammages, e.g., beverage cartons with a high variation of projection areas but similar weights (orange dots; Fig. 7b), and is unable to cope with outliers as shown, e.g., by the overestimation of large NF particles (purple dots in lower right corner; Fig. 7b).

In contrast, the best-performing ML model (Fig. 7c) allows decent PMP, sophisticatedly handles outliers, and outperforms the best reference model (RM2) by 43.2% higher R^2-score and a 32.3% lower *nMAE*. However, when assessing model performance, it has to be considered that in this first-of-a-kind study, only five material classes (PE, PP, BC, NF, PPC) and the particle size range 60 mm – 240 mm (PSC I and PSC II) was analyzed and outliers, as well as black particles, were removed beforehand using the interquartile range method (cf. Section 2.3.4).

3.4.2. Comparison with mono-material PMP models for primary raw materials

Comparing our best-performing models (Table 5) to mono-material PMP models for primary raw materials (cf. Table 1, Section 1.4.1) shows that these studies used significantly fewer shape measurements. For example, the final models of Banta et al. (2003) and Zhang et al. (2012) contain $n = 4$ shape measurements, and Vallebuona et al. (2003) used $n = 6$ shape measurements in their final model (excluding combinations). In contrast, our top 3 best performing models (RF, DT, linear regression) used between $n = 35$ and $n = 43$ shape measurements.

Furthermore, existing studies focussing on primary raw materials (Banta et al., 2003; Vallebuona et al., 2003; Zhang et al., 2012) used multiple linear regression models, while we identified a better performance of tree-based regression models for our LWP dataset. A direct

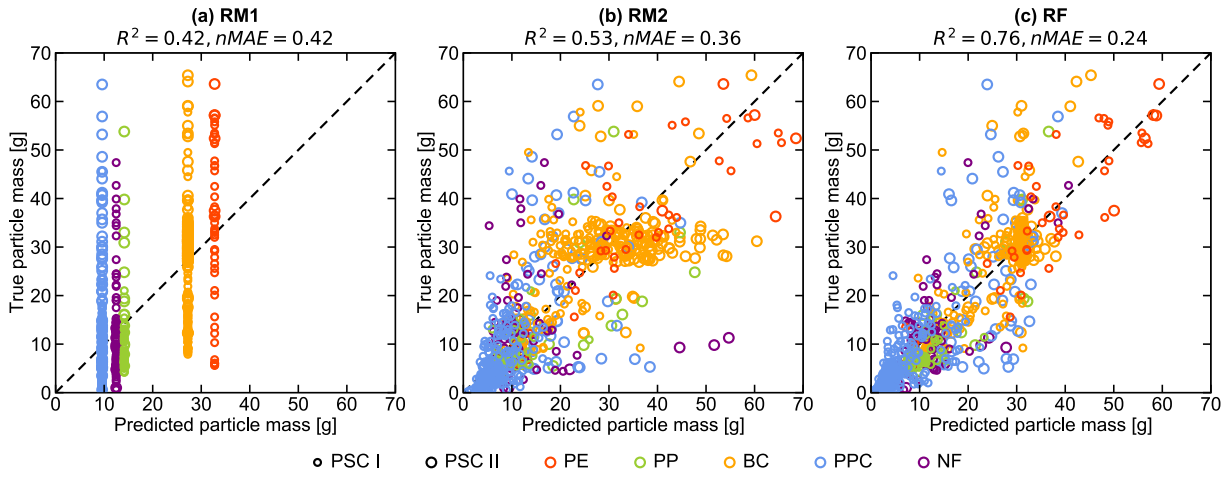

Fig. 7. Predicted and true particle masses for PMP using (a) material-specific mean particle masses (RM1), (b) material-specific mean grammages (RM2), and (c) hyperparameter-optimized random forest regression model (RF).

comparison between the prediction accuracies between rock (Vallebuona et al., 2003), limestone (Banta et al., 2003), and coal (Zhang et al., 2012) particles investigated in prior studies and the LWP particles in this study is (despite similar datasets sizes) difficult, as our LWP dataset contains five different material classes, while all prior PMP have studied mono-materials. Furthermore, our study focused on the particle size range 60 mm –240 mm compared to the particle size range of 3 mm – 75 mm in prior studies on primary raw materials.

Nevertheless, when comparing our best-performing linear regression model to the linear regression models of (Banta et al., 2003; Vallebuona et al., 2003; Zhang et al., 2012), it can be seen that the obtained R^2-score of 0.724 ± 0.064 is in a similar magnitude yet lower than those of mono-material studies (0.78 – 0.99; cf. Table 1). The lower R^2-score can most likely be explained by the higher complexity (e.g., post-consumer effects, LWP specific material design) in the LWP dataset as previously outlined. In addition to extending PMP to waste materials, we have shown that PMP can be improved by, e.g., applying tree-based regression models. Our overall best performing PMP model (RF) reaches similar R^2-scores to those of (Vallebuona et al., 2003). In the future, it would thus be interesting to compare different PMP models on different datasets to find out to which extend these findings are transferable to other datasets.

4. Conclusions and outlook

SBMC is an upcoming research topic based on which new applications like automatic quality control, process control, and material input characterization are envisioned. Monitoring mass-based MFCs requires knowledge about individual particle masses which can be predicted from sensor-based acquired images. Sensor-based PMP has yet only been investigated for primary raw materials. It was transferred to secondary raw materials on the example of LWP waste in the paper at hand: Based on a created dataset containing 3DLT and RGB images of $n = 3{,}830$ LWP particles, the technical feasibility of PMP for LWP wastes was demonstrated.

Analyzing the obtained dataset showed that particle masses vary significantly between different material classes. Distributions of masses and grammages are primarily influenced by the packaging design (e.g., size, shape, and material thicknesses) and post-consumer characteristics (e.g., folding or compression of packaging material during waste collection). Except for PPC, grammages generally decrease with increasing particle sizes due to a larger share of hollow spaces.

Over all material classes, 39 of 66 investigated shape measurements show moderate to high positive correlation coefficients ($SCC \geq 0.50$). The volume-equivalent diameter correlates best with the particle masses ($SCC = 0.71$, $PCC = 0.70$). Furthermore, shape measurements correlate strongly with each other, and 94.8% of their variance can be explained by one principal component.

Both reference models for PMP were outperformed by hyperparameter-optimized ML models when selecting an appropriate feature set. Tree-based regression algorithms (DT and RF) achieved better predictions for the investigated dataset than other regression methods (linear regression, kNN, SVR, and PLS). Better-performing PMP models generally used more shape measurements and were better at suppressing irrelevant features or instances. However, after about three to six included features, no significant increase in the prediction accuracy was observed. A random forest regressor was identified as the best-performing ML model based on 40 shape measurements achieving an $nMAE = 0.243 \pm 0.050$ and an R^2-score of 0.763 ± 0.091.

In future research, PMP could be extended to other LWP material classes (e.g., mixed plastic, plastic foils, ferrous metals, and residual fractions) or other material flows (e.g., metal concentrates or construction & demolition wastes). Moreover, information from other sensors (e.g., near-infrared) could be used to determine the material composition for individual particles, which could be used as an additional feature for PMP. Furthermore, we plan to apply artificial neural networks to the PMP problem, as their ability to detect and model complex nonlinear relationships could be advantageous for more precise PMP. In addition, we intend to use convolutional neural networks (CNNs) that would not be limited by the creativity of human researchers in inventing or selecting shape measurements. CNNs could potentially be able to identify more complex and potentially more relevant features directly from RGB or 3DLT images in the LWP dataset, since the weights in the convolutional layers required for feature extraction can be optimized by the model itself during the training phase.

CRediT authorship contribution statement

Nils Kroell: Conceptualization, Methodology, Software, Validation, Formal analysis, Investigation, Data curation, Writing – original draft, Writing – review & editing, Visualization, Project administration. **Xiaozheng Chen:** Conceptualization, Methodology, Software, Funding acquisition, Writing – review & editing. **Abtin Maghmoumi:** Software, Investigation, Data curation, Writing – review & editing, Visualization. **Morgane Koenig:** Validation, Investigation, Data curation, Writing – review & editing. **Alexander Feil:** Supervision, Funding acquisition, Writing – review & editing. **Kathrin Greiff:** Supervision, Writing – review & editing.

Declaration of Competing Interest

The authors declare that they have no known competing financial interests or personal relationships that could have appeared to influence the work reported in this paper.

Acknowledgments

We would like to thank Christian Hündgen and Frank Arleth from Hündgen Entsorgungs GmbH & Co. KG (Swisttal, Germany) for giving us access to their LWP sorting plant for the sampling campaign as well as for providing the LWP samples used in this study.

Funding

This work was supported by the National Austrian Research Promotion Agency (FFG) within the program “Production of the Future” under the project EsKorte (grant no. 877341) and the German Federal Ministry of Education and Research (BMBF) within the program "Resource-efficient circular economy - plastics recycling technologies (KuRT)" under the project ReVise (grant no. 033R341).

References

Altman, N.S., 1992. An introduction to kernel and nearest-neighbor nonparametric regression. The American Statistician 46, 175–185. https://doi.org/10.1080/00031305.1992.10475879.

Andersson, T., Thurley, M.J., Carlson, J.E., 2012. A machine vision system for estimation of size distributions by weight of limestone particles. Minerals Engineering 25, 38–46. https://doi.org/10.1016/j.mineng.2011.10.001.

Astrup, T., Fruergaard, T., Christensen, T.H., 2009. Recycling of plastic: accounting of greenhouse gases and global warming contributions. Waste management & research 27, 763–772. https://doi.org/10.1177/0734242X09345868.

Banta, L., Cheng, K., Zaniewski, J., 2003. Estimation of limestone particle mass from 2D images. Powder Technology 132, 184–189. https://doi.org/10.1016/S0032-5910(03)00061-5.

Baur, E., Osswald, T.A., Rudolph, N., Brinkmann, S., Schmachtenberg, E., 2013. Saechtling Kunststoff Taschenbuch. Carl Hanser Verlag GmbH & Co, KG, München.

Breiman, L., 2001. Random Forests. Machine Learning 45, 5–32. https://doi.org/10.1023/A:1010933404324.

Chang, C.-C., Lin, C.-J., 2011. LIBSVM: A library for support vector machines. ACM Transactions on Intelligent Systems and Technology 2, 1–27. https://doi.org/10.1145/1961189.1961199.

Chen, H., Zhang, B., Fuhlbrigge, T., 2019. Robot throwing trajectory planning for solid waste handling. The 9th IEEE International Conference on CYBER Technology in Automation, Control, and Intelligent Systems (IEEE-CYBER 2019) : July 29-August 2, 2019, Suzhou, China. IEEE, pp. 1372–1375.

Chen, X., Kroell, N., Feil, A., Pretz, T., 2020. Determination of the composition of multilayer plastic packaging with NIR spectroscopy. Detritus 13, 62–66. https://doi.org/10.31025/2611-4135/2020.14027.

Chen, X., Kroell, N., Li, K., Feil, A., Pretz, T., 2021a. Influences of bioplastic polylactic acid on near-infrared-based sorting of conventional plastic. Waste Management & Research 1–4. https://doi.org/10.1177/0734242X211003969.

Chen, X., Kroell, N., Wickel, J., Feil, A., 2021b. Determining the composition of post-consumer flexible multilayer plastic packaging with near-infrared spectroscopy. Waste management (New York, N.Y.) 123, 33–41. https://doi.org/10.1016/j.wasman.2021.01.015.

Conversio Market & Strategy GmbH, 2020. Stoffstrombild Kunststoffe in Deutschland 2019.

Curtis, A., Küppers, B., Möllnitz, S., Khodier, K., Sarc, R., 2021. Real time material flow monitoring in mechanical waste processing and the relevance of fluctuations. Waste Management (New York, N.Y.) 120, 687–697. https://doi.org/10.1016/j.wasman.2020.10.037.

Der Grüne Punkt, 2018. Produktspezifikation 329: Polyethylen. https://www.gruener-punkt.de/de/downloads (accessed 13 April 2021).

Deutsches Institut für Normung e. V., 2012. DIN EN 15934: Schlamm, behandelter Bioabfall, Boden und Abfall – Berechnung des Trockenmassenanteils nach Bestimmung des Trockenrückstands oder des Wassergehalts. Beuth Verlag GmbH, Berlin (accessed 15 April 2021).

Deutsches Institut für Normung e. V., 2012. DIN ISO 9276-6 – Darstellung der Ergebnisse von Partikelgrößenanalysen: Teil 6: Deskriptive und quantitative Darstellung der Form und Morphologie von Partikeln. Beuth Verlag, Berlin (accessed 12 May 2020), 27 pp.

Devore, J.L., 2012. Probability and Statistics for Engineering and the Sciences, eighth ed. Brooks/Cole, Australia.

European Union, 2018. European Parliament and Council Directive 94/62/EC of 20 December 1994 on packaging and packaging waste.

Eurostat, 2021. Packaging waste by waste management operations. https://ec.europa.eu/eurostat/databrowser/view/ENV_WASPAC__custom_797150/default/table?lang=en (accessed 12 April 2021).

Fahrmeir, L., 2013. Regression: Models, Methods and Applications. Springer, Berlin, Heidelberg.

Feil, A., Coskun, E., Bosling, M., Kaufeld, S., Pretz, T., 2019. Improvement of the recycling of plastics in lightweight packaging treatment plants by a process control concept. Waste management & research 37, 120–126. https://doi.org/10.1177/0734242X19826372.

Feil, A., Pretz, T., 2017. Aufbereitung fester Abfallstoffe. In: Kranert, M. (Ed.), Einführung in die Kreislaufwirtschaft. Springer Fachmedien Wiesbaden, Wiesbaden.

Feil, A., Pretz, T., 2020. Mechanical recycling of packaging waste. Plastic Waste Recycl. Elsevier, pp. 283–319. https://doi.org/10.1016/B978-0-12-817880-5.00011-6.

Feil, A., van Thoden Velzen, E.U., Jansen, M., Vitz, P., Go, N., Pretz, T., 2016. Technical assessment of processing plants as exemplified by the sorting of beverage cartons from lightweight packaging wastes. Waste Management (New York, N.Y.) 48, 95–105. https://doi.org/10.1016/j.wasman.2015.10.023.

Grajski, K.A., Breiman, L., Di Viana Prisco, G., Freeman, W.J., 1986. Classification of EEG spatial patterns with a tree-structured methodology: CART. IEEE Transactions on Biomedical Engineering 33, 1076–1086. https://doi.org/10.1109/TBME.1986.325684.

Harris, C.R., Millman, K.J., van der Walt, S.J., Gommers, R., Virtanen, P., Cournapeau, D., Wieser, E., Taylor, J., Berg, S., Smith, N.J., Kern, R., Picus, M., Hoyer, S., van Kerkwijk, M.H., Brett, M., Haldane, A., Del Río, J.F., Wiebe, M., Peterson, P., Gérard-Marchant, P., Sheppard, K., Reddy, T., Weckesser, W., Abbasi, H., Gohlke, C., Oliphant, T.E., 2020. Array programming with NumPy. Nature 585, 357–362. https://doi.org/10.1038/s41586-020-2649-2.

Hastie, T., Tibshirani, R., Friedman, J.H., 2009. The Elements of Statistical Learning: Data Mining, Inference, and Prediction, second ed. Springer, New York, NY.

Igathinathane, C., Ulusoy, U., 2012. Particle size distribution analysis of ground coal by machine vision ΣVolume approach. In: International Mineral Processing Congress (IMPC), New Delhi, Indien. 24.–28. September 2012, pp. 5581–5593.

Junjuri, R., Gundawar, M.K., 2020. A low-cost LIBS detection system combined with chemometrics for rapid identification of plastic waste. Waste Management (New York, N.Y.) 117, 48–57. https://doi.org/10.1016/j.wasman.2020.07.046.

Khodier, K., Curtis, A., Sarc, R., Lehner, M., O'Leary, P., Pomberger, R., 2019. Smart solid waste processing plant: vision and pathway. In: ISWA world congress 2019, Bilbao, Spain. 07 October 2019–09 October 2019.

Krämer, P., 2017. Entwicklung von Berechnungsmodellen zur Ermittlung relevanter Einflussgrößen auf die Genauigkeit von Systemen zur nahinfrarotgestützten Echtzeitanalytik von Ersatzbrennstoffen. Dissertation. Aachen.

Karagiannopoulos, M., Anyfantis, D., Kotsiantis, S.B., Pintelas, P.E., 2007. Feature selection for regression problems. Feature selection for regression problems. The 8th Hellenic European Research on Computer Mathematics & its Applications, HERCMA. https://thalis.math.upatras.gr/~dany/downloads/hercma07.pdf, 2007.

Kroell, N., 2021. imea: A Python package for extracting 2D and 3D shape measurements from images. Journal of Open Source Software 6, 3091. https://doi.org/10.21105/joss.03091.

Kroell, N., Johnen, K., Chen, X., Feil, A., 2021. Fine metal-rich waste stream characterization based on RGB data: comparison between feature-based and deep learning classification methods. In: Beyerer, J., Längle, T. (Eds.), OCM 2021 – Optical Characterization of Materials: Conference Proceedings. KIT Scientific Publishing, p. 3091. https://doi.org/10.5445/KSP/1000128686.

Kubat, M., 2017. An Introduction to Machine Learning, second ed. Springer International Publishing, Cham.

Küppers, B., Chen, X., Seidler, I., Friedrich, K., Raulf, K., Pretz, T., Feil, A., Pomberger, R., Vollprecht, D., 2019. Influences and consequences of mechanical delabelling on PET recycling. Detritus 6, 1. https://doi.org/10.31025/2611-4135/2019.13816.

Küppers, B., Schlögl, S., Friedrich, K., Lederle, L., Pichler, C., Freil, J., Pomberger, R., Vollprecht, D., 2020a. Influence of material alterations and machine impairment on throughput related sensor-based sorting performance. Waste Management & Research. https://doi.org/10.1177/0734242X20936745, 734242X20936745.

Küppers, B., Seidler, I., Koinig, G.R., Pomberger, R., Vollprecht, D., 2020b. Influence of throughput rate and input composition on sensor-based sorting efficiency. Detritus 59–67. https://doi.org/10.31025/2611-4135/2020.13906.

Küter, A., Reible, S., Geibig, T., Nüßler, D., Pohl, N., 2018. THz imaging for recycling of black plastics. Technisches Messen 85, 191–201. https://doi.org/10.1515/teme-2017-0062.

Lapusan, C., Rad, C., Hancu, O., Brisan, C., 2018. Vision-based robotic cell design for automated waste manipulation. Applied Sciences 444, 52030. https://doi.org/10.1088/1757-899X/444/5/052030.

Marsland, S., 2015. Machine Learning: An Algorithmic Perspective. CRC Press, Boca Raton, FL.

Möllnitz, S., Küppers, B., Curtis, A., Khodier, K., Sarc, R., 2021. Influence of pre-screening on down-stream processing for the production of plastic enriched fractions for recycling from mixed commercial and municipal waste. Waste management (New York, N.Y.) 119, 365–373. https://doi.org/10.1016/j.wasman.2020.10.007.

Moroni, M., Mei, A., 2020. Characterization and separation of traditional and bio-plastics by hyperspectral devices. Applied Sciences 10, 2800. https://doi.org/10.3390/app10082800.

Mukaka, M.M., 2012. Statistics corner: A guide to appropriate use of correlation coefficient in medical research. Malawi Medical Journal 24, 69–71.

Mukherjee, S., Tamayo, P., Rogers, S., Rifkin, R., Engle, A., Campbell, C., Golub, T.R., Mesirov, J.P., 2003. Estimating dataset size requirements for classifying DNA microarray data. Journal of Computational Biology 10, 119–142. https://doi.org/10.1089/106652703321825928.

Länderarbeitsgemeinschaft Abfall, 2001. LAGA PN 98: Richtlinie für das Vorgehen bei physikalischen und chemischen Untersuchungen im Zusammenhang mit der Verwertung/Beseitigung von Abfällen.
Papadakis, E., Raptopoulos, F., Koskinopoulou, M., Maniadakis, M., 2020. On the use of vacuum technology for applied robotic systems. IEEE Press, Piscataway, NJ, pp. 73–77.
Pearson, K., 1895. Note on regression and inheritance in the case of two parents. Proceedings of the Royal Society of London 58, 240–242. https://doi.org/10.1098/rspl.1895.0041.
Pedregosa, F., Varoquaux, G., Gramfort, A., Michel, V., Thirion, B., Grisel, O., Blondel, M., Prettenhofer, P., Weiss, R., Dubourg, V., Vanderplas, J., Passos, A., Cournapeau, D., Brucher, M., Perrot, M., Duchesnay, E., 2011. Scikit-learn: machine learning in python. Journal of Machine Learning Research 12, 2825–2830.
Pellenc ST SAS, 2021. The multi-material sorting machine for sorting and recycling centres. https://www.pellencst.com/products/mistralplus/ (accessed 14 April 2021).
Perugini, F., Mastellone, M.L., Arena, U., 2005. A life cycle assessment of mechanical and feedstock recycling options for management of plastic packaging wastes. Environmental Progress 24, 137–154. https://doi.org/10.1002/ep.10078.
Ragaert, K., Delva, L., van Geem, K., 2017. Mechanical and chemical recycling of solid plastic waste. Waste Management (New York, N.Y.) 69, 24–58. https://doi.org/10.1016/j.wasman.2017.07.044.
Rozenstein, O., Puckrin, E., Adamowski, J., 2017. Development of a new approach based on midwave infrared spectroscopy for post-consumer black plastic waste sorting in the recycling industry. Waste Management (New York, N.Y.) 68, 38–44. https://doi.org/10.1016/j.wasman.2017.07.023.
Sarc, R., Curtis, A., Kandlbauer, L., Khodier, K., Lorber, K.E., Pomberger, R., 2019. Digitalisation and intelligent robotics in value chain of circular economy oriented waste management – a review. Waste Management (New York, N.Y.) 95, 476–492. https://doi.org/10.1016/j.wasman.2019.06.035.
Serranti, S., Gargiulo, A., Bonifazi, G., 2011. Characterization of post-consumer polyolefin wastes by hyperspectral imaging for quality control in recycling processes. Waste Management (New York, N.Y.) 31, 2217–2227. https://doi.org/10.1016/j.wasman.2011.06.007.
Serranti, S., Luciani, V., Bonifazi, G., Hu, B., Rem, P.C., 2015. An innovative recycling process to obtain pure polyethylene and polypropylene from household waste. Waste Management (New York, N.Y.) 35, 12–20. https://doi.org/10.1016/j.wasman.2014.10.017.
Signoret, C., Caro-Bretelle, A.-S., Lopez-Cuesta, J.-M., Ienny, P., Perrin, D., 2019a. MIR spectral characterization of plastic to enable discrimination in an industrial recycling context: I. Specific case of styrenic polymers. Waste Management (New York, N.Y.) 95, 513–525. https://doi.org/10.1016/j.wasman.2019.05.050.
Signoret, C., Caro-Bretelle, A.-S., Lopez-Cuesta, J.-M., Ienny, P., Perrin, D., 2019b. MIR spectral characterization of plastic to enable discrimination in an industrial recycling context: II. Specific case of polyolefins. Waste Management (New York, N.Y.) 160–172. https://doi.org/10.1016/j.wasman.2019.08.010.
Spearman, C., 1961. The Proof and Measurement of Association Between Two Things. Appleton-Century-Crofts, East Norwalk, CT, US, p. 45.
STEINERT GmbH, 2021. Sorting of Post-consumer Packages. https://steinertglobal.com/magnets-sensor-sorting-units/sensor-sorting/ (accessed 14 April 2021).
TOMRA Sorting GmbH, 2021. Recover more resources with sensor-based sorting. https://www.tomra.com/en/sorting/recycling (accessed 14 April 2021).
Vallebuona, G., Arburo, K., Casali, A., 2003. A procedure to estimate weight particle distributions from area measurements. Minerals Engineering 16, 323–329. https://doi.org/10.1016/S0892-6875(03)00014-1.
van der Walt, S., Schönberger, J.L., Nunez-Iglesias, J., Boulogne, F., Warner, J.D., Yager, N., Gouillart, E., Yu, T., the scikit-image contributors, 2014. scikit-image: image processing in Python. PeerJ 2. https://doi.org/10.7717/peerj.453.
Vinutha, H.P., Poornima, B., Sagar, B.M., 2018. Detection of Outliers Using Interquartile Range Technique from Intrusion Dataset. Information and Decision Sciences. Springer, Singapore, pp. 511–518. https://doi.org/10.1007/978-981-10-7563-6_53.
Vrancken, C., Longhurst, P.J., Wagland, S.T., 2017. Critical review of real-time methods for solid waste characterisation: informing material recovery and fuel production. Waste Management (New York, N.Y.) 61, 40–57. https://doi.org/10.1016/j.wasman.2017.01.019.
Weissenbach, T., Sarc, R., 2021. Investigation of particle-specific characteristics of non-hazardous, fine shredded mixed waste. Waste Management (New York, N.Y.) 119, 162–171. https://doi.org/10.1016/j.wasman.2020.09.033.
Willmott, C.J., Matsuura, K., 2005. Advantages of the mean absolute error (MAE) over the root mean square error (RMSE) in assessing average model performance. Climate Research 30, 79–82. https://doi.org/10.3354/cr030079.
Wold, H., 2005. Partial least squares. In: Kotz, S., Read, C.B., Balakrishnan, N., Vidakovic, B., Johnson, N.L. (Eds.), Encyclopedia of Statistical Sciences. Wiley-InterScience, Hoboken, NJ.
Wolpert, D.H., 1996. The lack of a priori distinctions between learning algorithms. Neural Computation 8, 1341–1390. https://doi.org/10.1162/neco.1996.8.7.1341.
Wypych, G., 2012. Handbook of Polymers. ChemTec Publ, Toronto.
Zhang, Z., 2015. An estimation of coal density distributions by weight based on image analysis and MIV-SVM. IEEE, pp. 1110–1113.
Zhang, Z., Yang, J., Ding, L., Zhao, Y., 2012. An improved estimation of coal particle mass using image analysis. Powder Technology 229, 178–184. https://doi.org/10.1016/j.powtec.2012.06.027.

3.3 Publication D: Sensor-based prediction of mass-based material flow compositions

> **Kroell, N.**, Chen, X., Küppers, B., Lorenzo, J., Maghmoumi, A., Schlaak, M., Thor, E., Nordmann, C., & Greiff, K. (2023). Near-infrared-based determination of mass-based material flow compositions in mechanical recycling of post-consumer plastics: Technical feasibility enables novel applications. *Resources, Conservation and Recycling*, *191*, 106873. https://doi.org/10.1016/j.resconrec.2023.106873

While Publications B and C (Sections 3.1 and 3.2) have demonstrated the technical feasibility of a particle-level characterization approach by showing that particle masses can be predicted within reasonable accuracy by ML models at singled material flow presentations, there are many potential measuring points in sorting and processing plants where a singled material flow presentation is not available and/or not technically feasible (e.g., transport conveyor belts or bale press feeding conveyor belts). Therefore, Publication D (Figure 3.3) aims to demonstrate the technical feasibility of a material-flow-level approach, which can also be applied at unsingled or overlapping material flow presentations.

In the material-flow-based approach, first, the material flow surface is classified pixel-by-pixel into material classes based on NIR sensor data. From the resulting false-color image (representing the classification results), individual areas (*chunks*) are then extracted, in which the pixels of each material class are counted. The counted pixels reflect the area-based composition of the detected material flow surface. Regression models are then used to predict mass-based material flow composition from area-based compositions from the NIR sensor data.[3]

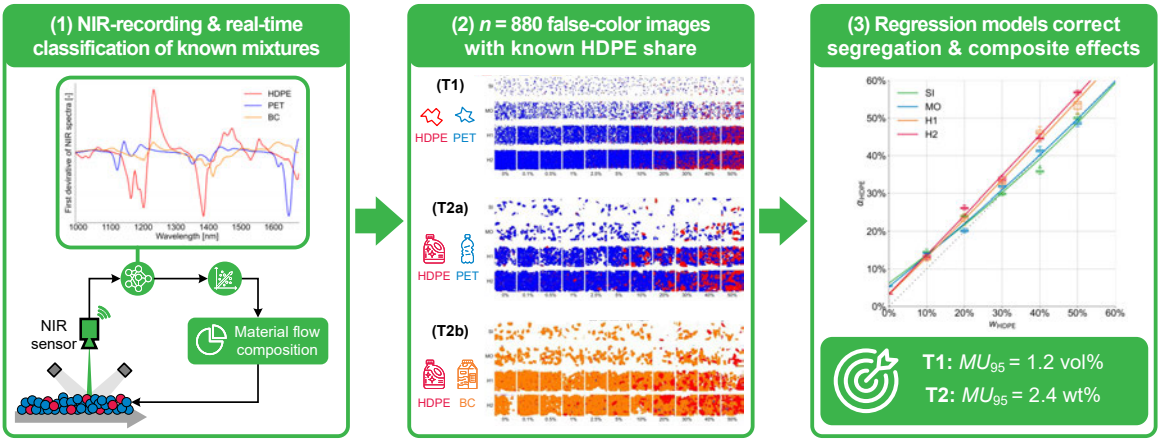

Figure 3.3. Graphical abstract Publication D.

[3]Supplementary materials for Publication D are provided in Appendix A.

Resources, Conservation & Recycling 191 (2023) 106873

Contents lists available at ScienceDirect

Resources, Conservation & Recycling

journal homepage: www.elsevier.com/locate/resconrec

Full length article

Near-infrared-based determination of mass-based material flow compositions in mechanical recycling of post-consumer plastics: Technical feasibility enables novel applications

Nils Kroell [a,*], Xiaozheng Chen [a], Bastian Küppers [b], Julius Lorenzo [a], Abtin Maghmoumi [a], Matthias Schlaak [a], Eric Thor [a], Christian Nordmann [b], Kathrin Greiff [a]

[a] Department of Anthropogenic Material Cycles, RWTH Aachen University, Wuellnerstr. 2, D-52062, Aachen, Germany
[b] STADLER Anlagenbau GmbH, Max-Planck-Str. 2, D-88361, Altshausen, Germany

ARTICLE INFO

Keywords:
Sensor-based material flow characterization
Sensor-based sorting
Automated quality control
Lightweight packaging waste
Machine learning
Circular economy

ABSTRACT

Mass-based material flow compositions (MFCOs) are crucial to assess and optimize mechanical plastic recycling processes. While MFCOs are determined by manual sorting analysis today, in the future MFCOs could be determined inline through near-infrared-based material flow characterization. This study aims to quantify the accuracy of near-infrared-based MFCO determinations to assess its technical feasibility. Binary mixtures of plastic flakes and post-consumer packaging were pixel-based classified at different material flow presentations, and mass-based MFCOs were predicted from the resulting false-color data using different data processing techniques. The results show high correlations between near-infrared-based false-color data and mass-based MFCOs. Through regression models and data aggregation, it was possible to predict mass-based MFCOs with mean absolute errors of 0.5% and 1.0% and R^2-scores of 99.9% and 99.4% for plastic flakes and packaging, respectively, across all material flow presentations. The demonstrated technical feasibility thus paves the way for new sensor technology applications in plastic recycling.

1. Introduction

Since the invention of the first synthetic polymer in 1907 (Crespy et al., 2008), more than 8,300 Mt of plastics have been produced worldwide (Geyer et al., 2017). While advantageous material properties and low production costs of plastics have led to their widespread use in the first place, these advantages have recently been overshadowed by negative environmental impacts (Dris et al., 2020). Production of new plastic requires fossil fuels as raw material, consumes large amounts of energy, and emits significant amounts of greenhouse gases (GHGs) (Zheng and Suh, 2019); it is estimated that cumulative GHG emissions associated with plastics could account for 10% to 13% of the total remaining carbon budget by 2050 (Shen et al., 2020). In 2010 alone, about 4.8 million to 12.7 million tons of plastics entered the oceans (Jambeck et al., 2015), where they endanger wildlife (Moore, 2008) and accumulate as microplastics in organisms and food chains (Avio et al., 2017; Chen et al., 2021a).

The global plastics crisis can only be tackled through a plethora of complementary measures (Nielsen et al., 2020). Starting with the reduction of plastic consumption, through longer use cycles and reuse of plastic products to zero-loss collection and high-quality recycling, these measures contribute to a reduction of the environmental impacts of plastics. In this regard, recycling processes play a key role: On the one hand, plastic recycling avoids negative impacts of alternative end-of-life operations (e.g., incineration, landfilling). On the other hand, produced plastic recyclates can substitute primary plastics and thus avoid negative environmental impacts of primary plastic production (Cudjoe et al., 2021). Among all recycling processes, mechanical recycling is considered particularly advantageous due to its low energy demand and low carbon footprint (Davidson et al., 2021).

Abbreviations: BC, beverage carton; GHG, greenhouse gases; HDPE, high-density polyethylene; LWP, lightweight packaging waste; MAE, mean absolute error; MFCO, material flow composition; MFP, material flow presentation; MO, monolayer; MU, measurement uncertainty; NIR, near-infrared; PET, polyethylene terephthalate; RR, reduction ratio; SBMC, sensor-based material flow characterization; SBS, sensor-based sorting; SI, singled.

* Corresponding author.
E-mail address: nils.kroell@ants.rwth-aachen.de (N. Kroell).

https://doi.org/10.1016/j.resconrec.2023.106873
Received 4 November 2022; Received in revised form 9 January 2023; Accepted 10 January 2023
Available online 9 February 2023

1.1. Mechanical recycling of post-consumer plastics

Mechanical recycling of post-consumer plastics involves three stages: First, end-of-life plastic products and packages are collected according to country-specific collection schemes (e.g., "lightweight packaging waste" [LWP] in Germany or "plastic packaging, metal packaging, drinks cartons" in Belgium). Second, *sorting plants* sort the collected plastic wastes into material-, polymer-, or color-specific preconcentrates. Third, specialized *processing plants* purify the preconcentrates into plastic recyclates. These recyclates can then substitute primary plastics and achieve environmental benefits as outlined above. (Feil and Pretz, 2020)

However, taking the EU27+3 countries as an example, only 8.5 wt% of the plastic demand in 2020 could be covered by post-consumer recyclates due to high material losses along the value chain (Plastic

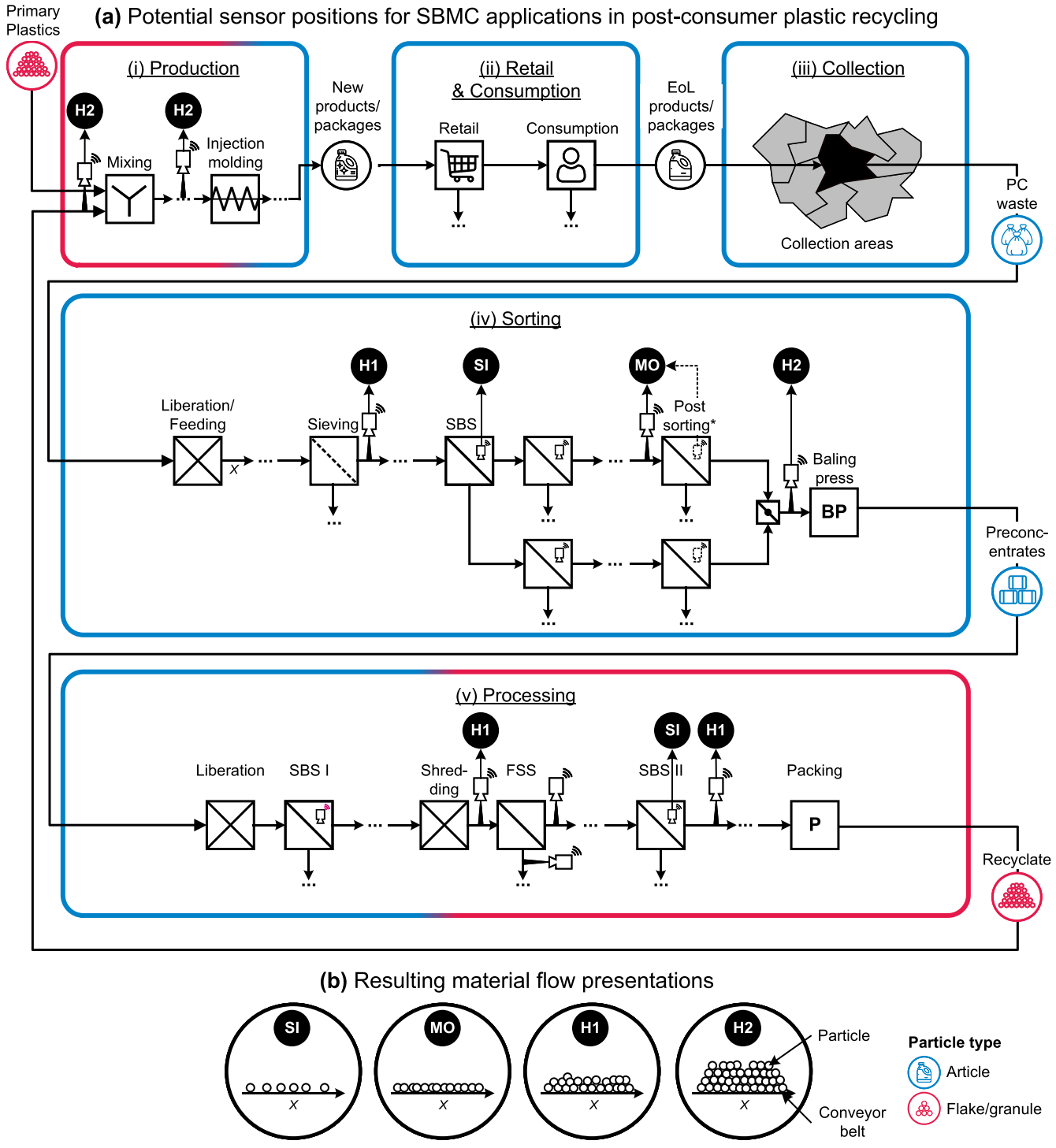

Fig. 1. Potential applications of novel SBMC methods in consumer-based plastic cycles and resulting material flow presentations. (a) Simplified overview of consumer-based plastic cycles with selected, potential sensor positions; (b) simplified cross-section view of different material flow presentations: singled (SI), monolayer (MO), multilayered bulk with bulk heights H1 and H2. *x*: conveying direction, BP: bale press, P: Packing, FSS: float sink separation, PC: post-consumer; *post sorting can be performed automatically with sorting robots, manually, or not at all; in the case of post sorting through sorting robots, the resulting data streams may also be available for material flow characterization.

Europe, 2022): From 29.5 Mt/a collected post-consumer plastics in the EU27+3, only 34.6 wt% (10.2 Mt/a) (Plastic Europe, 2022) were sent as plastic preconcentrates to processing plants. Of the 9.1 Mt/a plastic preconcentrates treated in EU27+3 processing plants, only 60.4 wt% (5.5 Mt/a) (Plastic Europe, 2022) resulted in plastic recyclates. In addition, low and/or unknown plastic recyclate qualities hamper primary plastic substitution in applications with high-quality requirements and the general acceptance of plastic recyclates (Alassali et al., 2021).

1.2. Sensor-based material flow characterization

A promising approach to both minimize material losses and increase product qualities in mechanical plastic recycling lies in novel *sensor-based material flow characterization* (SBMC) applications. In SBMC, sensors and (machine learning) algorithms are used to digitally characterize material flows. Based on material flow characteristics acquired through SBMC, new applications can be envisioned for the optimization of mechanical recycling processes (Fig. 1). (Kroell et al., 2022a)

For SBMC applications in mechanical recycling of post-consumer plastics, *material flow compositions* (MFCOs) are of particular interest (Kroell et al., 2022a). Today, MFCOs in plastic recycling are (almost exclusively) determined through sampling and manual sorting analysis, which is time- and cost-intensive and thus often only conducted on an irregular basis. The resulting intransparency due to the unknown MFCOs results potentially in large inefficiencies. In the future, SBMC methods could help achieve transparency at lower costs and pave the way to new applications that help increase the quality and quantity of recycled plastics:

First, MFCOs inside sorting and processing plants could enable an adaptive and intelligent process control to enhance the plant performance and availability (Fig. 1a.iv and v). For example, SBMC data could enable novel *sensor-based process monitoring* (e.g., Kroell et al., 2022b; Schlögl and Küppers, 2022) or *sensor-based process control* (e.g., Küppers et al., 2022) applications.

Second, information on output MFCOs could make *sensor-based quality control* of product fractions from sorting and processing plants possible (Fig. 1a.iv and v). For example, adaptive pricing models could be implemented based on SBMC data, or sorting products with low quality can be identified for possible reprocessing (Kroell et al., 2022a).

Third, input MFCOs based on SBMC in sorting plants could enable the monitoring and improvement of separate waste collection (Fig. 1a.iii). For example, material losses during waste collection could be reduced by more efficiently allocating and assessing public information campaigns for separate waste collection (Initiative „Mülltrennung wirkt“, 2021).

However, all SBMC applications rise and fall with the *accuracy* (ISO 5725, 2022) of the sensor-based determined MFCOs: If MFCOs cannot be quantified accurately, then (i) adaptive process control algorithms cannot identify optimal machine parameters (Küppers et al., 2022), (ii) confidence in statements of potential sensor-based quality monitoring systems is not given, and (iii) input material flows cannot be reliably monitored.

1.3. Accuracy of sensor-based determined MFCOs

SBMC data processing can be divided into pixel, particle, and material flow levels (Kroell et al., 2022a). At the pixel- and particle-level, several studies have already demonstrated that non-carbon-black standard plastics can be differentiated with > 99% classification accuracy by appropriate classification algorithms due to their unique near-infrared (NIR) spectra (Kroell et al., 2022a). While several SBS manufacturers are already providing area-based material statistics from existing SBS equipment to plant operators (e.g., Binder+Co AG, 2022; Pellenc ST SAS, 2022; REDWAVE, 2022; Sesotec GmbH, 2022; STEINERT GmbH, 2022; TOMRA System ASA, 2022), two critical research gaps remain unsolved:

Research gap 1: Provision of mass-based indicators. Pixel-based classified NIR data provides only *area-based* information on MFCOs, while product qualities and separation processes are assessed using *mass-based* indicators (Kroell et al., 2021; Kroell et al., 2022a). Due to different material densities and grammages, area-based material flows compositions cannot be directly converted into mass-based MFCOs (Kroell et al., 2021). In previous work (Kroell et al., 2021), it was demonstrated that individual particle masses can be predicted from 2D and 3D sensor data using material-specific grammages (mass per area occupied at the conveyor belt) or machine learning models at the particle level. However, the question of how the accuracy of mass predictions contributes to the overall accuracy of MFCO determination at the material flow level remains unsolved.

Research gap 2: Consideration of different material flow presentations. Within sorting and processing plants, material flows are conveyed in different *material flow presentations (MFPs)*:

- In sensor-based sorting (SBS) stages, material flows are usually presented as *singled monolayers* on acceleration belts to the SBS units to achieve sufficient sorting results (Feil et al., 2021; Kroell et al., 2022b), i.e., materials do not overlap or touch each other on the conveyor (Fig. 1b.SI).
- For preconditioning processes (e.g., wind-shifting), a MFP as *monolayers* (i.e., particles touch but do not largely overlap each other; Fig. 1b.MO) is often sufficient.
- For material transportation, material flows are often transported as *multilayered bulks* (i.e., particles overlap each other; Fig. 1b.H1/H2) (Kroell et al., 2022a).

Since NIR is a surface measurement technology with a limited penetration depth (Chen et al., 2021b), only the composition of the material flow surface can be determined with NIR, which might differ from that of the full material flow (Kroell et al., 2022a). Thus, it is still unclear (a) if SBMC of post-consumer plastics in the case of missing material singling is technically feasible at all and (b) how accurate the obtained MFCOs are under different MFPs (Kroell et al., 2022a).

1.4. Aim and research question

This study aims to evaluate the technical feasibility and quantify the accuracy of NIR-based MFCO determination of post-consumer plastics. More specifically, we aim to answer the following research question: *How accurate are NIR-based determined MFCOs (i) for different particle types (*i.e., *flakes and articles, cf. Fig. 1b), (ii) at different material flow presentations, and (iii) based on different data processing techniques?*

2. Material and methods

To answer this research question, we created binary material mixtures of plastic flakes and articles with defined MFOCs. We presented these mixtures at different MFPs (cf. Fig. 1b) to a state-of-the-art NIR sensor, which classifies the material flow pixel by pixel into pre-defined material classes. Subsequently, the number of pixels per material class of a given evaluation area were counted. Different models (density, grammages, and regression) were used to estimate MFCOs from NIR-based pixel counts. Estimated MFCOs were then compared to known MFCOs from creating the mixtures to assess the accuracy of NIR-based MFCO determination.

2.1. Materials and mixtures

Our investigations were structured into two test series: In test series T1, the determination of MFCOs of plastic flakes is investigated to simulate applications in processing plants (cf. Fig. 1a.v). In test series T2, post-consumer plastic packaging articles are studied to simulate applications in sorting plants (cf. Fig. 1a.iv).

2.1.1. Plastic flakes (T1)

To obtain pure plastic flakes, white high-density polyethylene (HDPE) and transparent polyethylene terephthalate (PET) plates of 3 mm thickness from S-POLYTEC GmbH (Goch, Germany) have been subsequently comminuted in rotary shear (see Table S1 in supplementary materials for technical data) for primary comminution and in a cutting mill (Table S2) for secondary comminution. Afterward, the ground plastic flakes have been sieved on a analytical sieve (Table S3) to obtain plastic flakes in the particle size range of 10 mm – 20 mm, which is a common particle size range in plastic processing (Maisel et al., 2020). Fig. 2a-c show exemplary RGB and false-color images as well as projection area distributions of the investigated plastic flakes.

2.1.2. LWP samples (T2)

For T2, HDPE packaging, PET bottles, and beverage cartons (BCs) were sampled from the LWP sorting plant Hündgen Entsorgungs GmbH & Co. KG (Swisttal, Germany). Each material fraction product fraction was sampled from the respective product fraction at the end of the sorting process (1 m^3 total sampling volume per product fraction). To ensure maximum representativity during sampling, the full material flow was sampled from a continuously falling material stream according to (Länderarbeitsgemeinschaft Abfall, 2001). The particle size range of the investigated LWP samples is approx. 60 mm – 240 mm (see [Kroell et al., 2021] for further details on the sampling campaign). Afterward, remaining impurities (fines [< 60 mm] and non-target material) were manually removed to obtain pure material fractions of each material (cf. Fig. 2d-f).

2.1.3. Binary mixtures

Three types of binary mixtures were generated to simulate the influence of different materials and particle types: (T1) HDPE and PET flakes, (T2a) post-consumer HDPE and PET packaging, and (T2b) post-consumer HDPE and BC packaging. For all three mixtures, $n = 11$ HDPE shares were investigated: 0%; 0.1%; 0.5%; 1%; 2.5%; 5%; 10%; 20%; 30%; 40%; and 50%.

For T1, raw densities of PET and HDPE flakes are known ($\rho_{V,\ HDPE} = 0.96$ g/cm^3, $\rho_{V,\ PET} = 1.27$ g/cm^3), thus mass-based (w_i) and volume-based MFCOs (φ_i) can be converted into each other using Eq. (1). To eliminate the known density influence on NIR-based determination from Eq. (1) and to make the results easier transferable to mixtures with different density combinations (e.g., polypropylene or polyvinyl chloride), HDPE shares for T1 are prepared in volume percent (φ_i) and we focus on the prediction from area-based (α_i) into volume-based (φ_i) MFCOs within this study.

$$w_i = \frac{\varphi_i{}^* \rho_{V,i}}{\sum_j \varphi_j{}^* \rho_j} \quad (1)$$

For T2 (post-consumer packaging waste), an indication of material densities is not possible due to post-consumer waste characteristics (e.g., post-consumer effects, residual content, material composites, hollow spaces). Thus, material mixtures of T2 were created in wt%.

2.2. Experimental setup

For both test series, the measuring situation in a processing plant (T1) and sorting plant (T2) was simulated using a lab-scale (T1) and technical-lab-scale (T2) test rig to take different particle sizes into account and to enable sufficiently high sample sizes. Each test rig consists of (i) a feeding unit and a conveyor belt to create different MFPs and (ii) a NIR sensor for data acquisition (Fig. 2g).

2.2.1. Material flow presentation

Mixtures were presented in four different MFPs to the NIR sensor to simulate different scenarios defined in Fig. 1b: singled monolayer (SI), monolayer (MO), bulk height h_1 (H1), and bulk height h_2 (H2) ($h_2 > h_1$; T1: $h_1 \approx 10$ mm, $h_2 \approx 17$ mm; T2: $h_1 \approx 150$ mm, $h_2 \approx 300$ mm). Fig. 2h-k show the belt occupation and bulk heights of the four different MFPs exemplarily for T1 based on 3D laser triangulation recordings.[1]

For T1, different MFPs were achieved through a vibrating conveyor operated at different conveying speeds (Fig. 2g.F1). For T2, an ascending conveyor was used for feeding in the SI and MO trials (Fig. 2g.F2) and a dosing bunker with a stamp for the feeding in the H1 and H2 trials (Fig. 2g.F3). In both test series, black conveyor belts were used for material transportation (conveyor width: $b_{T1} = 385$ mm, $b_{T2} = 845$ mm; conveying speed: $v_{T1} = 0.25$ m/s, $v_{T2} = 1$ m/s).

Since the recording of the sensor data was technically limited to 60 s per trial (maximum recording time of uninterrupted false-color data), the material mixtures per trial were adapted to the respective MFP: The feed volumes (V_i) in individual test series and MFPs were $V_{SI} \approx 6$ L, $V_{MO} \approx 10$ L, $V_{H1,H2} \approx 12$ L for T1 and $V_{SI,MO} \approx 300$ L, $V_{H1,H2} \approx 500$ L for T2. Each mixture was measured $n = 10$ (T1) and $n = 5$ (T2) times for each HDPE share and MFP, resulting in a total of $n = 880$ trials.

2.2.2. NIR recording and classification

2.2.2.1. Sensor. In both test series, a Helios-G2–320 NIR sensor from EVK DI Kerschhaggl GmbH (Raaba, Austria) was used to capture and classify the NIR spectra (see [EVK Kerschhaggl GmbH, 2022a] for further details). The used spectral range of the sensor was 990 nm to 1678 nm with a spectral resolution of 3.1 nm/band. The used NIR sensor has an on-chip classification engine, which is frequently used in different industrial and research applications (e.g., Curtis et al., 2021; Friedrich et al., 2022; Kleinhans et al., 2022; Kroell et al., 2022a; Küppers et al., 2022; Schlögl and Küppers, 2022). The resulting spatial resolution of the NIR sensors is 1.08 mm/px and 3.50 mm/px for T1 and T2, respectively[2]. Four halogen lamps with a power of 400 W each were used as emitters (T1: two halogen lamps each from front and back, T2: four halogen from front), and the reflection of radiation from the surface is captured by the NIR sensor. The sensor was calibrated using a white ceramic tile and emitters switch on (white calibration) and the black conveyor belt with emitters switched off (black calibration) as targets using the EVK SQALAR software (EVK Kerschhaggl GmbH, 2022b).

2.2.2.2. Classification model. For each test series, a classification model was developed to classify each spectrum into background (conveyor belt) and user-defined material classes (T1: HDPE, PET; T2: HDPE, PET, BC). For background definition, a threshold was defined to segment the recordings into background and foreground (materials) based on the mean intensity of each spectrum. For material classification, the on-sensor CLASS32 algorithm from EVK DI Kerschhaggl GmbH (Raaba, Austria) was used. In CLASS32, NIR spectra are firstly preprocessed (first derivative, normalization, and smoothing) and then compared to user-defined reference spectra.

For defining NIR reference spectra (cf. Fig. S1 and Fig. S2 in supplementary materials), representative regions of interest were selected for each material class. For T1, spectra were selected from the center of the plastic flakes to avoid edge effects (Chen and Feil, 2019; Küppers et al., 2019a). Accordingly, reference spectra of non-sleeved and non-labeled parts of the LWP samples were selected for T2. Additionally, overlays of transparent materials on top of other materials were added as reference spectra to avoid systematic misclassifications due to mixed NIR spectra in the case of transparency (e.g., a PET bottle on top of a HDPE bottle is classified as PET), cf. (Kleinhans et al., 2022).

[1] See Kroell et al. (2021) for a detailed method description on the used 3D laser triangulation recording.

[2] Length and width of square pixels after spatial calibration (Section 2.3.1).

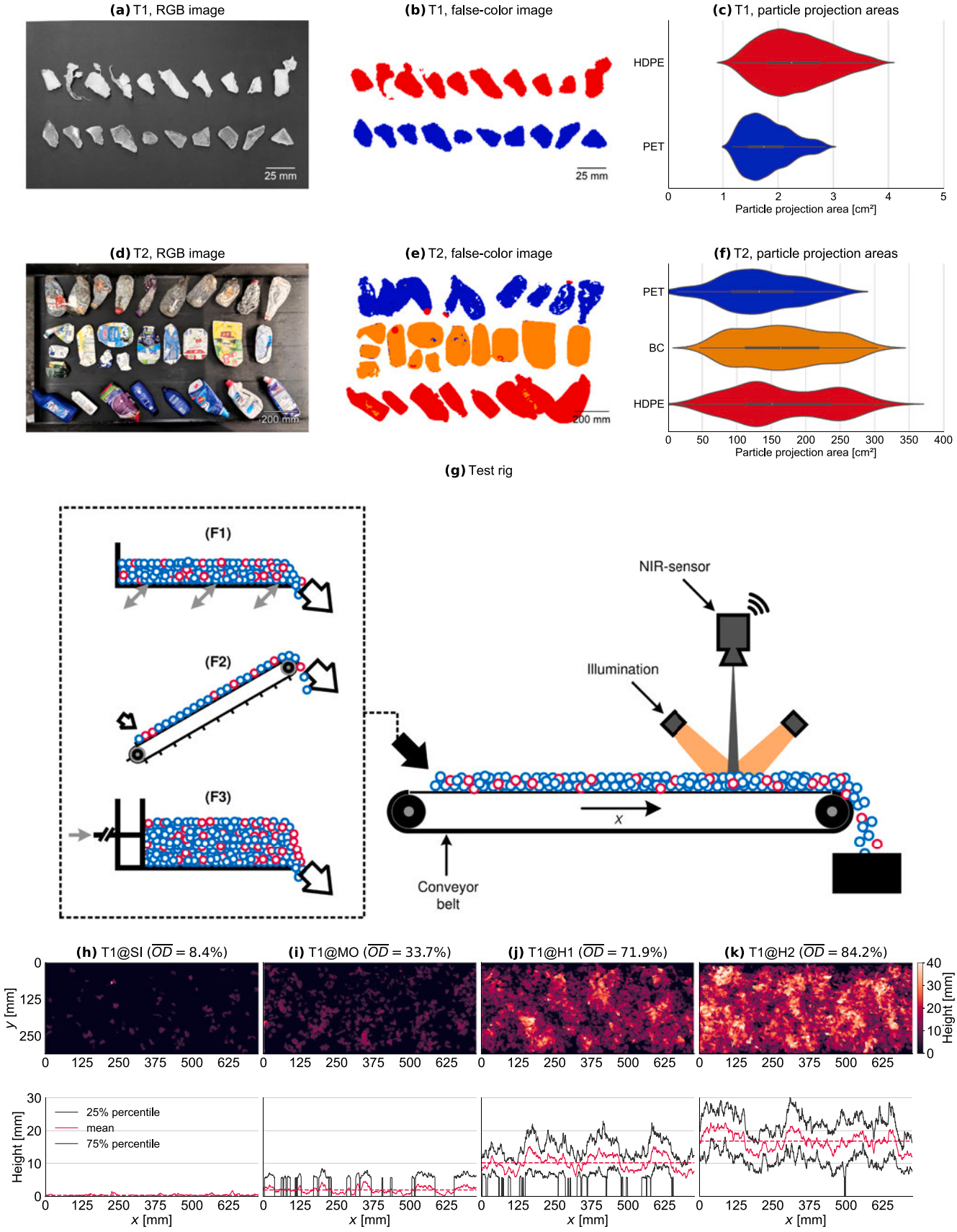

Fig. 2. Materials and methods. (a, d) RGB image, (b, e) resulting NIR false-color image (see [c] and [f] for color legend, respectively), (c, f) distribution of particle projection areas per material for test series T1 (plastic flakes) and T2 (post-consumer plastic packaging), respectively; (g) test rig for T1 and T2; F1: vibrating conveyor, F2: ascending conveyor, F3: dosing bunker with stamp; (h-k) 3DLT recording for different MFPs in T1; $\overline{OD}$: mean occupation density.

2.3. Data evaluation

For data evaluation, custom Python 3.10 scripts were developed. For data analysis and visualization, primary the open-source packages *NumPy* (Harris et al., 2020) [data storage and data processing], *pandas* (McKinney, 2010; The pandas development team, 2020) [data storage and data processing], *OpenCV* (Bradski, 2000) [pre-processing of false-color images], *scikit-image* (van der Walt et al., 2014) [pre-processing of false-color images], *imea* (Kroell, 2021) [extraction of particle measurements], *scikit-learn* (Pedregosa et al., 2011) [training and evaluation of regression models], *SciPy* (Virtanen et al., 2020) [statistics], *matplotlib* (Hunter, 2007) [data visualization], and *seaborn* (Waskom, 2021) [data visualization] have been applied.

2.3.1. Calibration and data extraction

Each image was firstly calibrated to ensure the same spatial resolution in *x*- (conveying direction) and *y*-direction ("square pixels"). Then, row-wise pixel counts are extracted from each image within a region of interest. Due to the batch-wise tests, lower particle throughputs occur at the beginning and the end of each trial, which could distort the results due to lower occupation densities (share of the conveyor belt covered by material) compared to the MFPs to be simulated. Therefore, an automated method for defining the region of interest has been developed: First, the cumulative distribution of non-background pixels from start until end of each trial is calculated and normalized to 100%. Then, the region of interest is defined as all rows that lie in an interval of $[t_1, t_2]$ of this cumulative distribution. In this study, the selected interval was [20%, 80%], i.e., the middle 60% of the total material area per trial is extracted to eliminate lower, unrepresentative belt occupations at the beginning and the end of each trial.

2.3.2. Data aggregation: chunks and moving averages

To determine time-resolved MFCOs, false-color pixels of a given area must first be aggregated before they can be converted to MFCOs. In the following, we will refer to these aggregation areas as *chunks*.

To quantify the influence of different chunk sizes on SBMC accuracies, a range of different chunk sizes is investigated. For broad applicability of the results, we report the investigated chunk sizes in [m^2] instead of [s] since this allows universal indications independent of specific conveyor belt widths and speeds. For defining the chunk area, we compare two approaches: (i) the projection area of the total conveyor surface incl. material (*conveyor area,* $A_{\text{chunk,conveyor}}$) and (ii) the projection area covered by material (*material area,* $A_{\text{chunk,material}}$). For a given application, the area-based chunk definition ($A_{\text{chunk,conveyor}}$ or $A_{\text{chunk,material}}$) can be converted to a time-based chunk definition based on the known belt speed v, conveyor width b, and occupation density OD using Eq. (2):

$$\Delta t_{\text{chunk}} = \frac{A_{\text{chunk,conveyor}}}{v^*b} = \frac{A_{\text{chunk,material}}}{OD^*v^*b} \tag{2}$$

For example, a material-area-based chunk size of $A_{\text{chunk, material}} = 1\ \text{m}^2$ on a sensor-based sorter with the parameters $v = 3\ \text{m/s}$, $b = 2\ \text{m}$ and $OD = 20\%$ equals a time-based chunk size of $\Delta t_{\text{chunk}} = 0.83\ \text{s}$.

2.3.3. Pixel-to-MFCO-models

While pixel-based NIR classification describes material flows in terms of areas, mass-based MFCOs are needed in most SBMC applications (cf. research gap 1, Section 1.3). Therefore, we differentiate between three types of MFCOs within this study: The *mass share* w_i (Eq. (3)) (DIN 1310, 1984), the *volume share* φ_i (Eq. (4)) (DIN 1310, 1984), and the *area share* α_i (Eq. (5)). Where m_i, V_i, and A_i are the mass, volume, and projection area (as recorded by the NIR sensor) of fraction i, and m, V, and A are the total masses, volumes, and projections areas, respectively.

$$w_i = \frac{m_i}{m} \tag{3}$$

$$\varphi_i = \frac{V_i}{V} \tag{4}$$

$$\alpha_i = \frac{A_i}{A} \tag{5}$$

As elaborated in Section 2.1.3, material mixtures for T1 are given in HDPE volume shares (φ_{HDPE}) and we will determine how accurately these can be predicted from the area-based HDPE shares (α_{HDPE}) from the NIR false-color data. In the following, we will refer to this model as the *density model*.

For T2, two pixel-to-MFCO models are compared. First, we apply material-specific grammages (Eq. (6)) to transform the area-based HDPE shares (α_{HDPE}) into estimated mass-based HDPE shares ($\widehat{w}_{\text{HDPE}}$) according to Kroell et al. (2021) by using Eq. (7) (*grammage model*). The determined grammages for T2 in this study are $\rho_{A,\ \text{HDPE}} = 2.38\ \text{kg/m}^2$, $\rho_{A,\ \text{PET}} = 2.19\ \text{kg/m}^2$, and $\rho_{A,\ \text{BC}} = 1.49\ \text{kg/m}^2$.

$$\rho_{A,i} = \frac{m_i}{A_i} \tag{6}$$

$$w_i = \frac{\alpha_i{}^*\rho_{A,i}}{\sum_j \alpha_j{}^*\rho_{A,j}} \tag{7}$$

Second, we apply a *regression model* to convert area-based (α_{HDPE}) into mass-based HDPE shares ($\widehat{w}_{\text{HDPE}}$). Therefore, we split the NIR data into 70% training and 30% test data. The regression model is then trained on the training data and its prediction accuracy is assessed based on the test data. To avoid overfitting due to the limited investigated HDPE share range (0% – 50%, cf. Section 2.1.3), a polynomial regression model (cf. Fahrmeir et al., 2013) with a polynomial degree of two is chosen to investigate a first technical feasibility[3,4].

2.3.4. Accuracy assessment

A variety of different metrics exist to assess the accuracy of measurements (ISO 5725, 2022). To translate the intuition of many practitioners regarding the accuracy of SBMC methods into a single metric, we propose the *95% measurement uncertainty* (MU_{95}). The MU_{95} is the 95th percentile (P_{95}) of all absolute errors between a set of measurands X_{measured} and its corresponding true values X_{true} (Eq. (8)).

$$MU_{95} = P_{95}(|X_{\text{measured}} - X_{\text{true}}|)$$

$$\text{with } X = \{x_1, \ldots, x_n\} \tag{8}$$

The MU_{95} for a set of measurements indicates that in 95% of all cases in the measurements, the true MFCO (x_{true}) is in the range $x_{\text{measured}} \pm MU_{95}$. For example, if a plant operator is using an inline-NIR material flow monitoring system with a MU_{95} of 5 wt% and the NIR system is displaying a value of $x_{\text{measured}} = 50$ wt%, the true MFCO is between 45 wt% and 55 wt% in 95 of 100 measurements. The motivation behind using a 95% percentile instead of, e.g., maximum errors is to exclude potential outliers and thus to account for the often high heterogeneity of anthropogenic material flows. In addition to the proposed MU_{95} metric, results are reported as mean absolute errors (*MAE*) and R^2-scores to provide better comparability for readers used to *MAE* and R^2 metrics. Accurate measurements are characterized by low MU_{95} and *MAE* values and R^2-scores close to 100%.

[3] Note that the presented approach can be easily extended to more complex regression models (e.g., neural networks), if wider ranges of training data is available.

[4] The motivation behind using a polynomial regression model of the second degree is that (a) the relation between area-based and mass-based MFCOs is non-linear (cf. Eq. (7)). A linear regression would result in *underfitting*, while (b) higher polynomial degrees would result in *overfitting* due to limited training data (0%–50% HDPE share).

3. Results and discussion

The following sections aim at answering the research question raised in Section 1.4 regarding the influence of different particle types (Section 3.1), MFPs (Section 3.2), and data processing techniques (Section 3.3).

3.1. Influence of particle types

3.1.1. Classifyability

As evident from Fig. 2b and Fig. 3a-b, the trained classification model for T1 can differentiate HDPE, PET and background very accurately. The classification model for T2 also succeeds in providing a satisfactory distinction between HDPE, PET, BC, and background (Fig. 2e; Fig. 3c,e). However, the overall classification accuracy is lower, likely due to three major effects:

(1) Thin-walled areas of PET bottles are sometimes falsely classified as background (Fig. 2e, Fig. 3c). Due to their transparency, most of the radiation is transmitted through the PET bottles and absorbed by the black conveyor belt. Thus, only a small proportion of the radiation is reflected and captured by the NIR sensor (cf. Küppers et al., 2019b).
(2) Combinations of sleeves or labels and packaging material result in mixed NIR spectra, which can influence the classification result (Chen et al., 2023; Küppers et al., 2019a; Schlögl and Küppers, 2022). For example, a paper label on top of a HDPE canister has mixed NIR spectra of paper and HDPE, which is similar to the NIR spectra of BC (made from a HDPE inlay and paper fibers); thus, some paper labels are classified falsely as BC (Fig. 2e, Fig. 3c,e).
(3) We observe some misclassifications from dark parts of BCs as PET (Fig. 2e, Fig. 3e), which might be caused by the lower NIR reflectance due to the dark color or by a direct reflectance of shiny BC parts.

3.1.2. Correlation between NIR-based and true MFCOs

3.1.2.1. Plastic flakes (T1). Fig. 3b compares the pixel-based HDPE shares obtained through the NIR classification (α_{HDPE}) with the true volume-based HDPE share (φ_{HDPE}) obtained when creating the material mixtures. Overall, the pixel-based and true HDPE shares correlate strongly with a Pearson correlation coefficient (Pearson, 1895) of $PCC_{T1} = 99.5\%$.

However, with increasing true HDPE share, the area-based HDPE share from the NIR sensor increasingly overestimates the corresponding true HDPE share ($p < 0.001$)[5]. A likely reason for this overestimation could be the different surface-area-to-volume ratios of the investigated HDPE and PET flakes, which can be traced back to the different comminution behavior of both polymers: Since HDPE is softer, more fraying of HDPE occurred during shredding compared to PET (cf. Fig. 2a), resulting in an increased projection area of HDPE compared to PET (HDPE flakes: 718 m^2/m^3, PET flakes: 476 m^2/m^3). As a result, the area-based HDPE share is overestimated by +4.90 vol% at $\varphi_{HDPE} =$ 50 vol%.

3.1.2.2. Plastic packaging articles (T2). Fig. 3d and Fig. 3f compare the predicted mass-based HDPE shares based on NIR data using the grammage model ($\widehat{w}_{HDPE}$, cf. Section 2.3.3) with the true mass-based HDPE shares (w_{HDPE}). For T2, predicted and true HDPE-shares correlate strongly with each other ($PCC_{T2a} = 98.8\%$, $PCC_{T2b} = 96.4\%$), but slightly lower than T1.

Similar to T1, the NIR-based characterization overestimates the true HDPE share for T2a and T2b, but because of different reasons. While the samples shown far left in Fig. 3c-e represent pure PET and BC fractions ($w_{HDPE} = 0\%$) in article-based manual sorting analysis, the pixel-based NIR characterization identifies HDPE shares of 5.4 a% (5.9 wt%) and 2.0 a% (3.2 wt%) for T2a and T2b, respectively. Reason for this difference is the different counting basis of both methods: While HDPE caps, e.g., on PET bottles, count as "PET" in manual analysis, they are (correctly) classified and counted as "HDPE" in the pixel-by-pixel NIR characterization.

The HDPE-overestimation decreases with higher true HDPE share, as the material flow contains more "true" HDPE from HDPE packaging and fewer "false" HDPE caps from PET bottles. Additionally, labels on true HDPE packaging classified as BC reduce the predicted HDPE share and simultaneously increase the predicted share of other material classes (e.g., paper-based labels on HDPE containers that are classified as BC).

3.2. Influence of material flow presentation

3.2.1. Plastic flakes (T1)

HDPE-overestimation in T1 differs significantly between different MFPs (mean over all trials: SI: +2.63%, MO: +0.92%, H1: +0.08%, H2: +0.32%), see Fig. 3b. Quantitatively, we can show that the HDPE-overestimation decreases with increasing occupancy density ($p = 0.04$).

A possible reason for this effect could be the lower thickness of frays compared to the main part of the flakes: If a HDPE fray overlays the black conveyor belt, it is usually classified either as HDPE or as background (depending on material thickness and background definition in the NIR classification; cf. Fig. 2b). At higher occupation densities, HDPE flakes lie on top of other flakes. If a HDPE fray is on top of another HDPE flake, it is usually classified as HDPE, but if a HDPE fray overlays a PET flake, a mixed HDPE/PET spectra can occur due to the penetration depth of NIR (Chen et al., 2021b, 2023). Since mixed PET/HDPE spectra from transparent PET on top of HDPE are trained as "PET" to the classification model[6] (cf. Section 2.2.2.2), the HDPE frays on top of PET might be classified as PET in some cases, resulting in a lower HDPE-overestimation at higher occupation densities.

3.2.2. Plastic packaging articles (T2)

No significant differences are observed when comparing the predicted MFCOs of SI vs. MO as well as H1 vs. H2. In contrast, the predicted MFCOs differ significantly between non-overlapping (SI, MO) and overlapping (H1, H2) MFPs, which might be explained by the following two mechanisms.

3.2.2.1. Classification behavior at different MFPs. For T2a, HDPE-overestimation of pure fractions ($w_{HDPE} = 0\%$) is significantly ($p < 0.001$) higher for non-overlapping (SI: +5.87 wt%, MO: +5.84 wt%) compared to overlapping MFPs (H1: +3.61 wt%, H2: +3.60 wt%). A possible explanation for this is the better detectability of thin-walled PET bottles on top of other materials in comparison to the black conveyor belt: Two thin-walled PET bottles on top of each other have a higher overall material thickness, which results in a higher mean intensity of the reflected NIR spectra that is usually more often classified as PET instead of background. A thin-walled PET bottle on top of HDPE packaging results in mixed PET/HDPE spectra, which are trained as PET to the classification model (cf. Section 2.2.2.2). Thus, less PET is recognized at non-overlapping MFPs, which results in higher predicted HDPE shares compared to overlapping MFPs.

For T2b, the HDPE-overestimation is higher at overlapping vs. non-overlapping MFPs (e.g., at $w_{HDPE} = 0\%$: H1: +4.47 wt%, H2: +4.37

[5] *p*-values express the level of significance: differences are considered statistically significant if the *p*-value is lower than 0.05.

[6] HDPE on top of PET is trained as "HDPE", but the PET influence on a PET+HDPE spectra is lower than the PET influence on HDPE+PET due to the opaque color of HDPE flakes compared to transparent color of PET in this study (cf. Section 2.1.1).

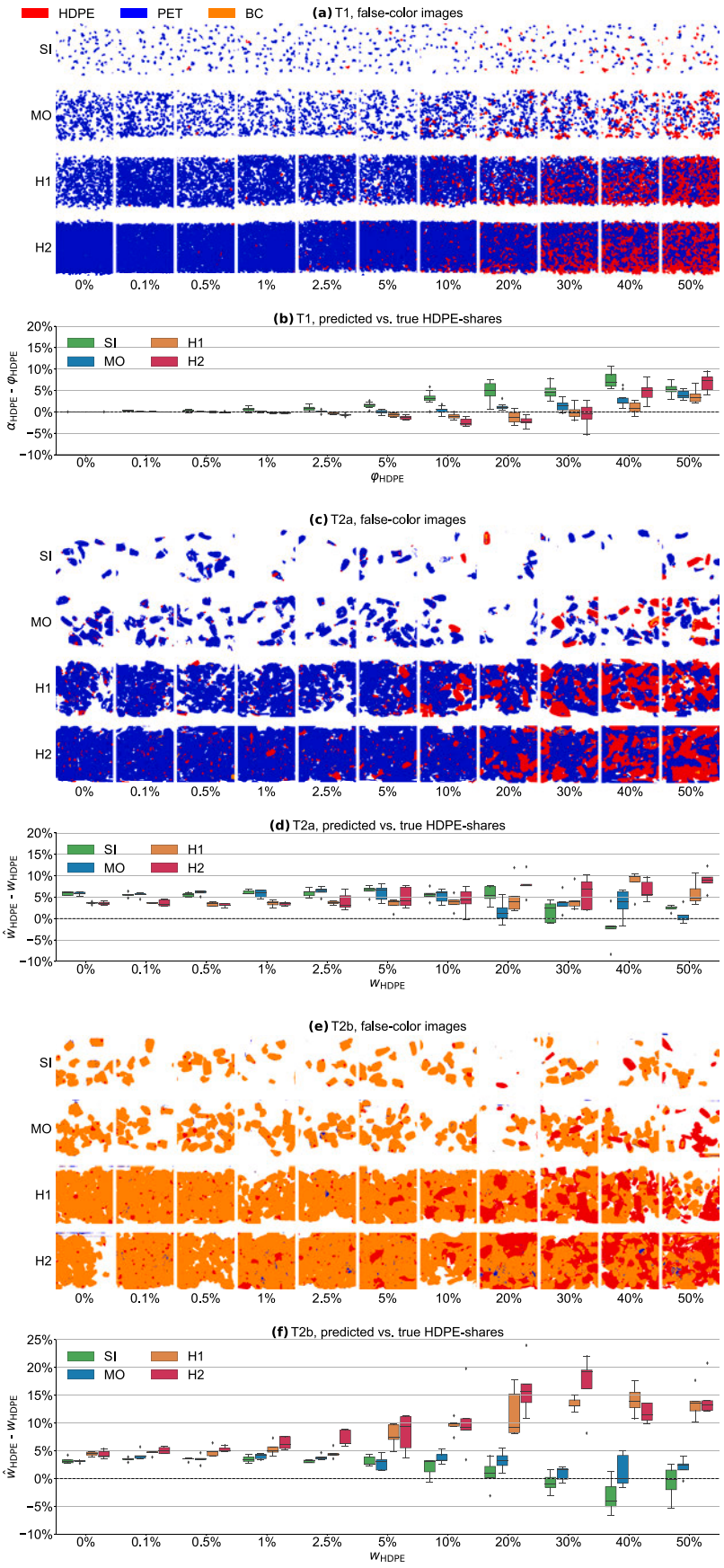

Fig. 3. Influence of particle types and MFP on trial-based prediction errors. (a, c, e) randomly selected quadratic sections of false color images per MFP and true HDPE share; (b, d, f) comparison between predicted and true HDPE share per trial for T1, T2a, and T2b, respectively.

wt% vs. SI: +3.24 wt%, MO: +3.09 wt%). The causes of this behavior cannot be reliably assessed on the data basis of this study. A possible hypothesis for this effect could be different particle orientations, which could result in more HDPE caps facing toward the NIR sensor at overlapping MFPs. However, further research is needed to clarify the mechanisms behind these observations.

3.2.2.2. Segregation effects. In both test series, HDPE shares are disproportionately overestimated with increasing HDPE share: For T2a, the difference between overlapping vs. non-overlapping MFPs ($w_{\text{HDPE, (H1,H2)}} - w_{\text{HDPE, (SI,MO)}}$) increases from -2.2 wt% ($w_{\text{HDPE}} = 0\%$) to +5.8 wt% ($w_{\text{HDPE}} = 50\%$); for T2b, HDPE-overestimation increases from +1.3% ($w_{\text{HDPE}} = 0\%$) to +13.3% ($w_{\text{HDPE}} = 50\%$), cf. Fig. 3d,f.

A possible reason for the accumulation of HDPE articles on the captured material flow surface could be higher particle volumes and three-dimensional shapes of HDPE packaging compared to smaller and/or flattened PET bottles and BCs. Due to the *brazil nut effect* (Rosato et al., 1987), larger HDPE packaging could have accumulated on the material flow surface. Since NIR is a surface measurement method, accumulation of larger articles on the material flow surface will lead to an overestimation of the corresponding material fraction compared to the true MFCO.

3.3. Influence of data processing techniques

This section investigates two data processing techniques to increase the accuracy of NIR-based determined MFCOs: Appropriate *chunk sizes* (Section 3.3.1) aim at reducing random measurement errors (i.e., increasing precision [ISO 5725, 2022]), e.g., due to different particle orientations or particle artifacts. *Pixel-to-MFCO-models* (Section 3.3.2) aim at reducing systematic measurement errors (i.e., increasing trueness [ISO 5725, 2022]), e.g., due to different counting basis of composite materials (cf. Section 3.1) or segregation errors (cf. Section 3.2).[7]

3.3.1. Chunk sizes

Fig. 4 shows the influence of chunk sizes on prediction accuracies (quantified by the MU_{95} metric) and the resulting MFCO time series. As shown in Fig. 4a-l, MUs decrease continuously with increasing chunk size and asymptotically approach a plateau, which represents the systematic differences between NIR-based and manual material flow characterization known from Fig. 3.

3.3.1.1. Definition of reduction ratios. From Fig. 4a-l, we observe a trade-off between low chunk size and low MU: Smaller chunks enable a lower latency between data acquisition and delivery of chunk-based information and higher temporal data resolution. Larger chunks, however, can smooth out unwanted fluctuations and reduce data noise.

To quantitatively describe different weighings between MU and chunk size, we define *reduction ratios* (*RR*, Eq. (9)) that describe the relative reduction of MU from raw false-color data ($MU_{95,\max}$) towards the MU plateau ($MU_{95,\min}$):

$$RR = \frac{MU_{95,\max} - MU_{95,i}}{MU_{95,\max} - MU_{95,\min}} \tag{9}$$

Based on the reduction ratios, we define three RR scenarios (80%, 95%, and 99% RR) that describe three different weighing between MU and chunk size (from a focus on small chunk sizes [$RR = 80\%$] to focus on low MUs [$RR = 99\%$]).

[7] To avoid an overrepresentation of the HDPE shares between 0% - 10% (due to the trials at 0.1%, 0.5%, 1%, 2.5%, 5% HDPE share), the ground truth data in Section 3.3 is limited to 0%, 10%, 20%, 30%, 40%, and 50% true HDPE share to achieve an equidistant distribution.

3.3.1.2. Influence of particle types and sizes. As shown in Fig. 4a-l, MUs decrease significantly faster for T1 (99% RR at 3.14 m^2 [mean over all T1 trials]) compared to T2a (13.32 m^2) and T2b (16.88 m^2). Two possible reasons for the faster decrease of T1 compared to T2 could be (i) higher homogeneity of plastic flakes from T1 compared to plastic packaging articles in T2 (e.g., due to composite packaging, a higher variety of particle sizes and shapes, and post-consumer effects [cf. Fig. 2a,d]) as well as (ii) larger particle sizes in T2 compared to T1 (cf. Fig. 2c,f), which might require larger chunk sizes for smoothing.

3.3.1.3. Influence of MFPs and chunk size definition. As shown in Fig. 4a,e,I, MUs for SI and MO decrease slower and later compared to H1 and H2, when a conveyor-area-based chunk size definition is used (cf. Section 2.3.2). A likely explanation for this observation are different occupation densities for different MFPs: While 1 m^2 conveyor area for T1 at SI contains on average 0.08 m^2 material, 1 m^2 conveyor area at MO, H1, and H2 contain 0.34 m^2, 0.72 m^2, and 0.84 m^2 material, respectively (cf. Fig. 2h-k). Thus, a higher amount of material is aggregated in a chunk at higher occupation densities, which results in stronger smoothing.

In contrast, when a material-area-based chunk size definition is used, MUs decrease almost simultaneously and at a similar pace for different MFPs (Fig. 4b,f,j). The resulting curve trajectories are thus more generalizable and could be used, e.g., to derive chunk sizes in specific SBMC applications.

3.3.1.4. Influence of target material share. Similar chunk sizes are needed to achieve the same RRs across different HDPE shares (cf. Fig. 4c, d,g,h,k,l) and no statistically significant correlation between HDPE share and chunk size at different RRs is found (conveyor-area-based chunk size: $\bar{p} = 0.544$, material-area-based chunk size: $\bar{p} = 0.668$ [mean p-value across all test series and RRs]).

3.3.1.5. Influence of chunk sizes on the resulting MFCO time series. Fig. 4m-x shows the influence of applying different chunk sizes to an exemplary time series (50% HDPE true share) across different MFPs and test series. For all test series, a decreased deviation of the raw sensor data from SI, over MO, H1 to H2 is observed (mean standard deviation of raw sensor data over all test series and HDPE shares: SI: 20.9%, MO: 16.2%, H1: 9.8%, H2: 8.7%). While finer details such as small fluctuations in the HDPE share are still present at 80% RR, these are smoothed out at 95% and 99% RR (cf. Fig. 4m-p).

3.3.2. Pixel-to-MFCO-models

As we have shown in Section 3.1 and Section 3.2, systematic effects such as different area-to-volume ratios, composite effects, and segregation errors lead to less accurate MFCO predictions. This raises the question if information about these effects can be used to correct them and make the MFCO predictions more accurate.

To answer this question, Fig. 5 shows the ground truth data and compares the prediction curves of the investigated models (T1: density and regression model, T2: grammage and regression model): True HDPE shares and pixel-based shares are shown on the *x*- and *y*-axis, respectively, and boxplots indicate the distribution of the raw data after applying a moving average (99% RR). Prediction accuracies of both models at different MFPs are quantified in Table 1 using the MU_{95}, *MAE*, R^2 metric (cf. Section 2.3.4).

In all cases, the regression model outperforms the density/grammage models. For T1 (Fig. 5a), the density model achieves a mean MU_{95} of 5.6 vol% over all MFPs due to the HDPE-overestimation (frays) discussed in Section 3.1.2.1 and Section 3.2.1. In contrast, the polynomial regression model successfully compensates higher area-based HDPE shares and reduces the MU_{95} by a factor of 4.6 down to 1.2 vol%.

For T2a (Fig. 5b), the grammage model results in similar predictions as a naïve prediction would predict ($\widehat{w}_i = \alpha_i$), due to similar grammage

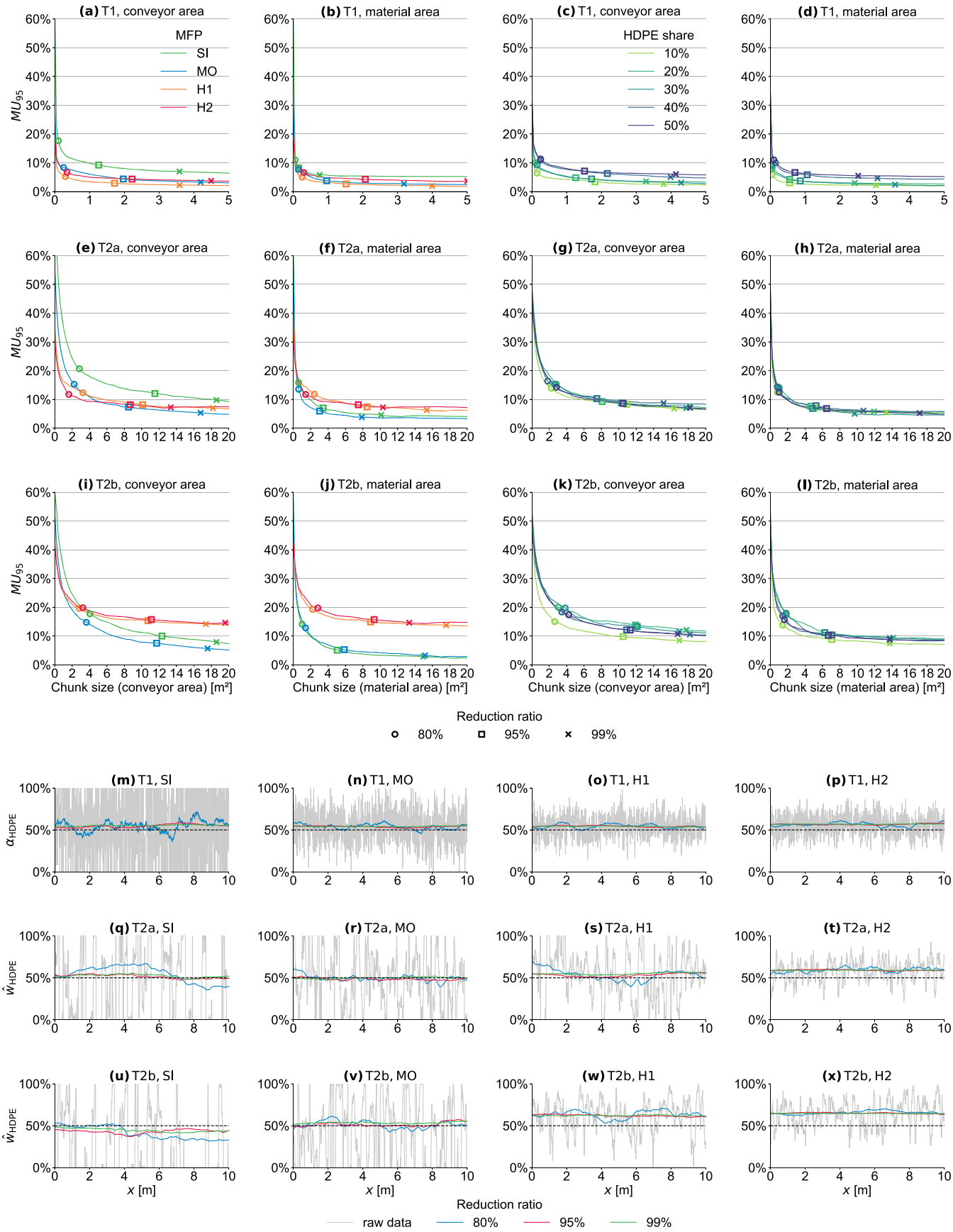

Fig. 4. Influence of chunk size and chunk definition on measurement uncertainty (MU). (a-l) influence of chunk size on MU for different test series, MFPs, and HDPE shares. (m-x) effect of exemplary chunk sizes (80%, 95%, and 99% reduction ratio) on exemplary time series (predicted HDPE share over time) on the example of 50% true HDPE share; T1: percentages in vol%, T2: percentages in wt%.

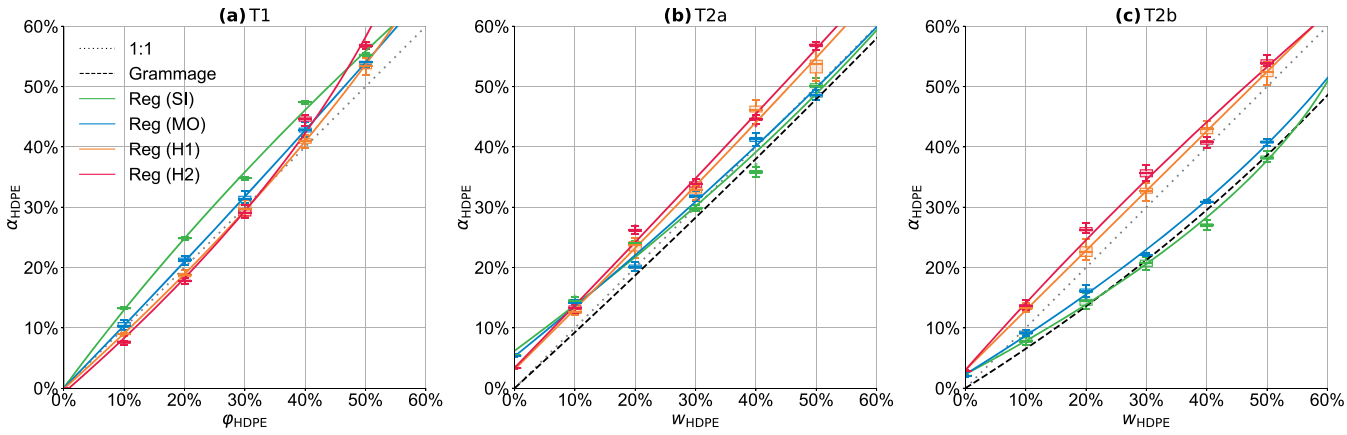

Fig. 5. Comparison of different pixel-to-MFCO-models at 99% reduction ratio (material-based chunk sizes: T1: 3.14 m^2, T2a: 13.32 m^2, T2b: 16.88 m^2).

Table 1
Accuracy of investigated pixel-to-MFCO-models at 99% reduction ratio (material-based chunk sizes: T1: 3.14 m^2, T2a: 13.32 m^2, T2b: 16.88 m^2); highest accuracies per test series are highlighted in bold.

Metric	Test series	Model	SI	MO	H1	H2	mean
MU_{95}	T1	**Density**	7.4%	4.1%	4.0%	7.0%	5.6%
		Regression	**1.3%**	**0.8%**	**1.0%**	**1.8%**	**1.2%**
	T2a	**Grammage**	5.9%	5.9%	8.6%	9.2%	7.4%
		Regression	**3.9%**	**2.5%**	**2.7%**	**2.0%**	**2.8%**
	T2b	**Grammage**	3.4%	4.2%	14.7%	17.3%	9.9%
		Regression	**1.9%**	**1.3%**	**1.5%**	**3.7%**	**2.1%**
MAE	T1	**Density**	4.2%	1.7%	1.2%	2.8%	2.5%
		Regression	**0.5%**	**0.3%**	**0.3%**	**0.8%**	**0.5%**
	T2a	**Grammage**	3.9%	3.8%	5.2%	6.2%	4.8%
		Regression	**1.7%**	**1.0%**	**0.9%**	**0.8%**	**1.1%**
	T2b	**Grammage**	1.8%	2.5%	11.3%	12.3%	7.0%
		Regression	**0.8%**	**0.7%**	**0.6%**	**1.3%**	**0.8%**
R^2	T1	**Density**	93.7%	98.5%	99.2%	96.7%	97.0%
		Regression	**99.8%**	**99.9%**	**99.9%**	**99.7%**	**99.9%**
	T2a	**Grammage**	91.3%	92.5%	91.8%	88.1%	90.9%
		Regression	**98.5%**	**99.4%**	**99.5%**	**99.6%**	**99.3%**
	T2b	**Grammage**	97.9%	97.2%	64.7%	58.0%	79.5%
		Regression	**99.7%**	**99.8%**	**99.8%**	**98.9%**	**99.5%**

of HDPE and PET (caused partially by a lower PET recognition compared to HDPE) (cf. Section 3.1.1). For T2b (Fig. 5c), the grammage model corrects the different grammages of HDPE and BC and is thus closer to the SI and MO data. As a consequence, the grammage model predictions are further away from the H1 and H2 data since the segregation errors are not included. In contrast, the regression model fits the training data of both test series and successfully corrects, e.g., HDPE-overestimations due to segregation errors at H1 and H2 or compound effects (HDPE caps) downward (Fig. 5c). On average, MUs are reduced by a factor of 3.5 ($MU_{95,grammage} = 8.6$ wt% → $MU_{95,regression} = 2.4$ wt%).

The final prediction results when combining sufficiently high chunk sizes (cf. Section 3.3.1) with the polynomial regression model of degree two show that NIR-based MFCOs determination for plastic flakes and LWP packaging is technically feasible. For plastic flakes (T1), mean MU_{95} values of 1.2 vol% (*MAE*: 0.5 vol%, R^2: 99.9%) are achieved, for post-consumer plastic packaging (T2), mean MU_{95} values were located at 2.4 wt% (*MAE*: 1.0 wt%, R^2: 99.4%).

4. Conclusion and outlook

SBMC methods promise to significantly improve post-consumer plastic recycling by enabling new applications of sensor technology such as adaptive process control or sensor-based quality control (Kroell et al., 2022a). Fulfilling these promises, however, is only feasible if the generated SBMC data is *accurate* enough.

While numerous studies have demonstrated high accuracy of NIR-based plastics classification at the pixel and particle level, it has been unclear what accuracies can be achieved at the material flow level. This study assessed the accuracy of NIR-based MFCO determinations based on three binary mixtures (T1: HDPE and PET plastic flakes, T2a: post-consumer HDPE packaging and PET bottles, T2b: post-consumer HDPE packaging and BCs) and investigated the effects of particle types, MFPs, and data processing techniques on the achievable accuracy.

User-defined settings in the NIR classification model have a large impact on NIR-based MFCO predictions of both **particle types**. Predicted MFCOs are especially influenced by (i) the discrimination between background and (transparent) materials and (ii) the classification of mixed NIR spectra (e.g., labels and sleeves for plastic packaging). For plastic flakes (T1), different surface area-to-volume ratios can result in significant over- and underestimations of the true material share, if area-based NIR classifications are used to determine volume- or mass-based MFCOs. For post-consumer plastic packaging (T2), prediction errors result mainly from the different counting basis of article-based manual sorting and pixel-based NIR characterization. For instance, it was determined that pure PET bottle (T2a) and BC (T2b) fractions from LWP contain approx. 5.4 a% and 2.1 a% HDPE, e.g., due to HDPE bottle caps, respectively.

Concerning the **material flow presentation**, it is important to distinguish between non-overlapping (SI, MO) and overlapping MFPs (H1, H2). On the one hand, material overlays influence the NIR classification behavior in that transparent materials are better detected. On the other hand, segregation errors were detected which led to an

overrepresentation of larger HDPE plastic packaging compared to smaller PET bottles and BCs on the material flow surface captured by the NIR sensor (brazil nut effect). For instance, HDPE contents were overestimated by an additional +5.8 wt% (T2a) and +13.3 wt% (T2b) for overlapping (H1, H2) compared to non-overlapping MFPs (SI, MO) at $w_{HDPE} = 50$ wt%.

Adequate **data processing** can significantly correct the effects presented above and thus increase the accuracy of NIR-based MFCOs: *Random errors* (e.g., due to different particle orientations) can be compensated by aggregating the data over sufficiently large *chunk sizes*. The influence of chunk sizes on measurement accuracies can be described by the material area per chunk: with increasing chunk size, the MU decreases asymptotically. *Systematic errors*, such as composite effects of plastic packaging and segregation errors, can be compensated through regression models. By using a polynomial regression model (polynomial degree two), the MU was on average reduced by a factor of 4.6 and 3.5 compared to density- or grammage-based conversion approaches for T1 and T2, respectively. By combining all findings, accuracies of $MU_{95} = 1.2$ vol% ($MAE = 0.5$ vol%; $R^2 = 99.9\%$) for plastic flakes (T1) and $MU_{95} = 2.4$ wt% ($MAE = 1.0$ wt%; $R^2 = 99.4\%$) for plastic packaging (T2) could be achieved.

Our results show that NIR-based determination of mass-based MFCOs in mechanical recycling of post-consumer plastics is technically feasible. However, they also indicate how significantly external factors like particle characteristics and MFPs can influence measurement accuracy and thus highlight the importance of material- and application-specific data processing techniques.

In future research, our results should be further scaled up. In addition to plant-scale investigations, we consider investigations on non-binary LWP mixtures; transfer to other polymers, particle size distributions, and material flows; as well as gaining a better understanding of segregation processes of anthropogenic material systems like LWP to be of particular importance.

Combining inline NIR sensors and adequate data processing techniques provides meaningful material information not only at the pixel and particle level but also at the material flow level and beyond. Based on the technical feasibility demonstrated in this study, new SBMC applications can be developed to accelerate the transition to more sustainable and efficient post-consumer plastics loops.

Funding

This work was funded by the German Federal Ministry of Education and Research (BMBF) within the program "Resource-efficient circular economy - plastics recycling technologies (KuRT)" under the project *ReVise* (grant no. 033R341) and the National Austrian Research Promotion Agency (FFG) within the program "Production of the Future" under the project *EsKorte* (grant no. 877341). The responsibility for the content of this publication lies with the authors.

CRediT authorship contribution statement

Nils Kroell: Conceptualization, Methodology, Software, Validation, Formal analysis, Investigation, Data curation, Writing – original draft, Writing – review & editing, Visualization, Supervision, Project administration, Funding acquisition. **Xiaozheng Chen:** Conceptualization, Methodology, Software, Validation, Writing – review & editing, Visualization, Funding acquisition. **Bastian Küppers:** Conceptualization, Methodology, Validation, Writing – review & editing. **Julius Lorenzo:** Investigation, Data curation, Writing – review & editing. **Abtin Maghmoumi:** Software, Data curation, Writing – review & editing, Visualization. **Matthias Schlaak:** Investigation, Writing – review & editing. **Eric Thor:** Software, Data curation, Writing – review & editing, Visualization. **Christian Nordmann:** Resources, Writing – review & editing, Funding acquisition. **Kathrin Greiff:** Supervision, Writing – review & editing, Funding acquisition.

Declaration of Competing Interest

The authors declared no potential conflicts of interest concerning the research, authorship, and/or publication of this article.

Data availability

Data will be made available on request.

Acknowledgments

We would like to thank STADLER Anlagenbau GmbH for providing the conveyor belt for T2 and Hündgen Entsorgungs GmbH & Co. KG for providing the LWP samples for T2. Many thanks to Christian de Ridder for his support in the practical investigations (T2).

Supplementary materials

Supplementary material associated with this article can be found, in the online version, at doi:10.1016/j.resconrec.2023.106873.

References

Alassali, A., Picuno, C., Chong, Z.K., Guo, J., Maletz, R., Kuchta, K., 2021. Towards higher quality of recycled plastics: limitations from the material's perspective. Sustainability 13 (23), 13266. https://doi.org/10.3390/su132313266.

Avio, C.G., Gorbi, S., Regoli, F., 2017. Plastics and microplastics in the oceans: from emerging pollutants to emerged threat. Mar. Environ. Res. 128, 2–11. https://doi.org/10.1016/j.marenvres.2016.05.012.

Binder+Co AG. Service Products, 2022. https://www.binder-co.com/1342/Service-Products#Plant-Improvements (accessed August 16, 2022).

Bradski, G., 2000. The OpenCV Library. Dr. Dobb's. Journal of Software Tools.

Chen, X., Feil, A., 2019. Detection and classification of heterogeneous materials as well as small particles using NIR-spectroscopy by validation of algorithms. In: Beyerer, J, Puente León, F, Längle, T (Eds.), OCM 2019 - Optical Characterization of Materials Conference Proceedings. KIT Scientific Publishing, pp. 63–77.

Chen, X., Kroell, N., Althaus, M., Pretz, T., Pomberger, R., Greiff, K., 2023. Enabling mechanical recycling of plastic bottles with shrink sleeves through near-infrared spectroscopy and machine learning algorithms. Resour. Conserv. Recycl. 188, 106719 https://doi.org/10.1016/j.resconrec.2022.106719.

Chen, X., Kroell, N., Dietl, T., Feil, A., Greiff, K., 2021a. Influence of long-term natural degradation processes on near-infrared spectra and sorting of post-consumer plastics. Waste Manag. 136, 213–218. https://doi.org/10.1016/j.wasman.2021.10.006.

Chen, X., Kroell, N., Wickel, J., Feil, A., 2021b. Determining the composition of post-consumer flexible multilayer plastic packaging with near-infrared spectroscopy. Waste Manag. 123, 33–41. https://doi.org/10.1016/j.wasman.2021.01.015.

Crespy, D., Bozonnet, M., Meier, M., 2008. 100 years of bakelite, the material of a 1000 uses. Angew. Chem. Int. Ed. Engl. 47 (18), 3322–3328. https://doi.org/10.1002/anie.200704281.

Cudjoe, D., Zhu, B., Nketiah, E., Wang, H., Chen, W., Qianqian, Y., 2021. The potential energy and environmental benefits of global recyclable resources. Sci. Total Environ. 798, 149258 https://doi.org/10.1016/j.scitotenv.2021.149258.

Curtis, A., Küppers, B., Möllnitz, S., Khodier, K., Sarc, R., 2021. Real time material flow monitoring in mechanical waste processing and the relevance of fluctuations. Waste Manag. 120 (1), 687–697. https://doi.org/10.1016/j.wasman.2020.10.037.

Davidson, M.G., Furlong, R.A., McManus, M.C., 2021. Developments in the life cycle assessment of chemical recycling of plastic waste – a review. J. Clean. Prod. 293, 126163 https://doi.org/10.1016/j.jclepro.2021.126163.

Deutsches Institut für Normung e.V. In: DIN 1310: Zusammensetzung von Mischphasen, 1984. Gasgemische, Lösungen, Mischkristalle); Begriffe, Formelzeichen.

Dris, R., Agarwal, S., Laforsch, C., 2020. Plastics: from a success story to an environmental problem and a global challenge. ***Global challenges*** (Hoboken, NJ) 4 (6), 2000026. https://doi.org/10.1002/gch2.202000026.

EVK Kerschhaggl GmbH. EVK HELIOS NIR G2-320: smart hyperspectral imaging camera, 2022a. https://www.evk.biz/en/products/hyperspectral-camera/evk-helios-nir-g2-320-class/(accessed December 11, 2022).

EVK Kerschhaggl GmbH. EVK SQALAR: software Tool for the qualitative and quantitative analysis, 2022b. https://www.evk.biz/en/products/analysis-software-tool/evk-sqalar/(accessed December 11, 2022).

Fahrmeir, L., Kneib, T., Lang, S., Marx, B., 2013. *Regression: Models, Methods and Applications*. Springer, Berlin, Heidelberg.

Feil, A., Kroell, N., Pretz, T., Greiff, K., 2021. Anforderungen an eine effiziente technologische Behandlung von Post-Consumer Verpackungsmaterialien in Sortieranlagen. Müll und Abfall 21 (7), 362–370. https://doi.org/10.37307/j.1863-9763.2021.07.04.

Feil, A., Pretz, T., 2020. Mechanical recycling of packaging waste. In: Letcher, T.M. (Ed.), *Plastic Waste and recycling: Environmental impact, Societal issues, prevention, and*

Solutions. Academic Press, Amsterdam, San Diego, Cambridge, MA, Kidlington, pp. 283–319.
Friedrich, K., Koinig, G., Pomberger, R., Vollprecht, D., 2022. Qualitative analysis of post-consumer and post-industrial waste via near-infrared, visual and induction identification with experimental sensor-based sorting setup. MethodsX 9, 101686. https://doi.org/10.1016/j.mex.2022.101686.
Geyer, R., Jambeck, J.R., Law, K.L., 2017. Production, use, and fate of all plastics ever made. Sci. Adv. 3 (7), e1700782 https://doi.org/10.1126/sciadv.1700782.
Harris, C.R., Millman, K.J., van der Walt, S.J., Gommers, R., Virtanen, P., Cournapeau, D., et al., 2020. Array programming with NumPy. Nature 585 (7825), 357–362. https://doi.org/10.1038/s41586-020-2649-2.
Hunter, J.D, 2007. Matplotlib: a 2D graphics environment. Comput. Sci. Eng. 9 (3), 90–95. https://doi.org/10.1109/MCSE.2007.55.
Initiative „Mülltrennung wirkt, 2021. ". Ein Jahr Initiative „Mülltrennung wirkt": von den Herausforderungen zum Erfolg: duale Systeme bilden eine starke Allianz für mehr Aufklärung. Müll und Abfall (7), 352–360. https://doi.org/10.37307/j.1863-9763.2021.07.03.
ISO, 2022. ISO 5725. International Organization for Standardization, Geneva accessed October 22, 2022.
Jambeck, J.R., Geyer, R., Wilcox, C., Siegler, T.R., Perryman, M., Andrady, A., et al., 2015. Marine pollution. Plastic waste inputs from land into the ocean. Science 347 (6223), 768–771. https://doi.org/10.1126/science.1260352.
Kleinhans, K., Küppers, B., Hernández Parrodi, J.C., Raegert, K., Dewulf, J., de, Meester S, et al., 2022. Challenges faced during a near-infrared-based material flow characterization study of commercial and industrial waste. In: Greiff, K, Wotruba, H, Feil, A, Kroell, N, Chen, X, Gürsel, D, et al. (Eds.), 9th Sensor-Based Sorting & Control, 13.04.2022 - 14.04.2022: Aachen; 2022.
Kroell, N., 2021. imea: a Python package for extracting 2D and 3D shape measurements from images. J. Open Source Softw. 6 (60), 3091 https://doi.org/10.21105/joss.03091.
Kroell, N., Chen, X., Greiff, K., Feil, A., 2022a. Optical sensors and machine learning algorithms in sensor-based material flow characterization for mechanical recycling processes: a systematic literature review. Waste Manag. 149, 259–290. https://doi.org/10.1016/j.wasman.2022.05.015.
Kroell, N., Chen, X., Maghmoumi, A., Koenig, M., Feil, A., Greiff, K., 2021. Sensor-based particle mass prediction of lightweight packaging waste using machine learning algorithms. Waste Manag. 136, 253–265. https://doi.org/10.1016/j.wasman.2021.10.017.
Kroell, N., Dietl, T., Maghmoumi, A., Chen, X., Küppers, B., Feil, A., et al., 2022b. Assessment of sensor-based sorting performance for lightweight packaging waste through sensor-based material flow monitoring: concept and preliminary results. In: Greiff, K, Wotruba, H, Feil, A, Kroell, N, Chen, X, Gürsel, D, et al. (Eds.), 9th Sensor-Based Sorting & Control, 13.04.2022 - 14.04.2022: Aachen, 2022.
Küppers, B., Chen, X., Seidler, I., Friedrich, K., Raulf, K., Pretz, T., et al., 2019a. Influences and consequences of mechanical delabelling on pet recycling. Detritus 06 (0), 1. https://doi.org/10.31025/2611-4135/2019.13816. - June 2019.
Küppers, B., Schloegl, S., Oreski, G., Pomberger, R., Vollprecht, D., 2019b. Influence of surface roughness and surface moisture of plastics on sensor-based sorting in the near infrared range. Waste management & research the journal of the International Solid Wastes and Public Cleansing Association. ISWA 37 (8), 843–850. https://doi.org/10.1177/0734242X19855433.
Küppers, B., Schlögl, S., Kroell, N., Radkohl, V., et al., 2022. Relevance and challenges of plant control in the pre-processing stage for enhanced sorting performance. In: Greiff, K, Wotruba, H, Feil, A, Kroell, N, Chen, X, Gürsel, D, et al. (Eds.), 9th Sensor-Based Sorting & Control, 13.04.2022 - 14.04.2022: Aachen; 2022.
Länderarbeitsgemeinschaft Abfall, 2001. Richtlinie für das Vorgehen bei physikalischen und chemischen Untersuchungen im Zusammenhang mit der Verwertung/Beseitigung von Abfällen (LAGA PN 98).
Maisel, F., Chancerel, P., Dimitrova, G., Emmerich, J., Nissen, N.F., Schneider-Ramelow, M., 2020. Preparing WEEE plastics for recycling – How optimal particle sizes in pre-processing can improve the separation efficiency of high quality plastics. Resourc. Conserv. Recycl. 154, 104619 https://doi.org/10.1016/j.resconrec.2019.104619.
McKinney, W., 2010. Data structures for statistical computing in Python. In: Stéfan van der Walt, Jarrod Millman. Proceedings of the 9th Python in Science Conference.
Moore, C.J., 2008. Synthetic polymers in the marine environment: a rapidly increasing, long-term threat. Environ. Res. 108 (2), 131–139. https://doi.org/10.1016/j.envres.2008.07.025.
Nielsen, T.D., Hasselbalch, J., Holmberg, K., Stripple, J., 2020. Politics and the plastic crisis: a review throughout the plastic life cycle. WIREs Energy Environ. 9 (1) https://doi.org/10.1002/wene.360.
Pearson, K.VII, 1895. Note on regression and inheritance in the case of two parents. Proc. Royal Soc. London 58 (347–352), 240–242. https://doi.org/10.1098/rspl.1895.0041.
Pedregosa, F., Varoquaux, G., Gramfort, A., Michel, V., Thirion, B., Grisel, O., et al., 2011. Scikit-learn: machine learning in Python. J. Open Source Softw. 12, 2825–2830.
Pellenc ST SAS. MISTRAL+ CONNECT, 2022. https://www.pellencst.com/products (accessed August 16, 2022).
Plastic Europe. The circular economy for plastics: a European overview, 2022. https://plasticseurope.org/knowledge-hub/the-circular-economy-for-plastics-a-european-overview-2/(accessed May 27, 2022).
REDWAVE. REDWAVE mate, 2022. https://redwave.com/en/products?setLang=1 (accessed August 16, 2022).
Rosato, Strandburg, Prinz, Swendsen, 1987. Why the Brazil nuts are on top: size segregation of particulate matter by shaking. Phys. Rev. Lett. 58 (10), 1038–1040. https://doi.org/10.1103/PhysRevLett.58.1038.
Schlögl, S., Küppers, B., et al., 2022. Quantifying the delabelling performance using sensor-based material flow monitoring. In: Greiff, K, Wotruba, H, Feil, A, Kroell, N, Chen, X, Gürsel, D, et al. (Eds.), 9th Sensor-Based Sorting & Control, 13.04.2022 - 14.04.2022: Aachen; 2022.
Sesotec GmbH. Recycling sorting systems with conveyor belt, 2022. https://www.sesotec.com/emea/en/products/groups/recycling-sorting-systems-with-conveyor-belt (accessed August 16, 2022).
Shen, M., Huang, W., Chen, M., Song, B., Zeng, G., Zhang, Y., 2020. Micro)plastic crisis: un-ignorable contribution to global greenhouse gas emissions and climate change. J. Clean. Prod. 254, 120138 https://doi.org/10.1016/j.jclepro.2020.120138.
STEINERT GmbH. STEINERT.view, 2022. https://steinertglobal.com/de/steinert-digital/dashboard-view/(accessed August 16, 2022).
The pandas development team. pandas-dev/pandas: pandas: zenodo, 2020.
TOMRA System ASA. TOMRA Insight, 2022. https://www.tomra.com/en/solutions/waste-metal-recycling/tomra-insight (accessed August 16, 2022).
van der, Walt S, Schönberger, J.L., Nunez-Iglesias, J., Boulogne, F., Warner, J.D., Yager, N., et al., 2014. scikit-image: image processing in Python. PeerJ 2, e453. https://doi.org/10.7717/peerj.453.
Virtanen, P., Gommers, R., Oliphant, T.E., Haberland, M., Reddy, T., Cournapeau, D., et al., 2020. SciPy 1.0: fundamental algorithms for scientific computing in Python. Nat. Methods 17, 261–272. https://doi.org/10.1038/s41592-019-0686-2.
Waskom, M.L., 2021. seaborn: statistical data visualization. J. Open Source Softw. 6 (60), 3021. https://doi.org/10.21105/joss.03021.
Zheng, J., Suh, S., 2019. Strategies to reduce the global carbon footprint of plastics. Nat. Clim. Chang. 9 (5), 374–378. https://doi.org/10.1038/s41558-019-0459-z.

3.4 Publication E: NIR-MFCO dataset

> **Kroell**, **N.**, Chen, X., Maghmoumi, A., Lorenzo, J., Schlaak, M., Nordmann, C., Küppers, B., Thor, E., & Greiff, K. (2023). NIR-MFCO dataset: Near-infrared-based false-color images of post-consumer plastics at different material flow compositions and material flow presentations. *Data in brief*, *48*, 109054. https://doi.org/10.1016/j.dib.2023.109054

Although Publication D (Section 3.3) has proven the technical feasibility of predicting mass-based material flow composition of binary, post-consumer material mixtures using NIR-sensors and regression models, the presented approach could be developed further. For example, image pre-processing techniques or deep-learning algorithms could be applied to the false-color images before the pixel counting or for an even better prediction of mass-based material flow compositions from area-based false-color images. However, the creation of the data basis (NIR false-color images of binary waste mixtures with known composition) for Publication D (Section 3.3) involved considerable time and logistical effort. This is consistent with common surveys, which indicate that data scientists spend about 80% of their time creating and preparing datasets (Forbes, 2016). At the same time, Publication A (Section 2.1) shows that there have been few open-access datasets in SBMC research and 94% of all reviewed investigations by Publication A had to create the dataset themselves. To allow other researchers to develop and test additional machine and deep learning models to the presented challenge of predicting mass-based material flow compositions from NIR-based false-color data, the underlying *NIR-MFCO dataset* (Figure 3.4) of Publication D (Section 3.3) was published in Publication E. The *NIR-MFCO dataset* contains $n = 880$ NIR-based false-color images at different material flow compositions and material flow presentations. The associated data article describes in detail the creation and design as well as potential new use-cases of the dataset and makes it accessible to the global research community to further advance SBMC characterization methods and validate the stated hypothesis.

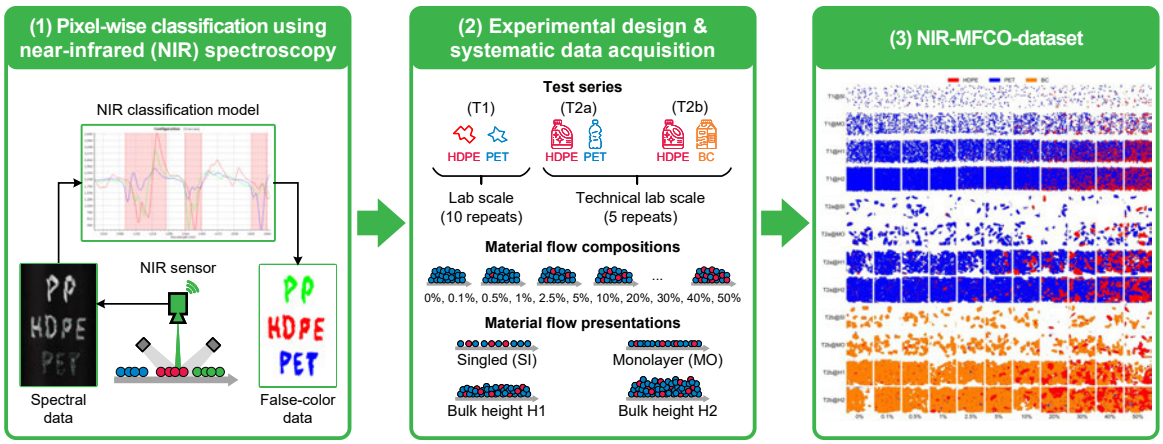

Figure 3.4. Graphical abstract Publication E.

Data in Brief 48 (2023) 109054

Contents lists available at ScienceDirect

Data in Brief

journal homepage: www.elsevier.com/locate/dib

Data Article

NIR-MFCO dataset: Near-infrared-based false-color images of post-consumer plastics at different material flow compositions and material flow presentations

Nils Kroell[a,*], Xiaozheng Chen[a], Abtin Maghmoumi[a], Julius Lorenzo[a], Matthias Schlaak[a], Christian Nordmann[b], Bastian Küppers[b], Eric Thor[a], Kathrin Greiff[a]

[a] Department of Anthropogenic Material Cycles, RWTH Aachen University, Wuellnerstr. 2, Aachen D-52062, Germany
[b] STADLER Anlagenbau GmbH, Max-Planck-Str. 2, Altshausen D-88361, Germany

ARTICLE INFO

Article history:
Received 16 February 2023
Revised 3 March 2023
Accepted 6 March 2023
Available online 14 March 2023

Dataset link: NIR-MFCO dataset: Near-infrared-based false-color images of post-consumer plastics at different material flow compositions and material flow presentations (Original data)

ABSTRACT

Determining mass-based material flow compositions (MFCOs) is crucial for assessing and optimizing the recycling of post-consumer plastics. Currently, MFCOs in plastic recycling are primarily determined through manual sorting analysis, but the use of inline near-infrared (NIR) sensors holds potential to automate the characterization process, paving the way for novel sensor-based material flow characterization (SBMC) applications. This data article aims to expedite SBMC research by providing NIR-based false-color images of plastic material flows with their corresponding MFCOs. The false-color images were created through the pixel-based classification of binary material mixtures using a hyperspectral imaging camera (EVK HELIOS NIR G2–320; 990 nm–1678 nm wavelength range) and the on-chip classification algorithm (CLASS 32). The resulting NIR-MFCO dataset includes $n = 880$ false-color images from three test series: (T1) high-density polyethylene (HDPE) and polyethylene terephthalate (PET)

Abbreviations: BC, beverage carton; HDPE, high-density polyethylene; LWP, lightweight packaging; MFCO, material flow composition; MFP, material flow presentation; MO, monolayer; NIR, near-infrared; PET, polyethylene terephthalate; RGB, red-green-blue; SBMC, sensor-based material characterization; SI, singled.

DOI of original article: 10.1016/j.resconrec.2023.106873

* Corresponding author.
E-mail address: nils.kroell@ants.rwth-aachen.de (N. Kroell).

https://doi.org/10.1016/j.dib.2023.109054

Keywords:
Sensor-based material flow characterization
Lightweight packaging waste
Mechanical plastic recycling
Circular economy
Machine learning
Computer vision
NIR spectroscopy
Polymers

flakes, (T2a) post-consumer HDPE packaging and PET bottles, and (T2b) post-consumer HDPE packaging and beverage cartons for $n = 11$ different HDPE shares (0% - 50%) at four different material flow presentations (singled, monolayer, bulk height H1, bulk height H2). The dataset can be used, e.g., to train machine learning algorithms, evaluate the accuracy of inline SBMC applications, and deepen the understanding of segregation effects of anthropogenic material flows, thus further advancing SBMC research and enhancing post-consumer plastic recycling.

Specifications Table

Subject	Environmental Engineering
Specific subject area	Sensor-based material flow characterization in mechanical recycling processes
Type of data	Images
How the data were acquired	1. Binary mixtures of (i) high-density polyethylene (HDPE) and polyethylene terephthalate (PET) flakes, (ii) post-consumer HDPE packaging and PET bottles, and (iii) HDPE packaging and beverage cartons were created with different HDPE contents. 2. The binary mixtures were repeatedly captured on a conveyor belt under different material flow presentations simulating different measurement situations of inline-sensor technology in sorting and processing plants. 3. A *HELIOS NIR G2–320* hyperspectral imaging camera (990 nm – 1678 nm wavelength range) from EVK Kerschhaggl GmbH (Raaba, Austria) was used to pixel-based classify the material flows into pre-defined material classes. The resulting false-color images were captured.
Data format	• Raw • Preprocessed (cropped, spatially calibrated, white space removed)
Description of data collection	False-color images were created using the on-chip CLASS32 classification algorithm from EVK Kerschhaggl GmbH (Raaba, Austria) and exported as bitmap files ("raw data"). Afterward, the bitmap files were preprocessed in Python to ensure a spatially equidistant data representation and exported uncompressed as PNG files to ensure interoperability ("preprocessed data"). Both, raw and preprocessed data are available within the NIR-MFCO dataset, along with the Python code for preprocessing.
Data source location	• Institution: Department of Anthropogenic Material Cycles • City: Aachen • Country: Germany
Data accessibility	Repository name: Zenodo Data identification number: 10.5281/zenodo.7638775 Direct URL to data: doi.org/10.5281/zenodo.7638775
Related research article	N. Kroell, X. Chen, B. Küppers, J. Lorenzo, A. Maghmoumi, M. Schlaak, E. Thor, C. Nordmann, K. Greiff, Near-infrared-based determination of mass-based material flow compositions in mechanical recycling of post-consumer plastics: Technical feasibility enables novel applications, Resources, Conservation and Recycling 191 (2023) 106873. https://doi.org/10.1016/j.resconrec.2023.106873. [1]

Value of the Data

- Contains false-color images from a total of $n = 880$ experiments of monitoring plastic material flows using near-infrared-based inline sensor technology on conveyor belts in combination with known material flow compositions for each experiment.
- The dataset is intended for researchers investigating novel applications of inline-sensor technology for the optimization of (mechanical) recycling processes [2]. Machine learning and computer vision researchers can use this dataset to train and assess different (machine learning) algorithms for predicting (mass-based) material flow compositions [1].
- Machine learning and image processing algorithms can be trained and assessed on predicting material flow compositions from near-infrared-based false-color images [1]. Furthermore, this dataset enables researchers to assess the accuracy of near-infrared-based inline material flow characterization under different measurement situations and can help gaining a better understanding of segregation effects of anthropogenic material flows [2].
- Data was collected from three test series (T1: HDPE and PET plastic flakes, T2a: post-consumer HDPE packaging and PET bottles, T2b: post-consumer HDPE packaging and beverage cartons) to simulate inline sensor technology applications in processing (T1) and sorting plants (T2).
- False-color images of four different material flow presentations (singled, monolayer, bulk height H1, bulk height H2 [1]) are included to simulate different sensor measurement situations in mechanical sorting and processing plants [1].
- For each test series and material flow presentation, $n = 11$ different material flow compositions have been recorded (0%; 0.1%; 0.5%; 1%; 2.5%; 5%; 10%; 20%; 30%; 40%; and 50% HDPE). Each experiment was repeated $n = 10$ (T1) and $n = 5$ (T2) times such that measurement repeatability and influences of different particle orientations can be quantified.

1. Objective

To increase plastic recirculation [3], mechanical plastic recycling processes need to be assessed and optimized, which requires known material flow compositions (MFCOs) [1,2,4]. Today, MFCOs in mechanical recycling are primarily determined through manual sorting analysis, which is time- and cost-intensive and thus often conducted on an irregular basis. In the future, inline sensor-based material flow characterization (SBMC) methods [2] could automate material flow characterization and enable novel SBMC applications to enhance plastic recirculation [4–6].

Numerous studies have demonstrated that post-consumer plastics can be classified with $>$ 99% accuracy using near-infrared (NIR) spectroscopy at pixel and particle level [2]. However, little research has been conducted so far at the material flow level, specifically on predicting MFCOs [2]. A particular barrier for SBMC research on the material flow level is the higher experimental effort for creating ground truth data since a material flow comprises hundreds to thousands of individual particles. The NIR-MFCO dataset aims at expediting SBMC research by lowering the experimental barrier at the material flow level through providing NIR-based false-color images of post-consumer plastics for different particle types, materials, and material flow presentations in combination with their corresponding MFCOs.

2. Data Description

2.1. Dataset Structure

2.1.1. Folder Structure

The NIR-MFCO dataset is constructed as a zip archive containing multiple levels of subfolders (Fig. 1a). In the first subfolder level, the full dataset is made available as *raw* (subfolder “raw”)

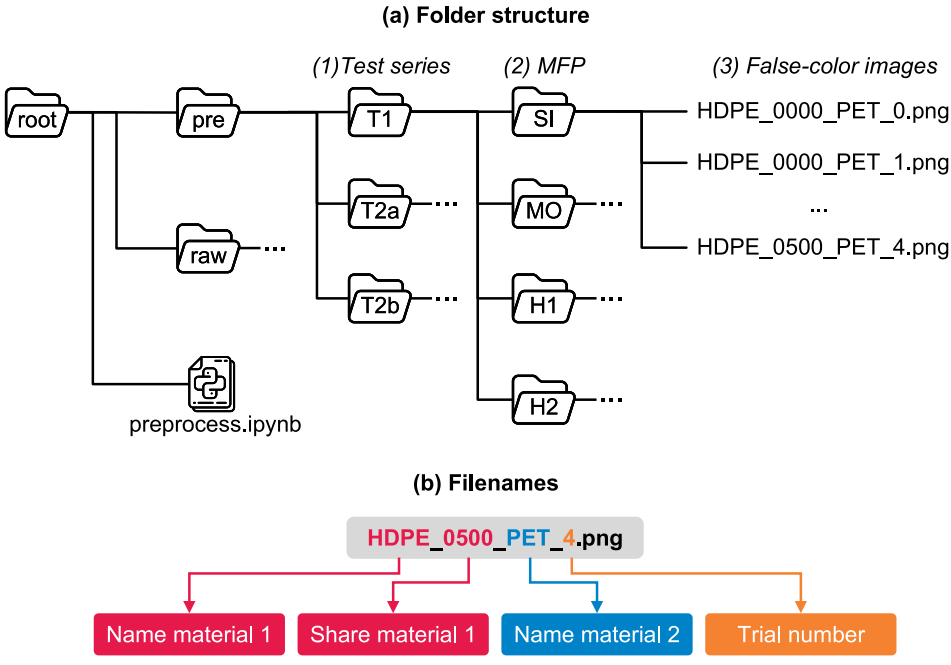

Fig. 1. Overview of the NIR-MFCO dataset.

Table 1
Summary of the three test series included in the NIR-MFCO dataset.

Test series	T1	T2a	T2b
Test rig	lab	technical lab	technical lab
Material 1	HDPE	HDPE	HDPE
Material 2	PET	PET bottles	BC
Particle type	flakes	LWP articles	LWP articles
Particle size range	10 mm – 20 mm	60 mm – 240 mm	60 mm – 240 mm
Share unit	vol%	wt%	wt%
#Repetitions	10	5	5
MFPs	SI, MO, H1, H2		
Material 1 shares	0%; 0.1%; 0.5%; 1%; 2.5%; 5%; 10%; 20%; 30%; 40%; 50%		
#Images	440	220	220

and *preprocessed* (subfolder "pre") data (cf. Section 3.4). Furthermore, we provide a Jupyter notebook to transform the raw into the preprocessed data ("preprocess.ipynb").

At the second subfolder level, the dataset is structured in three individual **test series** (T1, T2a, T2b). Test series T1 contains false-color images of HDPE and PET plastic flakes at different material flow presentations (MFPs) and with different HDPE shares in volume percent (cf. Section 3.1.1). Test series T2a contains false-color images of post-consumer HDPE packaging and post-consumer PET bottles, while test series T2b contains false-color images of post-consumer HDPE packaging and post-consumer beverage cartons (BCs). The materials for T2 were sampled from a LWP sorting plant and HDPE shares are given in mass percent (cf. Section 3.1.2).

At the third subfolder level, the false-color images of each test series are structured into four different **MFPs** (SI, MO, H1, H2; cf. Section 3.2). Within each subfolder, false-color images of binary mixtures at $n = 11$ different HDPE shares are provided (cf. Table 1). Each experiment was repeated $n = 10$ (T1) and $n = 5$ (T2) times (each repetition is referred to as a *trial* in the

Table 2
Definition of false colors (8-bit red-green-blue [RGB] values) used for all three test series.

Material class	Color name	R	G	B
HDPE	red	255	0	0
PET	blue	0	0	255
BC	orange	255	127	0
Background	white	255	255	255

following), resulting in $n = 110$ (T1) and $n = 55$ (T2a, T2b) false-color images per subfolder. Additionally, the third subfolder level of the *raw* dataset contains a folder "_calib" for spatially calibrating the false-color images (cf. Section 3.4.3). Table 1 summarizes the main characteristics of the NIR-MFCO dataset.

2.1.2. Format of Filenames

The material names of the binary mixtures (material 1 and material 2), material shares, and trial numbers are encoded within the filename as shown in Fig. 1b. In the filename, the share of a material is given directly after its name (cf. Fig. 1b). The material share is encoded as a dimensionless float (between 0 and 1) with three decimal place precision, and the comma point is not printed. For example, "0200" refers to a material share of 0.200, i.e., 20%; "0001" equals 0.1%, etc.

The share of the last material (material 2 for this dataset [$\emptyset_{\text{material 2}}$]) is not given since it can directly be calculated from the other material shares (all material shares sum up to 100%), see Eq. (1).

$$\emptyset_{\text{material 2}} = 1 - \emptyset_{\text{material 1}} \tag{1}$$

2.2. False-Color Images

2.2.1. False-Colors

In each image, the pixel-based classification results from the near-infrared (NIR) sensor are represented as 8-bit RGB false-colors, as shown by the example image sections in Fig. 2. Table 2 summarizes the color values of all three classified materials (HDPE, PET, BC) and background color including their RGB values.

2.2.2. Spatial Resolution

The raw false-color images of T1 have a spatial resolution of 1.64 mm/px in *x*-direction (conveyor direction, cf. Fig. 4) and 1.08 mm/px in *y*-direction (orthogonal to conveyor direction). For T2, the spatial resolutions are 3.98 mm/px and 3.50 mm/px in *x*- and *y*-direction, respectively. The preprocessed false-color images were spatially calibrated and thus have spatial resolutions of 1.08 mm/px in *x*- and *y*-direction for T1, and 3.50 mm/px in *x*- and *y*-direction for T2.

2.2.3. Image Formats

The original false-color images from the NIR sensor are saved as 8-bit bitmap (".bmp") images (as provided by the EVK SQALAR software). For better interoperability, we save the preprocessed false-color images as 8-bit ".png" images.

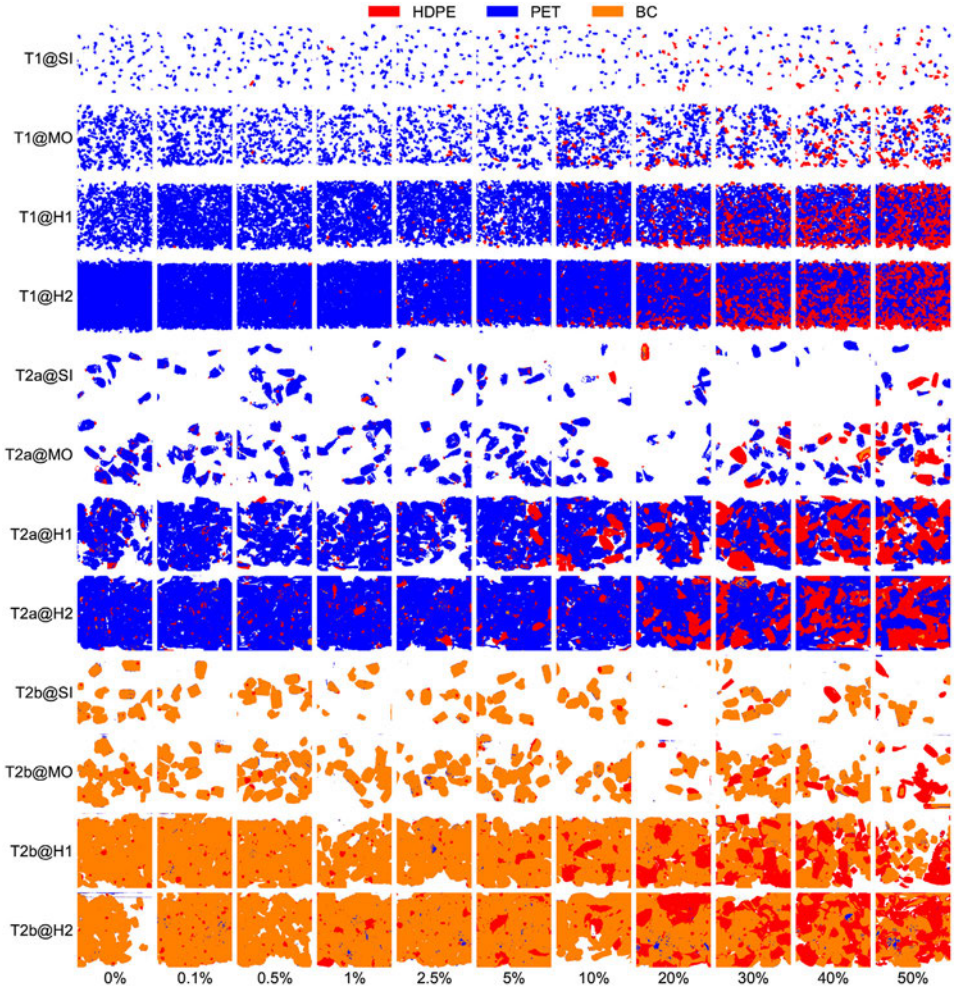

Fig. 2. Exemplary false-color-image sections for test series T1, T2a, and T2b at different MFPs (rows) and HDPE shares (columns), cf. [1].

3. Experimental Design, Materials and Methods

3.1. Materials

3.1.1. Plastic Flakes (T1)

For test series T1, plastic flakes with a particle size between 10 mm and 20 mm were created to simulate typical SBMC applications in processing plants [7]. The plastic flakes were created using white high-density polyethylene (HDPE) and transparent polyethylene terephthalate (PET) plates with a thickness of 3 mm from S-POLYTEC GmbH (Goch, Germany).

First, the HDPE and PET plates were comminuted in a rotary shear (MOCO Maschinen- und Apparatebau GmbH & Co. KG AZ 7 [Viernheim, Germany]) with a peripheral speed of 0.5 m/s, cutting disk width of 28 mm, and drive power of 7.5 kW for pre-crushing. Second, the pre-crushed HDPE and PET particles were further comminuted in a cutting mill (RETO RE-CYCLINGTECHNIK GmbH GA 37/450 [Bergkamen, Germany]) with a peripheral speed of 9 m/s,

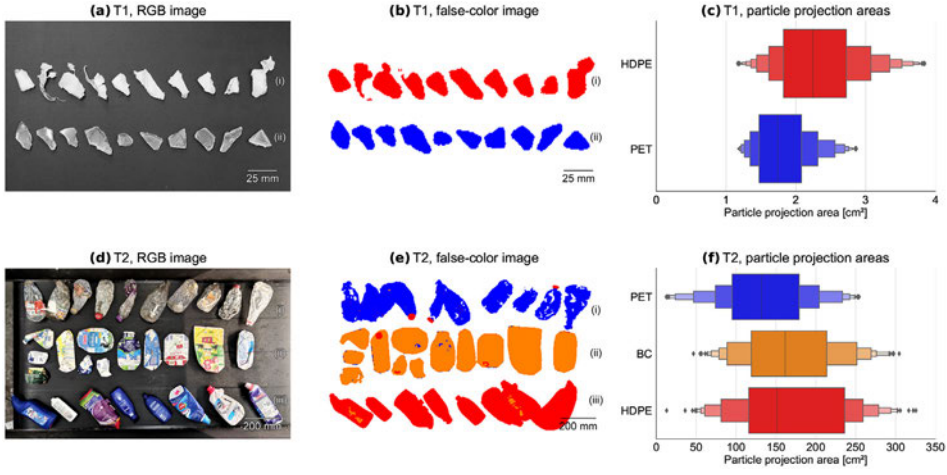

Fig. 3. Materials. (a) RGB images and (b) NIR false-color images for test series T1 [(i) HDPE, (ii) PET], (d) RGB images and (e) NIR false-color images for test series T2 [(i) PET, (ii) BC, (iii) HDPE], (c, f) distribution of particle projection areas per material for test series T1 (plastic flakes) and T2 (post-consumer plastic packaging), respectively, cf. [1].

Table 3
Grammages and raw densities of used materials within the NIR-MFCO dataset.

Test series	Material	Grammage [kg/m²]	Raw density [kg/m³]
T1	HDPE flakes	1.34[a]	960[b]
	PET flakes	2.66[a]	1270[b]
T2	HDPE packaging	2.46[a]	–
	PET bottles	2.30[a]	–
	BC	3.50[a]	–

Data source: [a]determined based on bulk mass from balance and total projection area per bulk determined by NIR recordings, [b]data sheet from S-POLYTEC GmbH (Goch, Germany).

rotor diameter of 350 mm, rotor length of 450 mm, output mesh size of 30 mm, and drive power of 37 kW.

Third, the plastic flakes were screened on an analytical sieve machine from Siebtechnik GmbH (Mühlheim [Ruhr], Germany) to produce plastic flakes in the desired size range of 10 mm to 20 mm, which is typically used in mechanical plastic recycling [7]. We used 10 mm and 20 mm round meshes and operated the screen at a speed of 1400 rpm for a sieving duration of 90 s.

Fig. 3a-c shows exemplary RGB images (a) and false-color images (b), as well as projection area distributions (c) of the investigated plastic flakes. Grammages and raw densities of the investigated materials are summarized in Table 3.

3.1.2. Lightweight Packaging (T2)

The goal of test series T2 is to simulate typical SBMC applications within sorting plants, in which material flows are presented as packaging articles [1]. Therefore, a sampling campaign was conducted in December 2020 at the LWP sorting plant Hündgen Entsorgungs GmbH & Co. KG in Swisttal (Germany). During the sampling campaign, each product fraction was sampled from the respective product fraction at the end of the technical sorting process and before manual sorting. From each product fraction (HDPE, PET bottles, and BC), a total volume of 1 m³ was sampled. To ensure maximum representativity during sampling, the full material flow was sampled from a continuously falling material stream according to LAGA PN98 [8]. The particle size range of the investigated LWP samples is approx. 60 mm – 240 mm [9]. Afterward, re-

maining impurities in the product fractions (fines [< 60 mm] and non-target material) were manually removed to obtain pure material fractions of each material. Fig. 3d–f shows exemplary RGB (d) and false-color images (e), as well as projection area distributions (f) of the investigated post-consumer plastic packaging. Grammages of the investigated materials are summarized in Table 3.

3.1.3. Binary Mixtures

Three types of binary mixtures were generated to simulate the influence of different materials and particle types: (T1) HDPE and PET flakes, (T2a) post-consumer HDPE and PET packaging, and (T2b) post-consumer HDPE and BC packaging. For all three mixtures, $n = 11$ HDPE shares were investigated: 0%; 0.1%; 0.5%; 1%; 2.5%; 5%; 10%; 20%; 30%; 40%; and 50%.

To make the dataset easier transferable to mixtures with different density combinations (e.g., polypropylene, or polyvinyl chloride), HDPE shares for T1 are prepared in volume percent (φ_i [vol%]). Since raw densities ρ_V of PET and HDPE flakes are known (Table 3), mass- (w_i) and volume-based MFCOs (φ_i) can be converted into each other using Eq. (2).

$$w_i = \frac{\varphi_i * \rho_{V,i}}{\sum_j \varphi_j * \rho_j} \tag{2}$$

For T2 (post-consumer packaging waste), an indication of material densities is not possible due to post-consumer waste characteristics (e.g., residual content, composites, hollow spaces). Therefore, material mixtures of T2 are created in mass percent (w_i [*wt%*]).

3.2. Test Rigs

To simulate applications of inline sensor technology in processing and sorting plants, a lab-scale and technical lab-scale test rig were constructed. Each test rig consists of (i) a feeding unit and conveyor belt to create different MFPs and (ii) a NIR sensor for data acquisition (Fig. 4).

The created mixtures were presented in four different MFPs to the NIR sensor:

- Singled (**SI**): Particles do not overlap and (mostly) do not touch each other.
- Monolayer (**MO**): Particles (mostly) do not overlap but touch each other.
- Bulk height (**H1, H2)**: Particles overlap and touch each other and thus create a multi-layered material bulk [1,2]. ($h_2 > h_1$; $h_{1,T1} \approx 10$ mm, $h_{2,T1} \approx 17$ mm, $h_{1,T2} \approx 150$ mm, $h_{2,T2} \approx 300$ mm).

For T1, different MFPs were achieved through a vibrating conveyor (AViTEQ Vibrationstechnik GmbH KF 12–2 [Hattersheim am Main, Germany]) operated at different conveying speeds (Fig. 4a). For T2, an ascending conveyor (1 m/s conveying speed, 600 mm belt width, 25° ascending angle) was used for feeding in the SI and MO trials (Fig. 4b.F1), and a dosing bunker (1000 mm width; 850 mm height; 2000 mm length) with a stamp were used for the feeding in the H1 and H2 trials (Fig. 4b.F2). In both test series, black conveyor belts were used for material transportation (conveyor width: $b_{T1} = 385$ mm, $b_{T2} = 845$ mm; conveying speed: $v_{T1} = 0.25$ m/s, $v_{T2} = 1$ m/s).

Since the recording of the sensor data was technically limited to 60 s per trial (maximum recording time of uninterrupted false-color data), the material mixtures per trial were adapted to the respective MFP (Table 4). Each mixture was measured $n = 10$ (T1) and $n = 5$ (T2) times for each HDPE share and MFP, resulting in a total of $n = 880$ trials.

3.3. Data Acquisition

3.3.1. NIR Sensor

A *HELIOS NIR G2–320* hyperspectral imaging camera from EVK DI Kerschhaggl GmbH (Raaba, Austria) was used to capture and classify the NIR spectra in both test series. The used spectral

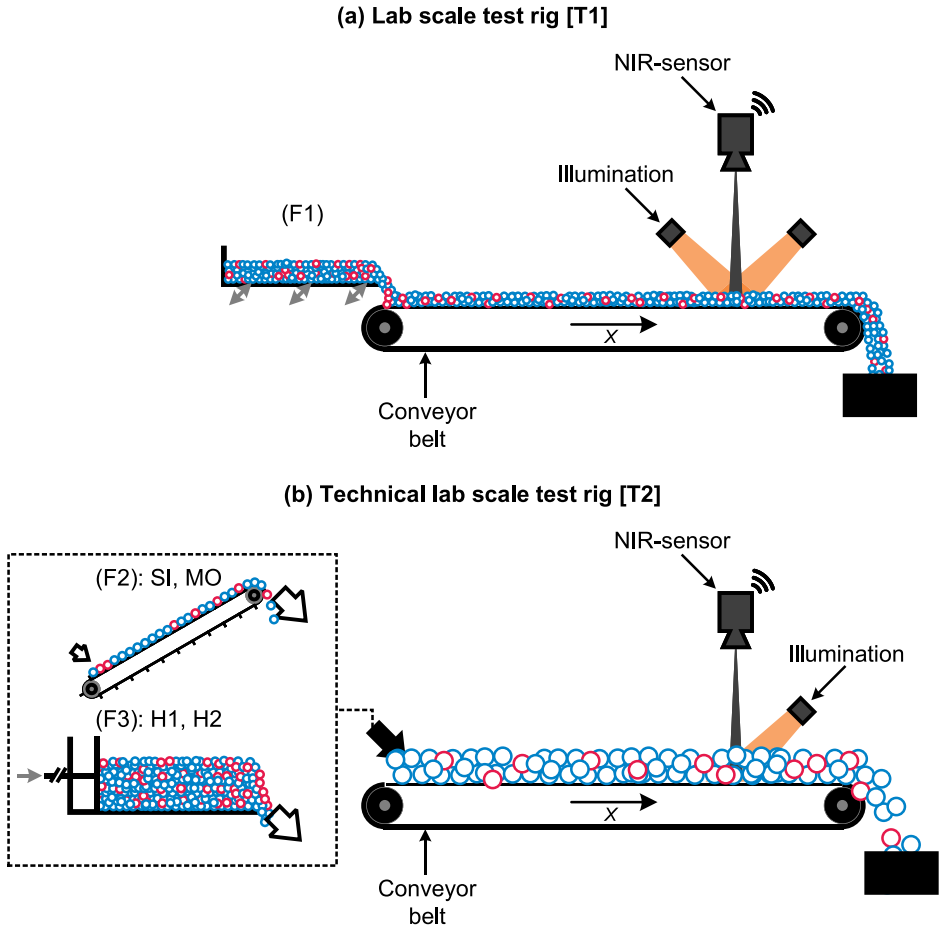

Fig. 4. NIR test rigs for test series T1 (lab scale) and test series T2 (technical lab scale). Material feeding: (F1): vibrating conveyor, (F2): ascending conveyor, (F3): dosing bunker with stamp, cf. [1].

Table 4
Feed volume for individual test series and MFPs in liter [L].

MFP	T1	T2
SI	6	300
MO	10	300
H1	12	500
H2	12	500

range of the sensor was 990 nm to 1678 nm with a spectral resolution of 3.1 nm/band. The used NIR sensor has an on-chip classification engine, which is frequently used in different industrial and research applications [5,10–16]. The resulting spatial resolution of the NIR sensor is 1.08 mm/px and 3.50 mm/px for T1 and T2, respectively (cf. Section 2.2.2). Four halogen lamps with a power of 400 W each were used as emitters and the reflection of radiation from the surface is captured by the NIR sensor. For test series T1, two halogen lamps each were illuminating the conveyor surface from front and back (Fig. 4a); for test series T2, four halogen lamps were illuminating the conveyor surface from front (against the conveyor direction) (Fig. 4b). Before

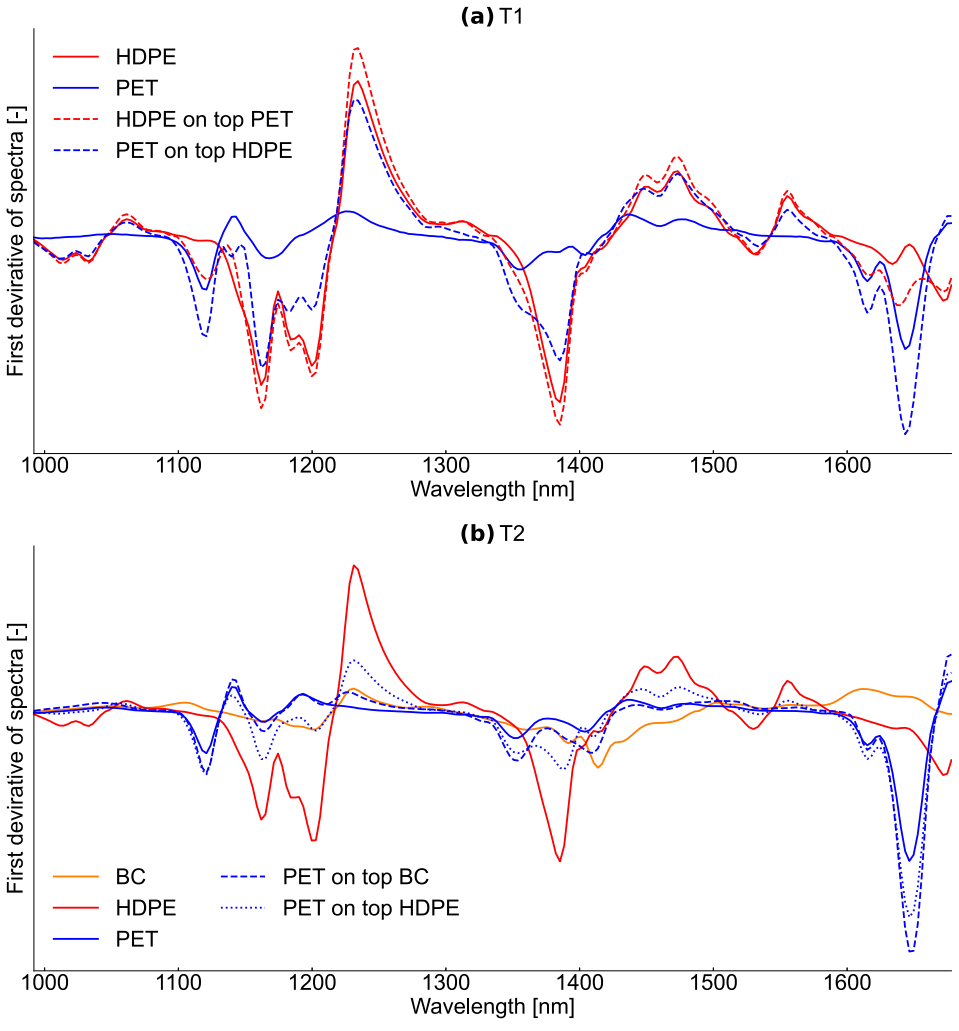

Fig. 5. NIR reference spectra used for NIR classification at test series T1 and T2, cf. [1].

each recording day, a black and white calibration of the NIR sensor was performed with the EVK SQALAR software using a white ceramic tile and switched on emitters (white calibration) and the black conveyor surface with switched off emitters (black calibration) [17].

3.3.2. NIR Classification Model

For each test rig, a NIR classification model was developed to classify each spectrum into background (conveyor belt) and user-defined material classes (T1: HDPE, PET; T2: HDPE, PET, BC). For background definition, a threshold was defined to segment the recordings into background and foreground (materials) based on the mean intensity of each spectrum. For material classification, the on-sensor CLASS32 algorithm from EVK DI Kerschhaggl GmbH (Raaba, Austria) was used. In CLASS32, NIR spectra are first preprocessed (first derivative, normalization, and smoothing) and then compared to user-defined reference spectra.

For defining NIR reference spectra shown in Fig. 5, representative regions of interest were selected for each material class. For T1, spectra were selected from the center of the plastic flakes

to avoid edge effects [18,19]. Accordingly, reference spectra of non-sleeved and non-labeled parts of the LWP samples were selected for T2. Additionally, overlays of transparent materials on top of other materials were added as reference spectra to avoid systematic misclassifications due to mixed NIR spectra in the case of transparency (e.g., a PET bottle on top of a HDPE bottle is classified as PET), cf. [16].

3.3.3. Export of False-Color Image

After each trial, the recorded false-color images of the "raw" section of this dataset were directly exported as ".bmp"-files. No further data processing was applied to the raw false-color images.

3.4. Data Preprocessing

The data preprocessing described below is intended to simplify subsequent data processing of users. However, users may also use the "raw" false-color images which are not affected by the data preprocessing. The described data preprocessing steps can be executed using the "preprocess.ipynb" Jupyter notebook included in the NIR-MFCO dataset. The preprocessing steps aim to remove irrelevant data (noise at the horizontal borders of the image and recordings of empty conveyor belt section at the beginning and end of each trial [white space]) and spatially calibrate the false-color images to ensure measurements independent of the particle orientation.

3.4.1. Horizontal Cropping

During the false-color image recording, disturbances can occur at the edge of the conveyor belt (e.g., entangled particles at the edge of the conveyor belt). Therefore, horizontal cropping is applied as a first step in the data preprocessing to cut off these disturbances. Per default, 15 px are cropped off from the left and right border of each false-color image.

3.4.2. White Space Removal

For the removal of white space, the false-color image is first segmented into a binary image, with the material areas representing the foreground ("True") and the conveyor belt representing the background ("False"). Second, small image noise (e.g., dust particles that are classified as material) is removed by area-opening with an area threshold of 40 px. Third, the first and last continuous image lines without material pixels are vertically cropped off.

3.4.3. Spatial Calibration

Each image is then spatially calibrated to ensure the same spatial resolution in x- (conveyor direction) and y-direction ("square pixels") by resizing the image in conveying direction. The resizing factor depends on the frame rate and resolution (#pixels per line) of the NIR sensor as well as speed and width of the used conveyor belt. For spatial calibration, we recorded multiple circle calibration targets (T1: $d = 60$ mm, T2: $d = 270$ mm; cf. folder "_calib" in the raw folder of the dataset) and determined the mean bounding box dimension in x- and y-direction ($\overline{BB}_x$, $\overline{BB}_y$). We then use these bounding box dimensions to determine a resize factor RF according to Eq. (3) and rescale the image by using the function *transform.rescale()* from *scikit-image* [20].

$$RF = \frac{\overline{BB}_y}{\overline{BB}_x} \tag{3}$$

Ethics Statement

This study does not involve experiments on humans or animals.

Declaration of Competing Interest

The authors declare that they have no known competing financial interests or personal relationships that could have appeared to influence the work reported in this paper.

Data Availability

NIR-MFCO dataset: Near-infrared-based false-color images of post-consumer plastics at different material flow compositions and material flow presentations (Original data) (Zenodo).

CRediT Author Statement

Nils Kroell: Conceptualization, Methodology, Software, Validation, Investigation, Data curation, Writing – original draft, Writing – review & editing, Visualization, Supervision, Project administration, Funding acquisition; **Xiaozheng Chen:** Conceptualization, Methodology, Validation, Writing – review & editing, Visualization, Funding acquisition; **Abtin Maghmoumi:** Software, Data curation, Writing – review & editing, Visualization; **Julius Lorenzo:** Investigation, Data curation, Writing – review & editing; **Matthias Schlaak:** Investigation, Writing – review & editing; **Christian Nordmann:** Resources, Writing – review & editing, Funding acquisition; **Bastian Küppers:** Conceptualization, Methodology, Writing – review & editing; **Eric Thor:** Writing – review & editing, Visualization; **Kathrin Greiff:** Supervision, Writing – review & editing, Funding acquisition.

Acknowledgments

We would like to thank STADLER Anlagenbau GmbH for providing the conveyor belt for T2 and Hündgen Entsorgungs GmbH & Co. KG for providing the LWP samples for T2. Many thanks to Christian de Ridder for his support in the practical investigations (T2).

Funding: This work was funded by the German Federal Ministry of Education and Research (BMBF) within the program “Resource-efficient circular economy - plastics recycling technologies (KuRT)” under the project ReVise (Grant No. 033R341) and the National Austrian Research Promotion Agency (FFG) within the program “Production of the Future” under the project EsKorte (Grant No. 877341). The responsibility for the content of this publication lies with the authors.

Supplementary Materials

Supplementary material associated with this article can be found, in the online version, at doi:10.1016/j.dib.2023.109054.

References

[1] N. Kroell, X. Chen, B. Küppers, J. Lorenzo, A. Maghmoumi, M. Schlaak, E. Thor, C. Nordmann, K. Greiff, Near-infrared-based determination of mass-based material flow compositions in mechanical recycling of post-consumer plastics: technical feasibility enables novel applications, Resour. Conserv. Recycl. 191 (2023) 106873, doi:10.1016/j.resconrec.2023.106873.

[2] N. Kroell, X. Chen, K. Greiff, A. Feil, Optical sensors and machine learning algorithms in sensor-based material flow characterization for mechanical recycling processes: a systematic literature review, Waste Manag. 149 (2022) 259–290, doi:10.1016/j.wasman.2022.05.015.

[3] European Commission, Circular Economy Action Plan: For A Cleaner and More Competitive, European Commission, Europe, 2020.

[4] R. Sarc, A. Curtis, L. Kandlbauer, K. Khodier, K.E. Lorber, R. Pomberger, Digitalisation and intelligent robotics in value chain of circular economy oriented waste management - a review, Waste Manag. 95 (2019) 476–492, doi:10.1016/j.wasman.2019.06.035.

[5] B. Küppers, S. Schlögl, N. Kroell, V. Radkohl, Relevance and challenges of plant control in the pre-processing stage for enhanced sorting performance, in: Proceedings of the 9th Sensor-Based Sorting & Control 2022, Aachen, 2022, doi:10.2370/9783844085457.
[6] N. Kroell, T. Dietl, A. Maghmoumi, X. Chen, B. Küppers, A. Feil, K. Greiff, Assessment of sensor-based sorting performance for lightweight packaging waste through sensor-based material flow monitoring: concept and preliminary results, in: Proceedings of the 9th Sensor-Based Sorting & Control 2022, Aachen, 2022, doi:10.2370/9783844085457.
[7] F. Maisel, P. Chancerel, G. Dimitrova, J. Emmerich, N.F. Nissen, M. Schneider-Ramelow, Preparing WEEE plastics for recycling – how optimal particle sizes in pre-processing can improve the separation efficiency of high quality plastics, Resour. Conserv. Recycl. 154 (2020) 104619, doi:10.1016/j.resconrec.2019.104619.
[8] Länderarbeitsgemeinschaft Abfall, Richtlinie für das Vorgehen bei physikalischen und chemischen Untersuchungen im Zusammenhang mit der Verwertung/Beseitigung von Abfällen, 2001 https://www.laga-online.de/documents/m32_laga_pn98_1503993280.pdf.
[9] N. Kroell, X. Chen, A. Maghmoumi, M. Koenig, A. Feil, K. Greiff, Sensor-based particle mass prediction of lightweight packaging waste using machine learning algorithms, Waste Manag. 136 (2021) 253–265, doi:10.1016/j.wasman.2021.10.017.
[10] A. Curtis, B. Küppers, S. Möllnitz, K. Khodier, R. Sarc, Real time material flow monitoring in mechanical waste processing and the relevance of fluctuations, Waste Manag. 120 (2021) 687–697, doi:10.1016/j.wasman.2020.10.037.
[11] X. Chen, N. Kroell, T. Dietl, A. Feil, K. Greiff, Influence of long-term natural degradation processes on near-infrared spectra and sorting of post-consumer plastics, Waste Manag. 136 (2021) 213–218, doi:10.1016/j.wasman.2021.10.006.
[12] X. Chen, N. Kroell, K. Li, A. Feil, T. Pretz, Influences of bioplastic polylactic acid on near-infrared-based sorting of conventional plastic, Waste Manag. Res. 39 (2021) 734242X211003969, doi:10.1177/0734242X211003969.
[13] X. Chen, N. Kroell, J. Wickel, A. Feil, Determining the composition of post-consumer flexible multilayer plastic packaging with near-infrared spectroscopy, Waste Manag. 123 (2021) 33–41, doi:10.1016/j.wasman.2021.01.015.
[14] X. Chen, N. Kroell, M. Althaus, T. Pretz, R. Pomberger, K. Greiff, Enabling mechanical recycling of plastic bottles with shrink sleeves through near-infrared spectroscopy and machine learning algorithms, Resour. Conserv. Recycl. 188 (2023) 106719, doi:10.1016/j.resconrec.2022.106719.
[15] K. Friedrich, G. Koinig, R. Pomberger, D. Vollprecht, Qualitative analysis of post-consumer and post-industrial waste via near-infrared, visual and induction identification with experimental sensor-based sorting setup, MethodsX 9 (2022) 101686, doi:10.1016/j.mex.2022.101686.
[16] K. Kleinhans, B. Küppers, J.C. Hernández Parrodi, K. Raegert, J. Dewulf, S. de Meester, Challenges faced during a near-infrared-based material flow characterization study of commercial and industrial waste, in: Proceedings of the 9th Sensor-Based Sorting & Control 2022, Aachen, 2022, pp. 71–84.
[17] EVK Kerschhaggl GmbH, EVK SQALAR: Software Tool for the Qualitative and Quantitative Analysis, 2022 https://www.evk.biz/en/products/analysis-software-tool/evk-sqalar/. Accessed March 16, 2023.
[18] X. Chen, A. Feil, Detection and classification of heterogeneous materials as well as small particles using NIR-spectroscopy by validation of algorithms, in: J. Beyerer, F. Puente León, T. Längle (Eds.), Proceedings of the Optical Characterization of Materials Conference Proceedings OCM 2019, KIT Scientific Publishing, 2019, pp. 63–77, doi:10.5445/KSP/1000087509.
[19] B. Küppers, X. Chen, I. Seidler, K. Friedrich, K. Raulf, T. Pretz, A. Feil, R. Pomberger, D. Vollprecht, Influences and consequences of mechanical delabelling on pet recycling, Detritus 6 (2019) 39–46, doi:10.31025/2611-4135/2019.13816.
[20] S. van der Walt, J.L. Schönberger, J. Nunez-Iglesias, F. Boulogne, J.D. Warner, N. Yager, E. Gouillart, T. Yu, the scikit-image contributors, scikit-image: image processing in Python, PeerJ 2 (2014) e453, doi:10.7717/peerj.453.

4 Novel SBMC applications

Chapter 3 demonstrated that mass-based material flow compositions of post-consumer material flows can be determined with high accuracy using sensor technology and application-specific ML models. Chapter 4 aims to transfer the developed characterization methods into two novel SBMC applications (RQ III) and prove their technical feasibility at an industrial scale.

4.1 Publication F: Sensor-based quality control

> **Kroell, N.**, Chen, X., Küppers, B., Schlögl, S., Feil, A., & Greiff, K. (2024). Near-infrared-based quality control of plastic pre-concentrates in lightweight-packaging waste sorting plants. *Resources, Conservation and Recycling*, *201*, 107256. https://doi.org/10.1016/j.resconrec.2023.107256

As outlined in Section 1.2, the lack of transparency of up-to-date pre-concentrate qualities leads to inefficient secondary raw material markets and a lack of incentives for plant operators to further improve pre-concentrate qualities. Based on the characterization methods from Chapter 3, Publication F therefore aims at demonstrating the technical feasibility of an inline NIR-based pre-concentrate quality monitoring in a state-of-the-art LWP sorting plant (Figure 4.1). In particular, it should be investigated to what extent the encouraging results from Section 3.3 for binary mixtures of LWP packaging at technical scale can be reproduced for heterogeneous material flows at industrial plant scale and to what extent the developed sensor-based quality control (SBQC) approach can compete with state-of-the-art manual quality control procedures.[4]

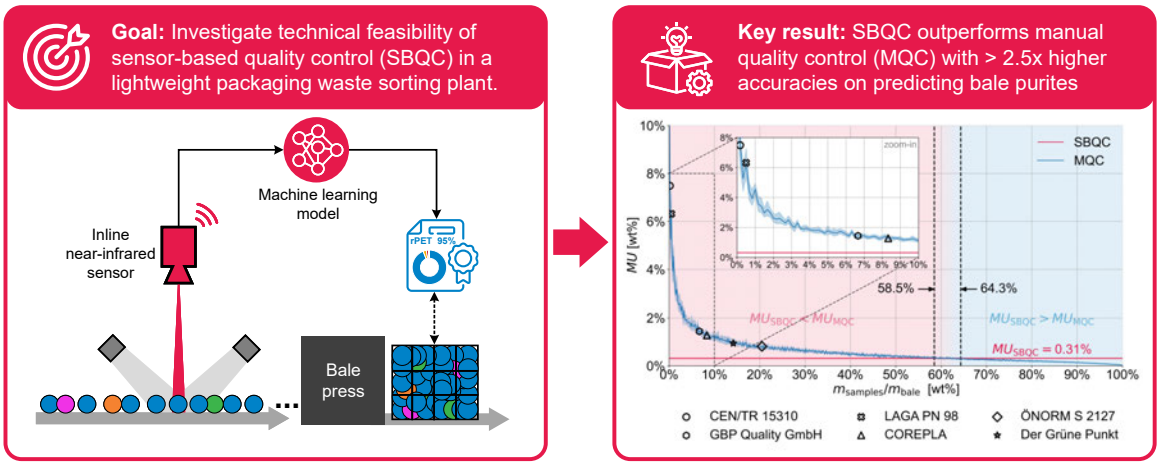

Figure 4.1. Graphical abstract Publication F.

[4]Supplementary materials for Publication F are provided in Appendix B.

Resources, Conservation & Recycling 201 (2024) 107256

Contents lists available at ScienceDirect

Resources, Conservation & Recycling

journal homepage: www.elsevier.com/locate/resconrec

Near-infrared-based quality control of plastic pre-concentrates in lightweight-packaging waste sorting plants

Nils Kroell [a,*], Xiaozheng Chen [b], Bastian Küppers [b], Sabine Schlögl [c], Alexander Feil [a], Kathrin Greiff [a]

[a] Department of Anthropogenic Material Cycles, RWTH Aachen University, Wuellnerstr. 2, D-52062, Aachen, Germany
[b] STADLER Anlagenbau GmbH, Max-Planck-Str. 2, D-88361, Altshausen, Germany
[c] Chair of Waste Processing Technology and Waste Management, Montanuniversity Leoben, A-8700, Leoben, Austria

ARTICLE INFO

Keywords:
Sensor-based material flow characterization
Automated quality control
Inline quality monitoring
Circular economy
Mechanical post-consumer plastic recycling
Machine learning

ABSTRACT

Today's post-consumer plastic recycling is limited by labor-intensive manual quality control (MQC) procedures, resulting in largely unknown pre-concentrate purities. Sensor-based quality control (SBQC) could enable an automated inline quality monitoring and thus contribute to a more transparent and enhanced plastic recycling. Therefore, we investigated the technical feasibility of near-infrared-based SBQC for plastic pre-concentrates in a lightweight packaging waste sorting plant. The developed SBQC method outperformed MQC methods by reducing measurement uncertainties from between ±0.8 wt% and ±6.7 wt% (MQC) to ±0.31 wt% (SBQC) for bale-specific purities at monolayered material flow presentations. In addition, we show that SBQC may even be possible at multilayered material flow presentations, although further research is needed to address identified segregation effects. The demonstrated technical feasibility of SBQC at plant scale represents a major breakthrough as it opens new opportunities in plastic recycling, such as adaptive pricing models and intelligent process control in sorting plants.

Abbreviations

BC	beverage carton;
BG	background;
CSV	comma-separated value;
DSD	Der Grüne Punkt Duales System Deutschland GmbH;
EU	European Union;
HDPE	high-density polyethylene;
LWP	lightweight packaging;
ML	machine learning;
MQC	manual quality control;
MU	measurement uncertainty;
NIR	near-infrared;
nMU	normalized measurement uncertainty;
PCC	Pearson correlation coefficient;
PET	polyethylene terephthalate;
PP	polypropylene;
PPC	paper, paperboard, and cardboard;
PS	polystyrene;
RGB	red, green, blue;
RQ	research question;
SBQC	sensor-based quality control;
SP	sensor position;
UNDEF	undefined

1. Introduction

In 2020, the European Union (EU) 27+3 collected 29.5 Mt/a of post-consumer plastic waste, but only 18.6 wt%[1] to 22.0 wt%[2] of the collected plastics were turned into plastic recyclates, while the remainder was incinerated or landfilled (Plastic Europe, 2022b). Therefore, massive improvements in post-consumer plastic recycling are needed to make a relevant contribution to climate and resource protection (European Commission, 2019; United Nations, 2015) and a competitive circular economy (Bachmann et al., 2023; European Commission, 2020).

* Corresponding author at: Department of Anthropogenic Material Cycles, RWTH Aachen University, Wuellnerstr. 2, D-52062, Aachen, Germany.
E-mail address: nils.kroell@ants.rwth-aachen.de (N. Kroell).

[1] Assuming all exported material was incinerated or landfilled.
[2] Assuming all exported material was processed into 100% recyclates.

https://doi.org/10.1016/j.resconrec.2023.107256
Received 26 May 2023; Received in revised form 6 September 2023; Accepted 10 October 2023

Plastic packaging is the largest source of post-consumer plastic waste in the EU 27+3, amounting to 17.9 Mt/a (60.7 wt% of the total post-consumer plastic waste) in 2020 (Plastic Europe, 2022a). Recycling of post-consumer packaging waste involves three stages: plastic waste collection based on country/region-specific collection schemes, sorting into material-specific pre-concentrates in *sorting plants*, and processing pre-concentrates into recyclates in *processing plants* (Feil and Pretz, 2020). Generated plastic recyclates can then substitute primary plastics during production processes and achieve significant environmental benefits, e.g., in terms of energy and greenhouse gas emission savings (Bachmann et al., 2023; Cudjoe et al., 2021).

As the crucial intermediate between collection and processing, the *quality of pre-concentrates* generated in sorting plants significantly affects the overall process efficiency in post-consumer plastic recycling (Feil and Pretz, 2020). Low-quality pre-concentrates can lead to significant material losses and to sub-optimal recyclate quality in processing plants (Dehoust and Christiani, 2012), thereby hampering the substitution of primary plastics and ultimately limiting the achievable environmental benefits (bvse-Fachverband Kunststoffrecycling, 2017; Hahladakis and Iacovidou, 2018). Suboptimal pre-concentrate qualities have been criticized in the past (e.g., bvse-Fachverband Kunststoffrecycling, 2016; 2017; EU Recycling, 2018) and significant deviations from purity specifications have been documented (bvse-Fachverband Kunststoffrecycling, 2017; Knappe et al., 2021).

1.1. Limitations of manual quality control

Currently, the quality of plastic pre-concentrates is determined by manual quality control (MQC), i.e., sampling and manual sorting analysis (Borowski, 2018; Der Grüne Punkt, 2016). Because of the necessary sampling and manual sorting analysis, MQC is time-consuming and cost-intensive, and thus often only performed on an irregular basis (Borowski, 2018). For example, Borowski (2018) reports that a quality control team consisting of two to three experienced employees needs about two hours to analyze a single pre-concentrate bale (=4–6 person hours per bale), while modern sorting plants produce several hundred bales per day. Hence, quality control with MQC methods can only be performed on a spot-check basis for selected bales.

The lacking transparency on batch-specific pre-concentrate qualities currently results in pre-concentrates being traded on a *flat-rate basis*, i.e., irrespective of their (bale-specific) quality (plasticker, 2023). Thus, combined with high disposal costs for residual fractions, sorting plant operators have thus a business interest in sorting only "as good as necessary" instead of "as good as possible", since better sorting would lead to higher disposal costs for the higher quantity of the then generated sorting residues as well as lower income due to the reduced overall quantity of pre-concentrates (Knappe et al., 2021). In addition, technical optimizations in sorting plants can be challenging due to the missing benchmark without a reliable and in-time measurement of produced pre-concentrate qualities (Kroell et al., 2022a).

1.2. Opportunities through sensor-based quality control

Sensor-based quality control (SBQC) could enable automatic, real-time, and batch-specific knowledge of the quality (i.e., purity) of pre-concentrates and thus considerably enhance post-consumer plastic recycling (Kroell et al., 2022a):

1.2.1. Adaptive pricing models

By monitoring the quality of each batch, the pricing of pre-concentrates could transition from a flat-rate basis to adaptive pricing models, where higher pre-concentrate quality results in higher prices, thereby adjusting the incentives for sorting plant operators.

1.2.2. Process optimization in sorting plants

Automatic monitoring of pre-concentrate qualities would allow for timely detection and correction of quality deficits, e.g., by using adaptive process control of the sorting plant to improve overall sorting quality.

1.2.3. Evaluation and optimization of separate collection

Information on material composition and quantity of output fractions could be used to calculate back to the sorting plant input (collected mixed lightweight packaging waste), thus, enabling the evaluation and optimization of separate collection (e.g., assessment of public campaigns to improve separate collection [Initiative „Mülltrennung wirkt“, 2021]).

1.2.4. Process optimization in processing plants

By sharing data along the value chain, processing plants could benefit from known input qualities, e.g., through input-adaptive process parameterization to varying pre-concentrates qualities or an optimized distribution of pre-concentrate qualities across processing plants with different processing technologies and depths.

1.3. Related work and research gap

Data analysis for SBQC applications can be divided into pixel, particle, and material flow levels (Kroell et al., 2022a). At the pixel and particle level, numerous studies (e.g., Bonifazi et al., 2018; Calvini et al., 2018; Chen et al., 2021; Duan and Li, 2021; Xia et al., 2021; Zheng et al., 2018) have demonstrated that non-carbon-black plastics can be differentiated with $\geq$ 99% accuracy using near-infrared (NIR) spectroscopy.

However, the quality of plastic pre-concentrates is not defined in terms of pixels and particles but by the mass-based composition of the entire material flow, i.e., the aggregation of thousands of particles (cf. Section 2.1). Yet, little research has been conducted for sensor-based determination on mass-based material flow composition, which comes with a new set of challenges such as finding appropriate data aggregation methods, area-to-mass-conversion, and different counting basis (cf. Section 2.2) (Kroell et al., 2022a).

Kroell et al. (2023a) recently demonstrated the technical feasibility of predicting mass-based material flow compositions from NIR-based false-color data using machine learning (ML). Through regression models and data aggregation, it was possible to predict mass-based material flow compositions of binary post-consumer plastic packaging mixtures with a measurement uncertainty of $\pm$2.0 wt% across different material flow presentations at technical lab scale (Kroell et al., 2023a; Kroell et al., 2023b). However, to our best knowledge, the technical feasibility of NIR-based quality control of plastic pre-concentrates at plant scale has yet to be shown.

1.4. Aim and research questions

With the present paper, we aim to demonstrate the technical feasibility of inline-SBQC of plastic pre-concentrates from lightweight-packaging (LWP) sorting at plant scale by answering the following four research questions (RQs):

- **RQ 1:** What prediction accuracies can be achieved for monitoring impurity contents using NIR sensors at monolayer presentation and which data processing techniques and training dataset sizes are feasible for accurate predictions?
- **RQ 2**: How accurate is the prediction of bale-specific purities using SBQC methods compared to MQC at monolayer presentation?
- **RQ 3**: What is the variation of plastic pre-concentrate purities in a LWP sorting plant?
- **RQ 4**: How feasible is SBQC at a multilayered material flow presentation?

2. Background

2.1. Quality definitions of plastic pre-concentrates

Pre-concentrate qualities are defined by their purity, i.e., the mass-based share of target material in a pre-concentrate batch (Borowski, 2018; Der Grüne Punkt, 2023; Feil et al., 2021). As pre-concentrates are transported as *bales* between sorting and processing plants, a batch in sorting plants refers to a compressed cuboid plastic bale with median dimensions of approx. 1100 mm x 1100 mm x 1200 mm and a mass of approx. 200 kg to 1000 kg (depending on the pressed material) (Borowski, 2018).

For example in Germany, pre-concentrate purities are often specified based on the Der Grüne Punkt Duales System Deutschland GmbH (DSD) specifications (Der Grüne Punkt, 2023). A transparent polyethylene terephthalate (PET) bottle bale, for example, must contain at least 98 wt % transparent PET bottles according to the DSD specifications (Der Grüne Punkt, 2023).

2.2. Purity definitions

Along the plastic recycling value chain, different stakeholders use different references for defining the term *purity*, which can cause confusion, especially at the interfaces between different stakeholders. Therefore, we propose to differentiate between three different *purity definitions* (Table 1):

- **Article-based purity:** An article is a piece of packaging that may consist of several components and materials. It may also contain residues or contaminants. Article-based purity is defined as 100 % when the target material content exceeds an application-specific threshold. For example, a post-consumer PET bottle is considered 100 % pure, even if it contains, e.g., a bottle cap made of high-density polyethylene (HDPE), a label made of polypropylene (PP), remaining residual contents (e.g., liquids), and adhering dust.
- **Material-based purity:** In contrast to article-based purity, all mechanically removable non-target materials connected to a target article are considered impurities for material-based purity. In the PET bottle example, HDPE bottle caps, PP labels, remaining residual contents, and adhering dust are now considered impurities, since they can be mechanically removed (e.g., through separation steps like washing processes).
- **Chemical purity:** In addition to the material-based purity, all non-target molecules are considered impurities when defining a chemical purity, even if they cannot be (mechanically) removed. This includes, for example, additives, fillers, and reinforcing materials. For example, a washed and cleaned PET flake would not be considered 100 % pure as it contains non-PET molecules such as color pigments or UV stabilizers.

Article-based purity definitions are typically used during waste collection and in sorting plants, while material-based purity definitions are frequently used in plastic processing and chemical purity definitions are used, e.g., in chemical recycling. The stricter the purity definition, the lower is the determined purity $P_{m,\,i}$ (Eq. (1)).

$$P_{m,\ \text{article-based}} \geq P_{m,\ \text{material-based}} \geq P_{m,\ \text{chemical}} \quad (1)$$

Table 1
Proposed definition of article-based, material-based and chemical purities; ✔: included in purity definition, –: not included in purity definition.

Constituents	Examples	Included in Article-based purity[a]	Material-based purity	Chemical purity
Agglomerates	Multiple interlocking packages, e.g., through post-consumer influences	✔[b]	–	–
Secondary components	Labels and sleeves inclusive adhesives, lids	✔	–	–
Residual content	Remaining liquids	✔	–	–
Adhesive contamination	Dust, adhesive organics	✔	–	–
Material-bound additives, fillers, and reinforcing materials	Color pigments, UV stabilizers, antistatic agents, plasticizers, flame retardants, glass fibers	✔	✔	–
Target molecule	Polypropylene, aluminum	✔	✔	✔
Unit		wt% wet	wt% dry	wt% dry

[a] oriented on Der Grüne Punkt (2023)
[b] depending application-specific target-material threshold and definition of the sorting catalogue.

2.3. Potential SBQC sensor positions

As SBQC aims to analyze final pre-concentrate purities, it should take place *after* the last sorting stage and *before* the bale press. For most modern sorting plants, two sensor positions fulfill both criteria (see Fig. 1b):

- **Sensor position 1 (P1)**: product conveyor belts feeding the material into product bunkers,
- **Sensor position 2 (P2)**: feeding conveyor belts towards the bale press.

Sensor position P1 allows SBQC at a *monolayer* material flow presentation, i.e., particles do not overlap each other, while material flows at sensor position P2 are transported as *multilayered* bulks, i.e., particles strongly overlap each other (Kroell et al., 2023a). As NIR spectroscopy is a surface measurement technology (Workman and Weyer, 2007), NIR-based characterization of multilayered bulks (P2) can be challenging, e.g., due to segregation effects (Kroell et al., 2023a). However, sensor position P2 permits the monitoring of multiple pre-concentrate types with a single sensor, while sensor position P1 requires separate sensors for each pre-concentrate type, thus reducing potential investment costs (Kroell et al., 2022a).

3. Material and methods

To compare both sensor positions and answer the RQs from Section 1.4, we conducted two test series A and B in a state-of-the-art LWP sorting plant in Germany.

3.1. Experimental setup

3.1.1. Test series A

Test series A aimed at investigating the technical feasibility of SBQC at plant scale at monolayer material flow presentation (sensor position P1; RQ 1) and then comparing the SBQC results with MQC (RQ 2). As shown in Fig. 1a, a state-of-the-art NIR sensor ("NIR A1") was mounted on the conveyor belt of a PET tray product belt (P1) for inline monitoring of the full material flow (Section 3.2.1 to Section 3.2.3).

To validate the NIR data with MQC, all impurities were manually sorted out by two human experts with several hundred hours of experience in manual sorting analysis of post-consumer plastic packaging. The human experts were positioned directly after the NIR sensor

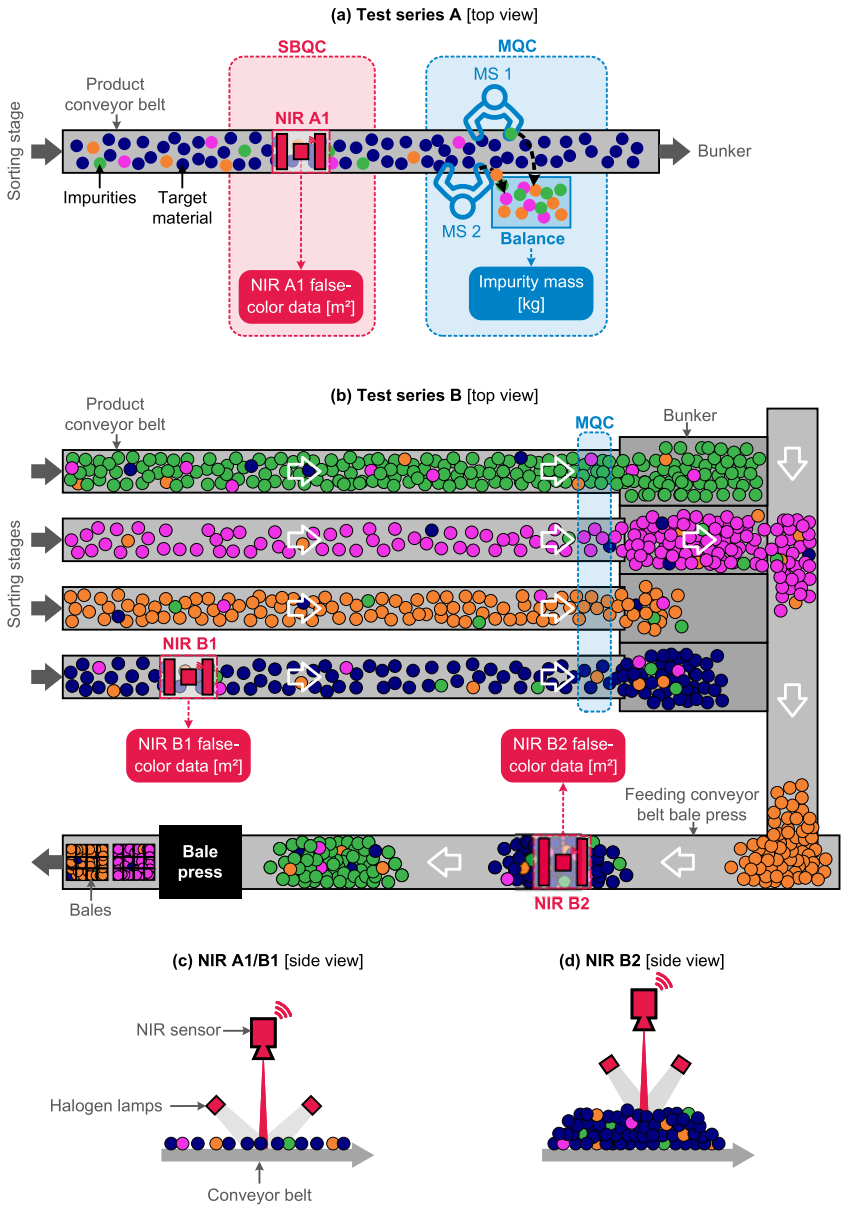

Fig. 1. Experimental setup of (a) test series A and (b) test series B as well as NIR sensor setup and material flow presentation at (c) sensor position P1 [PET tray product conveyor belt, monolayer material flow presentation] and (d) sensor position P2 [feeding conveyor belt bale press, multilayered material flow presentation].

(Fig. 1a) and immediately dropped any impurities in a sample container (V = 90 L), whose weight was recorded every second using a digital balance (Section 3.2.4).

Each trial lasted for 25 s during which the data of NIR A1 and the digital balance was recorded. After each 25 s trial, the sample container was emptied and time was given to the human experts to recover from the intense sorting, such that all sorting trials could be conducted at maximum concentration and with maximum accuracy over the course of three days. In total, n = 417 trials were recorded resulting in 174 minutes of manual sorting data during which 1,562 kg of PET tray product was manually sorted and recorded.

3.1.2. Test series B

Test series B aimed at quantifying purity variations (RQ 3) and assessing the technical feasibility of SBQC at multilayered material flow presentation (sensor position P2; RQ 4). During test series B, the full NIR data of two NIR sensors were recorded for a duration of 30 h. As shown in Fig. 1b, the first NIR sensor ("NIR B1") was positioned at the identical position and with the same configuration as NIR A1 (=sensor position P1), and the second NIR sensor (NIR B2) was positioned over the feeding conveyor belt to a bale press (sensor position P2), thus monitoring the bale-wise composition of PET tray and other plastic pre-concentrates (PET bottle, PP, HDPE, and polystyrene [PS]). In addition, all recorded fractions were sampled, manually analyzed, and immediately returned to the bunker to generate additional MQC data to validate the NIR results without influencing the NIR B2 measurements (Section 3.2.5).

3.2. Data acquisition

3.2.1. NIR sensor configuration

In both test series, hyperspectral imaging NIR sensors EVK HELIOS EQ32 from EVK Kerschhaggl GmbH (Raaba, Austria) were used. The used wavelength range was 1,017 nm to 1,702 nm at a spectral resolution of 3.1 nm per channel. All sensors were operated at a framerate of 446 Hz.

At sensor position P1 (Fig. 1c), the effective belt width was $b \approx$ 520 mm and the conveyor belt speed was $v \approx$ 0.42 m/s, resulting in a

spatial resolution of 3.31 mm^2/px. At sensor position P2 (Fig. 1d), the effective belt width was $b \approx 830$ mm, and the conveyor belt speed was $v \approx 1.2$ m/s, resulting in a spatial resolution of 13.41 mm^2/px.

Halogen lamps with 400 W each were used to illuminate the material flow as it moved below the NIR sensor (cf. Fig. 1c+d). At sensor position P1, two halogen lamps from the front and two halogen lamps from the back were used (4 × 400 W = 1,600 W in total). At sensor position P2, four halogen lamps from the front and four halogen lamps from the back were used (8 × 400 W = 3,200W in total). To prevent overheating of the conveyor belt at a belt standstill and recording redundant data, the power supply of the NIR illumination was coupled with the belt control such that the NIR illumination switched off automatically when the conveyor belt stopped.

3.2.2. NIR classification models

The material flow was classified pixel-based in real-time using the on-chip classification algorithm CLASS32 from EVK Kerschhaggl GmbH (Raaba, Austria) based on normalized first-derivatives of the acquired NIR spectra (EVK Kerschhaggl GmbH, 2023a).

Six material classes were trained to the classification model: PET, PP, polyethylene (PE), PS, beverage carton (BC), as well as paper, paperboard, and cardboard (PPC). For each material class, a variety of different packaging articles was sampled from the sorting plant, recorded, and added as reference spectra to the classification model (see Fig. S1 and Fig. S2 in supplementary materials) to ensure a high classification accuracy. For defining the reference spectra, representative regions of the recorded raw spectra were selected, such that, e.g., edge effects are avoided (Chen and Feil, 2019; Küppers et al., 2019).

The reference spectra also include sleeved and labeled parts of plastic bottles, which can have a significant influence on the NIR classification (Chen et al., 2023). These sleeved and labeled parts were added as reference spectra to the material class of the bottle material (e.g., an HDPE bottle with a PET sleeved is trained as "PE"), to assure a classification of the plastic article as fully correct as possible (cf. Chen et al., 2023). Likewise, wet articles were used as training materials to exclude the influence of NIR absorption of water on the classification (cf. Küppers et al., 2019). Lastly, overlays of transparent material on top of other materials (e.g., PET tray on top of an HDPE bottle) are trained as reference spectra, such that always the material on top is classified, to avoid systematic over/underestimation of certain materials (cf. Kroell et al., 2023a).

Background (BG) pixels (black conveyor belt) and material pixels were differentiated using the mean intensity of the raw NIR spectra based on a user-defined threshold. NIR spectra that differ significantly from the reference spectra are classified as "undefined" (UNDEF) by the CLASS32 algorithm, resulting in a total of eight different NIR outputs (PET, PP, PE, PS, BC, PPC, UNDEF, BG). Within CLASS32, three spectral regions of interest for classification were defined (NIR 1: 1082 nm – 1261 nm, 1352 nm – 1514 nm, 1621 nm – 1702 nm; NIR 2: 1107 nm – 1242 nm, 1342 nm – 1505 nm, 1615 nm – 1696 nm), where the NIR spectra of the investigated materials differ most (see Fig. S1 and Fig. S2). As shown in Fig. S3, the classification model classifies all six material classes correctly. Smaller classification errors occur between BC and PPC (especially for plastic coated PPC) and due to labeled or sleeved parts of packaging items.

3.2.3. NIR data acquisition

After uploading the NIR classification model from Section 3.2.2 to the NIR sensor, the CLASS32 algorithm then assigns a material class (represented as a false-color) to each recorded pixel. The resulting false-color data was captured using the EVK Stream Supervisor software (EVK Kerschhaggl GmbH, 2023b). In the EVK Stream Supervisor software, the false-color images are aggregated over 0.1 s and the pixel counts are then saved along with a timestamp in a comma-separated value (CSV) file.

3.2.4. Digital balance

For test series A, the impurity masses were recorded with a digital balance (KERN IFB 60L-3L; KERN & SOHN GmbH [Balingen-Frommern, Germany]) with a precision of ±0.002 kg and a maximum weight of 60 kg. The weight was written automatically every second along with a timestamp to an Excel file through the software SCD-4.0-PRO from KERN & SOHN GmbH.

3.2.5. Manual sorting analysis

For test series B, the plastic pre-concentrate fractions (PET tray, PET bottle, PP, HDPE, and PS) recorded by NIR B2 were additionally sampled, and their composition was analyzed through manual sorting analysis. The sampling was performed according to LAGA PN 98 (2001) using the existing automatic sampling system based on temporarily reversing the respective bunker feeding belt into a sampling container to create ideal sampling conditions with a sample volume of 180 L.

After sampling, the sample was immediately manually sorted into the following material fractions by human experts: PET tray, PET bottle, PP, PE, PS, BC, PPC, non-ferrous metals, ferrous metals, composites, and residual. Each sorted fraction was weighted using a digital balance (KERN DS 150K1, KERN & SOHN GmbH [Balingen-Frommern, Germany]) with a precision of ±0.001 kg and a maximum weight of 150 kg to determine the material composition of each sample. After manual sorting analysis, the full sampled material (incl. impurities) was mixed together, homogenized, and returned to the bunker feeding belt to make sure that the NIR B2 recordings were as little as possible influenced by the sampling[3]. Since the focus is on PET tray, the PET tray fraction and all other fractions were sampled alternatively resulting in the following sampling schedule: PET tray, PET bottle, HDPE, PET tray, PS, PET tray, PP. After each cycle, the sampling schedule was repeated. In total, n = 46 samples were taken and manually analyzed resulting in a total analyzed sample volume of 8,280 L and a total sample mass of 244 kg.

3.3. Data processing

For data processing, data visualization, and ML model training and evaluation, custom Python scripts were developed. The following open-source packages were primarily used: *NumPy* (Harris et al., 2020) [data storage and data processing], *pandas* (McKinney, 2010; The pandas development team, 2020) [data storage and data processing], *scikit-learn* (Pedregosa et al., 2011) [training and evaluation of regression models], *SciPy* (Virtanen et al., 2020) [statistics], *matplotlib* (Hunter, 2007) [data visualization], and *seaborn* (Waskom, 2021) [data visualization].

3.3.1. Spatial calibration

First, the pixel counts per 0.1 s from Section 3.2.3 were transformed into area flows [m^2/h] by using the spatial resolution from Section 3.2.1. For determining the spatial resolutions, false-color recordings of circular calibration targets of 170 mm diameter were recorded. The spatial resolution was then calculated by dividing the area of the calibration targets by the number of pixels of the calibration target.

3.3.2. Area-to-mass conversion using material-specific grammages

For the conversion between area-based NIR recordings and mass-based impurity masses, material-specific grammages were determined. Therefore, product material flows were sampled according to LAGA PN 98 (2001) (cf. Section 3.2.5) and the sampled material was manually sorted into pure material classes (PET tray, PET bottle, PP, HDPE, PS, BC, and PPC). Afterward, material feeding on the PET tray belt was

[3] Due to the sample homogenization, multiple belt transfers between the point where the sample were returned and NIR 2 as well as the relative low share (≤ 1.5 wt%) of sample masses (2.4 kg to 9.0 kg, mean: 5.3 kg) compared to the pre-concentrate bale masses (600 kg), the influences on the sampling on NIR 2 are considered as neglectable in the following.

manually stopped and the mono-material fractions were batch-wise recorded using NIR B1. For each batch, the false-color data from NIR B1 and the total mass of the batch were recorded. In total, the following masses per mono material fractions were recorded: PET bottle: 12.2 kg, PET tray: 2.7 kg, PP: 6.3 kg, PE: 7.1 kg, PS: 3.8 kg, BC: 12.2 kg, PPC: 3.6 kg.

Afterward, material-specific grammages were calculated according to Eq. (2) based on the total mass of recorded mono-material fractions m_i and the total area per recorded mono material fraction (incl. non-target pixels) A_i.

$$\rho_{A,i} = \frac{m_i}{A_i} \tag{2}$$

Table 2 summarizes the determined grammages. Since no sample material for the NIR material class UNDEF can be collected, a grammage of $\rho_{A,\ \mathrm{UNDEF}} = 1.63\ \mathrm{kg/m^2}$ was used, which is the mean grammage over all other seven material classes from Table 2.

3.3.3. Area-to-mass conversion using machine learning

Based on the insights from Kroell et al. (2023a), ML models were used as an alternative for predicting the mass-based impurity contents and material flow compositions from area-based NIR data.

For test series A, the total impurity mass flow can be calculated from the impurity mass of one trial measured by the digital balance (m_{impurity}) and the duration of one trial ($\Delta t_{\mathrm{trial}} = 25$ s) using Eq. (3).

$$\dot{m}_{\mathrm{impurity}} = \frac{\Delta m}{\Delta t} = \frac{m_{\mathrm{impurity}}}{\Delta t_{\mathrm{trial}}} \tag{3}$$

Therefore, a multivariate linear regression model (f_{A}, Eq. (4)) was trained to predict the total impurity mass flow $\hat{\dot{m}}_{\mathrm{impurity}}$ [kg/h] from the area flows $\dot{A}_i$ [$\mathrm{m^2/h}$] of each material class detected by the NIR sensor (cf. Section 3.2.2) excluding background[4].

$$\hat{\dot{m}}_{\mathrm{impurity}} = f_{\mathrm{A}}(\dot{A}_{\mathrm{PET}}, \dot{A}_{\mathrm{PP}}, \dot{A}_{\mathrm{PE}}, \dot{A}_{\mathrm{PS}}, \dot{A}_{\mathrm{BC}}, \dot{A}_{\mathrm{PPC}}, \dot{A}_{\mathrm{UNDEF}}) \tag{4}$$

To increase the practicality and robustness of our ML model in lightweight-packaging waste sorting plants, we divided our dataset into 20% ($n = 83$ trials) training data and 80% ($n = 334$ trials) test data. Our goal was to demonstrate that a satisfactory model could be achieved even with a small training set, thereby increasing efficiency for industrial applications by reducing data collection needs. Moreover, a large test dataset was employed for a robust analysis of the ML model performance and the comparison with MQC methods (cf. Section 4.2).

3.3.4. Throughput estimation

Besides impurity masses, it is necessary to know the total product mass flow to calculate the purities of a material flow or pre-concentrate bale (cf. Eq. (6)). For industrial SBQC applications, information on product masses is often available from the bunker system in terms of the total mass of each produced bale. However, for calculations in Section 3.4, it is necessary to estimate the PET tray product mass flow at a higher temporal resolution (25 s).

Previous research (e.g., Curtis et al., 2021; Kroell et al., 2022b; Küppers et al., 2020; Küppers et al., 2022) has established a strong correlation between mass flows and area flows. To enhance throughput estimation, we therefore calculated the throughput $\dot{m}_{\mathrm{PET\ tray\ product}}$ using the total area flow measured by NIR A1 ($\dot{A}_{\mathrm{PET\ tray\ product}}$) as follows:

$$\dot{m}_{\mathrm{PET\ tray\ product}} = \dot{A}_{\mathrm{PET\ tray\ product}} * \rho_{A,\ \mathrm{PET\ tray\ product}} \tag{5}$$

To determine the mean grammage $\rho_{A,\ \mathrm{PET\ tray\ product}}$, we first measured the total occupied area (including impurities) of the 39.7 Mg PET tray product using NIR A1. Then, we employed Eq. (2) to calculate the mean grammage as $\rho_{A,\mathrm{PET\ tray\ product}} = 1.79\ \mathrm{kg/m^2}$.

3.3.5. Outlier removal

During preprocessing of test series A, we removed two non-representative outliers (trials no. 127 and 128; 0.5% of the total dataset) with impurity mass flows of 395.7 kg/h and 332.4 kg/h, as both outliers deviated significantly both from the median (25.3 kg/h) and the next largest impurity mass flow (117.5 kg/h). The outliers resulted from two water-soaked shoes with an approximate mass of approx. 2 kg each in the PET tray material flow and not removing them would make ML model training and evaluation practically infeasible. While, in the current study, the two outliers were omitted to demonstrate the general technical feasibility of the SBQC approach, given their low frequency and significant deviation from the other datapoints, a detailed consideration of such outliers regarding the application-specific relevance is recommended when applying our findings into operational practice and the evaluation of future SBQC measurement systems (cf. Section 5).

3.4. Comparison of SBQC and MQC (bale sampling simulation)

To answer RQ 2, SBQC and MQC methods were compared with each other on the task of predicting the purity of a PET tray bale with an average mass of 600 kg. As it is unfeasible to manually sort hundreds of PET tray bales to determine the necessary ground truth, different bale compositions were digitally generated from test series A.

Therefore, the data from test series A was first randomly split into 20% training and 80% test data (cf. Fig. 2a). The training set was used to train ML model A (Section 3.3.3) for SBQC and the test set was used as the ground truth for creating simulated PET tray bales with known compositions.

3.4.1. Simulation of different PET tray bales

The test set consists of $n = 334$ trials containing in total 1242.4 kg manually sorted material (approx. 2.1 bales) each with the corresponding impurity (Section 3.1.1) and total masses (Section 3.3.4). To create a simulated PET tray bale, we randomly sampled n trials from the test set without replacement until a total sample mass of 600 kg was reached. These n trials then represent one simulated PET tray bale with its known mass m_{bale} and known purity $P_{m,\mathrm{bale}}$ according to Eq. (6).

$$P_{m,\ \mathrm{bale}} = \frac{m_{\mathrm{impurity}}}{m_{\mathrm{bale}}} = \frac{\sum_{i=1}^{n} m_{\mathrm{impurity},\ i}}{\sum_{i=1}^{n} m_i} \tag{6}$$

3.4.2. Simulation of MQC sampling

State-of-the-art MQC of pre-concentrates in LWP sorting plants involves sampling. The required sample sizes for a pre-concentrate bale can be calculated based on different technical norms and guidelines (see Section 1 in supplementary materials). In the case of a 600 kg PET tray bale, applying these norms and guidelines results in required sample sizes of 0.9 kg (CEN/TR 15310-1, 2006), 3.2 kg (LAGA PN 98, 2001), 40.0 kg (GBP Quality GmbH, 2023), 50.0 kg (COREPLA, 2022), 80.0 kg–90.0 kg (Der Grüne Punkt, 2016), and 123.0 kg (ÖNORM S

Table 2
Determined material-specific grammages.

Material class	Grammage [kg/m²]
PET bottle	2.17
PET tray	1.22
PP	1.79
PE	2.64
PS	1.34
BC	1.97
PPC	0.79

[4] Since the total area flow (materials + background) is constant, the background area flow is linear dependent on the sum of all material area flows and thus excluded from model training, cf. Fahrmeir et al. (2013).

2127, 2011).

To simulate the influence of different sample sizes, we randomly sampled k of these n trials, which then represents a sample with the total sample mass $m_{\text{samples}}(k)$. As in traditional MQC, the purity of the total bale is estimated by the purity of the sample according to Eq. (7).

$$\widehat{P}_{m,\,\text{bale},\,\text{MQC}}(k) = \frac{m_{\text{impurity}}(k)}{m_{\text{samples}}(k)} = \frac{\sum_{i=1}^{k} m_{\text{impurity},i}}{\sum_{i=1}^{k} m_i} \text{ with } k \leq n \tag{7}$$

3.4.3. Simulation of SBQC inline monitoring

In contrast to MQC, SBQC methods analyze the full material flow, therefore no sampling is involved. Thus, ML model A was used to predict the impurity mass for each of the n trials ($\widehat{m}_{\text{impurity},\,\text{SBQC},\,i}$). The predicted purity of the bale ($\widehat{P}_{m,\,\text{bale},\,\text{SBQC}}$) is then calculated by dividing the summed-up impurity mass ($\widehat{m}_{\text{impurity},\,\text{SBQC}}$) through the total bale mass (Eq. (8)).

$$\widehat{P}_{m,\,\text{bale},\,\text{SBQC}} = \frac{\widehat{m}_{\text{impurity},\,\text{SBQC}}}{m_{\text{bale}}} = \frac{\sum_{i=1}^{n} \widehat{m}_{\text{impurity},\,\text{SBQC},\,i}}{\sum_{i=1}^{n} m_i} \tag{8}$$

This process was repeated for a total of 1,000 different PET tray bales. This was the basis for the assessment of the measurement uncertainty of MQC methods with different sample sizes and the proposed SBQC methods.

3.5. Assessment of measurement uncertainty

To assess the predicted (im)purities for answering RQ 1 and RQ 2, we use the 95 %-percentile measurement uncertainty (MU) metric according to Kroell et al. (2023a). The MU_{95} is the 95th percentile (P_{95}) of all absolute errors between a set of measurands X_{measured} and its corresponding true values X_{true} (Eq. (9))

$$MU_{95} = P_{95}(|X_{\text{measured}} - X_{\text{true}}|)$$

$$\text{with } X = \{x_1, \ldots, x_n\} \tag{9}$$

The MU_{95} indicates that in 95 % of all cases, the true value (x_{true}) is in the range $x_{\text{measured}} \pm MU_{95}$ (Kroell et al., 2023a). For example, if an SBQC system is predicting a purity of 96 wt%, with a MU_{95} of 2 wt%, then the true purity is between 94 wt% and 98 wt% in 95 of 100 measurements. The lower the MU_{95} values, the more accurate are the predictions.

As the MU_{95} indicates the deviations in absolute terms, we use the normalized MU (nMU_{95}) defined in Eq. (10) to express relative deviations. The nMU_{95} is the MU_{95} devided by the mean measurement values ($\bar{x}_{\text{measured}}$).

$$nMU_{95} = \frac{MU_{95}(X_{\text{measured}})}{\bar{x}_{\text{measured}}} \tag{10}$$

4. Results and discussion

4.1. Impurity mass flow prediction at monolayer presentation (RQ 1)

Fig. 2a shows the impurity mass flows of test series A determined by manual sorting of human experts over the course of $n = 417$ trials and the applied random train-test-split. High variations in the measured impurity flows between 0 kg/h and 117.5 kg/h (mean: 28.3 kg/h) can be observed.

4.1.1. Comparison of material-specific grammage and ML model

Fig. 2b compares the grammage (Section 3.3.2) and ML model (Section 3.3.3) in predicting the impurity mass flow based on the NIR A1 data. As shown in Fig. 2b, the grammage model overestimates the impurity mass flow on average by a factor of 2.11, resulting in an nMU_{95} of 218.0%. In contrast, the predictions of ML model A are more accurate with an nMU_{95} of 94.6% on the raw data.

A likely reason for the overestimation of the grammage model is the discrepancy between article-based and material-based purity definitions (cf. Section 2.2, esp. Eq. (1)). In an article-based purity definition, used by human experts, non-PET materials are counted as impurities only if they are not physically connected to a PET article. The NIR sensor, however, classifies each pixel independently of its connection to other materials. Since each non-PET pixel directly contributes to the predicted impurity for the grammage model, non-PET pixels from PET articles (e.g., PP films, PPC labels belonging to PET trays) are always counted as impurities.

In contrast, the ML model is trained on the article-based impurity definition by the human experts in the manual sorting (training) data. It can thus correct these composite effects by adjusting its model coefficients. However, as shown in Fig. 2c, especially high impurity mass flows are still difficult to be predicted for the model. A possible reason for this is a large variance of grammages in post-consumer packaging waste (cf. Kroell et al., 2021), which makes accurate predictions on the unaggregated raw data (here: 25 s chunks) challenging (cf. Kroell et al., 2023a).

4.1.2. Influence of data aggregation (chunk size)

Since the investigated sorting plant produces a PET tray bale approximately every $\Delta t_{\text{bale}} = 67$ min, 25 s values of SBQC are not necessary for this use case. Aggregation of sensor-based material flow data has been demonstrated to improve prediction accuracy (Kroell et al., 2023a), as, e.g., particle-specific deviations in grammages can be smoothed out. Therefore, Fig. 2d shows the influence of different chunk sizes (time windows over which the data was aggregated [Kroell et al., 2023a]) on the model performance.

As shown in Fig. 2d, prediction errors decline super-linear with increasing chunk size. For chunk sizes above 30 minutes, nMUs of $\leq$ 6.9 % are achieved. As illustrated for exemplary chunk sizes in Fig. 2d, even small data aggregation can already effectively reduce prediction errors.

4.1.3. Influences of training size

Another way to improve model performance is to increase the amount of provided training data (Goodfellow et al., 2016). As the original training set was relatively small ($n = 83$ trials; 20% of the total dataset), the question arises whether the performance of the model could be improved with more training data. On the other hand, as the generation of training data is costly (e.g., high personal expenses for manual sorting), it is also of high practical interest whether a similar level of performance could be achieved with even less training data.

To address both questions, Fig. 2d shows the model performance for different training sizes across different chunk sizes. It becomes evident that in this case, the model performance does not substantially increase with increasing training size: While the mean nMU_{95} over all investigated chunk sizes (25 s – 80 min) at 20% training size ($n = 83$ trials) is 11.1%, it only decreases to 10.8%, when doubling the training size to 40% ($n = 166$ trials). Furthermore, with only 10% training data ($n = 41$ trials), a comparable model performance with a mean nMU_{95} of 11.8% over all chunk sizes was still achieved.

4.1.4. Model robustness

Fig. 2e shows the coefficients of the trained models for different training sizes to further validate the model robustness and study the influence of different training sizes on the model. As shown, the model demonstrates increased stability with increasing training size, showing stable predictions for training sizes greater than 10%.

The model predictions appear plausible, since the coefficient for the material class PET (= target material class in the investigated PET tray fraction) is nearly zero across all trained models, thus not influencing the impurity content. Negative model coefficients are observed for the material classes PE, PP, and UNDEF. The negative PE and PP coefficients

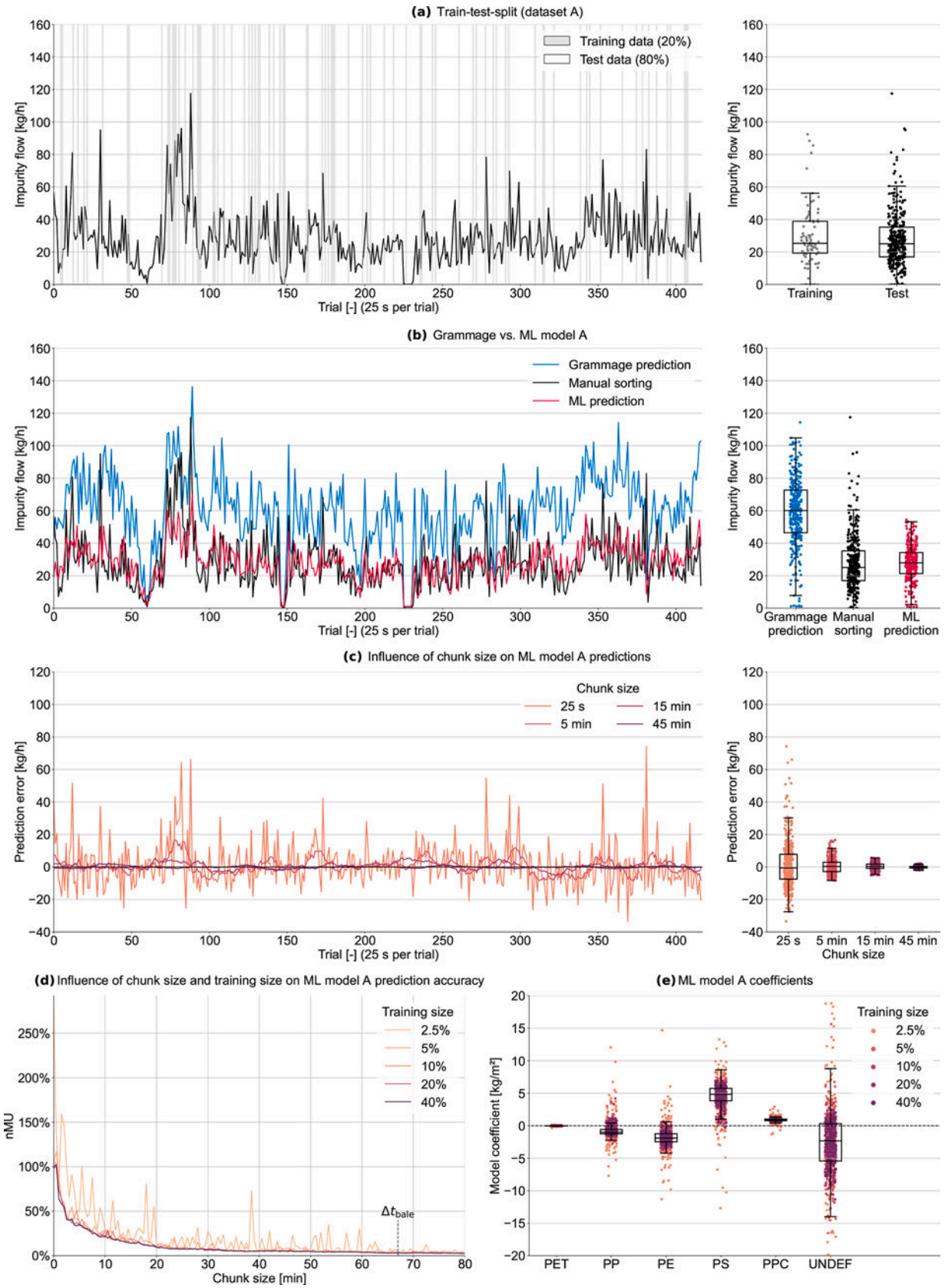

Fig. 2. NIR-based impurity mass flow prediction at monolayer presentation [NIR A1]. (a) Overview of measured impurities determined by human experts and applied train-test-split, (b) impurity prediction using grammages and ML compared to ground truth, (c) influence of data aggregation on prediction errors of ML model A, (d) influence of training size on the prediction performance of ML model A, (e) distribution of model coefficients of ML model A trained across different training sizes and chunk sizes from [d]. Δt_{bale}: average production time of a PET tray bale in test series A.

are likely the model's correction for composite effects (discrepancy between article- and material-based purity, cf. Section 2.2) as films of PET tray packaging and bottle caps belonging to PET bottles are frequently made of PE and PP (Roosen et al., 2020). The negative value and high variation of the UNDEF coefficient could indicate an attempt of the model to correct misclassifications as well as unknown material classes within the UNDEF material classes from the NIR A1 sensor. In contrast, positive model coefficients are especially found for PS and PPC, which supports the hypothesis that the model might have chosen PS and PPC as leading indicators for high impurity contents.

In summary, ML model A demonstrates superior performance in predicting impurity mass flows compared to the grammage model by effectively taking discrepancies between article-based and material-based purity definitions into account through material-specific weight adjustments. Data aggregation has a significant impact on model performance, with prediction errors declining super-linearly as chunk size increases. Notably, even a small amount of training data (10% of the full dataset) can yield comparable model performance. The final model, trained on only $n = 83$ trials (20% training size) combined with a 67-minute aggregation (corresponding to the average production time of one PET tray bale), can predict impurity mass flows with a nMU_{95} of 3.2%.

4.2. Comparison between SBQC and MQC at monolayer presentation (RQ 2)

Fig. 3 compares the accuracy (MU [wt%]) between SBQC based on NIR A1 and MQC across different sample sizes for 1,000 simulated PET tray bales (cf. Section 3.4). As shown by the MQC line in Fig. 3, the measurement uncertainty of MQC caused by the sampling error decreases quadratically with increasing sample sizes, and a "diminishing return" effect is observed, i.e., with increasing sample sizes the additional measurement accuracy gained by larger sample sizes flattens out. High MUs (> 5 wt%) are observed when simulating MQC according to CEN/TR 15310-1 (2006) [$MU_{95} = 6.7$ wt%] and LAGA PN 98 (2001) [$MU_{95} = 5.6$ wt%]. In contrast, higher sample sizes specified in technical MQC guidelines for pre-concentrates as well as the ÖNORM S 2127 (2011) lead to reasonable MUs (≤ 1.5 wt%) when simulating MQC according to GBP Quality GmbH (2023) [$MU_{95} = 1.5$ wt%], COREPLA (2022) [$MU_{95} = 1.3$ wt%], Der Grüne Punkt (2016) [$MU_{95} = 1.0$ wt%], and ÖNORM S 2127 (2011) [$MU_{95} = 0.8$ wt%].

Since SBQC methods require no sampling, the proposed method using ML model A achieves a constant MU_{95} of 0.31 wt%, which is significantly lower than MUs of MQC with sample sizes specified by technical norms and guidelines (Fig. 3). In fact, between 351 kg (58.5 wt%) and 386 kg (64.3 wt%) of the simulated PET tray bales must have been sampled and manually sorted to achieve equal or lower MUs by traditional MQC methods. Using the estimate of 4 to 6 person-hours to analyze a sample of 80 kg to 90 kg from Borowski (2018) (cf. Section 1.1), this would amount to between 15.6 to 29.0 person-hours per bale to achieve the same accuracy using MQC than with the proposed SBQC method.

4.3. Variation in predicted pre-concentrate purities (RQ 3)

To demonstrate the potential benefits of SBQC and to estimate purity fluctuations (RQ 3), Fig. 4a shows the area-based purity distribution of the $n = 17$ PET tray bales that were produced during the sensor measurements of test series B. Among these analyzed bales, the area-based purities ranged between 68.3 area percent (a%) and 77.6 a% and with a standard deviation of 3.1 a%.

Notably, the area-based purity of bales produced during the early and late shifts (mean purity: 75.8 a%) was statistically significantly higher ($p \leq 0.01$[5]) compared to night shifts (70.3 a%). A likely reason for this are the different input materials, which are processed during the early and late shifts (input material 1) and night shifts (input material 2) in the investigated sorting plant.

According to the SBQC data, the two input materials affect different impurities to different degrees (Fig. 4b). When input material 2 is processed (night shift), the PET tray product contains statistically significant ($p \leq 0.01$) more PPC (+6.5 a%) and UNDEF (+0.6 a%) material and significantly less target material and other plastics (PET: -5.5 a%, PP: -0.8 a%, PE: -0.9 a%, PS: -0.1 a%). A likely reason for this is the different characteristics of the two input materials (e.g., material flow composition, particle size distribution, and water content), which influence the sorting plant operation (e.g., Kroell et al., 2022b; Küppers et al., 2020; Küppers et al., 2021; Küppers et al., 2022).

4.4. SBQC at multilayered material flow presentation (RQ 4)

Fig. 5 shows the feasibility of SBQC at multilayered material flow presentations ($\alpha_{\text{NIR B2}}$) by comparing the material flow composition of plastic pre-concentrate bales measured with MQC ($\widehat{w}_{\text{MQC}}$; Section 4.4.1) and SBQC at monolayer presentation ($\alpha_{\text{NIR B1}}$; Section 4.4.2). In addition to individual values (unfilled markers), mean values (filled markers) and their distance from the ideal correlation line are displayed.

4.4.1. NIR B2 vs. MQC

In test series B, $n = 103$ pre-concentrate bales were analyzed in total by NIR B2. $n = 30$ of these bales ($n_{\text{PET tray}} = 13$, $n_{\text{PET bottle}} = 4$, $n_{\text{PP}} = 5$, $n_{\text{HDPE}} = 4$, $n_{\text{PS}} = 4$) were also sampled and their composition was manually analyzed (cf. Section 3.2.5).

In Fig. 5, all bales other than the PET tray bale marked with "**", which is determined by NIR B1, are determined by MQC. These Non-"X"-markers for PET tray, PET bottle, PP, HDPE and PS compare the bale compositions determined by MQC (mass-based and article-based purity definition; cf. Section 2.2) with bale compositions determined by NIR B2 (area-based and material-based purity definition; cf. Section 2.2). Different colors indicate material fractions within a bale. For example, a red circle represents the mass-based PE share (red) within a PP bale (circle).

Even though the estimated material shares of NIR B2 and MQC are determined based on a different counting basis (mass-based vs. area-based) and based on different purity definitions (article- and material-based), a general correspondence between NIR B2 and MQC purities can be observed across all bale types ($MU_{95,\ \text{purity},\ \text{PET tray}} = 10.3\%$, $MU_{95,\ \text{purity},\ \text{PET bottle}} = 5.0\%$, $MU_{95,\ \text{purity},\ \text{PP}} = 5.7\%$, $MU_{95,\ \text{purity},\ \text{HDPE}} = 3.4\%$, $MU_{95,\ \text{purity,PS}} = 8.6\%$).

Likewise, there is a reasonable correspondence between MQC- and NIR-based impurity shares. Here, MU_{95} values are slightly lower since the impurities have a much lower share compared to the purities ($\overline{MU}_{95,\ \text{impurities},\ \text{PET tray}} = 2.4\%$, $\overline{MU}_{95,\ \text{impurities},\ \text{PET bottle}} = 0.9\%$, $\overline{MU}_{95,\ \text{impurities},\ \text{PP}} = 1.3\%$, $\overline{MU}_{95,\ \text{impurities},\ \text{HDPE}} = 1.3\%$, $\overline{MU}_{95,\ \text{impurities},\ \text{PS}} = 1.7\%$). However, in relative terms, the consistency of purities ($\overline{nMU}_{95,\ \text{purity}} = 7.2\%$) is considerably more accurate compared to impurities ($\overline{nMU}_{95,\ \text{impurity}} = 202.1\%$). A possible explanation may be that the influence of individual particles on the total material content is higher for impurities due to the lower particle number of impurities compared to target materials.

While these numbers indicate the general feasibility of SBQC at multilayered material flow presentations, the following limitations of this comparison have to be considered:

[5] p-values express the level of significance. Here, we calculated the p-value based on the Mann–Whitney U test, Mann and Whitney (1947).

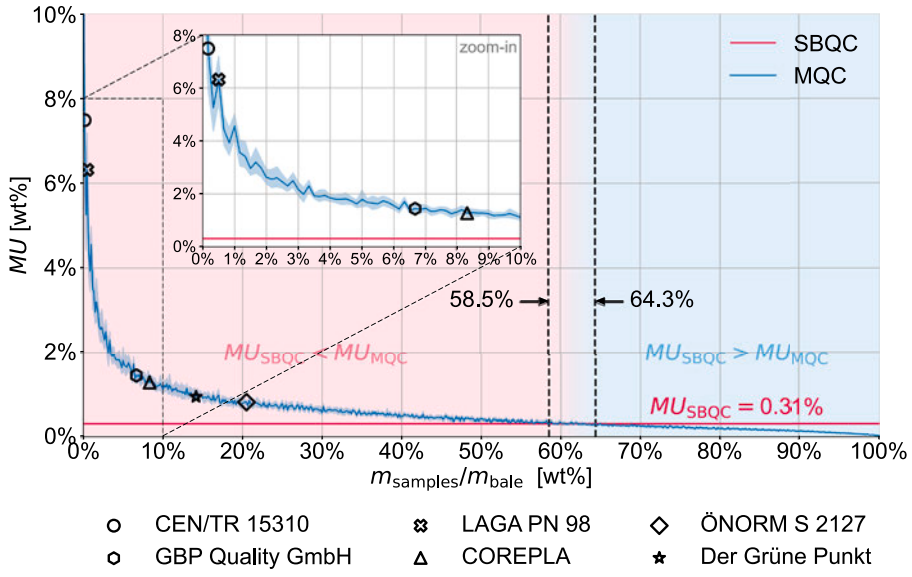

Fig. 3. Comparison of inline SBQC using NIR and ML with MQC using different sampling sizes at monolayer presentation [NIR A1]; markers: minimum sample sizes according to CEN/TR 15310-1 (2006), LAGA PN 98 (2001), ÖNORM S 2127 (2011), GBP Quality GmbH (2023), COREPLA (2022), and Der Grüne Punkt (2016).

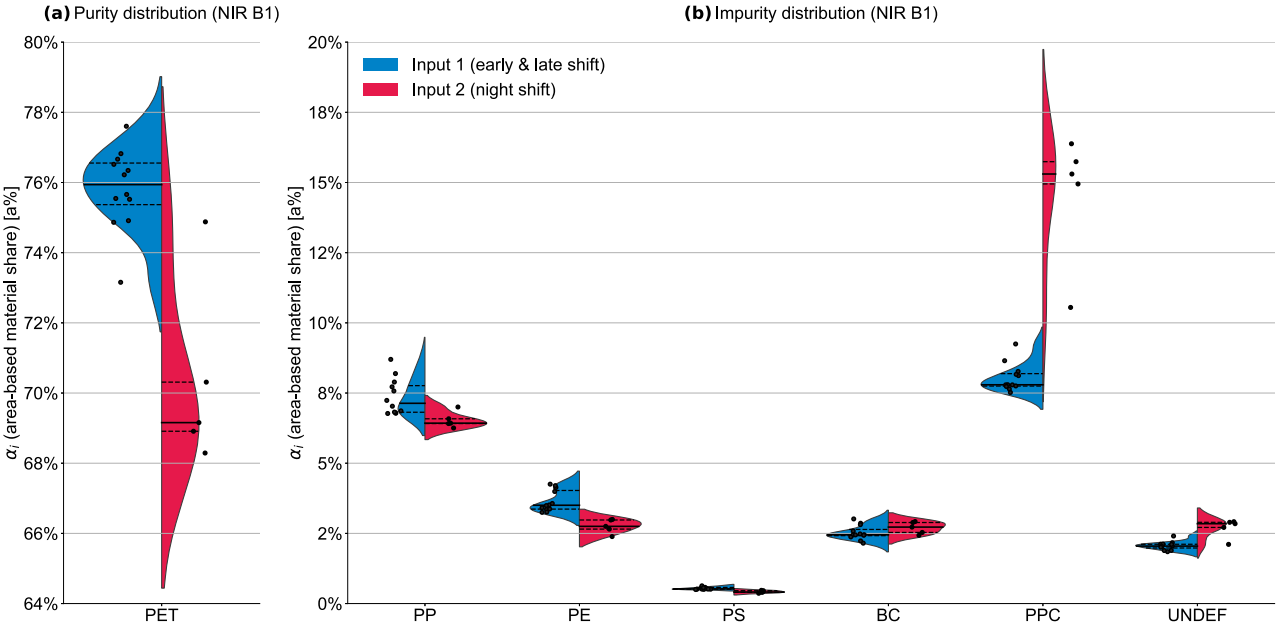

Fig. 4. Area-based (a) purity and (b) impurity distribution per bale between plant input 1 (early and late shift, left violin) and plant input 2 (night shift, right violin) [NIR B1]; solid line: median, dashed line: 25 % and 75 % percentile.

- First, MQC with the initially chosen sample sizes in this study (180 L) is associated with a considerable **sampling error** (see Section 4.2), which can, for example, be observed by high variation of the MQC analysis results (0.97 wt% standard deviations [per material class and bale type, macro-average]) compared to the lower variation in the NIR B2 compositions (0.19 a% standard deviation).
- Second, as discussed earlier, NIR B2 and MQC data have different **counting basis** (mass-based vs. area-based) and purity definitions (cf. Section 2.2). Applying appropriate area-to-mass-prediction models and pixel-to-article-based conversion models might thus reduce the differences between both data sources (Kroell et al., 2021; Kroell et al., 2023a).
- Third, independent of the previous effects, SBQC at a **multilayered material flow presentation** can differ from SBQC at a monolayered material flow presentation and MQC, if the analyzed material flow surface by NIR B2 differs from the area-based composition of the full bale (see Section 4.4.2).

To investigate the influences of multilayered material flow presentation independent from the previous effects, Section 4.4.2 compares the area-based bale compositions determined by NIR B1 and NIR B2 for the investigated PET tray bales.

4.4.2. NIR B2 vs. NIR B1

"X"-markers in Fig. 5 compare the area-based bale compositions determined by NIR B2 and NIR B1 for PET tray bales. Due to the absence of a sampling error, less deviation occurs in NIR B1 measurements compared to MQC, such that potential systematic effects are easier to be

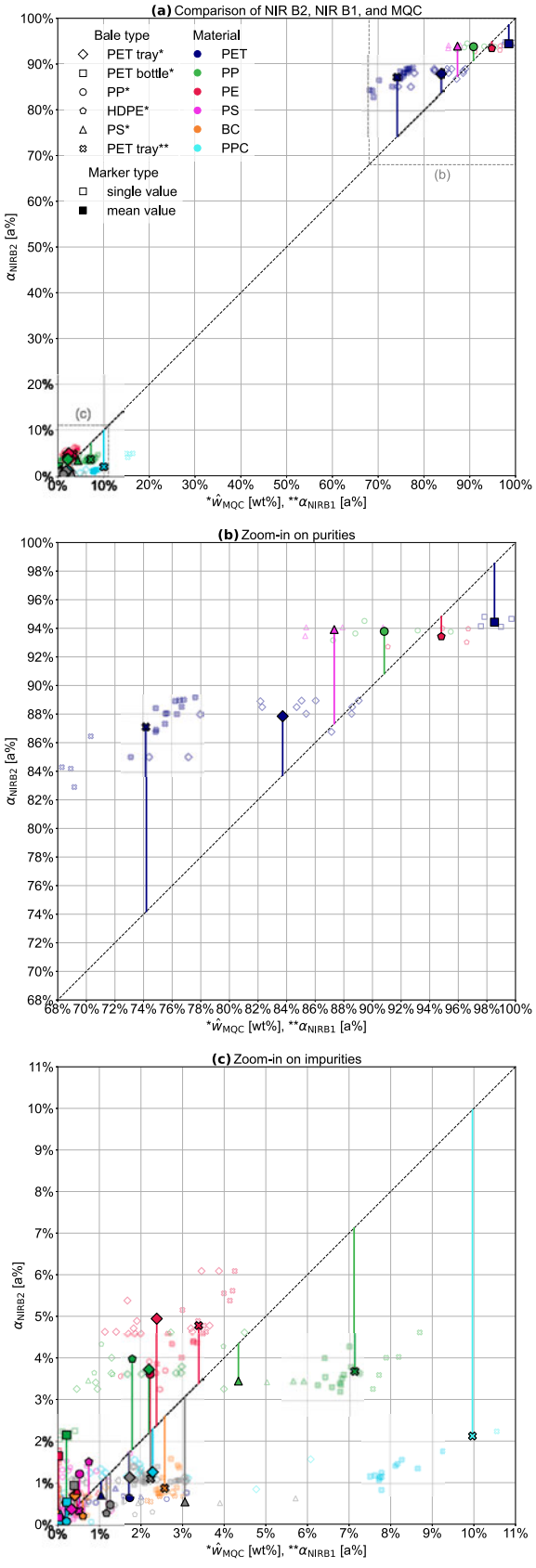

(caption on next column)

Fig. 5. Feasibility of SBQC at multilayered material flow presentation. (a) Differences in area-based material flow compositions between NIR B1 (monolayered material flow presentation, sensor position P1) and NIR B2 (multilayered material flow presentation, sensor position P2) for PET-tray bales and between area-based material flow composition using NIR B2 and mass-based MQC (sample size = 180 L) for plastic pre-concentrate bales, (b) zoom-in of [a] on purities, (c) zoom-in of [a] on impurities; * mass-based and article-based purity determined by MQC ($\widehat{w}_{\mathrm{MQC}}$), ** area-based and material-based purity determined by NIR B1 ($\alpha_{\mathrm{NIR\ B1}}$).

identified.

When analyzing the PET tray purities (Fig. 5b), a high correlation between NIR B2 and NIR B1 can be observed with a Pearson correlation coefficient (PCC) of 0.915 (Pearson, 1895). A systematic overestimation of NIR B2 is observed with area-based PET shares on average +12.9 a% higher when measured with NIR B2 compared with NIR B1.

Likewise, PET tray impurity shares (Fig. 5c) correlate to a higher extent between NIR B2 and NIR B1 for the material classes PPC (PCC = 0.989), PS (PCC = 0.873), PE (PCC = 0.831), to a lower extent for PP (PCC = 0.601) and BC (PCC = 0.529), and no correlation is found for UNDEF materials. A closer look at Fig. 5c reveals that PE shares were always overestimated by NIR B2 compared to NIR B1 by +1.4 a% on average, while other material classes were mostly underestimated by NIR B2 to different extents (PPC: -7.8 a%, PP: -3.4 a%, BC: -1.7 a%, PS: -0.2 a%, UNDEF: -1.1 a%). These observations are consistent with the findings described in (Kroell et al., 2023a) and might have been caused by the following two mechanisms:

4.4.2.1. Different classification behavior at multilayered material flow presentation. At NIR B1, NIR spectra of particles are measured as a monolayer on top of a carbon-black conveyor belt. For transparent material, like PET trays, very thin-walled parts of packaging articles can result in a low spectral intensity due to the carbon-black surface underneath, which can cause the classification of some article parts as background by the NIR classification algorithms. However, at NIR B2, the material flow surface is measured on top of several underlying material layers. Therefore, even thin-walled parts of transparent articles are laying on top of several other particles, which results in higher spectral intensity and the classification of all article parts as the corresponding material instead of background (mixed NIR spectra are classified as the material on top with the used algorithm, cf. Section 3.2.2). As a consequence, the recognized area of transparent and thin-walled articles is higher at NIR B2 compared to NIR B1, resulting in a higher material share. As a lot of transparent and thin-walled packaging items (e.g., trays, foils, multilayered packaging) are made of PET and PE, this mechanism might partially explain why the material classes PET and PE were overestimated by NIR B2.

4.4.2.2. Segregation effects. Based on our previous experience, the results of Kroell et al. (2023a), and the analysis of the NIR false-color images, we assume that the +12.9% PET overestimation is too high to be caused solely by differences in the NIR classification behavior. The PET overestimation could have been caused by segregation effects, e.g., by the accumulation of two-dimensional PET trays on the material flow surface measured by NIR B2. In addition, variations in particle characteristics such as particle size and shape resulting from different materials used in different packaging applications could further increase segregation effects. Further research and a more robust understanding of segregation mechanisms for post-consumer packaging are required to verify or falsify this hypothesis.

In summary, NIR-based SBQC at multilayered material flow presentation (bale press feeding belt, P2) seems feasible in general with reasonable correspondence between NIR B2 and MQC as well as NIR B1 measurement. However, a deeper understanding of segregation effects and a development of correction as well as area-to-mass models is

necessary to achieve SBQC predictions with accuracies of practical relevance at multilayered material flow presentations (sensor position P2) in the future.

5. Conclusions

The plastic recycling value chain is currently suffering from a high degree of intransparency since MQC procedures for post-consumer plastic pre-concentrates are time-consuming, cost-intensive, and thus only performed on an irregular basis. Inline sensor technology promises to overcome these limitations by enabling an automated monitoring of produced pre-concentrate qualities. While numerous studies showed the high accuracy of plastic discrimination using NIR spectroscopy at pixel- and particle levels, it remained unclear if NIR-based quality control of plastic pre-concentrates at the material flow level and plant scale is technically feasible. Further, it remained unclear how the achieved accuracy of an SBQC approach compares to traditional MQC in the form of manual sorting analysis of taken samples.

In two test series, we showed that SBQC at plant scale is not only technically feasible, but ML-based SBQC predictions can be even more accurate than traditional sampling-based methods. Since the purities of plastic pre-concentrates are determined by a mass- and article-based purity definition in current technical norms and industrial practice (cf. Section 2.2), comparable purities from the pixel-based NIR-false-color-data should be predicted using, e.g., ML methods, to account for composite effects in post-consumer packaging (difference between article- and material-based purity definition, cf. Section 2.2). The high data aggregation due to an average bale production time of several minutes up to an hour (here: 67 minutes) evens out prediction errors at lower time scales and achieves purity predictions with high accuracies (±3.2% normalized measurement uncertainty) [RQ 1].

A direct comparison of SBQC and MQC to predict the purity of 600 kg PET tray bales demonstrates the advantages of the SBQC method: When following technical norms and guidelines for MQC, bale purities could be determined with measurement uncertainties (95^{th} percentile of absolute errors) between ±6.7 wt% (0.9 kg sample size [CEN/TR 15310-1, 2006]) to ±0.8 wt% (123 kg sample size [ÖNORM S 2127, 2011]). The proposed SBQC method predicted bale purities within ±0.31 wt% measurement uncertainty. In fact, we estimate that the required total sample mass for MQC must have been ≥ 350 kg, i.e., more than half of the total PET tray bale and thus way beyond any reasonable MQC practice, to be more accurate than SBQC [RQ 2].

Another benefit of SBQC data could be demonstrated by identifying significant variations in the area-based material flow composition of the PET tray pre-concentrate caused by two different input materials of the sorting plant coming from two different collection areas. To obtain comparable knowledge using MQC, a high personnel effort in both day and night shifts would be necessary. Since investigation of this type are costly, many relevant parameters in sorting plants have remained undetected in the past [RQ 3].

To potentially monitor several pre-concentrates simultaneously with a single NIR sensor in the future, the technical feasibility of SBQC with multi-layered material flow presentations (feeding conveyor belt to bale press) was investigated. A good correlation was found between area-based purities measured at mono- and multi-layered material flow presentation with a high Pearson correlation coefficient of 0.915. Systematic deviations between monolayered and multilayered material flow presentations due to segregation effects and changes in the NIR classification behavior reported by previous studies (Kroell et al., 2023a) were confirmed, resulting in the need for a better understanding of segregation effects and the development of possible correction models [RQ 4].

Several directions for future research emerge from our work: Our investigations could be extended to other pre-concentrates or types of sorting and processing plants. In addition, the NIR sensor could be complemented by additional sensors such as RGB cameras and/or with deep learning techniques, e.g., to detect contaminants of the same material such as HDPE silicon cartridges in a HDPE pre-concentrate or to enable a quality assessment for color-sorted fractions. Further, long-term sensor measurements are needed to analyze the stability of the developed ML models under seasonal fluctuations, changing packaging designs, different waste collection areas/schemes, frequency of outlier impurities, or differing plant operations and to develop and test potential recalibration strategies (e.g., DIN 54390, 2022; Flamme et al., 2020). The economics of SBQC could be enhanced by either utilizing more cost-effective sensor technologies (e.g., RGB cameras) or enabling the previously mentioned SBQC at multilayered material flow presentations to monitor multiple pre-concentrates with a single sensor. To reduce the costs for model training and adaptation at multiple measuring points or in multiple sorting plants, the development of time-/cost-efficient methods for generating the necessary ground truth data as well as the application of transfer and feathered learning approaches could be of further interest.

Ultimately, our research underlines the promising opportunities of sensor technology in post-consumer plastic recycling beyond today's sorting applications. By fostering transparency, incentives for improved sorting could be established and realized through adaptive process control in sorting and processing plants, contributing to a boost in recyclate quality and yields and a sustainable circular economy.

Funding

This work was funded by the National Austrian Research Promotion Agency (FFG) within the program "Production of the Future" under the project *EsKorte* (grant no. 877341) and the German Federal Ministry of Education and Research (BMBF) within the program "Resource-efficient circular economy - plastic recycling technologies (KuRT)" under the project *ReVise* (grant no. 033R341). The responsibility for the content of this publication lies with the authors.

CRediT authorship contribution statement

Nils Kroell: Conceptualization, Methodology, Software, Validation, Formal analysis, Investigation, Data curation, Writing – original draft, Writing – review & editing, Visualization, Supervision, Project administration, Funding acquisition. **Xiaozheng Chen:** Conceptualization, Methodology, Validation, Writing – review & editing, Funding acquisition. **Bastian Küppers:** Conceptualization, Methodology, Validation, Investigation, Supervision, Writing – review & editing, Funding acquisition. **Sabine Schlögl:** Validation, Writing – review & editing, Funding acquisition. **Alexander Feil:** Writing – review & editing, Funding acquisition. **Kathrin Greiff:** Writing – review & editing, Supervision, Funding acquisition.

Declaration of Competing Interest

The authors declare that they have no known competing financial interests or personal relationships that could have appeared to influence the work reported in this paper.

Data availability

The data that has been used is confidential.

Acknowledgments

We would like to thank the following individuals for their much-appreciated support in our research: **Peter Bardenheuer**: support in literature review (Section 1, Section 2), **Abtin Maghmoumi**: data preprocessing (test series B), **Alena Spies**: sensor setup & manual sorting (test series A), **Johanna Beaupoil**: sensor setup & manual sorting (test series A), **Julius Lorenzo**: sensor setup & manual sorting (test series B),

Matthias Schlaak: sensor setup & manual sorting (test series B), and **Elias Pfund**: sensor setup (test series B).

Supplementary materials

Supplementary material associated with this article can be found, in the online version, at doi:10.1016/j.resconrec.2023.107256.

References

Bachmann, M, Zibunas, C, Hartmann, J, Tulus, V, Suh, S, Guillén-Gosálbez, G, et al., 2023. Towards circular plastics within planetary boundaries. Nat. Sustain. https://doi.org/10.1038/s41893-022-01054-9.

Bonifazi, G, Capobianco, G, Serranti, S., 2018. A hierarchical classification approach for recognition of low-density (LDPE) and high-density polyethylene (HDPE) in mixed plastic waste based on short-wave infrared (SWIR) hyperspectral imaging. Spectrochim. Acta A Mol. Biomol. Spectrosc. 198, 115–122. https://doi.org/10.1016/j.saa.2018.03.006.

Borowski C. Entwicklung von Verfahren und Bohrtechniken zur zufälligen Volumenelemententnahme aus Ballen; 2018.

bvse-Fachverband Kunststoffrecycling. bvse-Altkunststofftag hat begonnen - Qualität bleibt Thema Gastland ist die Türkei; 2016.

bvse-Fachverband Kunststoffrecycling. Kunststoffrecycler erhalten weiterhin ungenügende Qualität, 2017. https://www.bvse.de/gut-informiert-kunststoffrecycling/nachrichten-kunststoffrecycling/1650-kunststoffrecycler-erhalten-weiterhin-ungenuegende-qualitaet.html.

Calvini, R, Orlandi, G, Foca, G, Ulrici, A., 2018. Development of a classification algorithm for efficient handling of multiple classes in sorting systems based on hyperspectral imaging. J. Spectral Imag. https://doi.org/10.1255/jsi.2018.a13.

CEN/TR 15310-1, 2006. Characterisation of waste—sampling of waste materials—part 1: guidance on selection and application of criteria for sampling under various conditions. European Committee for Standardization, Brussels.

Chen, X, Feil, A., 2019. Detection and classification of heterogeneous materials as well as small particles using NIR-spectroscopy by validation of algorithms. In: Beyerer, J, Puente León, F, Längle, T (Eds.), OCM 2019 - Optical Characterization of Materials Conference Proceedings. KIT Scientific Publishing, pp. 63–77.

Chen, X, Kroell, N, Althaus, M, Pretz, T, Pomberger, R, Greiff, K, 2023. Enabling mechanical recycling of plastic bottles with shrink sleeves through near-infrared spectroscopy and machine learning algorithms. Resour. Conserv. Recycl. 188, 106719. https://doi.org/10.1016/j.resconrec.2022.106719.

Chen, X, Kroell, N, Li, K, Feil, A, Pretz, T., 2021. Influences of bioplastic polylactic acid on near-infrared-based sorting of conventional plastic. Waste management & research the journal of the International Solid Wastes and Public Cleansing Association. ISWA 39 (9), 734242X211003969. https://doi.org/10.1177/0734242X211003969.

COREPLA. General terms and conditions for sale by auction, 2022. https://www.corepla.it/sites/default/files/documenti/generaltermscond_rev._no15_march_2022.pdf (accessed April 15, 2023).

Cudjoe, D, Zhu, B, Nketiah, E, Wang, H, Chen, W, Qianqian, Y., 2021. The potential energy and environmental benefits of global recyclable resources. Sci. Total Environ. 798, 149258 https://doi.org/10.1016/j.scitotenv.2021.149258.

Curtis, A, Küppers, B, Möllnitz, S, Khodier, K, Sarc, R., 2021. Real time material flow monitoring in mechanical waste processing and the relevance of fluctuations. Waste Manage. 120 (1), 687–697. https://doi.org/10.1016/j.wasman.2020.10.037.

Dehoust G, Christiani J. Analyse und Fortentwicklung der Verwertungsquoten für Wertstoffe: Sammel- und Verwertungsquoten für Verpackungen und stoffgleiche Nichtverpackungen als Lenkungsinstrument zur Ressourcenschonung; 2012.

Der Grüne Punkt. Allgemeine Vertragsbedingungen der Der Grüne Punkt – Duales System Deutschland GmbH (DSD) für Verwerterverträge (AVBV) - Erlöskunden - Stand 07.2016, 2016. https://www.gruener-punkt.de/fileadmin/Dateien/Downloads/PDFs/geschaeftsbedingungen/AVBV_Erloeskunden_2016_07_04.pdf (accessed April 15, 2023).

Der Grüne Punkt. DSD Rohstofffraktionsspezifikationen, 2023. https://www.gruener-punkt.de/de/downloads (accessed April 17, 2023).

DIN 54390, 2022. Deutsches Institut für Normung e.V. Beuth Verlag, Berlin.

Duan, Q, Li, J., 2021. Classification of common household plastic wastes combining multiple methods based on near-infrared spectroscopy. ACS ES&T Engg 1 (7), 1065–1073. https://doi.org/10.1021/acsestengg.0c00183.

EU Recycling. Wie können mehr Kunststoffe in Leichtverpackungen recycelt werden?, 2018. https://eu-recycling.com/Archive/20131.

European Commission. The European Green Deal. Brussels, Belgium; 2019.

European Commission, 2020. Circular Economy Action Plan: For a cleaner and more competitive Europe. Brussels.

EVK Kerschhaggl GmbH. EVK SQALAR: Software Tool for the qualitative and quantitative analysis, 2023a. https://www.evk.biz/en/products/analysis-software-tool/evk-sqalar/(accessed April 21, 2023).

EVK Kerschhaggl GmbH. EVK STREAM Supervisor, 2023b. https://www.evk.biz/en/products/analysis-software-tool/evk-stream-supervisor/(accessed March 19, 2023).

Fahrmeir, L, Kneib, T, Lang, S, Marx, B., 2013. Regression: Models, methods and applications. Springer, Berlin, Heidelberg.

Feil, A, Kroell, N, Pretz, T, Greiff, K., 2021. Anforderungen an eine effiziente technologische Behandlung von Post-Consumer Verpackungsmaterialien in Sortieranlagen. Müll und Abfall 21 (7), 362–370. https://doi.org/10.37307/j.1863-9763.2021.07.04.

Feil, A, Pretz, T., 2020. Mechanical recycling of packaging waste. editor. In: Letcher, TM (Ed.), Plastic waste and recycling: Environmental impact, societal issues, prevention, and solutions. Academic Press, Amsterdam, San Diego, Cambridge, MA, Kidlington, pp. 283–319.

GBP Quality GmbH. Sortieranalysen: Aufgabe und Lösung, 2023. https://www.gbp-quality.eu/ablauf-arbeitsweise-gbp-sortieranalysen/(accessed April 15, 2023).

Goodfellow, I, Bengio, Y, Courville, A, 2016. Deep Learning. MIT Press.

Hahladakis, JN, Iacovidou, E., 2018. Closing the loop on plastic packaging materials: What is quality and how does it affect their circularity? Sci. Total Environ. 630, 1394–1400. https://doi.org/10.1016/j.scitotenv.2018.02.330.

Harris, CR, Millman, KJ, van der Walt, SJ, Gommers, R, Virtanen, P, Cournapeau, D, et al., 2020. Array programming with NumPy. Nature 585 (7825), 357–362. https://doi.org/10.1038/s41586-020-2649-2.

Hunter, JD, 2007. Matplotlib: A 2D graphics environment. Comput. Sci. Eng. 9 (3), 90–95. https://doi.org/10.1109/MCSE.2007.55.

Initiative „Mülltrennung wirkt“, 2021. Ein Jahr Initiative „Mülltrennung wirkt“: Von den Herausforderungen zum Erfolg: Duale Systeme bilden eine starke Allianz für mehr Aufklärung. Müll und Abfall (7), 352–360. https://doi.org/10.37307/j.1863-9763.2021.07.03.

Knappe F, Reinhardt J, Kauertz B, Oetjen-Dehne R, Buschow N, Ritthoff M, et al. Technische Potenzialanalyse zur Steigerung des Kunststoffrecyclings und des Rezyklateinsatzes; 2021. TEXTE 92.

Kroell, N, Chen, X, Greiff, K, Feil, A., 2022a. Optical sensors and machine learning algorithms in sensor-based material flow characterization for mechanical recycling processes: A systematic literature review. Waste Manage. 149, 259–290. https://doi.org/10.1016/j.wasman.2022.05.015.

Kroell, N, Chen, X, Küppers, B, Lorenzo, J, Maghmoumi, A, Schlaak, M, et al., 2023a. Near-infrared-based determination of mass-based material flow compositions in mechanical recycling of post-consumer plastics: Technical feasibility enables novel applications. Resour. Conserv. Recycl. 191, 106873 https://doi.org/10.1016/j.resconrec.2023.106873.

Kroell, N, Chen, X, Maghmoumi, A, Koenig, M, Feil, A, Greiff, K., 2021. Sensor-based particle mass prediction of lightweight packaging waste using machine learning algorithms. Waste Manage. 136, 253–265. https://doi.org/10.1016/j.wasman.2021.10.017.

Kroell, N, Chen, X, Maghmoumi, A, Lorenzo, J, Schlaak, M, Nordmann, C, et al., 2023b. NIR-MFCO dataset: Near-infrared-based false-color images of post-consumer plastics at different material flow compositions and material flow presentations. Data Brief 48, 109054. https://doi.org/10.1016/j.dib.2023.109054.

Kroell, N, Dietl, T, Maghmoumi, A, Chen, X, Küppers, B, Feil, A, et al., 2022b. Assessment of sensor-based sorting performance for lightweight packaging waste through sensor-based material flow monitoring: Concept and preliminary results. In: Greiff, K, Wotruba, H, Feil, A, Kroell, N, Chen, X, Gürsel, D, Merz, V (Eds.), 9th Sensor-Based Sorting & Control 2022; 13.04.2022 - 14.04.2022: Aachen.

Küppers, B, Schloegl, S, Oreski, G, Pomberger, R, Vollprecht, D., 2019. Influence of surface roughness and surface moisture of plastics on sensor-based sorting in the near infrared range. Waste management & research the journal of the International Solid Wastes and Public Cleansing Association. ISWA 37 (8), 843–850. https://doi.org/10.1177/0734242X19855433.

Küppers, B, Schlögl, S, Friedrich, K, Lederle, L, Pichler, C, Freil, J, et al., 2021. Influence of material alterations and machine impairment on throughput related sensor-based sorting performance. Waste management & research the journal of the International Solid Wastes and Public Cleansing Association. ISWA 39 (1), 122–129. https://doi.org/10.1177/0734242X20936745.

Küppers, B, Schlögl, S, Kroell, N, Radkohl, V., 2022. Relevance and challenges of plant control in the pre-processing stage for enhanced sorting performance. In: Greiff, K, Wotruba, H, Feil, A, Kroell, N, Chen, X, Gürsel, D, Merz, V (Eds.), 9th Sensor-Based Sorting & Control 2022; 13.04.2022 - 14.04.2022: Aachen.

Küppers, B, Seidler, I, Koinig, GR, Pomberger, R, Vollprecht, D., 2020. Influence of throughput rate and input composition on sensor-based sorting efficiency //Volume 09 - March 2020. Detritus (9), 59–67. https://doi.org/10.31025/2611-4135/2020.13906.

Länderarbeitsgemeinschaft Abfall LAGA PN 98, 2001.

Mann, HB, Whitney, DR., 1947. On a test of whether one of two random variables is stochastically larger than the other. Ann. Math. Statist. 18 (1), 50–60. https://doi.org/10.1214/aoms/1177730491.

McKinney, W., 2010. Data structures for statistical computing in python. In: Stéfan van der Walt, Jarrod Millman. Proceedings of the 9th Python in Science Conference.

Österreichisches Normungsinstitut. ÖNORM S 2127, 2011 (accessed February 11, 2023).

Pearson, K., 1895. VII. Note on regression and inheritance in the case of two parents. Proc. R. Soc. Lond. 58 (347-352), 240–242. https://doi.org/10.1098/rspl.1895.0041.

Pedregosa, F, Varoquaux, G, Gramfort, A, Michel, V, Thirion, B, Grisel, O, et al., 2011. Scikit-learn: machine learning in python. J. Open Source Software 12, 2825–2830.

Flamme, S, Kölking, M, Glorius, T, Mayer, S, 2020. Langzeituntersuchungen zur stoffstromspezifischen Kalibrierung eines nahinfrarotgestützten Echtzeitanalyse-Systems. In: Pomberger, R: Konferenzband zur 15. Recy & DepoTech-Konferenz, Montanuniversität Leoben, Österreich sowie virtuelle Konferenzwelt auf meetyoo, 18.-20. November 2020: Leoben, Österreich: AVW, Abfallverwertungstechnik & Abfallwirtschaft Eigenverlag, 2020.

Plastic Europe. Plastics – the Facts 2022; 2022a.

Plastic Europe. The circular economy for plastics: a European overview, 2022b. https://plasticseurope.org/knowledge-hub/the-circular-economy-for-plastics-a-european-overview-2/(accessed May 27, 2022).

plasticker. "Recybase" - Börse für Kunststoff-Rohstoffe, 2023. https://plasticker.de/recybase/(accessed April 19, 2023).
Roosen, M, Mys, N, Kusenberg, M, Billen, P, Dumoulin, A, Dewulf, J, et al., 2020. Detailed analysis of the composition of selected plastic packaging waste products and its implications for mechanical and thermochemical recycling. Environ. Sci. Technol. 54 (20), 13282–13293. https://doi.org/10.1021/acs.est.0c03371A.
The pandas development team. pandas-dev/pandas: Pandas: Zenodo, 2020.
United Nations. Paris Agreement. United Nations Framework Convention on Climate Change; 2015.
Virtanen, P, Gommers, R, Oliphant, TE, Haberland, M, Reddy, T, Cournapeau, D, et al., 2020. SciPy 1.0: fundamental algorithms for scientific computing in python. Nat. Methods 17, 261–272. https://doi.org/10.1038/s41592-019-0686-2.
Waskom, ML., 2021. Seaborn: statistical data visualization. J. Open Source Softw. 6 (60), 3021. https://doi.org/10.21105/joss.03021.
Workman, JJ, Weyer, L., 2007. Practical Guide to Interpretive Near-Infrared Spectroscopy. CRC Press.
Xia, J, Huang, Y, Li, Q, Xiong, Y, Min, S., 2021. Convolutional neural network with near-infrared spectroscopy for plastic discrimination. Environ. Chem. Lett. 19 (5), 3547–3555. https://doi.org/10.1007/s10311-021-01240-9.
Zheng, Y, Bai, J, Xu, J, Li, X, Zhang, Y., 2018. A discrimination model in waste plastics sorting using NIR hyperspectral imaging system. Waste Manage. 72, 87–98. https://doi.org/10.1016/j.wasman.2017.10.015.

4.2 Publication G: Data-driven process models and digital twins

> **Kroell**, **N.**, Maghmoumi, A., Dietl, T., Chen, X., Küppers, B., Scherling, T., Feil, A., & Greiff, K. (2024). Towards digital twins of waste sorting plants: Developing data-driven process models of industrial-scale sensor-based sorting units by combining machine learning with near-infrared-based process monitoring. *Resources, Conservation and Recycling*, *200*, 107257. https://doi.org/10.1016/j.resconrec.2023.107257

The second SBMC application (Publication G) targets the process level, which has rarely been addressed in previous SBMC research (cf. Publication A [Section 2.1]). Due to the high efforts of manual material flow characterization, which is needed for process assessment, most processes in recycling are difficult to be modeled and are often treated as black boxes. Based on the insight from Chapter 3 that material flows can be especially satisfactorily sensor-based monitored at singled or monolayer material flow presentations, Publication G addressed this gap by using inline NIR-sensors to automatically assess the sorting behavior of an industrial-scale SBS unit (Figure 4.2). Based on the obtained process monitoring data, ML models are trained to form a data-driven process model, which is then used as a building block to simulate and optimize an entire SBS cascade and to be utilized for the long-term development of digital sorting plant twins.[5]

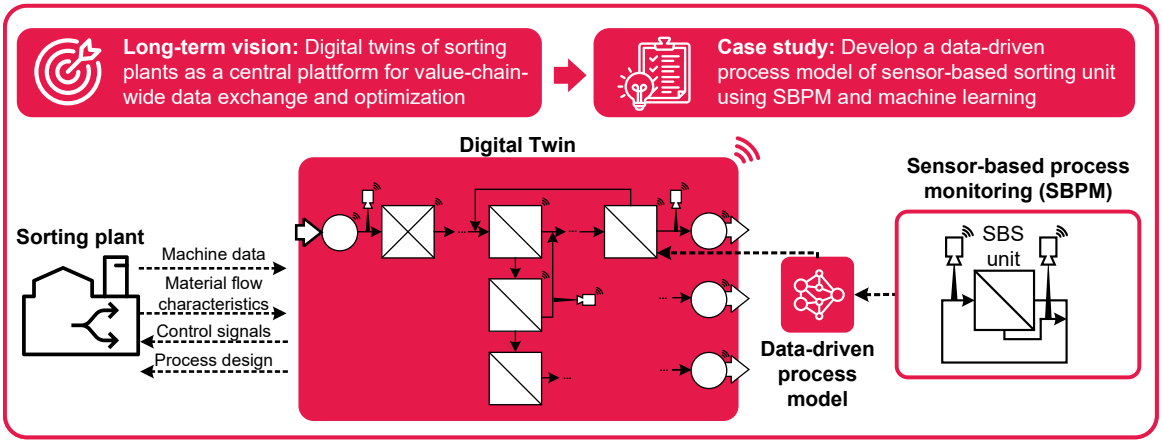

Figure 4.2. Graphical abstract Publication G; SBPM: sensor-based process monitoring.

[5]Supplementary materials for Publication G are provided in Appendix C.

Resources, Conservation & Recycling 200 (2024) 107257

Contents lists available at ScienceDirect

Resources, Conservation & Recycling

journal homepage: www.elsevier.com/locate/resconrec

Towards digital twins of waste sorting plants: Developing data-driven process models of industrial-scale sensor-based sorting units by combining machine learning with near-infrared-based process monitoring

Nils Kroell [a,*], Abtin Maghmoumi [a], Tobias Dietl [a,b], Xiaozheng Chen [b], Bastian Küppers [b], Tabea Scherling [a], Alexander Feil [a], Kathrin Greiff [a]

[a] Department of Anthropogenic Material Cycles, RWTH Aachen University, Wuellnerstr. 2, D-52062 Aachen, Germany
[b] STADLER Anlagenbau GmbH, Max-Planck-Str. 2, D-88361 Altshausen, Germany

ARTICLE INFO

Keywords:
Sensor-based material flow characterization
Circular economy
Mechanical post-consumer plastic recycling
Data-driven process simulation
Artificial intelligence
Lightweight packaging waste

ABSTRACT

Sorting plants are crucial for effective recycling, but their optimization can be challenging due to the heterogeneity of waste streams. We introduce a novel approach to holistically optimize sorting plants using digital twins containing data-driven process models. To demonstrate their technical feasibility, we developed a data-driven process model for industrial-scale sensor-based sorting (SBS) units by combining near-infrared process monitoring with machine learning. Our results indicate a sorting performance change (F_1-score) in the SBS unit by 0.22 a% for +1% occupation density and +0.19 a% for +1 wt% target material share. An artificial neural network predicted the SBS behavior with a 3.0% mean absolute error. Our case study demonstrates the potential of data-driven process models for digital twins by clarifying the influence of throughput fluctuations on SBS performance and simulating different SBS cascade designs, thus paving the way towards improved design and operation of sorting plants and a more circular future.

1. Introduction

Natural resource extraction and processing is responsible for about 50% of global greenhouse gas emissions and more than 90% of water and biodiversity issues (IRP, 2019). Substituting primary raw materials with secondary raw materials from recycling processes can significantly reduce these environmental impacts (e.g., Schwarz et al., 2021; Schyns and Shaver, 2021; Zhang et al., 2023), but the amount of substituted primary raw materials is still very limited (IRP, 2019). For example, the European Union, considered to be one of the pioneers of circular economy (European Commission, 2019, 2020), was able to obtain only about 12.7 wt% of its raw material supply from secondary raw material sources in 2021 (Eurostat, 2023).

Significant improvements in today's recycling systems are thus necessary to increase the quantity and quality of recovered secondary raw materials (European Parliament and Council, 2018; Hahladakis and Iacovidou, 2018; Schwarz et al., 2021). Modern recycling systems of mixed waste streams often comprise three stages: (i) waste collection, (ii) sorting mixed waste into pre-concentrates in sorting plants, and (iii) processing pre-concentrates into secondary raw materials in processing plants (Pretz et al., 2020; Ragaert et al., 2017). The performance of *sorting plants* is crucial for the overall recycling performance as (a) material losses in sorting plants towards energy recovery cannot be recovered at later process stages and (b) the pre-concentrate qualities generated by sorting plants can limit the performance of subsequent processing stages (Dehoust and Christiani, 2012; Knappe et al., 2021; Ragaert et al., 2017).

1.1. Optimization potentials in sorting plants

The performance of a sorting plant is influenced by both its design and operation. In the **design stage**, engineers develop an initial process

Abbreviations: ANN, artificial neural networks; BC, beverage carton; BG, background; C, cleaner; DEM, discrete element method; LWP, lightweight packaging; ML, machine learning; MSOD, material-specific occupation density; NIR, near-infrared; OD, occupation density; PE, polyethylene; PET, Polyethylene terephthalate; PP, polypropylene; PPC, paper, paperboard, and cardboard; PR, polynomial regression; PS, polystyrene; R, rougher; RF, random forest; S, scavenger; SBS, sensor-based sorting; TC, transfer coefficient; UNDEF, undefined..

* Corresponding author at: Department of Anthropogenic Material Cycles, RWTH Aachen University, Wuellnerstr. 2, D-52062, Aachen, Germany.
E-mail address: nils.kroell@ants.rwth-aachen.de (N. Kroell).

https://doi.org/10.1016/j.resconrec.2023.107257
Received 4 July 2023; Received in revised form 25 September 2023; Accepted 10 October 2023

design and then simulate the sorting plant to dimension individual process steps (e.g., conveyor belt widths or component sizes) based on the obtained mass balance. Due to missing information on the exact sorting behavior of individual process steps for different material flow characteristics, this process simulation is currently based on fixed, manually estimated transfer coefficients depending on expert knowledge and experience (Bárkányi et al., 2022; Kleinhans et al., 2021; Tanguay-Rioux et al., 2022). Inaccuracies in the process simulation resulting from these estimations can lead to a suboptimal process design and dimensioning, resulting in avoidable additional costs (over--dimensioning) or a suboptimal sorting plant performance (under--dimensioning), i.e., lower product qualities and yields with respective economic and ecological consequences (Kroell et al., 2023b).

In the **operational phase**, fluctuations in the input material flows can make an effective plant operation challenging. For example, changing product designs (Eriksen et al., 2019; Kleinhans et al., 2021; Singh et al., 2014), consumer behavior (Denafas et al., 2014; Umweltbundesamt, 2012), seasonal influences (Denafas et al., 2014; Gómez et al., 2009; Kleinhans et al., 2021), or different waste collection areas (Denafas et al., 2014; Kleinhans et al., 2021; Umweltbundesamt, 2012; van Thoden Velzen et al., 2019) can significantly change the characteristics of the input material flows in terms of, e.g., material composition, particle size distribution, or moisture content. Today, most sorting plants are operated with constant process parameters (e.g., screen cuts, wind sifter speeds, or settings of sensor-based sorting units), which are often optimized during plant commissioning but then rarely adjusted during plant operation. This combination of fluctuating input material flows and constant process parameters can lead to significant performance losses (Küppers et al., 2022).

1.2. Digital twins of sorting plants

Both design and operation of sorting plants could therefore be significantly enhanced by developing and utilizing a *digital twin* of the sorting plant (Fig. 1), which reflects a virtual representation of the sorting plant and could become a central platform for simulating, controlling, and optimizing the sorting in real-time among different stakeholders (cf. Tao et al., 2018).

During the **design phase**, the digital twin could be used to simulate the material flow distribution dynamically and more accurately in the designed sorting plant, thus enhancing the dimensioning of individual processes. Further, an accurate process simulation enabled by the digital twin serves as a basis for iterative and potentially artificial-intelligence-assisted optimization of the process design to increase the overall sorting plant performance and/or maximize, e.g., economic or ecological goal functions.

During the **operational phase**, real-time machine and material flow data (cf. Kroell et al., 2022a) from the physical sorting plant could be fed back into the digital twin. Based on the simulation results inside the digital twin, improved process parameters could be generated and sent to the process control of the sorting plant, thereby adapting the sorting plant to changing input material flows and enhancing the overall plant

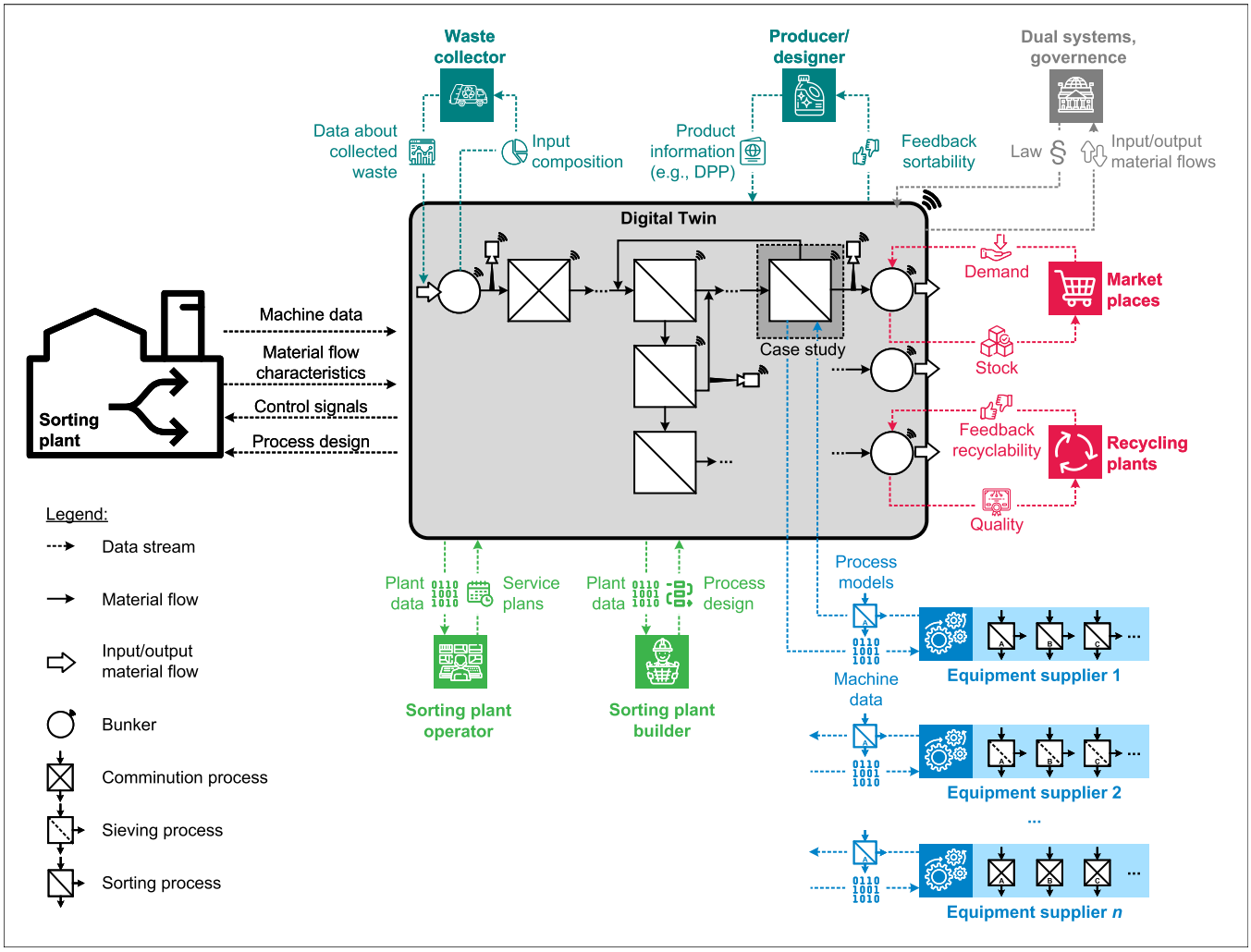

Fig. 1. Concept for a digital twin of a waste sorting plant with exemplary use cases and stakeholders (not exhaustive).

performance.

A prerequisite for the development of such a digital twin is that the behavior of the sorting plant can be simulated within reasonable accuracy. As sorting plants can be represented by an interlinked set of process steps, modeling the entire sorting plant can be achieved by individually replicating these steps and subsequently integrating them to create an entire virtual sorting plant. While process models are well established in, e.g., chemical process engineering (Arizmendi-Sánchez and Sharratt, 2008; Jawad et al., 2021) or processing of bulk materials (Jovanović et al., 2015; McCoy and Auret, 2019), process models for sorting of anthropogenic waste streams are rather scarce. Sorting units of particular importance in sorting plants are sensor-based sorting (SBS) units due to its widespread application and high number of installed units in modern sorting plants (Gundupalli et al., 2017; Kroell et al., 2022a; Sarc et al., 2019), on which we will therefore focus in the following case study.

1.3. Related work: process models of sensor-based sorting units

In the primary raw material sector, detailed process models of SBS units have already been developed, for instance, based on discrete element methods (DEM) (Pieper et al., 2016) or computational fluid dynamics coupled with DEM (Bauer et al., 2023; Fitzpatrick et al., 2015) for bulk materials like peppercorns, coffee beans, and minerals.

However, these physics-based process models require detailed knowledge of material parameters such as particle masses, particle shapes, densities, and various friction coefficients, as well as experimental calibration of these parameters. For heterogeneous waste streams like post-consumer plastic packaging waste, such material parameters vary significantly between each waste particle due to, e.g., individual product/packaging designs and their waste genesis (e.g., residual contents, particle deformation during waste collection and sorting, post-consumer effects) (Kroell et al., 2021). In addition, the material flow behavior is influenced by moisture, surface contaminations, and adhering dust as well as missing bulk properties (Feil and Pretz, 2020). As it is currently infeasible to determine such detailed characteristics for thousands of waste particles, a direct transfer of existing SBS models from the primary raw material to the waste management sector seems infeasible.

In the waste management sector, previous studies have investigated the influence of surface roughness and moisture (Küppers et al., 2019b), throughput and eject-share (Küppers et al., 2020b), machine malfunctions and impurities (Küppers et al., 2020a), as well as volume flow fluctuations (Curtis et al., 2021) on the SBS behavior. The process evaluation in these investigations was carried out in *batch-wise* sorting trials, with the mass and composition of product and residual fractions being determined after sorting. Because of this batch-wise process evaluation, there is only a limited number of data points available to describe the sorting behavior at different material and process parameters, which leads to only statements with limited statistical significance.

1.4. Research aim and approach

With the present paper, we aim to enable the creation of digital sorting plant twins by developing a method for creating *data-driven process models* in waste sorting and processing. On the example of an industrial-scale SBS unit, we want to demonstrate how such data-driven models can be developed and what potentials they bring for dynamic sorting plant simulations.

Our modeling approach is based on the combination of (i) sensor-based process monitoring (Kroell et al., 2022a) for creating the necessary empirical data basis in an automated manner and (ii) machine learning models trained on the process monitoring data to allow a precise prediction of the sorting behavior across different material and machine parameters.

Thus, our approach overcomes the limitations of previous approaches in three ways: First, the model development is based on inline sensor-based process monitoring data, thus eliminating the need for a detailed input characterization at the individual particle level (cf. Section 1.3). Second, the creation of the necessary data basis is not done manually and batch-wise, but sensor-based and inline, which generates a wide data basis for training the models. Third, the investigations are carried out for an industrial-scale SBS unit using actual waste particles on a real scale, making them more applicable to SBS units in real-world applications.

Based on the findings of previous research (Section 1.3), our model development focusses on three main factors influencing on the SBS behavior, which shall be investigated in detail with our novel sensor-based process assessment method and included in the data-driven process model: throughput, input composition, and throughput fluctuations.

2. Material and methods

To reach our research aim defined in Section 1.4, an experimental setup was created to automatically assess the sorting performance of an industrial-scale SBS unit using near-infrared (NIR)-based process monitoring. Based on the acquired process monitoring data, machine learning (ML) models were trained to develop a data-driven process model of the investigated SBS unit and showcase its benefits for developing digital twins of waste sorting plants. The SBS unit investigated the example of sorting out polyethylene terephthalate (PET) bottles from a 3D plastic fraction from lightweight packaging (LWP), which is one of the most common SBS applications (Kroell et al., 2022a).

2.1. Experimental setup

To enable continuous test operation and data acquisition, our experimental setup consisted of a closed material loop, as shown in Fig. 2a. First, the test material (Section 2.1.2) was presented on an acceleration belt to the industrial-scale SBS unit (Section 2.1.1), which sorts the material flow into an eject and drop fraction. Second, two external NIR sensors monitored the acceleration belt and sorting result (eject and drop conveyor belt) (Section 2.1.3) and thus created the necessary data for assessing the SBS unit and developing a data-driven process model. Third, the eject and drop material flows were mixed via a belt transfer and a modified ballistic separator and several additional belt transfers, which completed the homogenization of the material flow before re-entering the SBS unit again.

2.1.1. SBS unit

The investigated SBS unit was an industrial-scale NIR-based SBS belt sorter with a total working width of 2,000 mm, an acceleration belt speed of $v_1 = 3$ m/s, an air nozzle bar with 12.5 mm nozzle distance for material ejection operated at 5.5 bar air pressure. To investigate a high range of occupation densities despite the limited transport capacity of the sorting line, the effective belt width of the SBS unit was reduced to $b_1 = 1{,}000$ mm (Fig. 2b).

The SBS unit was programmed to actively sort out PET (bottles and trays) based on an industry-standard NIR sorting recipe for plastic sorting applications trained on LWP articles and was provided directly by the SBS manufacturer. The same LWP sorting recipe is operiatonially used in several LWP sorting plants, and no further modifications were made to the sorting recipe to keep the sorting results as close to the reality of LWP sorting plants as possible. After sorting, the ejected and non-ejected particles landed on an eject and drop conveyor belt, respectively, with the same belt width of $b_2 = 830$ mm and the same belt speed of $v_2 = 1.2$ m/s each (Fig. 2b).

2.1.2. Sample material

To create a 3D plastic fraction for the desired sorting application

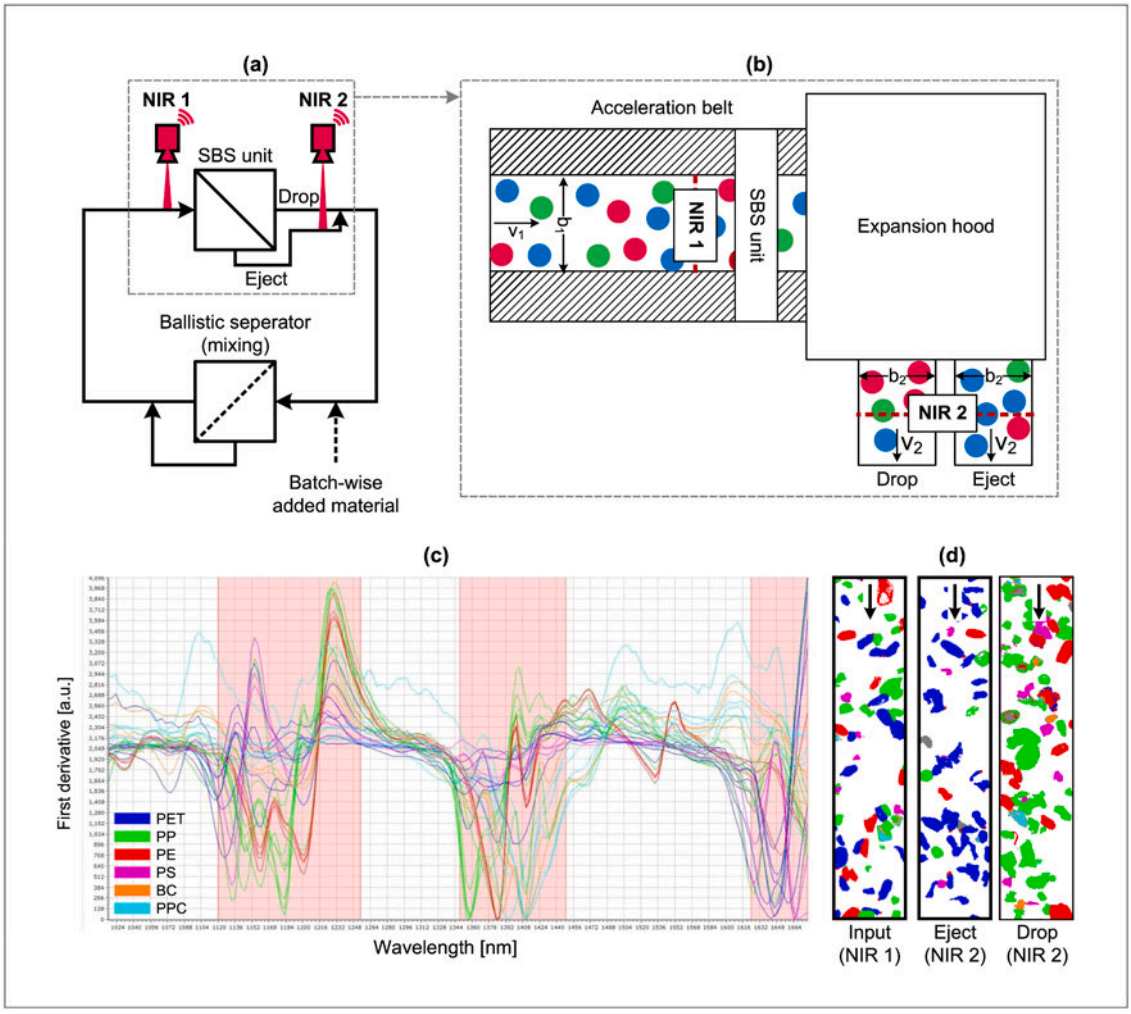

Fig. 2. Experimental setup. (a) simplified process layout of the material loop, (b) top-view on industrial-scale SBS unit with added external NIR sensors, (c) NIR classification recipe, (d) resulting false-color recordings of NIR 1 and NIR 2 [see (c) for color legend].

(sorting out PET bottles from a 3D plastic LWP fraction), a PET fraction and a non-PET plastic fraction were created and subsequently mixed in defined mass ratios to create defined shares of the target (PET) material ("target share") (see Fig. S1 in Supplementary Materials).

For the PET fraction, post-consumer PET bottles from a LWP sorting plant (product fraction) from Slovenia were pre-treated with the STADLER label remover (Küppers et al., 2019a) to improve sortability for the SBS unit and classifiability for external NIR sensors by removing the influence of labels and sleeves (Chen et al., 2023a) and increasing the surface roughness (Küppers et al., 2019b).

For the non-PET fraction, LWP waste from the city of Maribor (Slovenia) was pre-conditioned to create a 3D plastic fraction. The pre-conditioning simulated typical pre-conditioning processes in a state-of-the-art LWP sorting plant by subsequently removing 2D materials and fines (< 45 mm) using a ballistic separator, ferrous metals with a magnetic separator, and non-ferrous metals with an eddy current separator. All PET contents from the pre-conditioned 3D plastic fraction were removed using the SBS unit (Section 2.1.1). To ensure complete removal of PET bottles by the SBS unit, the material flow was consecutively sorted five times by the SBS unit at low ODs and manually post-sorted afterwards. The sample material was then created by mixing defined masses of PET- and non-PET materials (Section 2.1.4). Table S1 summarizes the material flow composition of the non-PET fraction.

2.1.3. NIR-based process monitoring

2.1.3.1. NIR sensors. Due to the excellent classificability of LWP materials in the NIR range (Kroell et al., 2022a; Neo et al., 2022), two external NIR sensors (Fig. 2b) were used to monitor the acceleration belt ("NIR 1") and eject and drop belt ("NIR 2"). Both external NIR sensors were EVK HELIOS EQ32 hyperspectral imaging sensors from EVK Kerschhaggl GmbH (Raaba, Austria) with a spectral resolution of 3.1 nm/channel, a used wavelength range of 1,016 nm to 1,676 nm, operated at a frame rate of 450 Hz.

2.1.3.2. NIR classification model. The recorded NIR data were then pixel-based classified using the on-chip CLASS32 classification algorithm from EVK Kerschhaggl GmbH (2023) based on a developed NIR classification model (cf. Friedrich et al., 2022), which was trained on six material classes (Fig. 2c): PET; polypropylene (PP); polyethylene (PE); polystyrene (PS); beverage carton (BC); and paper, paperboard, and cardboard (PPC). The reference spectra were recorded from various packaging articles from the sample material and selected from the center part of the packaging articles to avoid spectral anomalies such as edge effects (Chen and Feil, 2019; Küppers et al., 2019b).

Furthermore, NIR spectra from labeled and sleeved plastic bottle parts, known to significantly affect NIR classification (Chen et al., 2023a), were added as reference spectra. This addition helped training the model to identify bottle materials accurately, even when covered

with different sleeve or label materials. The same approach was used for wet articles and overlays of transparent material on others to mitigate NIR absorption influence and systematic misclassification (Kroell et al., 2023a; Küppers et al., 2019b).

Differentiation between background (BG) pixels (conveyor belt) and material pixels was achieved by setting a user-defined threshold based on the dynamic of the raw NIR spectra. Before the classification, the following pre-processing techniques are applied to the NIR spectra using the EVK SQALAR software: intensity calibration (white and black reference), first derivative, normalization, and smoothing (cf. Küppers et al., 2019b). The classification in CLASS32 was based on three spectral regions of interest shown in Fig. 2c (1120 nm – 1254 nm, 1348 nm – 1448nm, 1624 nm – 1676 nm), where material spectra showed maximum differentiation. NIR spectra significantly differing from references are classified as "undefined" (UNDEF) by the CLASS32 algorithm, resulting in eight distinct NIR outputs (PET, PP, PE, PS, BC, PPC, UNDEF, and BG).

2.1.3.3. Recording of NIR-false-color images. The developed NIR classification model was then uploaded to the NIR sensor, thus enabling an NIR classification in real-time. The classification results (material class per pixel) were then continuously recorded using a self-developed recording software and stored as false-color images as shown in Fig. 2d.

2.1.4. Experimental procedure

To investigate the influence of different target shares, throughputs, and throughput fluctuations on the SBS performance and develop a process model for their prediction, all influence factor combinations were investigated as follows.

First, the **target share** was set by mixing a pre-defined amount of PET and non-PET material (cf. Section 2.1.2). Five different input compositions were investigated: 5 wt% PET (simulation of a SBS scavenger), 30 wt% PET (simulation of a SBS rougher), 50 wt% PET (dataset completion), 70 wt% PET (dataset completion), and 90 wt% PET (simulation of a SBS cleaner). The SBS unit was set to *positive sorting* (ejecting PET) for the trials with 5 wt%, 30 wt%, 50 wt% PET content and to *negative sorting* (ejecting all non-PET materials) for the trials with 70 wt% and 90 wt% PET content.

Second, the throughput, measured by the **occupation density** (OD; share of acceleration belt area that is covered by material), was varied by adding defined amounts of sample material to the material loop resulting in $n = 16$ investigated throughput steps.

Third, the influence of **throughput fluctuations** was studied by operating the feeding conveyor belt at constant belt speed ($v = 1.2$ m/s) ("constant throughput") and fluctuating belt speeds alternating between 4 s at $v_a = 1.2$ m/s belt speed and 8 s at $v_b = 0.6$ m/s belt speed ("fluctuating throughput"). These alternating belt speeds resulted in a throughput fluctuation ratio of $\dot{V}_b/\dot{V}_a = 2{:}1$.

Each target share and throughput step was divided into a 5 min section for adding sample material to the material loop (cf. Fig. 2a) and equalizing the material flow, a 10 min section with constant throughput, and a 10 min section with fluctuating throughput. In total, 2000 min (33.3 h) of SBS sorting at different target shares, ODs, and fluctuations were investigated and recorded (excluding time for material and test setup preparation).

2.2. Data preprocessing

After conducting the experiments, the recorded false-color images were processed for subsequent ML model training. The following open-source packages were primarily used for data processing, visualization, and ML training: *NumPy* (Harris et al., 2020) [data storage and data processing], *pandas* (McKinney, 2010; The pandas development team, 2020) [data storage and data processing], *scikit-learn* (Pedregosa et al., 2011) [training and evaluation of ML models], *SciPy* (Virtanen et al., 2020) [statistics], *matplotlib* (Hunter, 2007) [data visualization], and *seaborn* (Waskom, 2021) [data visualization].

2.2.1. Image calibration and splitting

Firstly, each image was calibrated to ensure the same spatial resolution in *x*- (conveying direction) and *y*-direction ("square pixels"). Then, the images from NIR 2 were vertically split into images of the eject and drop conveyor belt (cf. Fig. 2d).

2.2.2. Data aggregation

As shown by Kroell et al. (2023a), it is necessary to aggregate NIR-based false-color data to draw insights from it at the material flow level and reduce the effect of particle artifacts. In addition, Kroell et al. (2023a) showed that aggregating over a certain material area (e.g., aggregating 1 m^2 material) is advantageous compared to time-based data aggregation (e.g., aggregating 1 s).

Since the assessment of sorting performance is based on the target material area (cf. Section 2.3.1), we aggregated the pixel-based false-color images from NIR 1 until the area of the target material (here: PET) reached a chunk size of 0.1 m^2 (approx. 5–10 post-consumer PET bottles [cf. Kroell et al., 2023c]) by accumulating the pixel counts from each row in the NIR 1 false-color images. This aggregated NIR 1 area containing 0.1 m^2 PET is referred to as a *chunk* in the following (cf. Kroell et al., 2023a).

Based on the beginning time stamp ($t_{start,\ NIR1}$) and end timestamp ($t_{stop,\ NIR1}$) of each chunk representing 0.1 m^2 PET from NIR 1, the time stamps for the corresponding chunks at NIR 2 were calculated. Therefore, the transport time $\Delta t_{transport} = 3.5$ s between NIR 1 and NIR 2 (cf. Fig. 2b) was added to the timestamps of NIR 1:

$$t_{i,\ NIR2} = t_{i,\ NIR1} + \Delta t_{transport} \quad (1)$$

As the traveling time of each particle between NIR 1 and NIR 2 can differ whether it is ejected ("eject") or not ("drop") and depending on where it lies on the acceleration belt (cf. Fig. 2b), the created chunks were thus further smoothed using a moving average with a window size of 100 chunks (10 m^2). The combination of data aggregation over 0.1 m^2 combined with a moving average over 10 m^2, thus combines the advantages of a sufficiently high number of chunks for ML model training and a sufficiently high data aggregation to reduce noise from different transport times and particle artifacts.

2.2.3. Feature extraction

To describe the input material flow on the acceleration belt independently from the belt width and belt speed, we then normalize the material-specific area flows per chunk ($\dot{A}_i$) by area flow of the total conveyor belt ($\dot{A}_{belt}$) using the material-specific occupation density (MSOD) (Schlögl et al., 2023) as shown in Eq. (2).

$$MSOD_i = \frac{\dot{A}_i}{\dot{A}_{belt}} \ with\ \dot{A}_{belt} = v^* b \quad (2)$$

Further, we describe the throughput of the SBS unit using the OD (Küppers et al., 2020a) as shown in Eq. (3).

$$OD = \frac{\dot{A}_{covered}}{\dot{A}_{belt}} = \sum_i MSOD_i \quad (3)$$

While we have shown in previous work (Kroell et al., 2022b) that more detailed indicators (singling ratio and particle distances) can be calculated from the NIR-based false-color images, evidence has shown that for the investigations conducted on SBS units so far, these indicators do not correlate better than OD with SBS performance (Kroell et al.,

2022b). Since the OD is an established indicator and easier to calculate from the images compared to the singling ratio or particle distances,[1] we will focus on the OD to describe the acceleration belt in the following.

2.3. SBS assessment and modeling

2.3.1. Assessment of SBS performance

For evaluating the SBS performance based on the NIR 2 data, we will use the established indicators *purity* (Eq. (4)) and *yield* (Eq. (5)) (Feil et al., 2017). Purity describes the share of the target material ($\dot{A}_{\text{PET, eject}}$) in the eject fraction ($\dot{A}_{\text{eject}}$), while yield describes how much target material was sorted in the eject fraction ($\dot{A}_{\text{PET, eject}}$) compared to the total target material ($\dot{A}_{\text{PET, eject}} + \dot{A}_{\text{PET, drop}}$). As proposed in (Küppers et al., 2020b), we will use an area-based assessment of the SBS performance as SBS is based on the area-based detection and ejection of material flows.[2]

Since there is always a trade-off between high purity and high yield, we will additionally express the SBS performance using the F_1-score (Kroell et al., 2022b), shown in Eq. (6), which is the harmonic mean between purity and yield, and expresses the SBS performance in a single performance metric.

$$P_{a,\ \text{PET}} = \frac{\dot{A}_{\text{PET, eject}}}{\dot{A}_{\text{eject}}} = \frac{\dot{A}_{\text{PET, eject}}}{\sum_i \dot{A}_{i,\ \text{eject}}} \tag{4}$$

$$R_{a,\ \text{PET}} = \frac{\dot{A}_{\text{PET, eject}}}{\dot{A}_{\text{PET, eject}} + \dot{A}_{\text{PET, drop}}} \tag{5}$$

$$F_{1,\ \text{a, PET}} = 2 \cdot \frac{P_{\text{a, PET}} \cdot R_{\text{a, PET}}}{P_{\text{a, PET}} + R_{\text{a, PET}}} \tag{6}$$

2.3.2. Transfer coefficients

To fully simulate an entire sorting plant, it is not only necessary to describe the sorting behavior in terms of target and non-target material (Section 2.3.1) but to predict how the individual material classes are distributed among the individual output material flows (here: eject and drop).

Hence, we use *transfer coefficients* (TCs) (Eq. (7)) to describe how an area flow of a material class is distributed between eject and drop fractions (cf. Brunner and Rechberger, 2016). By convention, we will define the TC based on the actively ejected fraction that is sorted out, i.e., a TC of 100% describes a case where 100% of the input area flow is transferred to the eject fraction, and a TC of 0% where 100% of the area flow is transferred to the drop fraction.

$$TC_i = \frac{\dot{A}_{i,\ \text{eject}}}{\dot{A}_{i,\ \text{eject}} + \dot{A}_{i,\ \text{drop}}} \tag{7}$$

Since the input area flows approximately equals the sum of the output area flows (area constancy, Eq. (8)), a TC for each material class is sufficient to fully describe the sorting process. It is important to note that in contrast to mass flows, input and output area flows may not be exactly equal, e.g., due to particle deformations during ejection. However, over the time periods considered here, our data shows that these random effects even out and are therefore neglected in the following.

$$\dot{A}_{i,\ \text{input}} \approx \dot{A}_{i,\ \text{eject}} + \dot{A}_{i,\ \text{drop}} \tag{8}$$

Hence, the eject and drop fraction can be calculated from the TC and the material-specific input area flow, see Eq. (9) and Eq. (10).

$$\dot{A}_{i,\ \text{eject}} \approx TC_i * \dot{A}_{i,\ \text{input}} \tag{9}$$

$$\dot{A}_{i,\ \text{drop}} \approx (1 - TC_i) * \dot{A}_{i,\ \text{input}} \tag{10}$$

2.3.3. Transfer coefficients prediction using machine learning

To accurately and dynamically simulate a single SBS process, it is necessary to predict the material-specific TCs depending on the influence factors on the SBS process, such that the assumed TC in the digital twin reflects the TC in the actual sorting plant. This task can be solved using ML models, which predict the TC (=sorting behavior of the SBS unit) from the input material flow and SBS settings. More specifically, we will use the MSOD values determined by NIR 1 to predict the TCs determined by NIR 2 to simulate the SBS process with ML.

2.3.3.1. Train-validation-test split. To find the optimal set of hyperparameters for the ML model and to accurately assess the prediction performance of the ML model, it is necessary to split the model into a training, validation, and test dataset. The training set is used to train the ML model, enabling it to learn and extract patterns from the MSOD values determined by NIR 1. The validation set provides an unbiased evaluation of the model's performance during the tuning of hyperparameters, helping to prevent overfitting. Finally, the test set is used to assess the final performance of the model, providing an objective measure of how well the model generalizes to unseen data, thus ensuring the validity of the simulation of the SBS process.

To avoid data leakage from the validation and test data into the training data, we randomly split the $n = 16$ investigated throughput steps per target share (cf. Section 2.1.4) into $n = 13$ training and validation steps for ML model training and hyperparameter optimization (Section 2.3.3.3), and $n = 3$ test throughput steps for determining the final ML model performance. As each throughput step was investigated independently of each other in time, this approach ensures that the allocation of data to the training, validation, and test datasets is unbiased, and representative and avoids over-optimistic or -pessimistic model performance estimation.

2.3.3.2. Model selection and feature engineering. We will compare three types of ML regression models with increasing model complexity on the task of predicting the TCs from the MSOD values: polynomial regression (PR) models (cf. Fahrmeir et al., 2013), random forest (RF) regressors (Breiman, 2001), and artificial neural networks (ANN) (cf. Wang, 2003) (see Table S2 for the used ML model implementations). As most ML regression models are single-output models, we will use an ensemble of $n = 7$ individual regression models to predict the TC of all $n = 7$ material classes (PET, PP, HDPE, PS, BC, PPC, UNDEF). Furthermore, two different sets of models were trained for positive sorting and negative sorting of the SBS unit ("SBS mode"), as preliminary tests showed that the ML performance was better when training two separated ML models for positive and negative sorting compared to a joint ML model.

Each ML model is trained on two different types of input features: (i) the full set of MSOD values for each seven material classes ("full input feature set") and (ii) a reduced set of input features containing the OD, area-share of the target material (α_{target}), and the area-based share of the corresponding material fraction (α_j) ("reduced input feature set"). The features of the reduced input feature set can be directly calculated from the full input feature set using Eq. (11) to (13). The motivation behind comparing a reduced input feature set with the full input feature set is that input features like OD and target material share, which are of particular importance for the SBS result (cf. Section 3.1), are presented in a more direct form to the models and could therefore simplify the prediction for simpler ML models (cf. Liu and Dong, 2018).

$$OD = \sum_i MSOD_i \tag{11}$$

[1] The occupation density can be directly calculated from the pixel counts or material area, while the singling ratio and particle distances require a detection of individual particles or clusters.

[2] Readers interested in the conversion between area- to mass-based indicators may be, among others, interested into the following publications: Kroell et al. (2021); Kroell et al. (2023a); Kroell et al. (2023c).

$$\alpha_{target} = \frac{MSOD_{PET}}{OD} = \frac{MSOD_{PET}}{\sum_i MSOD_i} \quad (12)$$

$$\alpha_j = \frac{MSOD_j}{OD} = \frac{MSOD_j}{\sum_i MSOD_i} \quad (13)$$

2.3.3.3. Hyperparameter optimization. For each ML model type (PR, RF, ANN), material class, and SBS mode (positive or negative sorting), a systematic hyperparameter optimization was performed using a custom grid search. Therefore, each of the $n = 42$ ML models ($n = 3$ model types, $n = 7$ material class, $n = 2$ SBS modes) was trained on the training set and evaluated on the validation set for each hyperparameter combination. Table S3 summarizes the investigated hyperparameter settings for each ML model type. For each of the $n = 42$ ML models, the ML models with the lowest mean absolute error (MAE) value (cf. Section 2.3.3.4), i.e., the most precise TC prediction, were selected for evaluation on the test set and further investigations.

2.3.3.4. Machine learning model evaluation. The ML model performance was evaluated by comparing the TCs predicted by the ML models with the true TC determined through NIR 2 using the R^2-score and MAE (Devore, 2012; Willmott and Matsuura, 2005). Accurate TC predictions are indicated by low MAE values and R^2-scores close to 1.

2.4. Simulation of an SBS cascade

2.4.1. SBS process models

Based on the trained and best-performing ML models, a process model for a SBS unit was created to demonstrate the technical feasibility of simulating a SBS cascade containing multiple SBS units connected by conveyor belts. We simulated three types of SBS units: rougher, cleaner, and scavenger. Rougher units aim at positively sorting out target material, while cleaner units negatively sort out non-target materials from rougher ejects and scavengers recover target materials from rougher drops and cleaner ejects and sort them back into the input material flow for a second chance (Chen et al., 2023b).

For rougher and scavenger units, we used the ML models trained on positive sorting data; for cleaner units, we used the ML models trained on negative sorting data (cf. Section 2.3.3.2). Since our ML models were only trained on process monitoring data with PET as the target material, we used the "PET-as-target-material" ML model for all target material classes and the "PP-as-non-target-material" model cases where PET was the non-target material.[3] Table S4 gives an overview of the ML model configuration for the simulated SBS units.

2.4.2. Input material

To demonstrate the practical suitability of our process models, we simulate a NIR-based plastic-type separation in an LWP sorting plant, which is one of the most common SBS applications. In both input scenarios, the input area flow was consistent at 2.1 m^2 (equivalent to 25 a% OD in the initial rougher stage) across all investigated SBS cascades.

The assumed input composition ("input 1") into the SBS cascade (α_{PET} = 21.5 a%, α_{PP} = 35.1 a%, α_{HDPE} = 31.0 a%, α_{PS} = 2.3 a%, α_{BC} = 1.5 a%, α_{PPC} = 0.5 a%, α_{UNDEF} = 8.1 a%) was calculated based on an average LWP input composition in Germany published by Christiani (2017). For this purpose, the enrichment of plastics from an upstream plastic rougher into the SBS cascade was simulated with a TC of 0.9, and the removal of foreign materials such as films, metals, and beverage cartons was simulated with a TC of 0.1 (cf. Feil et al., 2021). In addition, the mass-based material flow composition was converted to an area-based material flow composition using the material-specific grammages from Kroell et al. (2023b).

As an alternative input scenario ("input 2"), an anticipated reduction of 50% in the PET content in LWP due to the expansion of Germany's deposit return system for PET bottles (Gesetz über das Inverkehrbringen, die Rücknahme und die hochwertige Verwertung von Verpackungen, 2023) was simulated. This resulted in a lower PET share and a higher share of other materials (α_{PET} = 12.5 a%, α_{PP} = 39.1 a%, α_{HDPE} = 34.5 a%, α_{PS} = 2.5 a%, α_{BC} = 1.7 a%, α_{PPC} = 0.6 a%, α_{UNDEF} = 9.1 a%) to be sorted by the simulated SBS cascade.

2.4.3. SBS settings and modeling of scavenger loops

Each SBS unit is modeled with a belt speed of $v = 3$ m/s and a specific belt width b_i (cf. Section 3.4). Based on the belt speed and belt width, the *MSOD* value of each material class is then calculated according to Eq. (2) as an input into the ML models from Section 2.3.3. For the simulation of material loops (e.g., due to scavengers) inside the SBS cascade, the simulation is run $n = 20$ times (=until area flows of the material loops converge at a stable value).

3. Results and discussion

3.1. Influence of occupation density and target share on SBS performance

Before developing an ML model for predicting the SBS sorting performance, we seek to understand the influence of OD and target share on the SBS performance to validate our automated process assessment using NIR-based process monitoring and compare our findings with previous studies. Fig. 3 shows the influence of OD (*x*-axis) and target share (color) on the SBS performance measured by (a) purity, (b) yield, and (c) F_1-score.

3.1.1. Influence on purity

As shown in Fig. 3a, the area-based product purity decreases linearly with increasing OD. The slope of this decrease depends on the target share and the negative slope increases with decreasing target share. Consequently, higher purities are produced at higher target shares ranging from 76.3 a% purity at 5 wt% target share to 98.1 a% purity at 90 wt% target share when comparing the produced purities at an exemplary OD of 25 a%.

In contrast to positive sorting, the produced purities with negative sorting are generally higher and less affected by higher ODs: In positive sorting, the average purity decreases with each additional 1 a% OD by −0.62 a%, −0.47 a%, and −0.35 a% for target shares of 5 wt%, 30 wt%, and 50wt%, respectively. In negative sorting, however, purity remains more or less constant over the investigated OD range (−0.01 a% and +0.02 a% slope at 70 wt% and 90 wt% target share, respectively).

3.1.2. Influence on yield

Similar to purities, the observed yields decrease with increasing OD (Fig. 3b). However, for the investigated SBS unit, the observed yields (82.6 a% - 99.7 a%) are generally higher than observed purities (56.1 a% - 99.0 a%), since the slopes are smaller. Compared to purities, the effects of positive and negative sorting reverse: Lower yields and steeper slopes are observed for negative sorting (70 wt% target share: −0.31 a% yield per additional 1 a% OD, 90wt%: −0.13 a%) compared to positive sorting (5 wt%: +0.06 a%, 30 wt%: −0.04 a%, 50 wt%: −0.03 a%).

3.1.3. Influence on F_1-score

As shown in Fig. 3c, the F_1-score demonstrates to be a good combination of purity and yield, compensates for the effects of positive and negative sorting, and thus reflects the general SBS performance well. It can be seen that the SBS performance (F_1-score) decreases with

[3] The "PP-as-non-target-material" model was chosen for cases where PET was the non-target material, because (i) the TC of PE is influenced by HDPE caps on top of PET bottles (difference between pixel- and article-based assessment, cf. Section 3.2) and (ii) we assumed that the SBS ejection behavior of PET bottles is more similar to PP packaging instead of PS (often present as smaller cups), PPC, and BC.

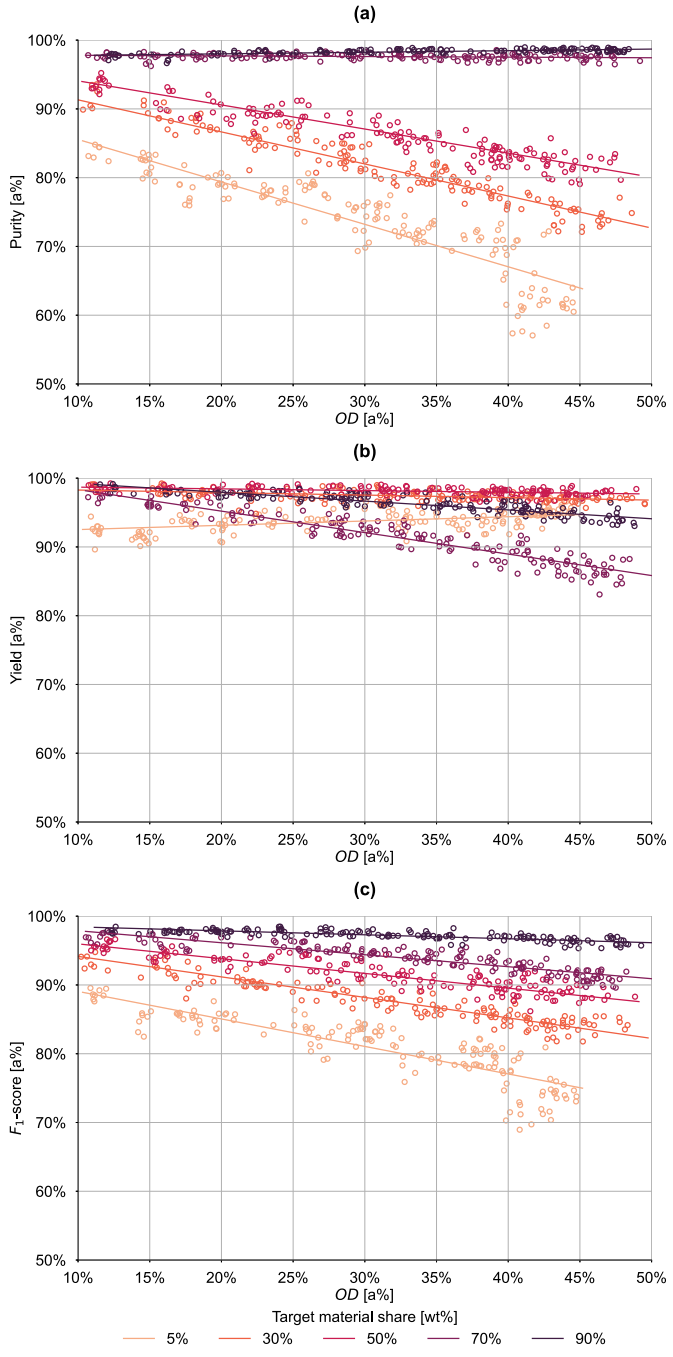

Fig. 3. Influence of occupation density (OD) and target share on SBS performance measured by area-based (a) purity, (b) yield, and (c) F_1-score. (Scatterplots limited to $n = 150$ randomly selected chunks per target share for better visualization.).

increasing OD and decreasing target share: Per additional +1 a% OD, the SBS performance decreases by −0.22 a% F_1-score and by additional +1 wt% target share, the SBS performance increases by +0.19 a% F_1-score.

3.1.4. Discussion

Our findings align with previous research, notably Küppers et al. (2020a, 2020b), Pascoe et al. (2010), and Pieper et al. (2016). The joint results indicate that SBS performance decreases with increasing OD and rises with higher target share, consistent across different material flows and SBS designs.

Regarding purity, both our study and Küppers et al. (2020a, 2020b) show that product purity decreases linearly with increasing OD. The slope of this decrease depends on the target share, meaning a higher target share leads to a higher purity.

However, our findings diverge from Küppers et al. (2020a, 2020b) when it comes to yield. In contrast to their assertion that yield is independent of input composition, our results show that the target share impacts the slope of the yield-OD curve (Fig. 3b), albeit to a lesser degree than purity. Moreover, Küppers et al. (2020a, 2020b) presented yield as a fourth-degree polynomial function, whereas we observe a more linear relationship with OD (cf. Fig. 3b).

These differences might arise from variations in the machine design of the investigated SBS units (e.g., chute sorter in Küppers et al. (2020a, 2020b) vs. belt sorter in our work, different air nozzle distances, transport speeds), SBS settings (e.g., applied air pressure), used SBS algorithm and sensors, material characteristics (e.g., particle size and shape, particle density/grammage, and material characteristics), and investigation scale (laboratory vs. industrial scale). As such, results should be interpreted within the specific context of each experimental setup and the materials processed.

3.2. Data-driven process model: TC prediction

To develop a data-driven process model for a digital twin of a multi-stage SBS sorting plant, it is not enough to characterize the SBS sorting behavior solely based on purity and yield (i.e., target and non-target material). Instead, it is crucial to predict how each material class is transferred into the eject and drop material flows since the ejection behavior of one sorting unit directly impacts the input material composition of the subsequent unit.

3.2.1. Material-specific TC distribution

Fig. 4 shows the transfer coefficients of each material class. For the target material PET (Fig. 4a), the TC is equivalent to the yield for positive sorting and (1 - yield) for negative sorting (cf. Eq. (5) and Eq. (7)). Therefore, the conclusions from Section 3.1.2 apply to the TCs of PET: For positive sorting, high TCs (= high yield) for PET are observed, which slightly decrease with increasing OD and increasing target share. For negative sorting, low TCs (=high yields) are observed, which slightly increase with increasing OD and decreasing target share.

For non-target materials, we observe systematic differences in the ejection behavior of different material classes (Fig. 4b-g). First, all TCs increase with increasing OD, which explains the decreasing purity with increasing OD identified in Section 3.1.1. A likely mechanism for this effect is the higher particle entrainment with increasing OD: With increasing OD, both the particle proximity (Kroell et al., 2022b) as well as the number of air valve activations increases, resulting in a higher probability of particle entrainment due to air valve turbulences (Fitzpatrick et al., 2015) and thus higher TCs with increasing ODs. It is surprising that the TCs of non-target materials also increase with increasing OD at negative sorting, which explains the higher and more constant purity at negative compared to positive sorting (cf. Section 3.1). A possible reason for this observation could be the accidental particle entrainment of additional non-target particles at higher ODs due to higher particle proximities and air valve activations.

Second, we observe that most non-target TCs increase with increasing target share for positive sorting but decrease with increasing target share for negative sorting. It can thus be beneficial to interpret the input material flow in terms of *eject area* (α_{eject}) instead of target share (α_{target}). As shown in Eq. (11), the eject share describes the area share of input material to be actively ejected and thus incorporates the effects of positive and negative sorting.

$$\alpha_{\text{eject}} = \begin{cases} \alpha_{\text{target}} \text{ for positive sorting} \\ (1 - \alpha_{\text{target}}) \text{ for negative sorting} \end{cases} \quad (14)$$

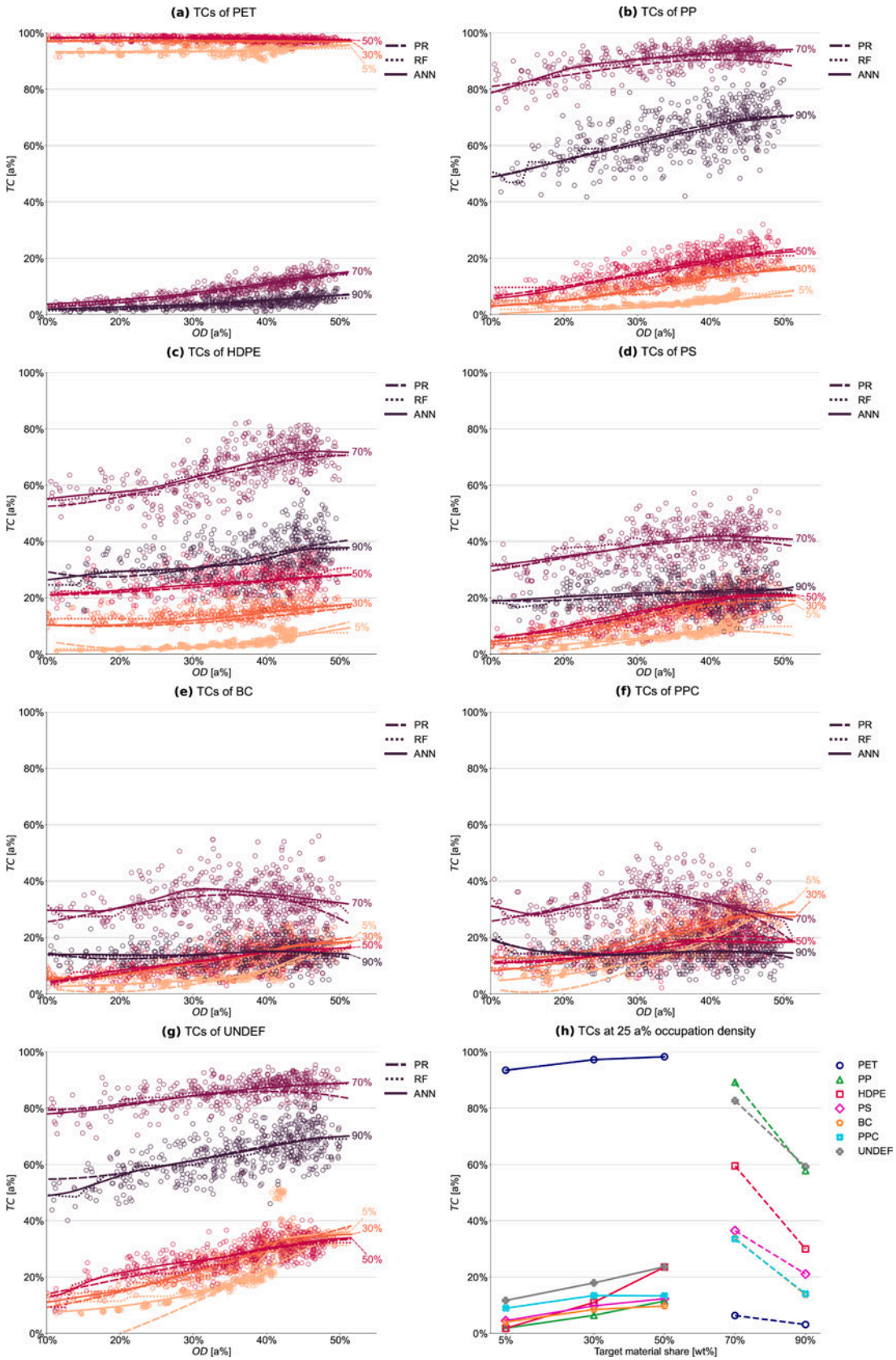

Fig. 4. Transfer coefficients (TCs) of the investigated SBS unit. (a-g) true transfer coefficients (circles) determined through NIR-based process monitoring and predicted TCs using ML (lines) per material class for different target shares and occupation densities (ODs). (h) average transfer coefficient at 25 a% occupation density for different target shares and material classes predicted using the ANN model; solid line: positive sorting, dashed line: negative sorting. (Scatterplots in [a-g] limited to $n = 500$ randomly selected chunks per target share for better visualization.).

When taking the eject area into account, it can be seen that all non-target TCs generally increase with increasing eject area. A likely mechanism for this observation is the higher air valve activations at higher eject shares resulting in higher particle entrainment at higher eject shares and thus higher TCs.

Third, systematic differences in the TCs between different material classes can be observed as shown by the mean TC at 25 a% OD in Fig. 4h. For example, the mean TCs differ by more than a factor of 2.4 across all eject shares and some material classes such as PP can be better sorted (=low TC at positive sorting and high TC at negative sorting) than other material classes such as PPC and HDPE.

3.2.2. Discussion on material-specific TC distribution

Several reasons and mechanisms could explain the systematic differences: First, it is important to note that our TC calculation is based on a pixel-based process monitoring, while the SBS ejection is article-based.[4] Therefore, material composites can have a direct influence on the TCs. For example, PET bottles often contain HDPE bottle caps (Kroell et al., 2023a; Roosen et al., 2020), thus positively sorting out a PET bottle increases the TC both of PET and HDPE. For instance, we observe that the TC of HDPE compared to PP is higher at positive sorting and lower at negative sorting, which could be caused by composite effects.

Second, the eject behavior of different material classes might affected by different particle and material flow characteristics. For example, more constant TCs are observed for PPC and BC (especially for negative sorting) compared to other material classes, which could be caused, e.g., by the higher flexibility and different geometry of PPC and BC compared to 3D plastics fractions. In addition, e.g., material-specific particle size and particle shape distributions, grammages, and mechanical properties as well as influences of the settings (sorting recipe) and classification of the SBS unit could explain the material-specific TC distributions. However, the scope of our study did not encompass the investigation of different non-target material shares and different particle characteristics (e.g., particle sizes) that could affect our hypotheses. Therefore, future research should further explore and test these hypotheses, for example, by systematically altering particle characteristics and non-target material shares to examine the effects on the SBS behavior.

3.2.3. TC prediction with ML

As shown qualitatively by the prediction lines in Fig. 4a-g, these systematic effects can be accurately predicted by all three investigated ML models (PR, RF, ANN). The models react robustly to outliers and reasonably predict the TCs across different material classes, ODs, and target shares. However, the RF predictions appear to be more fidgety, whereas PR and ANN predictions are significantly smoother.

Quantitatively, Table 1 shows that all investigated ML models can reasonably predict the TCs of all material classes with MAEs below 6.3%. The reduced input feature set (cf. Section 2.3.3.2) lowers the MAEs across all three models on average by −0.2% MAE (macro-average); however, the observed effect is not strong enough to be statistically significant ($p = 0.155$[5]).

Table 1
MAEs on test dataset (constant throughput) of different ML models and input feature sets on predicting the TCs for each material class based on the input material flow (MSODs); PR: polynomial regression, RF: random forest, ANN: artificial neural network.

Input	Full input feature set (MSODs)			Reduced input feature set (OD, α_{target}, α_i)		
ML model	**PR**	**RF**	**ANN**	**PR**	**RF**	**ANN**
PET	0.9%	1.1%	0.9%	1.2%	0.9%	0.8%
PP	3.6%	4.8%	3.4%	3.1%	3.8%	3.2%
HDPE	4.2%	6.3%	5.0%	4.9%	4.2%	3.8%
PS	3.2%	3.4%	3.2%	3.8%	3.7%	3.1%
BC	3.3%	3.4%	3.2%	3.0%	3.2%	3.1%
PPC	3.5%	3.7%	3.6%	3.8%	3.9%	3.5%
UNDEF	4.0%	5.3%	3.6%	4.1%	4.4%	3.7%
macro-average	**3.2%**	**4.0%**	**3.3%**	**3.4%**	**3.5%**	**3.0%**

3.2.4. Discussion on TC prediction with ML

TCs of the target material (PET; average MAE: 1.0%) are significantly ($p < 0.001$[6]) better predicted compared to the TCs of non-target materials target (average MAE: 3.8%) across all models and input feature sets. A likely reason for the lower MAEs of the PET TCs could be the lower fluctuations of the TCs of PET compared to other material classes (Fig. 4). Among the non-target material classes, MAEs are roughly similar except for HDPE, which is significantly ($p = 0.027$[7]) higher than all other material classes. A likely reason for this effect could be the composite effect of PET bottles and HDPE caps (cf. Section 3.2.1).

ANNs in combination with a reduced input feature set achieved the best model performance with an average MAE of 3.0% and are thus further applied to understand the influence of throughput fluctuations on the SBS performance (Section 3.3) and to simulate an SBS cascade (Section 3.4).

3.3. Process model application I: understanding the influence of throughput fluctuations

3.3.1. SBS performance prediction on constant and fluctuating throughput data

Fig. 5a-c compares the SBS performance in terms of purity, yield, and F_1-score between the sorting trials with constant and fluctuating throughputs. The simulated throughput fluctuations show no significant influence on SBS performance ($p = 0.768$) and a good correspondence between predicted and ground truth SBS performance can be observed.

The missing influence of throughput fluctuations on the SBS performance seems surprising at first glance since several previous studies (e.g., Curtis et al., 2021; Feil et al., 2019; Feil and Pretz, 2018; Küppers et al., 2020b) have emphasized the influence of throughput fluctuations on (sensor-based) sorting performance and a reduced SBS performance caused by throughput fluctuations was shown by Curtis et al. (2021). To understand and explain this discrepancy, we will utilize the SBS prediction model developed in Section 3.2.3.

First, Fig. 5d-f compare the predicted SBS performance using the ANN process model with the true SBS performance measured by NIR 2. As one would expect from Section 3.2.3, the ANN process model achieves very reasonable predictions. The purity, yield, and F1-score predictions ($MAE_{\text{purity, const.}} = 0.50\%$, $MAE_{\text{yield, const.}} = 0.32\%$, $MAE_{\text{F1-score, const.}} = 0.34\%$) are even lower compared to individual TCs (cf. Table 1), most likely due to the mutual compensation of individual prediction errors when aggregating multiple material classes into a single performance score.

Second, Fig. 5g-i show the predictions of the ANN process model on

[4] Within this paper, we use the term *particle* to describe any physical objects contained in a material flow. We differ between between the two major particle types, as described by Kroell et al. (2023a). First, *articles* are larger and more complex particles that are often comprised of different materials (e.g., LWP packaging after collection). Second, *flakes* are smaller particles (often < 20 mm) that are often comprised of a single material and have a more regular shape (e.g., plastic flakes after shredding in processing plants).

[5] *p*-values express the level of significance. Here, we calculated the *p*-value based on a paired *t*-test.

[6] Average *p*-value of paired *t*-test between PET and all other material classes.

[7] Average *p*-value of paired *t*-test between HDPE and all other non-target material classes.

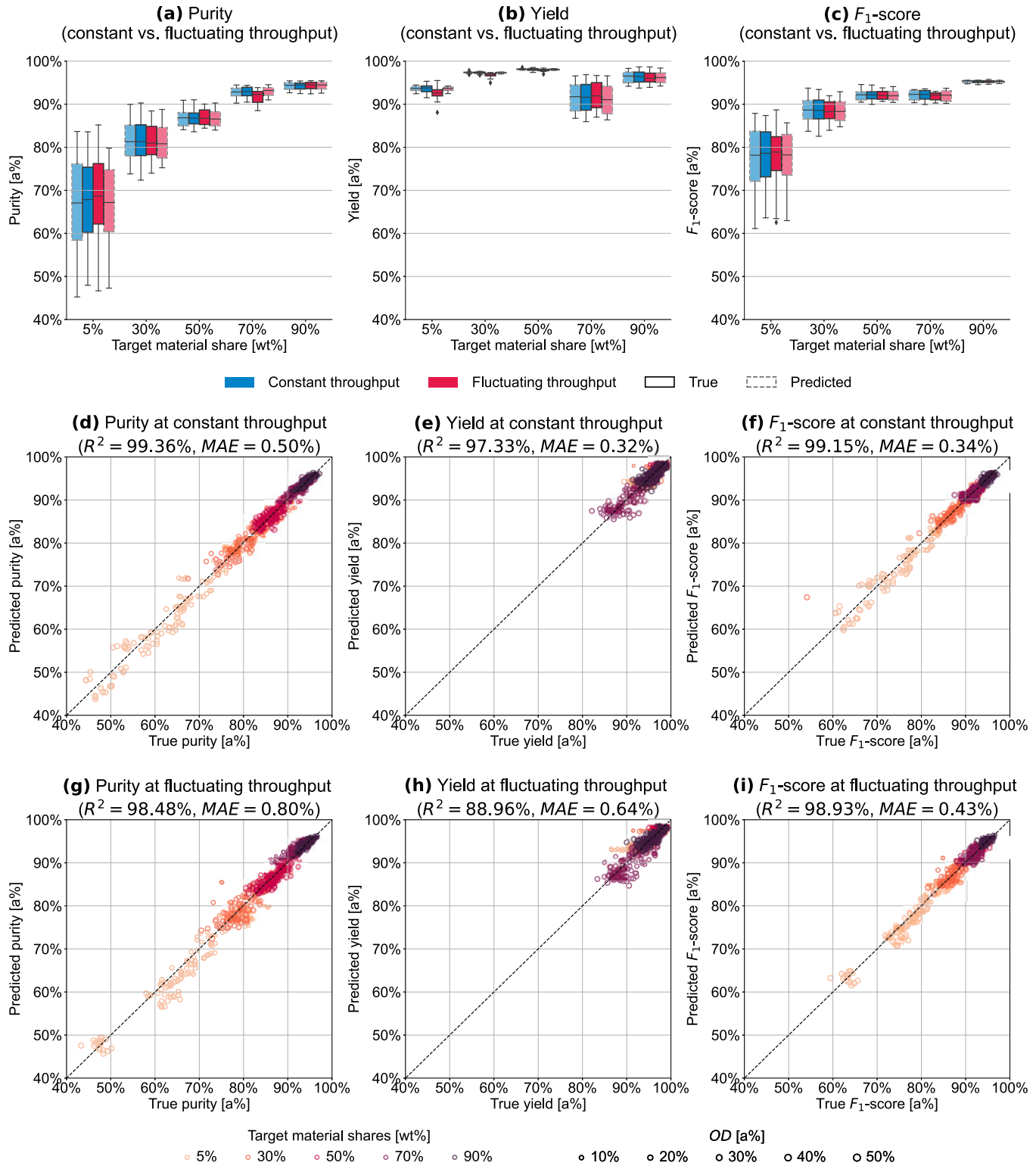

Fig. 5. Influence and prediction of fluctuations. (a-c) comparison of average SBS performance per sorting trial at constant vs. fluctuating throughput. True vs. predicted SBS performance at (d-f) constant and (g-i) fluctuating throughput with ANN model trained on constant throughput data; (Scatterplots in [a-f] limited to n = 10 randomly selected chunks per target share and throughput step [equal to n = 160 chunks per target share] for better visualization; boxplot in [a-c]: 25%, 50% and 75% percentiles.).

the fluctuating throughput data. Here, we observe that even though the model was trained only on constant throughput data, it is capable of very accurate predictions ($MAE_{\text{purity, fluct.}}$ = 0.80%, $MAE_{\text{yield, const.}}$ = 0.64%, $MAE_{\text{F1-score, const.}}$ = 0.43%).

3.3.2. *Discussion on the influence of throughput fluctuations*

Two main implications can be derived from these findings. First, it becomes evident that SBS performance over longer periods can be accurately predicted when dividing material flows into individual chunks (here: 10 m^2 of target material). The total SBS performance is

then the cumulative SBS performance of all chunks.

Second, the developed process model can be used to understand the lacking influence of the investigated throughput fluctuations: Since the SBS performance decreases linearly with increasing OD in the investigated OD range ($\leq$ 50 a%) (Fig. 4), temporarily higher ODs at fluctuating throughput result in a lower SBS performance during these high OD periods, however, the lower SBS performance is then compensated by the higher SBS performance during lower OD periods. Since the SBS performance decrease is linear, lower and higher SBS performance at higher and lower OD even out and the SBS performance is similar to a constant throughput scenario with the same mean OD.

At first glance, our results thus contradict those of Curtis et al. (2021) in which a lower SBS performance was found between constant and fluctuating throughput with the same average OD. At second glance, combining both findings result in a promising explanation mechanism: Our investigated throughput fluctuations had a fluctuation ratio of $\dot{V}_b$ / $\dot{V}_a = 2{:}1$ (cf. Section 2.1.4), hence even at high ODs and fluctuations, the material flows were always presented as a *monolayer* (i.e., no significant particle overlap) to the SBS unit, i.e., individual particles touched but did not overlap each other. The investigated throughput fluctuations of Curtis et al. (2021), however, were much larger ($\dot{V}_b/\dot{V}_a = 5{:}1$), and thus resulted in *particle overlaps* during high ODs (cf. Fig. 2 in [Curtis et al., 2021]).

At particle overlap, (i) only particles on the material flow surface can be detected by the sensor and (ii) the particle discharge could be mechanically hampered. It is thus likely that the SBS performance decreases disproportionately, i.e., super-linear, once a critical OD (e.g., >> 50 a%) is exceeded and particle stats overlap significantly. This super-linear performance decrease due to particle overlap is then no longer compensated by the relatively smaller increase in SBS performance at lower OD ranges, and the SBS performance would be lower compared to a constant throughput scenario. In further research, the SBS performance in the OD range > 50 a% should be investigated in more detail to determine whether the derived effect of the super-linear decrease of the SBS performance at higher ODs actually occurs.

3.4. Process model application II: simulation of SBS cascade

Lastly, we aim at demonstrating how the developed process model can be used to simulate an SBS cascade as part of a LWP sorting plant and determine what kind of insights can be derived from such a process simulation. Therefore, we will compare three different SBS stages (Fig. 6a) consisting of rougher, cleaner, and scavenger SBS units.

3.4.1. Simulated SBS cascades

The three SBS cascades are designed with industry-based interconnections varying in complexity and process design philosophies (Fig. 6a). Each SBS cascade is composed of seven units with a total belt width of 11.0 m. For this purpose, industry-standard working widths (1.0 m, 1.4 m, 2.0 m, 2.8 m) were allocated realistically across the different sensor positions (proportional to the expected area flow distribution based on the input composition) as shown in Fig. 6a.

In SBS cascade A, two parallel rougher lines (R1-R6 in Fig. 6a), each handling 50% of the total throughput, sort the target materials (PP, HDPE, and PET) in the order of their input share. A scavenger (S7) at the end of the SBS cascade is used to recover target material and send them back to the cascade input.

For SBS cascades B and C, the entire throughput is initially sorted by a single rougher line (R1, R3, R5), resulting in a higher OD and lower SBS performance (cf. Section 3.1). A cleaner line (C2, C4, C6) is then employed to remove non-target materials from the rougher ejects. Similar to SBS cascade A, a scavenger (S7) is positioned at the end of the SBS cascade for recovery of the lost target material.

While in SBS cascade B, the cleaner ejects are directly transported to the scavenger unit at the cascade's end, cleaner ejects in SBS cascade C are directly transported to the next rougher unit. This gives SBS cascade C an advantage as it can correct false rejects from the first rougher (e.g., R1) with the first cleaner (e.g., C2), then immediately re-sort them in the second rougher (e.g., R3). In contrast, SBS cascade B requires the false rejects to be returned to the circuit via the scavenger (S7).

3.4.2. Influence of process design on sorting performance

When assessing the produced output streams in Fig. 6b, we observe a better performance of SBS cascade B (F_1-score: 96.5 a% [macro-average]) and C (F_1-score: 96.2 a%) compared to SBS cascade A (F_1-score: 93.0 a%). The higher SBS performance is caused both by higher yields (A: 94.0 a%, B: 97.0 a%, C: 97.1 a%) and product purities (A: 92.1 a%, B: 96.0 a%, C: 95.4 a%). As shown by Fig. 6c, the higher SBS performance results from the cleaner stages, which sort out impurities (cf. cleaner ejects in Fig. 6c) leading to higher purities that can then be additionally sorted into correct pre-concentrate fractions leading to higher yields (cf. scavenger ejects in Fig. 6c).

In addition, Fig. 6c shows the effects of different SBS connections between SBS cascade B and C: Since all scavenger ejects in SBS cascade B are directly transported to the scavenger unit, the scavenger eject area flow is larger in SBS cascade B, as in SBS cascade C parts of the cleaner ejects have already been recovered by previous rougher stages (R3 and R5 in Fig. 6a).

3.4.3. Estimated energy consumption

To compare the energy consumption of the three SBS cascades, we estimate the relative energy demand of each SBS cascade by the total ejected area divided by the input area flow, which correlates with the energy needed for pressurized air supply. As shown in Fig. 6d, the estimated relative energy consumption of SBS cascade A is lower compared to SBS cascade B and C, since additional cleaner stages are avoided and increase less with increasing throughput. Combined with the results from Section 3.4.2, a trade-off between high SBS performance (SBS cascades B and C) and low energy demand (SBS cascade A) can be observed. When comparing SBS cascades B and C, we observe that the estimated energy demand of SBS cascade C is about 5.7% lower compared to SBS cascade B. A likely explanation for this effect is that HDPE and PET particles ejected by the cleaner units C2 and C4 require an additional loop through the scavenger S7 in SBS cascade B, while they are directly fed to the HDPE (R3) and PET (R5) rougher in SBS cascade C.

3.4.4. Influence of changing input composition (extension of PET deposit return system)

Fig. 6e shows that the developed SBS cascade models can be utilized to estimate the influence of changes in the input composition on the SBS performance. When a reduced PET share in the input composition, for example, caused by an extension of the PET deposit return system in Germany, is simulated, it can be seen that different output fractions are affected to disparate extents. Across all SBS cascades, the sorting performance (F_1-score) of PET decreases by −1.0 a% to −1.2 a%, while the sorting performance of HDPE and PP increase by +1.2 a% to +2.9 a% and +0.7 a% to +2.1 a%, respectively. An explanation for this effect is the reduced input share of PET and increased input share of PP and HDPE, which increase and decreases the SBS performance, respectively, as demonstrated in Section 3.4.4.

3.4.5. Discussion on SBS cascade simulation

Our process model proves to be effective in simulating SBS cascades within an LWP sorting plant, enabling precise performance analysis of differing process design philosophies. Through comparative evaluation of SBS cascades A, B, and C, we identified that the combination of a rougher and cleaner line increases the overall sorting performance compared to two parallel rougher lines with lower ODs, but also leads to increased energy consumption.

The developed process model further excels in quantifying the impact of changing input compositions on SBS performance, which is

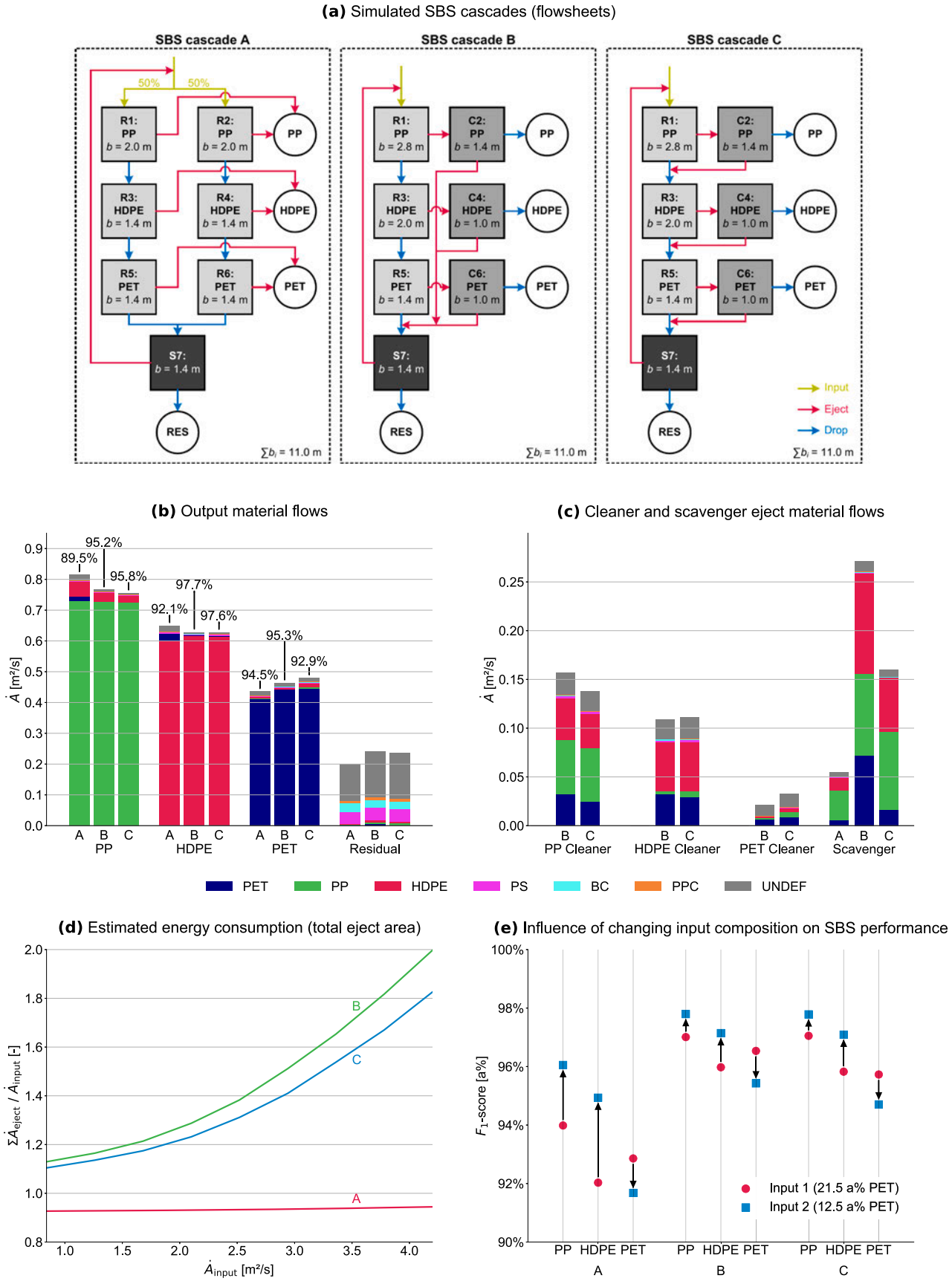

Fig. 6. Simulation of SBS cascades using the developed ANN process model. (a) simulated SBS cascades, (b) product material flows, (c) cleaner and scavenger ejects, (d) estimated energy consumption based on relative total ejection area, (e) effect of changing input material flow composition on SBS performance. R: rougher, C: cleaner, S: scavenger.

instrumental for proactive process adjustments. For instance, it helped anticipate the effect of an extended PET deposit return system in Germany on sorting performance. The developed cascade model presents an initial proof-of-concept for plant-scale process simulation. In future work, the developed model could be extended with process models of additional sorting and processing equipment and real-time data from a physical sorting plant to take additional steps towards a fully digital twin. Further, the digital process model could be extended with more detailed material flow and particle characteristics (e.g., moisture, packaging design, particle size distribution, packaging design) in future work.

4. Conclusions

Digital twins of sorting plants could significantly contribute to improve material recycling through enhanced plant performance. In the design phase, simulations inside the digital twin could help planning engineers develop an optimal process design for a given sorting task and optimize the dimensioning of individual process steps. In the operational phase, the digital twin could optimize the sorting plant parameterization based on data-driven process simulations and real-time data received from the physical sorting plant. A prerequisite for developing digital twins of sorting plants is the simulation of the sorting plants, which requires process models for each process.

With the present paper, we demonstrated that SBS units can be automatically evaluated at an industrial scale using NIR-based process monitoring. Based on the obtained process data, we showed that the sorting performance of SBS units is significantly influenced by both throughput (measured as OD) and input composition (measured as target share): For each additional 1% OD, the sorting performance of the investigated SBS unit decreased linearly by a -0.22 a% lower F_1-score. For each additional 1 wt% target share, the sorting performance of the investigated SBS unit increased linearly by $+0.19$ a% higher F_1-score. The observed sorting behavior can be explained by incorrect material discharges caused by particle entrainment due to (a) higher particle proximity at higher ODs and (b) increasing air nozzle activations ejected area share (= dependence on positive/negative sorting and input composition). The likelihood of incorrect discharges differs significantly between different material classes.

Further, we demonstrated that the sorting behavior of the SBS unit can accurately be described through material-specific TCs. Three different ML models (PR, RF, ANN) were used to predict TCs based on information on the input material flow (OD, target share, material share). ANNs achieved the highest prediction accuracy with an MAE of $\pm 3.0\%$. Based on the trained ANNs, a data-driven process model of the SBS plant was developed and the suitability of the model for optimizing sorting plants was demonstrated in two key applications.

In the first model application, it was shown that the sorting performance of the investigated SBS unit was not affected by throughput fluctuations despite claims and evidence of previous research. A likely mechanism for the missing influence of throughput fluctuations on the SBS performance is the linear decrease of SBS performance with increasing OD, as shown by the process models. Therefore, higher and lower SBS performance resulting from lower and higher ODs, respectively, even out and do not affect the SBS performance in the investigated OD range ($\leq$ 50% OD).

In the second model application, we successfully applied the developed process models to the simulation of three different SBS cascades containing seven different SBS units each. The obtained simulation results emphasize the influence of the process design as well as changing input compositions on the SBS performance. The simulation results are in line with previous research and indicate, e.g., a higher sorting performance but also increased energy demand of multi-stage sorting compared to single-stage sorting as well as changes in the material-specific sorting performance between -1.0 a% (PET) and $+2.9$ a% (PP) F_1-score, when a halving of the PET input share based on an extended PET deposit system in Germany is simulated.

In future work, our proposed sensor-based process assessment approach could be enhanced, e.g., by incorporating further pre-processing techniques to the false-color images (e.g., removal of HDPE caps on PET bottles) or by utilizing alternative sensor technologies that could enable a particle-specific tracking and process assessment (e.g., RFID-tags or digital watermarks for individual particles). Such a particle-based assessment could enable a more nuanced process modeling and allow, e.g., the investigation of different packaging designs on the SBS performance. Additionally, the scope could be extended to further material flow characteristics (e.g., different target materials, film share, particle size distribution, particle shape, material grammage/density) and machine parameters (e.g., SBS design, sorting algorithms) which could enable even more accurate SBS models. To manage the experimental effort, a design of experiment approach could be applied. In addition, our experiments should be further upscaled to plant-scale trials to investigate, e.g., the influence of a wider range of input compositions and impurities on the SBS behavior.

As our results of the missing influence of throughput fluctuations on SBS performance contradict the results of Curtis et al. (2021), additional sorting trials are recommended for clarification. Especially the comparison of different SBS machines, the investigation of SBS performance at high ODs ($>>$ 50%), and a systematic comparison of different throughput fluctuations may be of interest. Finally, to complete a digital twin, process models of other sorting and processing equipment, such as comminution units, screens, windsifters, eddy current separators, and magnetic separators, should be developed.

Ultimately, our work represents the first steps taken into a future, where the performance of sorting plants could be optimized by utilizing digital twins built upon sophisticated process models both in the planning and operational phases. These digital twins could serve as a central platform for value-chain-wide collaboration, ultimately resulting in secondary raw materials being recovered at higher quantities and qualities. While there is more work to be done, these first steps are already illuminating a promising path toward a more circular and sustainable future.

Funding

This work was funded by the German Federal Ministry of Education and Research (BMBF) within the program "Resource-efficient circular economy - plastics recycling technologies (KuRT)" under the project *ReVise* (grant no. 033R341) and the National Austrian Research Promotion Agency (FFG) within the program "Production of the Future" under the project *EsKorte* (grant no. 877341). The responsibility for the content of this publication lies with the authors.

CRediT authorship contribution statement

Nils Kroell: Conceptualization, Methodology, Software, Validation, Formal analysis, Investigation, Data curation, Writing – original draft, Writing – review & editing, Visualization, Supervision, Project administration, Funding acquisition. **Abtin Maghmoumi:** Methodology, Software, Data curation, Writing – review & editing, Visualization. **Tobias Dietl:** Methodology, Investigation, Data curation, Writing – review & editing. **Xiaozheng Chen:** Conceptualization, Methodology, Investigation, Writing – review & editing, Funding acquisition. **Bastian Küppers:** Conceptualization, Methodology, Writing – review & editing, Supervision, Funding acquisition. **Tabea Scherling:** Conceptualization, Writing – review & editing. **Alexander Feil:** Writing – review & editing, Funding acquisition. **Kathrin Greiff:** Writing – review & editing, Funding acquisition.

Declaration of Competing Interest

The authors declared no potential conflicts of interest concerning the

research, authorship, and/or publication of this article.

Data availability

The data that has been used is confidential.

Acknowledgments

We would like to thank Peter Bardenheuer for his support in the literature review.

Supplementary materials

Supplementary material associated with this article can be found, in the online version, at doi:10.1016/j.resconrec.2023.107257.

References

Arizmendi-Sánchez, J.A., Sharratt, P.N., 2008. Phenomena-based modularisation of chemical process models to approach intensive options. Chem. Eng. J. 135 (1–2), 83–94. https://doi.org/10.1016/j.cej.2007.02.017.

Bárkányi, Á., Egedy, A., Sarkady, A., Kurdi, R., Abonyi, J., 2022. Expert-based modular simulator for municipal waste processing technology design. Sustainability 14 (24), 16403. https://doi.org/10.3390/su142416403.

Bauer, A., Maier, G., Reith-Braun, M., Kruggel-Emden, H., Pfaff, F., Gruna, R., et al., 2023. Benchmarking a DEM-CFD model of an optical belt sorter by experimental comparison. Chem. Ing. Tech. 95 (1–2), 256–265. https://doi.org/10.1002/cite.202200124.

Breiman, L., 2001. Random forests. Mach. Learn. 45 (1), 5–32. https://doi.org/10.1023/A:1010933404324.

Brunner, P.H., Rechberger, H., 2016. Handbook of Material Flow Analysis. CRC Press.

Chen, X., Feil, A., 2019. Detection and classification of heterogeneous materials as well as small particles using NIR-spectroscopy by validation of algorithms. In: Beyerer, J, Puente León, F, Längle, T (Eds.), OCM 2019 - Optical Characterization of Materials Conference Proceedings. KIT Scientific Publishing, pp. 63–77.

Chen, X., Kroell, N., Althaus, M., Pretz, T., Pomberger, R., Greiff, K., 2023a. Enabling mechanical recycling of plastic bottles with shrink sleeves through near-infrared spectroscopy and machine learning algorithms. Res., Conserv. Recycl. 188, 106719 https://doi.org/10.1016/j.resconrec.2022.106719.

Chen, X., Kroell, N., Feil, A., Greiff, K., 2023b. Sensor-based sorting. In: Meskers, C., Worrell, E., Reuter, M.A. (Eds.), Handbook of Recycling: State-of-the-art for Practitioners, Analysts, and Scientists, pp. 145–159. https://doi.org/10.1016/B978-0-323-85514-3.00028-2.

Christiani, J., 2017. *Stand Der Technik und Herausforderungen für Einzelne Verpackungsmaterialien. Recycling und Recyclingfähigkeit von Verpackungen* (Berlin, 06. Dezember 2017).

Curtis, A., Küppers, B., Möllnitz, S., Khodier, K., Sarc, R., 2021. Real time material flow monitoring in mechanical waste processing and the relevance of fluctuations. Waste Manag. 120 (1), 687–697. https://doi.org/10.1016/j.wasman.2020.10.037.

Dehoust G., Christiani J. Analyse und Fortentwicklung der Verwertungsquoten für Wertstoffe: sammel- und Verwertungsquoten für Verpackungen und stoffgleiche Nichtverpackungen als Lenkungsinstrument zur Ressourcenschonung; 2012.

Denafas, G., Ruzgas, T., Martuzevičius, D., Shmarin, S., Hoffmann, M., Mykhaylenko, V., et al., 2014. Seasonal variation of municipal solid waste generation and composition in four East European cities. Res., Conserv. Recycl. 89, 22–30. https://doi.org/10.1016/j.resconrec.2014.06.001.

Devore, J.L., 2012. Probability and Statistics for Engineering and the Sciences, 8th ed. Brooks/Cole, Australia.

Eriksen, M.K., Christiansen, J.D., Daugaard, A.E., Astrup, T.F., 2019. Closing the loop for PET, PE and PP waste from households: influence of material properties and product design for plastic recycling. Waste Manag. 96, 75–85. https://doi.org/10.1016/j.wasman.2019.07.005.

European Commission, 2019. The European Green Deal. https://eur-lex.europa.eu/resource.html?uri=cellar:b828d165-1c22-11ea-8c1f-01aa75ed71a1.0002.02/DOC_1&format=PDF (accessed June 19, 2023).

European Commission, 2020. A New Circular Economy Action Plan: For a cleaner and More Competitive Europe (accessed June 19, 2023). https://eur-lex.europa.eu/legal-content/EN/TXT/?qid=1583933814386&uri=COM:2020:98:FIN.

European Parliament and Council, 2018. DIRECTIVE (EU) 2018/851 on Waste.

Eurostat, 2023. Circular Economy - Material Flows - Statistics Explained. https://ec.europa.eu/eurostat/statistics-explained/index.php?title=Circular_economy_-_material_flows.

EVK Kerschhaggl GmbH, 2023. EVK SQALAR: Software Tool for the Qualitative and Quantitative Analysis. https://www.evk.biz/en/products/analysis-software-tool/evk-sqalar/ (accessed April 21, 2023).

Fahrmeir, L., Kneib, T., Lang, S., Marx, B., 2013. Regression: Models, Methods and Applications. Springer, Berlin, Heidelberg.

Feil, A., Coskun, E., Bosling, M., Kaufeld, S., Pretz, T., 2019. Improvement of the recycling of plastics in lightweight packaging treatment plants by a process control concept. Waste Manag. Res. 37 (2), 120–126. https://doi.org/10.1177/0734242X19826372.

Feil, A., Kroell, N., Pretz, T., Greiff, K., 2021. Anforderungen an eine effiziente technologische behandlung von post-consumer verpackungsmaterialien in sortieranlagen. Müll und Abfall 21 (7), 362–370. https://doi.org/10.37307/j.1863-9763.2021.07.04.

Feil, A., Pretz, T., 2018. Ungenutzte potentiale in der abfallaufbereitung. Recy & DepoTech 2018: Recycling & Abfallverwertung, Abfallwirtschaft & Ressourcenmanagement, Deponietechnik & Altlasten, internationale Abfallwirtschaft & spezielle Recyclingthemen Vorträge-Konferenzband zur 14. Recy & DepoTech-Konferenz, 7.-9. November 2018. In: Pomberger, R, Adam, J, Aldrian, A. (Eds.), Leoben, Österreich: Leoben (Österreich). Leoben, Österreich: Abfallverwertungstechnik & Abfallwirtschaft Eigenverlag.

Feil, A., Pretz, T., 2020. Mechanical recycling of packaging waste. Plastic Waste and Recycling. Elsevier, pp. 283–319.

Feil, A., Pretz, T., Vitz, P., van Thoden Velzen, E.U., 2017. A methodical approach for the assessment of waste sorting plants. Waste Manag. Res. J. Int. Solid Wastes Public Cleans. Assoc., ISWA 35 (2), 147–154. https://doi.org/10.1177/0734242X16683270.

Fitzpatrick, R.S., Glass, H.J., 2015. Pascoe RD. CFD–DEM modelling of particle ejection by a sensor-based automated sorter. Miner. Eng. 79, 176–184. https://doi.org/10.1016/j.mineng.2015.06.009.

Friedrich, K., Koinig, G., Pomberger, R., Vollprecht, D., 2022. Qualitative analysis of post-consumer and post-industrial waste via near-infrared, visual and induction identification with experimental sensor-based sorting setup. MethodsX 9, 101686. https://doi.org/10.1016/j.mex.2022.101686.

Gesetz über das Inverkehrbringen, die Rücknahme und die hochwertige Verwertung von Verpackungen, 2023. VerpackG.

Gómez, G., Meneses, M., Ballinas, L., Castells, F., 2009. Seasonal characterization of municipal solid waste (MSW) in the city of Chihuahua, Mexico. Waste Manage. (Oxford) 29 (7), 2018–2024. https://doi.org/10.1016/j.wasman.2009.02.006.

Gundupalli, S.P., Hait, S., Thakur, A., 2017. A review on automated sorting of source-separated municipal solid waste for recycling. Waste Manag. 56–74. https://doi.org/10.1016/j.wasman.2016.09.015.

Hahladakis, J.N., Iacovidou, E., 2018. Closing the loop on plastic packaging materials: what is quality and how does it affect their circularity? Sci. Total Environ. 630, 1394–1400. https://doi.org/10.1016/j.scitotenv.2018.02.330.

Harris, C.R., Millman, K.J., van der Walt, S.J., Gommers, R., Virtanen, P., Cournapeau, D., et al., 2020. Array programming with NumPy. Nature 585 (7825), 357–362. https://doi.org/10.1038/s41586-020-2649-2.

Hunter, J.D., 2007. Matplotlib: a 2D graphics environment. Comput. Sci. Eng. 9 (3), 90–95. https://doi.org/10.1109/MCSE.2007.55.

IRP (2019). Global Resources Outlook 2019: Natural Resources for the Future We Want. Oberle, B., Bringezu, S., Hatfield-Dodds, S., Hellweg, S., Schandl, H., Clement, J., and Cabernard, L., Che, N., Chen, D., Droz-Georget , H., Ekins, P., Fischer-Kowalski, M., Flörke, M., Frank, S., Froemelt , A., Geschke, A., Haupt , M., Havlik, P., Hüfner, R., Lenzen, M., Lieber, M., Liu, B., Lu, Y., Lutter, S., Mehr , J., Miatto, A., Newth, D., Oberschelp , C., Obersteiner, M., Pfister, S., Piccoli, E., Schaldach, R., Schüngel, J., Sonderegger, T., Sudheshwar, A., Tanikawa, H., van der Voet, E., Walker, C., West, J., Wang, Z., Zhu, B. A Report of the International Resource Panel. United Nations Environment Programme. Nairobi, Kenya.

Jawad, J., Hawari, A.H., Javaid Zaidi, S., 2021. Artificial neural network modeling of wastewater treatment and desalination using membrane processes: a review. Chem. Eng. J. 419, 129540 https://doi.org/10.1016/j.cej.2021.129540.

Jovanović, I., Miljanović, I., Jovanović, T., 2015. Soft computing-based modeling of flotation processes – a review. Miner. Eng. 84, 34–63. https://doi.org/10.1016/j.mineng.2015.09.020.

Kleinhans, K., Hallemans, M., Huysveld, S., Thomassen, G., Ragaert, K., van Geem, K.M., et al., 2021. Development and application of a predictive modelling approach for household packaging waste flows in sorting facilities. Waste Manag. 120, 290–302. https://doi.org/10.1016/j.wasman.2020.11.056.

Knappe, F., Reinhardt, J., Kauertz, B., Oetjen-Dehne, R., Buschow, N., Ritthoff, M., et al., 2021. Technische Potenzialanalyse zur Steigerung des Kunststoffrecyclings und des Rezyklateinsatzes, p. 92. TEXTE.

Kroell, N., Chen, X., Greiff, K., Feil, A., 2022a. Optical sensors and machine learning algorithms in sensor-based material flow characterization for mechanical recycling processes: a systematic literature review. Waste Manag. 149, 259–290. https://doi.org/10.1016/j.wasman.2022.05.015.

Kroell, N., Chen, X., Küppers, B., Lorenzo, J., Maghmoumi, A., Schlaak, M., et al., 2023a. Near-infrared-based determination of mass-based material flow compositions in mechanical recycling of post-consumer plastics: technical feasibility enables novel applications. Resour. Conserv. Recycl. 191, 106873 https://doi.org/10.1016/j.resconrec.2023.106873.

Kroell, N., Chen, X., Küppers, B., Schlögl, S., Feil, A., Greiff, K., 2023b. Near-infrared-based quality control of plastic pre-concentrates in lightweight-packaging waste sorting plants. Resour. Conserv. Recycl. https://doi.org/10.1016/j.resconrec.2023.107256.

Kroell, N., Chen, X., Maghmoumi, A., Koenig, M., Feil, A., Greiff, K., 2021. Sensor-based particle mass prediction of lightweight packaging waste using machine learning algorithms. Waste Manag. 136, 253–265. https://doi.org/10.1016/j.wasman.2021.10.017.

Kroell, N., Chen, X., Maghmoumi, A., Lorenzo, J., Schlaak, M., Nordmann, C., et al., 2023c. NIR-MFCO dataset: near-infrared-based false-color images of post-consumer plastics at different material flow compositions and material flow presentations. Data Brief 48, 109054. https://doi.org/10.1016/j.dib.2023.109054.

Kroell, N., Dietl, T., Maghmoumi, A., Chen, X., Küppers, B., Feil, A., et al., 2022b. Assessment of sensor-based sorting performance for lightweight packaging waste through sensor-based material flow monitoring: concept and preliminary results [in print]. In: Greiff K., Wotruba H., Feil A., Kroell N., Chen X. Gürsel, Devrim, Merz, Vincent. 9th Sensor-Based Sorting & Control 2022, 13.04.2022 - 14.04.2022: Aachen.

Küppers, B., Chen, X., Seidler, I., Friedrich, K., Raulf, K., Pretz, T., et al., 2019a. Influences and consequences of mechanical delabeling on PET recycling. Detritus 6 (0), 39–46. https://doi.org/10.31025/2611-4135/2019.13816.

Küppers, B., Schloegl, S., Oreski, G., Pomberger, R., Vollprecht, D., 2019b. Influence of surface roughness and surface moisture of plastics on sensor-based sorting in the near infrared range. Waste Manag.ement & research the journal of the International Solid Wastes and Public Cleansing Association. ISWA 37 (8), 843–850. https://doi.org/10.1177/0734242X19855433.

Küppers, B., Schlögl, S., Friedrich, K., Lederle, L., Pichler, C., Freil, J., et al., 2020a. Influence of material alterations and machine impairment on throughput related sensor-based sorting performance. Waste Manag. Res. https://doi.org/10.1177/0734242X20936745.

Küppers, B., Schlögl, S., Kroell, N., Radkohl, V., Greiff, K., Wotruba, H., Feil, A., Kroell, N., Chen, X., Gürsel, D., Merz, V., 2022. Relevance and challenges of plant control in the pre-processing stage for enhanced sorting performance. 9th Sensor-Based Sorting & Control 2022, 13.04.2022 - 14.04.2022Aachen.

Küppers, B., Seidler, I., Koinig, G.R., Pomberger, R., Vollprecht, D., 2020b. Influence of throughput rate and input composition on sensor-based sorting efficiency. Detritus (9), 59–67. https://doi.org/10.31025/2611-4135/2020.13906.

Liu, H., Dong, G., 2018. Feature Engineering for Machine Learning and Data Analytics. CRC Press.

McCoy, J.T., Auret, L., 2019. Machine learning applications in minerals processing: a review. Miner. Eng. 132, 95–109. https://doi.org/10.1016/j.mineng.2018.12.004.

McKinney, W., 2010. Data structures for statistical computing in python. In: Stéfan van der Walt, Jarrod Millman. Proceedings of the 9th Python in Science Conference.

Neo, E.R.K., Yeo, Z., Low, J.S.C., Goodship, V., Debattista, K., 2022. A review on chemometric techniques with infrared, Raman and laser-induced breakdown spectroscopy for sorting plastic waste in the recycling industry. Resour. Conserv. Recycl. 180, 106217 https://doi.org/10.1016/j.resconrec.2022.106217.

Pascoe, R.D., Udoudo, O.B., Glass, H.J., 2010. Efficiency of automated sorter performance based on particle proximity information. Miner. Eng. 23 (10), 806–812. https://doi.org/10.1016/j.mineng.2010.05.021.

Pedregosa, F., Varoquaux, G., Gramfort, A., Michel, V., Thirion, B., Grisel, O., et al., 2011. Scikit-learn: machine learning in python. J. Open Source Software 12, 2825–2830.

Pieper, C., Maier, G., Pfaff, F., Kruggel-Emden, H., Wirtz, S., Gruna, R., et al., 2016. Numerical modeling of an automated optical belt sorter using the discrete element method. Powder Technol. 301, 805–814. https://doi.org/10.1016/j.powtec.2016.07.018.

Pretz, T., Raulf, K., Quicker, P., 2020. Waste, 4. Recycling. Ullmann's Encyclopedia of Industrial Chemistry. Wiley-VCH Verlag GmbH & Co. KGaA, Weinheim, Germany, pp. 1–39.

Ragaert, K., Delva, L., van Geem, K., 2017. Mechanical and chemical recycling of solid plastic waste. Waste Manag. 69, 24–58. https://doi.org/10.1016/j.wasman.2017.07.044.

Roosen, M., Mys, N., Kusenberg, M., Billen, P., Dumoulin, A., Dewulf, J., et al., 2020. Detailed analysis of the composition of selected plastic packaging waste products and its implications for mechanical and thermochemical recycling. Environ. Sci. Technol. 54 (20), 13282–13293. https://doi.org/10.1021/acs.est.0c03371A.

Sarc, R., Curtis, A., Kandlbauer, L., Khodier, K., Lorber, K.E., Pomberger, R., 2019. Digitalisation and intelligent robotics in value chain of circular economy oriented waste management–a review. Waste Manag. 95, 476–492.

Schlögl, S., Kamleitner, J., Kroell, N., Chen, X., Aldrian, A., 2023. Developing a Prediction Model in a Lightweight Packaging Waste Sorting Plant using Sensor-based Sorting Data Combined with Data of External Near-Infrared and LiDAR Sensors [Under Review]. Waste Manag.ement & research.

Schwarz, A.E., Ligthart, T.N., D, Godoi Bizarro, de, Wild P, Vreugdenhil, B., van Harmelen, T, 2021. Plastic recycling in a circular economy; determining environmental performance through an LCA matrix model approach. Waste Manag. 121, 331–342. https://doi.org/10.1016/j.wasman.2020.12.020.

Schyns, Z.O.G., Shaver, M.P., 2021. Mechanical recycling of packaging plastics: a review. Macromol. Rapid Commun. 42 (3), e2000415 https://doi.org/10.1002/marc.202000415.

Singh, J., Laurenti, R., Sinha, R., Frostell, B., 2014. Progress and challenges to the global waste management system. Waste Manag. Res. J. Int. Solid Wastes Public Cleans. Assoc., ISWA 32 (9), 800–812. https://doi.org/10.1177/0734242X14537868.

Tanguay-Rioux, F., Provost-Savard, A., Spreutels, L., Héroux, M., Legros, R., 2022. A method for assessing the performance of sorting unit operations in a material recovery facility based on waste characterizations. Can. J. Chem. Eng. 100 (9), 2572–2586. https://doi.org/10.1002/cjce.24466.

Tao, F., Cheng, J., Qi, Q., Zhang, M., Zhang, H., Sui, F., 2018. Digital twin-driven product design, manufacturing and service with big data. Int. J. Adv. Manuf. Technol. 94 (9–12), 3563–3576. https://doi.org/10.1007/S00170-017-0233-1.

The pandas development team, 2020. Pandas-dev/pandas: Pandas: Zenodo.

Umweltbundesamt, 2012. Analyse und Fortentwicklung der Verwertungsquoten für Wertstoffe (accessed June 19, 2023). https://www.umweltbundesamt.de/sites/default/files/medien/461/publikationen/4342.pdf.

van Thoden Velzen, E.U., Brouwer, M.T., Feil, A., 2019. Collection behaviour of lightweight packaging waste by individual households and implications for the analysis of collection schemes. Waste Manag. 89, 284–293. https://doi.org/10.1016/j.wasman.2019.04.021.

Virtanen, P., Gommers, R., Oliphant, T.E., Haberland, M., Reddy, T., Cournapeau, D., et al., 2020. SciPy 1.0: fundamental algorithms for scientific computing in python. Nat. Methods 17, 261–272. https://doi.org/10.1038/s41592-019-0686-2.

Wang, S.-C., 2003. Artificial Neural Network. editor. In: Wang, S-C (Ed.), Interdisciplinary Computing in Java Programming. Springer, Boston, MA, pp. 81–100.

Waskom, M.L., 2021. seaborn: statistical data visualization. J. Open Source Software 6 (60), 3021. https://doi.org/10.21105/joss.03021.

Willmott, C.J., Matsuura, K., 2005. Advantages of the mean absolute error (MAE) over the root mean square error (RMSE) in assessing average model performance. Climate Res. 30, 79–82. https://doi.org/10.3354/cr030079.

Zhang, C., Hu, M., van der Meide, M., Di Maio, F., Yang, X., Gao, X., et al., 2023. Life cycle assessment of material footprint in recycling: a case of concrete recycling. Waste Manag. 155, 311–319. https://doi.org/10.1016/j.wasman.2022.10.035.

5 Synthesis

Chapter 5 first summarizes the main findings of previous chapters (Section 5.1). Based on the joint findings, the overarching RQs and stated hypothesis are answered (Section 5.2), before use-cases are developed on how these findings can contribute to a CE and implications for different stakeholders are derived (Section 5.3), and suggestions on future work are given (Section 5.4).

5.1 Main findings and contributions

5.1.1 RQ I: State of research

In Chapter 2, a SLR of 267 investigations from 198 publications on SBMC based on optical sensors in mechanical recycling was conducted. The SLR revealed that applications of optical sensors and ML algorithms have received increased attention in recent years. However, it showed that SBMC research has so far not been recognized as a homogeneous research field (cf. Fig. 9 in Publication A [Section 2.1]). Therefore, a unified SBMC terminology has been developed.

5.1.1.1 SBMC terminology

SBMC can be defined as digitally capturing material flows with sensors and applying algorithms to extract MFCs from the acquired sensor data. The data analysis can be hierarchically structured between pixel, particle, material flow, and process levels (Figure 5.1).

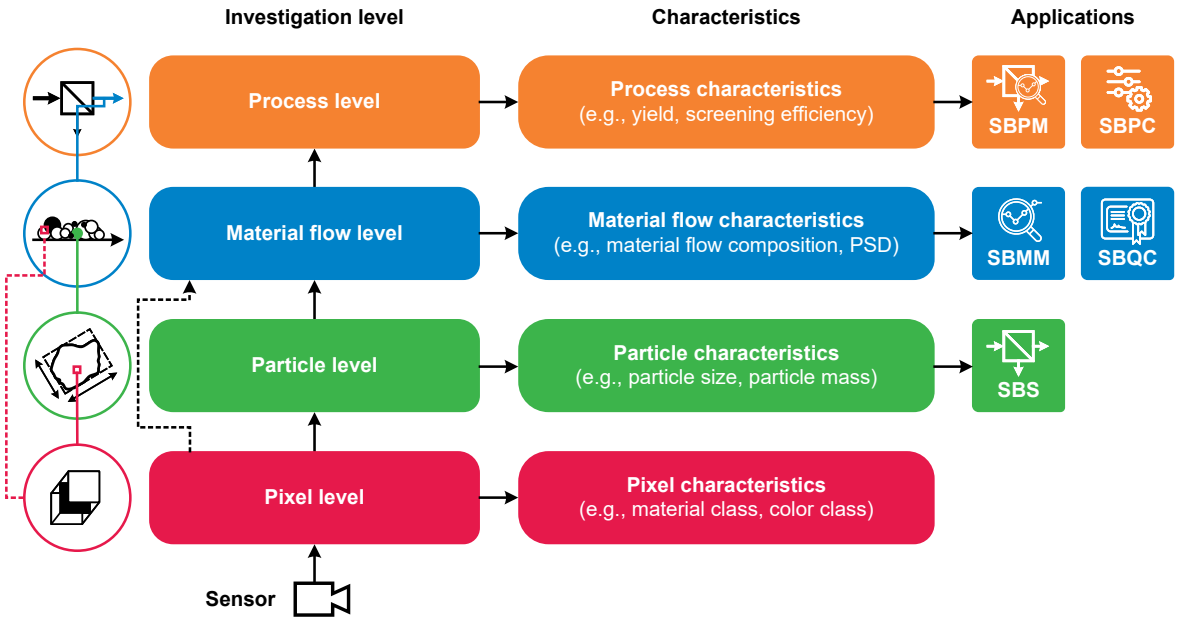

Figure 5.1. SBMC framework (Kroell, Chen, Greiff, et al., 2022); PSD: particle size distribution.

Depending on the investigation level and goal, six different SBMC applications can be identified: sensor-based sorting (SBS), sensor-based material flow monitoring (SBMM), sensor-based quality control (SBQC), sensor-based process monitoring (SBPM), and sensor-based process control (SBPC) (cf. Table 9 in Publication A [Section 2.1]).

5.1.1.2 Overview of SBMC research landscape

Based on the developed SBMC terminology, the SBMC research field was analyzed regarding six aspects:

(1) Material flows. Among the 17 material flows investigated by the reviewed publications, plastics (32.6%), waste from electrical and electronic equipment (11.2%), and construction and demolition waste (10.1%) have been studied most frequently. While 94.0% of all investigations collected their own data, only 6.0% of the SBMC research was conducted on public datasets. A correlation analysis of the 594 unique investigated material classes revealed two frequently reoccurring research topics: (i) polymer classification (especially with NIR spectroscopy) and (ii) classification of more general waste classes such as glass, paper, cardboard, plastic, metal (especially with visible [VIS]-RGB sensors and deep learning).

(2) Characteristics & investigation levels. SBMC researchers have so far focused almost exclusively on intensive MFCs. Only two publications (Curtis & Sarc, 2021; Feil et al., 2019) were conducted on extensive MFCs (volume flows). Among intensive MFCs, investigations focused mostly on material classification (78.4%), however, a shift from material and color classification to additional characteristics in recent years has been observed. Regarding investigation levels, SBMC research has so far focused mostly at the pixel (46.1%) and particle (49.8%) level. Only 4.1% of all reviewed investigations focused on the material flow level, and no investigations were found at the process level.

(3) Sensors. Among the ten different optical sensor types which have been applied in SBMC research so far, the VIS-NIR range has been addressed most frequently (83.0%) and especially VIS-RGB sensors have been increasingly investigated in recent years. Three broader SBMC tasks could be identified: (i) material identification, (ii) segmentation and measurement, and (iii) prediction of material properties.

(4) Algorithms & investigation scales. 76.4% of all investigations studied ML algorithms to extract characteristics from the acquired sensor data. Among the 36 different ML algorithms investigated, principal component analysis, convolutional neural networks (CNNs), partial least squares, k-nearest neighbors, and support vector machine were applied most often. Especially CNNs have received increasing attention in recent years. An innovative comparison of different ML algorithms based on Elo-ratings adopted from, e.g., chess games revealed

that especially CNN and random forest models are well suited for most SBMC applications due to their above-average prediction performance.

(5) Applications. Most SBMC research has focused on SBS and prediction applications, however, since 2008, SBMC research has expanded and shifted towards, e.g., SBMM, SBQC, SBPM, and SBPC. Besides a few publications on novel concepts (1.5%), the reviewed research has been mostly conducted at laboratory scale (90.6%). Little research has so far been conducted on a technical (6.7%) or plant scale (1.1%).

(6) Collaboration. A comprehensive network analysis revealed that SBMC frequently cite each others with 98.2% of all publications belonging to a large citation sub-graph. However, collaboration as co-authorships have been mostly limited to smaller researchers groups. The two largest research communities could be traced back to (i) a collaboration between RWTH Aachen University (Germany) and Montanuniversity Leoben (Austria) with $n = 33$ authors and (ii) the Sapienza University of Rome (Italy) with $n = 28$ authors. (cf. Fig. 9 in Publication A [Section 2.1]).

5.1.1.3 Future research potentials

Based on the overview of the SBMC research landscape, Publication A revealed ten future research potentials (cf. Section 5 and Fig. 10 in Publication A) to advance the SBMC research field in general. Of these ten future research potentials, five research potentials (Table 5.1) mark essential research gaps that needed to be specifically addressed by Publications B-G to prove the overarching hypothesis of this dissertation (cf. Section 1.4).

Table 5.1. Addressing of research potentials identified in Publication A through publications B-G in this dissertation; *[i]* research potential *i* according to Publication A (Section 2.1).

	Publication					
Research potential	**B**	**C**	**D**	**E**	**F**	**G**
Development & demonstration at material flow level *[6]*	✓	✓	✓	✓	✓	-
Open-access datasets & deep learning methods *[5]*	-	-	-	✓	-	-
Upscaling to plant scale *[9]*	-	-	-	-	✓	✓
Development of new business models around SBMC *[10]*	-	-	-	-	✓	✓
Development & demonstration at process level *[7]*	-	-	-	-	-	✓

5.1.2 RQ II: Characterization methods

A particular challenge and research gap in SBMC identified in Section 2.1 is the transformation of area- or volume-based sensor measurements into mass-based MFCs. This dissertation

addressed this challenge both on a particle (Section 5.1.2.1) and material flow (Section 5.1.2.2) level.

5.1.2.1 Particle level

At the particle level, the sensor-based prediction of individual particle masses was investigated. First, the *imea* package (Publication B [Section 3.1]) was developed, which allows the extraction of 53 different 2D and 13 different 3D particle descriptors with a single line function call. Based on the extracted particle measurements and measured particle masses of 3,830 LWP particles recorded with an innovative sensor-rig design in Publication C (Section 3.2), the following insights could be generated:

- Particle masses of LWP differ significantly between different material classes. The dominant factor causing these variations are not material-specific densities, but the packaging design, which differs between different applied materials.
- While particle masses generally increase with increasing particle size, material-specific grammage and 3DLT densities generally (except for the material class paper, paperboard, and cardboard) decrease with increasing particle sizes due to a larger share of hollow spaces. Both grammages and 3DLT densities are significantly influenced by post-consumer effects (e.g., folding of beverage cartons).
- The prediction of particle masses by grammages ($R^2 = 53.3\% \pm 22.4\%$) achieves more accurate predictions compared to mean particle masses ($R^2 = 42.2\% \pm 12.1\%$), since the influence of particle size is taken into account. However, the accuracy of both approaches is compromised by the strong heterogeneity of the material flow and post-consumer effects.
- Among the six investigated ML models, tree-based ML algorithms generally outperformed other ML models due to the selective suppression of irrelevant particle features. The most accurate particle mass prediction was using a random forest model ($R^2 = 76.3\% \pm 9.1\%$).

5.1.2.2 Material flow level

At the material flow level, the direct prediction of mass-based material flow compositions (MFCOs) from pixel-based classified NIR false-color images of binary plastic flake and post-consumer plastic packaging mixtures was investigated in Publication D and E (Sections 3.3 and 3.4). The results showed that the prediction of the MFCO is influenced by four main factors:

- **Classification model:** The design of the (NIR) classification model has a substantial impact on the predicted MFCO. The two main influencing factors are (i) the foreground/background definition, which in particular affects the detection of (partially) transparent particles, and (ii) the handling of mixed NIR spectra, such as in sleeved or labeled plastic packaging.

- **Surface-area-to-volume ratio:** In addition to the influence of different grammages and packaging design known from Section 5.1.2.1, different surface-area-to-volume ratios resulting, e.g., from material-specific comminution behavior, can also significantly influence MFCO prediction when area-based sensor data is used for volume- or mass-based MFCOs predictions.

- **Counting basis:** In manual analysis, objects are article-based sorted and one article is counted as 100% pure if the main material is the desired material. In pixel-based (NIR) characterization, materials in one object are classified to their own class. For instance, it was determined that pure polyethylene terephthalate (PET) bottle (T2a) and beverage carton (T2b) fractions from LWP contain approx. 5.4 a% and 2.1 a% high-density polyethylene (HDPE), respectively, e.g., due to HDPE bottle caps.

- **Particle overlap:** Regarding the material flow presentation, it is important to differentiate between non-overlapping- (singled and monolayer) and overlapping (different bulk heights) material flow presentations. Overlapping material flow presentations can result in (i) a higher share of detected transparent materials (better material detection in front of other materials compared to black conveyor belts) and (ii) segregation effects (e.g., accumulation of larger particles on the material flow surface due to the brazil nut effect).

The identified effects can be corrected by adequate data processing techniques, which have two complementary goals. First, the aggregation of sufficiently high material areas into chunks effectively reduces *random errors* (e.g., due to different particle orientations). Second, systematic errors such as difference between pixel- and article-based counting basis and segregation effects can be corrected through, e.g., regression models. In order to evaluate the effect of different corrective actions on accuracy of statements at material flow level in an application-oriented manner, the MU_{95} metric was developed. The MU_{95} metric compares the absolute prediction errors between true (X_{true}) and measured (X_{measured}) material flow characteristics and forms the 95th percentile (P_{95}).

$$\begin{aligned} MU_{95} &= P_{95}\left(|X_{\text{measured}} - X_{\text{true}}|\right) \\ \text{with } X &= \{x_1, \ldots, x_n\} \end{aligned} \tag{5.1}$$

By combining all findings, binary plastic flake and LWP mixtures could be predicted with a MU_{95} of 1.2 vol% ($R^2 = 99.9\%$) and 2.4 wt% ($R^2 = 99.4\%$), respectively, across the investigated material flow presentations (singled, monolayer, bulk heights H1 and H2). The underlying *NIR-MFCO dataset* was published open-access in the *Data in Brief* journal to further accelerate future SBMC research (Publication E [Section 3.4]).

5.1.2.3 Comparision between particle- and material-level approach

As shown in Figure 5.2a, both the particle-based approach from Section 5.1.2.1 and the material-flow-level approach from Section 5.1.2.2 can be used to transform area- or volume-based sensor-data into mass-based material flow compositions.

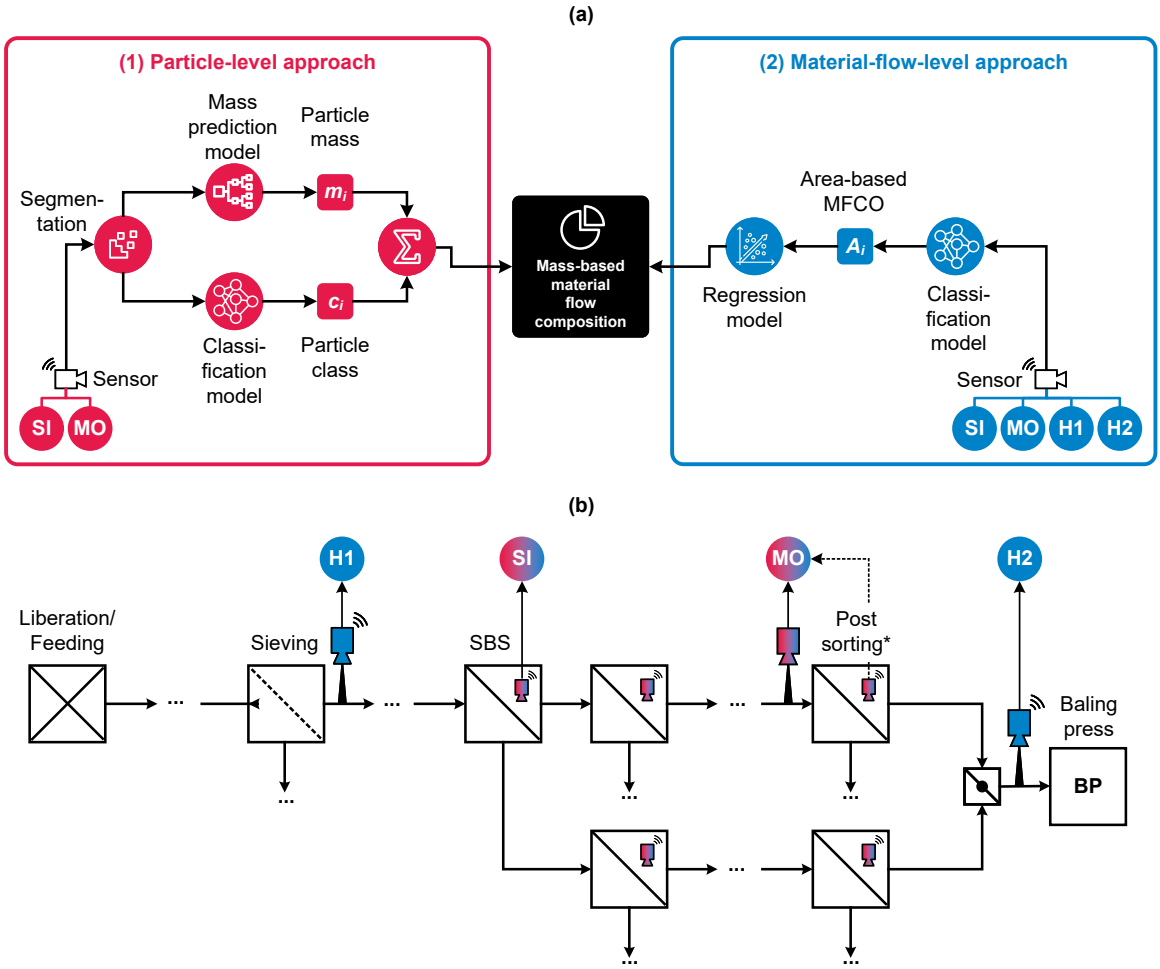

Figure 5.2. Comparison between particle- and material-flow-based approaches for sensor-based determinations of material flow compositions (MFCOs); **(a)** schematic flow sheets, **(b)** different material flow presentation in a simplified sorting plant; SI: singled, MO: monolayer, H1: bulk height H1, H2: bulk height H2 (H2 > H1).

Since the particle-based approach requires information on individual particles, from the experiences in this dissertation, it can be most likely only be applied to singled or monolayered material flow presentation (cf. Figure 5.2b). First, the sensor data needs to be segmented into individual particles which is relatively straightforward at a singled material flow presentation (singled particles against black conveyor belt), but it can become challenging at a monolayer material flow presentation due to particle overlaps, where deep-learning-based instance segmentation models could be applied. Then the segmented particles would be sent to a mass-prediction

model to prediction the individual particle masses m_i and a classification model to predict the particle class c_i. By summing up all predicted particle masses of each predicted particle class, the overall predicted mass-based material flow composition can then be obtained.

In the material-flow-level approach, the material flow would be firstly pixel-based classified, and the detected material areas A_i would then be sent to a regression model to predict mass-based material flow compositions from the given area-based material flow composition as demonstrated in Publication D (Section 3.3). As the material-flow-level approach requires no particle segmentation, it can thus also be applied at overlapping material flow presentations (H1 and H2 in Figure 5.2).

In practical implementation, the achievable accuracy of both methods (cf. Equation (5.1)) and the required amount of training data are of great importance. A direct comparison of these methods in further research (Section 5.4) would be particularly interesting, especially considering the different time needed to generate particle- and material flow-based training datasets.

5.1.3 RQ III: Novel SBMC applications

Based on the developed characterization methods, the technical feasibility of two novel SBMC applications was demonstrated at an industrial scale.

5.1.3.1 Sensor-based quality control

The first SBMC application addressed the NIR-based quality control of plastic pre-concentrates (Publication F [Section 4.1]). In LWP sorting plants, the quality of plastic pre-concentrates is determined by their purity. Since the term purity is interpreted differently by different stakeholders along the plastic recycling value chain, three different purity definitions have been proposed: article-based, material-based, and chemical purity (cf. Table 1 in Publication F [Section 4.1]). In a first test series, an inline NIR-sensor was used to monitor a PET tray product fraction on the manual sorting belt (monolayered material flow presentation) at the end of the sorting process, and ML predictions derived from the NIR data were compared with manual quality control (MQC) results.

Since the NIR sensor classifies the material flow pixel-wise, the NIR monitoring data represents an area- and material-based purity definition, while pre-concentrate qualities in LWP sorting plants are assessed mass- and article-based. Therefore, ML regression models have been used to predict article-based impurity mass flows from pixel-based NIR data.

Based on a total of 1,562 kg manually sorted and NIR-based analyzed PET tray product, the accuracy of MQC and SBQC was directly compared. When applying state-of-the-art MQC procedures with the sample masses defined in technical norms and guidelines, MU_{95}'s between 6.7 wt% (0.9 kg sample size [European Committee for Standardization, 2006]) and 0.8 wt% (123 kg sample size [2005]) were obtained. With the developed SBQC method, however, no sampling occurs

as the entire material flow can be monitored, and an MU_{95} of 0.31 wt% was achieved. It was estimated that more than 350 kg of a 600 kg PET tray bale must have been analyzed by MQC to become as accurate as the proposed SBQC method (cf. Fig. 3 in Publication F [Section 4.1]).

The developed SBQC method could be successfully applied to determine significant differences in the monitored PET tray product fractions due to different input materials sorted by the investigated LWP sorting plant. To reduce investment costs of the envisioned SBQC system, the technical feasibility of monitoring multiple pre-concentrates with a single NIR sensor at the bale press feeding conveyor belt was additionally investigated. While a good correlation between NIR measurements at the manual sorting belt (monolayered material flow presentation) and bale press feeding conveyor belt (multilayered material flow presentation) with a Pearson correlation of 0.915 was shown, systematic differences known from Section 5.1.2 were validated: Especially due to changes in NIR classification behaviour (transparent materials) and segregation effects, measured MFCOs between monolayered and multilayered material flows differed significantly.

5.1.3.2 Data-driven process models

The second SBMC application addressed the development of data-driven process models based on NIR-based process monitoring data (Publication G [Section 4.2]). Process models are an essential building block for the development of digital sorting plants twins, which could significantly enhance optimal design and adaptive parameterization of sorting plants. An industrial-scale SBS unit was automatically assessed using NIR-based process monitoring. The analysis of 2,000 minutes (33.3 h) systematically varied sorting trials showed that the SBS performance is significantly influenced by the throughput (measured as occupation density) and input composition (measured as target material share) but not by the investigated throughput fluctuations.

On the example of NIR-based SBS units for separating PET bottles from a LWP mixture, it was shown that the sorting behavior of SBS units can accurately be described using material-specific transfer coefficients (TCs). Using artificial neural network, material-specific TCs could be predicted with an mean absolute error (MAE) of 3.0%, which enables forming a sophisticated digital process model of the industrial-scale SBS unit. The developed process model was then successfully applied to simulate different SBS cascade designs, highlighting the influence of process design and changing input compositions on the sorting performance.

5.2 Answers to overarching research questions and hypothesis

Based on the findings from Section 5.1, the overarching RQs and the dissertation hypothesis from Section 1.4 can be answered as follows.

RQ I: Which existing research findings can be used, and which research gaps have to be filled to enable an inline SBMC of post-consumer waste streams?

Publication A revealed that especially classification methods at the pixel- and particle level from SBS are well-developed and can be applied to other SBMC applications. For example, NIR-based and pixel-based classification of different standard plastics can be achieved with $\geq 99\%$ accuracy and thus builds a strong basis for the development of, e.g., NIR-based characterization methods at the material flow and process level. From the ten identified future research potentials (cf. Section 5 and Fig. 10 in Publication A [Section 2.1]) to advance the SBMC research field in general, five critical research potentials have been identified to prove the stated hypothesis in Section 1.4 on the case study on LWP (cf. Table 5.1). These critical research potentials include the development and demonstration of characterizations methods at the material flow and process level, which has been insufficiently addressed so far, the upscaling to plant scale investigations, the accelerated development of SBMC methods through open-access datasets, and the development of new business models based on novel SBMC applications.

RQ II: How can the open research gaps from RQ I be closed and thus the sensor-based inline characterization of post-consumer material flows regarding their mass-based material flow compositions be enabled?

The sensor-based inline determination of mass-based MFCOs can be achieved through a particle-level approach and a material-flow-level approach. In the particle-level approach, the material class c_i and particle mass m_i of each particle is predicted from the sensor-data using, e.g., ML models. The mass-based MFCO is then determined by summing up the particle masses m_i in each material class c_i. Due to the need for a particle segmentation, the particle-level approach is only suitable for singled monolayered material flow presentations. The material-flow-level approach, however, can be applied across all material flow presentations. It comprises three stages: (i) the material flow surface is pixel-based classified, (ii) the resulting classifications (false-color data) are aggregated over defined material areas (chunks), and (iii) a regression model is used to transform the area-based composition of the detected material flow surface into a mass-based MFCO. Using data aggregation, random errors due to, e.g., particle artifacts are minimized. Using regression models, systematic errors caused, e.g., by different grammages or surface-area-to-volume ratios, different counting basis (material-based vs. article-based), and segregation effects at particle overlap are minimized. As demonstrated in Publication D, by applying these developed characterization methods, mass–based MFCOs of binary plastic flake and LWP mixtures can be determined within high accuracy (MU_{95} of 1.2 vol% and 2.4 wt%, respectively).

RQ III: Can the developed characterization methods from RQ II be translated into novel, industrial-scale SBMC applications to enhance CE?

Through two case studies, it was shown that the developed characterization methods can be translated into novel, industrial-scale SBMC applications to enhance CE. First, a SBQC of plastic pre-concentrates from LWP sorting plant was demonstrated in a state-of-the-art LWP sorting plant. Here, the material-flow-level approach from RQ II was used to predict bale-based purity of a PET tray pre-concentrate using inline-NIR-sensors. By verifying the model predictions with

manual sorting, it was demonstrated that the bale-based pre-concentrate purity can be determined within 0.31 wt% MU_{95} which surpasses the accuracy of state-of-the-art, sample-based manual quality control procedures (6.7 wt% to 0.8 wt% MU_{95}) with sample sizes defined in technical norms and guidelines. The high potential of the developed SBQC application was shown through that more than 350 kg of a 600 kg PET tray bale must have been analyzed by manual quality control procedures to become as accurate as the developed SBQC method.

Second, the demonstrated technical feasibility of monitoring LWP material flows with high accuracy using inline-NIR sensors from RQ II was used to develop a NIR-based process monitoring method. Based on the derived process monitoring data, ML models were trained to create a data-driven process model of an industrial-scale SBS unit. On the example of sorting out PET bottles from LWP mixture, it was shown that an artificial neural network could predict the sorting behavior of the investigated SBS-unit (measured by material-specific transfer coefficients) within 3.0% MAE. The developed process model was successfully used to explain systematic effects from different throughputs, input compositions and material flow fluctuations on the investigated SBS unit, and a SBS-cascade containing seven simulated SBS units was simulated to successfully illustrate the influences of different process designs and input material flows on the sorting behaviour of the SBS cascade.

Hypothesis: In addition to state-of-the-art sensor-based sorting, it is technical feasible to use sensor technology for the inline characterization of post-consumer material flows with industrial-relevant accuracies and at industrial scales. Based on the extracted material flow characteristics, novel SBMC applications can make the value-chain-wide material circulation more transparent and efficient.

By positively answering RQ I-III, this dissertation successfully demonstrated, on the example of LWP waste, that post-consumer material flows can be sensor-based characterized with industrial-relevant accuracies (MU_{95} of 1.2 vol% and 2.4 wt% for plastic flakes and LWP waste, respectively) and at industrial relevant scales (technical lab to plant scale). Based on two novel SBMC methods, the SBQC of plastic pre-concentrates in sorting plants and data-driven process models of industrial-scale SBS-units, it was shown how these applications make the value-chain-wide material circulation more transparent (automated and real-time SBQC of plastic pre-concentrated) and efficient (optimized process design and operation through data-driven process models). The hypothesis was thus successfully verified using the case study of LWP.

5.3 Implications

In the future, the demonstrated novel SBMC applications could be further applied in several use-cases. By implementing the developed SBMC applications across these use-cases, substantial positive implications on further developing the CE are to be expected (Figure 5.3).

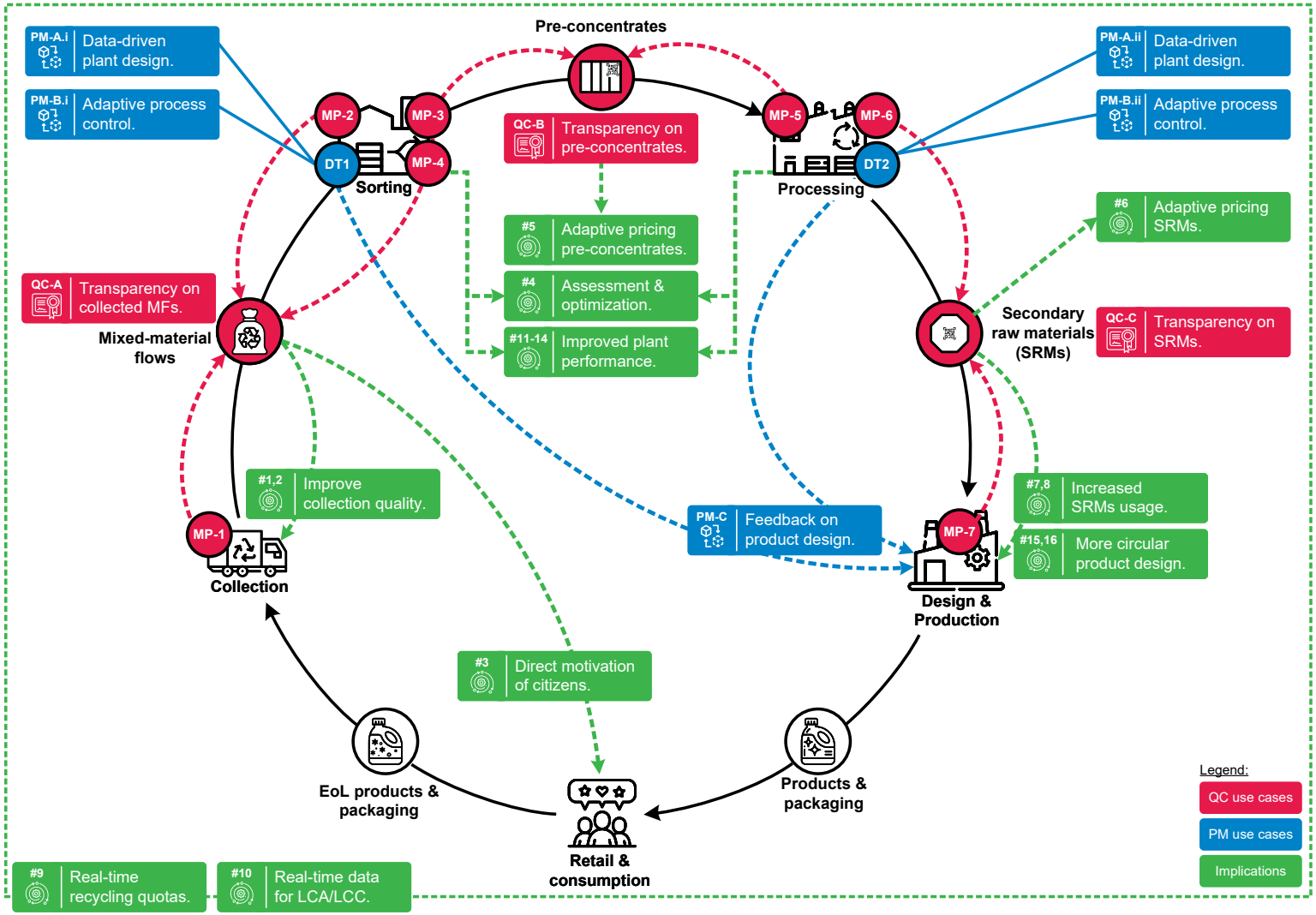

Figure 5.3. Overview on potential use-cases and implications of methods and applications developed in this dissertation; MF: material flow, SRM: secondary raw material, QC-*i*: use-cases based on SBQC, PM-*i*: use-cased based on SBPM, MP-*i*: measuring point for QC, #*i*: implications.

5.3.1 Sensor-based quality control

The first group of use-cases emerges from the demonstrated technical feasibility of sensor-based inline monitoring of material flow compositions, as demonstrated in Publication F (Section 4.1). As shown in Figure 5.3, transparency regarding up-to-date material flow compositions is especially relevant at the interface material flows between individual stages of the value chain (i.e., collected material flows, pre-concentrates, and secondary raw materials).

5.3.1.1 Measuring points

To measure the qualities (especially material flow compositions) of these individual interface material flows, seven different measurement points seem feasible to achieve material flow transparency at different interfaces of the value chain (cf. Figure 1.1):

(MP-1) Collection vehicles. The first possibility is the material characterization directly during collection in the collection vehicles, as it is already in pilot use in Austria (Mittermayr & Klüsner, 2019). Here, the material flow can be characterized container-specific by using additional sensors integrated in the pre-charging chamber of the waste collection vehicle. However, materials contained in collection bags and potential segregation effects (cf. Publication D [Section 3.3]) can complicate the detectability, and the characterization depth is currently only limited to broader material classes (packaging, paper, metal, bio-waste, residual waste).

(MP-2) SBS units in sorting plants. An alternative option for characterizing the collected material flows is the utilization of existing SBS data from sorting plants. Here, material flows are presented as singled monolayers to the SBS unit. Therefore, optimal detectability is ensured due to the absence of segregation effects (cf. Publication D [Section 3.3] and Publication F [Section 4.1]). In addition, the material flow characterization can also take place particle by particle (cf. Section 5.1.2 and Publication C [Section 3.2]). Since existing SBS data could be used, no investment in additional sensors is necessary. However, since only material flows can be monitored that are sensor-based sorted, it becomes necessary to monitor alternative measurement points, e.g., output material flows from preconditioning processes or the output material flows from SBS stages (cf. MP-3 and MP-4).

(MP-3) Output-SBQC of pre-concentrates at product conveyor belts in sorting plants. Pre-concentrates from sorting plants could be monitored with additionally installed sensors. As successfully demonstrated on an industrial scale in Publication F (Section 4.1) for a PET tray fraction, very accurate material flow characterization is possible due to the monolayer material flow presentation. However, as each output fraction requires an additional sensor, monitoring all output material flows with cost-intensive NIR-sensors is currently not considered economically feasible. A possible alternative is the use of low-cost sensors

such as VIS-RGB coupled with deep learning models (cf. future research potential 1 in Publication A [Section 2.1]), as currently developed by various startups (e.g., Greyparrot AI, 2023; PolyPerception, 2023; WeSort.AI GmbH, 2023) or the monitoring of multiple material flows with a single sensor (cf. MP-4).

(**MP-4**) **Output-SBQC of pre-concentrates at bale press feeding conveyor belts in sorting plants.** SBQC at bale press feeding conveyor belts allow multiple material flows to be monitored with just one sensor. This streamlining can not only reduce costs, with typically not more than three sensors needed for modern sorting plants, but also enables the investment in more cost-intensive sensors, such as NIR or multi-sensor combinations. Nonetheless, as highlighted in Publication F [Section 4.1], a current challenge in SBQC with multilayered bulks are segregation effects, requiring the development and validation of correction models.

(**MP-5**) **SBS units & input monitoring in processing plants.** Alternatively, pre-concentrate qualities could be monitored in processing plants, reducing the total number of required sensors, since processing plants bundle pre-concentrates from several sorting plants. Modern processing plants often feature SBS units for an initial sorting of pre-concentrates. Thus, the existing SBS unit data could be used for input monitoring, providing lower investment costs and enabling precise material flow characterization due to the singled material flow presentation on acceleration belts (cf. MP-2). However, additional sensor installations may be necessary for non-sensor-based-sorted material flows or if no SBS units are installed at the beginning of the processing plant (cf. MP-2).

(**MP-6**) **Output monitoring in processing plants.** After processing, the produced secondary raw materials are more homogeneous, which can simplify the characterization (cf. Publication D [Section 3.3]). While in collection and sorting processes, material flow compositions on an article basis are often decisive (cf. Publication F [Section 4.1]), additional material flow characteristics (e.g., melt flow rate, additives) might become important for secondary raw materials, which may require the use of alternative sensors or measurement techniques (e.g., middle-infrared).

(**MP-7**) **Input monitoring in production plants.** As an alternative to MP-6, secondary raw materials could also be sensor-based characterized in production plants, where similar measurement conditions as in the output of processing plants are to be expected (cf. MP-6).

From the captured material flow characteristics at one or more measuring points, three different use-cases based on the transparency of the individual interface material flows (Sections 5.3.1.2 to 5.3.1.4) can be derived.

5.3.1.2 Use-case QC-A: Transparency on collected material flows

The monitoring of collected material flows can take place either during collection (MP-1) or by back-calculation from the sorting plant (MP-2 to MP-4). A main advantage of MP-1 is that the material characterization can be household-specific, allowing citizens to be addressed more directly (see implication #3 below). A main advantage of monitoring in the sorting plant is that several collection areas can be monitored with the sensors from a single sorting plant, and a simplified/more accurate characterization can be expected due to the better material flow presentation (cf. Section 5.3.1.1). However, the back-calculation can at most be specific to collection vehicles or collection areas and requires the separation of the different input material flows in the sorting plant, which is common practice in only a few sorting plants so far.

The transparency about the material composition of the collected material flows generated by one of the measuring points or by the combination of several measuring points can be utilized in three aspects to maximize the amount of collected recyclables and to minimize the share of misdirected waste:

#1 Better targeted measures to improve collection quality. Based on the composition of the collected material flows (e.g., share of non-target materials), communication measures to improve the collection of separate waste could be applied in a more targeted manner in the future, e.g., by focusing on individual hot spots or addressing region-specific frequently false disposed items (e.g., lithium-ion batteries).

#2 Evaluation and comparison of measures to improve collection quality. Simultaneously, the effectiveness of the implemented measures can be evaluated directly in a before-and-after comparison based on the measured composition of collected material flow and systematically optimized, e.g., through A/B tests.

#3 Direct motivation of citizens (sensibilisation & gamification). The generated data-basis can be used to engage and sensitize citizens more directly for an effective separate collection as demonstrated, e.g., by the *Daheim* app in Austria (Mittermayr & Klüsner, 2019). Furthermore, the communication campaigns could be complimented with gamification elements (Sailer et al., 2013) to increase the motivation for separate collection.

5.3.1.3 Use-case QC-B: Transparency on pre-concentrates

As discussed in Section 5.3.1.1, pre-concentrate qualities can be either measured at the output of a sorting plant (MP-3 and MP-4) or the input of a processing plant (MP-5). Based on the created transparency, two key implications emerge.

#4 Automatic assessment and optimization of sorting plants. Due to the high effort of manual material flow characterization, the purity of pre-concentrates in sorting plants is often

monitored irregularly. Deficiencies in plant performance (e.g., technical disturbances in plant operation or changes in the input material) are therefore often only detected with considerable delay. Through an automatic monitoring of output fractions, such performance deficits could be detected and eliminated faster in the future, which would result in a higher consistency and higher quality of the pre-concentrates. At the same time, measurements to increase the sorting plant performance could be reproducibly assessed.

#5 Adaptive pricing models for pre-concentrates. Due to the lacking transparency regarding (bale-specific) pre-concentrate purities, pre-concentrates are currently mostly paid for on a flat-rate basis, i.e., independent of their purity (cf. Publication F [Section 4.1]). Combined with high disposal costs for sorting residues, sorting plants operators thus currently have only an incentive to sort "as good as necessary" instead of "as good as possible" (Knappe et al., 2021). Based on transparent pre-concentrate purities, adaptive pricing models could be developed in which higher pre-concentrate purities result in higher prices, thus fixing the lacking incentive for sorting plant operators to sort "as good as possible".

5.3.1.4 Use-case QC-C: Secondary raw materials

Based on MP-6 and MP-7, the quality of secondary raw materials could be automatically monitored and documented. This could result into three positive implications:

#6 Adaptive pricing models for secondary raw materials. Similar to use-case QC-B, adaptive pricing models could also be applied to secondary raw materials, thereby increasing the incentive for processing plant operators to produce high-quality secondary raw materials.

#7 Increased usage of secondary raw materials. Transparent monitoring and documentation of secondary raw materials could reduce reservations producers may have about using secondary raw materials, and thus strengthen the use of secondary raw materials overall.

#8 Adaptive secondary raw material usage. In addition, up-to-date material flow characteristics of secondary raw materials could be used for an adaptive process parameterization in production plants. For example, the addition of additives or the adjustment of process parameters (e.g., temperature, rotating speeds) could be dynamically adjusted to measured material flow characteristics. These adjustments could contribute to achieve more constant product specifications despite fluctuating secondary raw material characteristics, and thus help to increase the substitution of primary raw materials.

5.3.1.5 Use-case QC-D: Value-chain-wide assessment

Further, real-time material flow characteristics across several measuring points could enhance an up-to-date and more nuanced assessment of the plastic recycling value chain, resulting into

the following two positive implications:

#9 Real-time and more detailed calculation of recycling quotas. Recycling quotas could be calculated and presented on the basis of the monitored material flow characteristics in a more timely and spatially resolved manner, and contained non-target could be taken into account even more precisely in the quota calculation. As a result, a detailed and more up-to-date assessment of the circular economy would emerge, which, e.g., politicians could use for better decision-making and control.

#10 Material flow data for life-cycle assessments. In addition to the enhanced calculation of recycling quotas, the created data basis could also be used for a more precise ecological and economic evaluation of different circular economy strategies and measures. Based on the created data transparency, the ecological effectiveness of certain measures could be directly compared with each other (A/B tests) or critical hot spots with particularly high ecological impacts in the cycle could be identified and specifically addressed.

5.3.2 Digital process models and twins

A second group of use-cases (PM-A to PM-C) targets at utilizing an increased process transparency based on data-driven process models (cf. Publication G [Section 4.2]). This increased process transparency could significantly enhance material circulation through an improved data-driven design (PM-A) and operation (PM-B) of future-generation sorting and processing plants, as well as a better alignment of product/packaging design with sorting and processing technology (PM-C).

5.3.2.1 Use-case PM-A: Data-driven plant design

In the design phase of a sorting or processing plant, an accurate process simulation is crucial for the development of an optimal flow sheet and for an optimal dimensioning of individual process steps (e.g., conveyor belt widths or component sizes). In contrast to the currently often practiced simulation of sorting and processing plants based on fixed, manually estimated transfer coefficients, a data-driven process simulation could substantially improve the plant design and subsequent performance in the operational phase. Two positive implications could emerge:

#11 Optimal process dimensioning. Based on a data-driven and more accurate mass-balance, individual processes steps could be better dimensioned, resulting in lower investment cost (avoidance of over-dimensioning) or an improved sorting plant performance (avoidance of under-dimensioning).

#12 Data-driven process design. As the process simulation is able to estimate the future sorting performance of the sorting plant, multiple process designs could be compared to each

other and an optimal process design variant could be chosen during the design phase (as demonstrated in Publication G [Section 4.2]). In addition, the data-driven process simulation lays the foundation for a potential artificial intelligence (AI)-based process design, in which an AI algorithm could create and optimize process designs based on the results of the process simulation.

5.3.2.2 Use-case PM-B: Adaptive process control

The combination of fixed process parameters in many sorting/processing plants and fluctuating input material flow characteristics limits the overall plant performance (Küppers et al., 2022). In the future, digital twins of sorting and processing plants could first detect such changes based on the generated material flow transparency (cf. Section 5.3.1) and then propose optimized process parameters based on the process simulation. Two positive implications could emerge:

#13 Increased process performance. Through the adaptive process control, the plant performance could be enhanced, i.e., higher qualities and/or quantities of valuable output fractions could be produced. Examples for an increased process control could include, e.g., the dynamic adjustment of wind speeds in wind sifters depending on the input material flow (e.g., moisture content, particle size distribution, material flow composition), dynamic screen-cut control in drum screens (Küppers et al., 2022), or dynamic adjustments of SBS settings.

#14 Optimized energy consumption. Adaptive process control algorithms could be designed for more energy-efficient sorting and processing, e.g., by dynamically adjusting SBS compressed air pressures and valve opening times to reduce energy consumption. Likewise, the plant operation could be aligned with the electricity price (e.g., availability of low-cost solar or wind energy), for example, by scheduling maintenance intervals and the operation of energy-efficient processes in a targeted manner.

5.3.2.3 Use-case PM-C: Feedback on product and packaging design

On a value chain level, data-driven process models could additionally be used to provide valuable feedback to product and packaging manufacturers regarding the sortability and recyclability of products and packaging. Two positive implications could emerge:

#15 Feedback during design phase. During the design phase, particle-based process models of sorting and processing plants could be used to estimate the sortability and recyclability of packaging and products under development based on the product/packaging specification. In comparison with traditional physical tests, such digital assessments allow for faster iteration cycles and could thus contribute to a more circular product designs. Since the data-based process modeling approach reflects the actual sortability and recyclability

in real-world sorting and processing plants, they could greatly complement or be integrated in existing recyclability assessment tools (e.g., Institut cyclos-HTP GmbH, 2023; RecycleMe GmbH, 2023; Recyda GmbH, 2023).

#16 Feedback during use phase/after launch. In addition to the feedback during the design phase, real-time data from digital twins for sorting and processing plants could generate real-time feedback on the actual sortability and recyclability after the use phase of packaging and products in the market. This constant feedback could contribute to a better alignment of sorting and processing technology and product/packaging design (e.g., adjustments of SBS settings, more circular product design, automatic reporting of frequently wrongly sorted items).

5.4 Future work

Although this dissertation has demonstrated the high potentials of novel SBMC applications at an industrial scale, several research directions emerge from this dissertation with the goal of accelerating the transition of the developed methods and applications into industrial practice.

5.4.1 Improvement of economic feasibility

Sensor technology applications beyond SBS will only find their way into industrial practice, if they are economically viable. Therefore, future research could focus on demonstrating the feasibility of new SBMC business cases such as adaptive pricing models (=increase added value) or lowering the cost of sensor installations. Regarding the cost reduction, great potential is seen

1. on the application of cost-effective sensor-technologies like VIS-RGB- or light detection and ranging (LiDAR)-sensors (cf. future research potential 1 in Publication A [Section 2.1]),
2. on the positioning of sensors at strategic advantageous positions, e.g., bale press feeding conveyor belts, to monitor multiple material flows with a single sensor for which models for the correction of segregation effects need to be developed (cf. Publication F [Section 4.1]), and
3. on the use of data from existing SBS units (cf. future research potential 4 in Publication A [Section 2.1] and [Schlögl et al., 2023]).

5.4.2 Upscaling and long-term validation

The SBQC application demonstrated in this dissertation should be validated additionally by long-term tests on an industrial scale. In addition, the SBQC technology has the potential to be extended to other output fractions or material flows at other positions in a sorting or processing

plant. Regarding the data analysis, especially the question, if and if yes, how often the applied ML models should be retrained in industrial practice, could be of great interest for future research. Furthermore, as discussed in Section 5.1.2.3, it would be very interesting to compare particle- and material-flow-level approach for predicting mass-based material flow compositions at singled and monolayered material flow presentations with each other regarding achievable measurement uncertainties (MU_{95}) and required training dataset sizes.

5.4.3 Development of additional process models

The developed and demonstrated approach of creating data-driven process models based on sensor-based process monitoring data should be extended to other processes. For example, we have already demonstrated in (Chen, Kroell, Hofmann, et al., 2023) that 3DLT sensors can be used for the process monitoring of drum screens. As soon as process models of relevant processes are available, these could be interconnected and the entire sorting/processing plant could be simulated and assessed.

Furthermore, the modeling details could be enhanced. First, further process parameters or the influences of different construction types or manufacturers could be taken into account. Second, particle-based process models could include the influence of various particle characteristics into a transfer coefficient. For the creation of such particle-based process models, the use of marker technologies for a particle-based process assessment, such as radio-frequency identification (RFID)[6] (cf. Kaufeld et al., 2014; Rizvan et al., 2023) seems promising.

5.4.4 Transfer to other material flows

Great optimization potentials exist not only for LWP but also for other material flows (Figure 5.4). For the different material systems and process steps, the sensors and models used must be adapted to the respective process-relevant material flow characteristics, as it was demonstrated, e.g., for SBMM of paper waste using NIR (Spies et al., 2023), SBQC of non-ferrous metals using low-cost VIS-RGB sensors (Kroell, Johnen, et al., 2021), or the prediction of particle size distribution of construction and demolition waste using 3DLT (Kroell, Schönfelder, et al., 2022; Wu et al., 2023). Besides the extension to other material flows, especially the transfer of methods and best-practices between different material flows could thus be a great research focus in future work.

[6] radio-frequency identification

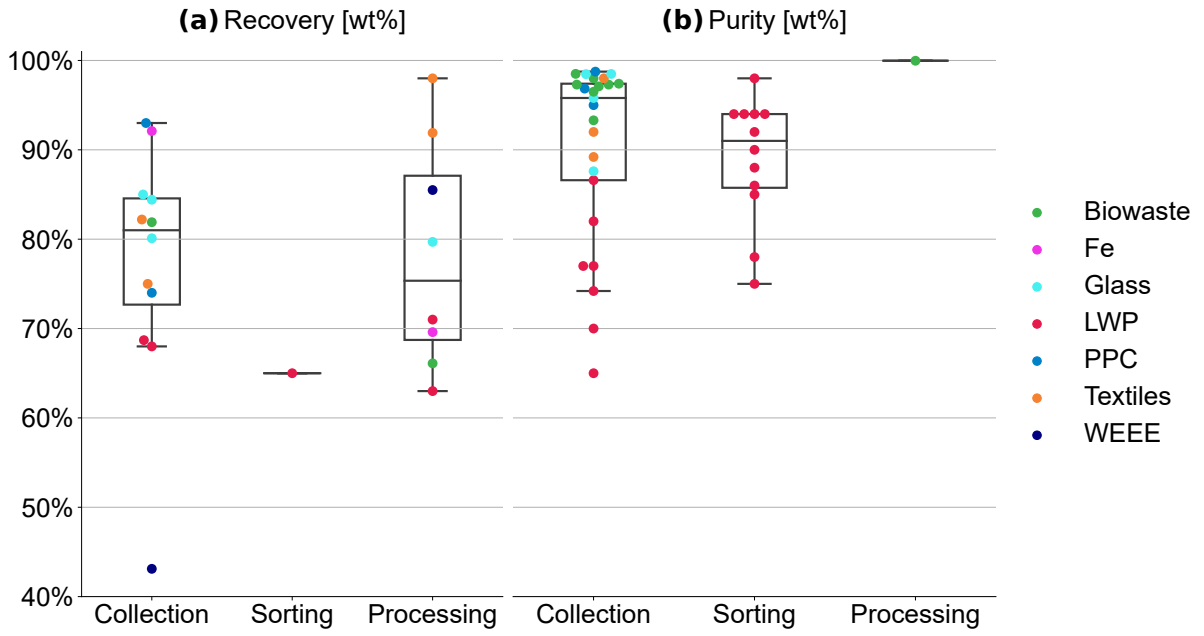

Figure 5.4. Overview on recovery and purity of different material flows during the collection, sorting, and processing stages[7] ; LWP: lightweight packaging; PPC: paper, paperboard & cardboard; WEEE: waste from electrical and electronic equipment.

5.4.5 Standardization and certification

Besides reducing costs and integrating SBMC applications into everyday operations, with increasing use of SBMC deployment, it becomes important that different stakeholders along the value chain have the same understanding and a high level of trust in the statements made by SBMC applications. In this context, standardization procedures can be essential, such as the recently published DIN 54390 for NIR-based monitoring of secondary fuels (Deutsches Institut für Normung e.V., 2022) or DIN-SPEC 91446 for the classification of recycled plastics by data quality levels (Deutsches Institut für Normung e.V., 2021). In addition, it may be useful to develop testing and certification processes to ensure and certify the accuracy of SBMC-data, especially in the area of SBQC. This standardization not only simplifies value chain-wide data exchange, but also creates the necessary trust in the transparency generated by SBMC, thereby contributing to more material circulation and actual use of the generated secondary raw materials.

[7]Data sources: (Aldrian et al., 2018; Bundesgütegemeinschaft Kompost e.V., 2022; Bundeskartellamt, 2012; Bünemann et al., 2011; Burger et al., 2022; Christiani, 2017; Cimpan et al., 2016; Conversio Market & Strategy GmbH, 2022; DIE PAPIERINDUSTRIE e.V., 2023; Dornbusch et al., 2019; European Container Glass Federation, 2023; Forbrig et al., 2020; Initiative Mülltrennung wirkt, 2021; Institut für Abfall, Abwasser und Infrastruktur-Management GmbH, 2014; Kehres, 2018; Knappe et al., 2021; Korolkow et al., 2015; Krebs et al., 2019; Krenn & Wellacher, 2018; Landesanstalt für Umwelt Baden-Württemberg, 2018; Löhle et al., 2020; Montag, 2017; Picuno et al., 2021; Pretz et al., 2022; Sabrowski, 2020; Sabrowski et al., 2018; Siepenkothen & Neumann, 2017; Steger et al., 2019; Wieczorek, 2017)

6 Conclusion

The current recycling industry is limited by a considerable lack of transparency due to the high effort of manual material flow characterization. While sensor technology in recycling has so far been used mainly as a sorting technology, this dissertation aimed at demonstrating that sensor technology could evolve into a new role by verifying the following hypothesis: *In addition to state-of-the-art sensor-based sorting, it is technical feasible to use sensor technology for the inline characterization of post-consumer material flows with industrial-relevant accuracies and at industrial scales. Based on the extracted material flow characteristics, novel SBMC applications can make the value-chain-wide material circulation more transparent and efficient.*

To verify this hypothesis, this dissertation aimed at answering three overarching research questions. For answering RQ I, a systematic literature review (Publication A) of 267 investigations from 198 peer-reviewed journal articles on the application of optical sensors in mechanical recycling was conducted. The review revealed that SBMC so far has not been recognized as a homogeneous research field and thus developed and proposed a unified SBMC terminology. While it became evident that especially pixel- and particle-based classification methods from SBS could also be transferred to new SBMC applications, significant research gaps were identified at the material flow and process level, which hamper the development of a novel SBMC applications such as SBMM, SBQC, SBPM, and SBPC. The review identified ten future research potentials to further advance the SBMC research field. Five of these future research potentials were identified as crucial for verifying the dissertation hypothesis and were thus addressed in RQ II and RQ III on the example of LWP waste.

For answering RQ II, new characterization methods were developed for determining mass-based material flow compositions of post-consumer material flows. In Publication B and C, a particle-level approach for determining mass-based material flow compositions from area- or volume-based measurements was developed. The trained random forest model outperformed traditional approaches such as mean particle masses or grammages by a 43% higher R^2-score ($R^2 = 76.3\%$). In Publications D and E, a material-flow-level approach was developed in which mass-based material flow compositions are directly predicted from pixel-based sensor data using data aggregation and regression models. Using the material-flow-level approach, binary plastic flake and LWP mixtures could be predicted with a MU_{95} of 1.2 vol% ($R^2 = 99.9\%$) and 2.4 wt% ($R^2 = 99.4\%$), respectively, across different material flow presentations.

For answering RQ III, the developed characterization methods from RQ II were transferred into two novel SBMC applications. First, an SBQC application for plastic pre-concentrates was developed (Publication F). It was demonstrated that the combination of inline NIR sensors and ML models can predict mass-based purities of post-consumer PET tray pre-concentrates with a

MU_{95} of 0.31 wt% at plant scale. In a direct comparison, the SBQC method outperformed state-of-the-art manual characterization methods with more than 2.5 times lower MU_{95}'s, and it was estimated that over 350 kg of a 600 kg PET tray bale would need to be manually sampled and sorted to achieve the same accuracy as the novel SBQC method. Second, a data-driven process model of an industrial SBS unit was developed by combining NIR-based process monitoring with artificial neural networks for predicting material-specific transfer coefficients, which achieved a 3.0% MAE across different throughputs, sorting modes, and input compositions (Publication G). The process model was successfully applied to simulate SBS cascades to illustrate the influences of different process designs and changing input compositions on the overall SBS performance. By positively answering RQ I-III, the stated hypothesis was verified and the dissertation proved that the potentials of a new role of sensor technology role in the recycling industry (Section 1.3) can be not only be theoretically envisioned but also be practically implemented.

The developed methods and applications can be applied further across various use-cases. First, the developed SBQC application could be transferred to other material flows and life cycle phases. At different measuring points during collection, sorting, and processing stages, the material composition of collected material flows, pre-concentrates, and secondary raw materials could be transparently monitored. The gained material flow transparency could contribute to an improvement in separate collection (e.g., through targeted campaigns and direct feedback to citizens), a technical optimization of sorting and processing plants, the creation of positive incentives by adaptive price models for higher pre-concentrate and secondary raw material qualities, and a more flexible use of secondary raw material in production processes.

Second, the developed process modelling approach could be applied to other processes (e.g., ballistic separators, wind-sifters, drum screens) and to the modeling of entire sorting and processing plants. In the plant design phase, such process models could be used to optimize the plant design and process dimensioning. During plant operation, data-driven process models could be used for adaptive process control to optimize the overall plant performance and energy consumption. Value chain-wide, data-driven process models could also be used to make products and packaging more circular during their design phase by providing direct feedback on real-world sortability and recyclability, and to contribute to a better alignment between sorting/processing technology and product/packaging design after the product launch.

While the conducted industrial-scale case studies and developed use-cases demonstrate the large future potentials of sensor technology in addition to today's SBS, future work will be required to improve the economic feasibility, integrate them into industrial practice and transfer them to additional processes and material flows. As these SBMC applications will grow into industrial practice, they can massively contribute to foster CE based on the created transparency, thereby reducing primary raw material dependency and increasing generated environmental benefits, ultimately ensuring a habitable planet for current and future generations.

Bibliography

Aldrian, A., Pomberger, R., Schipfer, C., & Gattermayer, K. (2018). Altglasrecycling - Anteil an Störstoffen im Altglas in Österreich. In R. Pomberger, J. Adam, A. Aldrian, L. Kranzinger, K. Lorber, S. Neuhold, T. Nigl, K. Pfandl, R. Sarc, T. Schwarz, P. Sedlazeck, M. Wellacher, A. Curtis, K. Friedrich, B. Küppers, S. Möllnitz, B. Rutrecht, T. M. Sattler, S. A. Viczek, … T. Weißenbach (Eds.), *Recy & DepoTech 2018* (pp. 193–198). Abfallverwertungstechnik & Abfallwirtschaft Eigenverlag.

Borowski, C. (2018). *Entwicklung von Verfahren und Bohrtechniken zur zufälligen Volumenelemententnahme aus Ballen* (Dissertation). Technischen Universität Clausthal. Clausthal, Fakultät für Energie- und Wirtschaftswissenschaften. Retrieved August 6, 2023, from https://dokumente.ub.tu-clausthal.de/servlets/MCRFileNodeServlet/clausthal_derivate_00000349/Db113597.pdf

Brand, A., Allen, L., Altman, M., Hlava, M., & Scott, J. (2015). Beyond authorship: attribution, contribution, collaboration, and credit. *Learned Publishing*, *28*(2), 151–155. https://doi.org/10.1087/20150211

Brune, M., & Feil, A. (2020). Fremdstoffgehalt in Biogut – Potential der Entfrachtung durch Vorbehandlung. In R. Pomberger, J. Adam, A. Aldrian, M. Altendorfer, A. Curtis, T. Dobra, K. Friedrich, L. Kandlbauer, K. E. Lorber, S. Möllnitz, T. Nigl, R. Sarc, T. Sattler, S. Viczek, D. Vollprecht, T. Weißenbach, & M. Wellacher (Eds.), *Recy & DepoTech 2020* (pp. 559–564). Abfallverwertungstechnik & Abfallwirtschaft Eigenverlag.

Bundesgütegemeinschaft Kompost e.V. (Ed.). (2022). Auswertung der gütegesicherten Kompostanalysen 2022. Retrieved August 6, 2023, from https://www.kompost.de/fileadmin/user_upload/Dateien/Zahlen/BGK_Auswertung_der_guetegesicherten_Kompostanalysen_2022.pdf

Bundeskartellamt. (2012). Sektoruntersuchung duale Systeme: Abschlussbericht. Retrieved August 6, 2023, from http://www.bundeskartellamt.de/SharedDocs/Publikation/DE/Sektoruntersuchungen/Sektoruntersuchung%20Duale%20Systeme%20-%20Abschlussbericht.pdf?__blob=publicationFile

Bünemann, Rachut, Christiani, Langen, & Wolters. (2011). Planspiel zur Fortentwicklung der Verpackungsverordnung: Teilvorhaben 1: Bestimmung der Idealzusammensetzung der Wertstofftonne (Umweltbundesamt, Ed.). Retrieved August 6, 2023, from https://www.umweltbundesamt.de/sites/default/files/medien/461/publikationen/4074.pdf

Burger, A., Cayé, N., & Schüler, K. (2022). Aufkommen und Verwertung von Verpackungsabfällen in Deutschland im Jahr 2020: Abschlussbericht (Umweltbundesamt, Ed.). Retrieved August 6, 2023, from https://www.umweltbundesamt.de/sites/default/files/

medien/1410/publikationen/2022-09-29_texte_109-2022_aufkommen-verwertung-verpackungsabfaelle-2020-d.pdf

Chen, X., Kroell, N., Althaus, M., Pretz, T., Pomberger, R., & Greiff, K. (2023). Enabling mechanical recycling of plastic bottles with shrink sleeves through near-infrared spectroscopy and machine learning algorithms. *Resources, Conservation and Recycling*, *188*, 106719. https://doi.org/10.1016/j.resconrec.2022.106719

Chen, X., Kroell, N., Dietl, T., Feil, A., & Greiff, K. (2021). Influence of long-term natural degradation processes on near-infrared spectra and sorting of post-consumer plastics. *Waste Management*, *136*, 213–218. https://doi.org/10.1016/j.wasman.2021.10.006

Chen, X., Kroell, N., Feil, A., & Greiff, K. (2023). Sensor-based sorting. In C. Meskers, E. Worrell, & M. A. Reuter (Eds.), *Handbook of recycling*. Elsevier.

Chen, X., Kroell, N., Feil, A., & Pretz, T. (2020). Determination of the composition of multilayer plastic packaging with nir spectroscopy. *Detritus*, (13), 62–66. https://doi.org/10.31025/2611-4135/2020.14027

Chen, X., Kroell, N., Hofmann, B., Schlögl, S., & Greiff, K. (2023). Improving drum sieve performance in lightweight packaging waste recycling by automatic parameter adjustment through 3D laser triangulation-based process monitoring. *Resources, Conservation and Recycling*, *192*, 106924. https://doi.org/10.1016/j.resconrec.2023.106924

Chen, X., Kroell, N., Li, K., Feil, A., & Pretz, T. (2021). Influences of bioplastic polylactic acid on near-infrared-based sorting of conventional plastic. *Waste management & research*, *39*(9), 1210–1213. https://doi.org/10.1177/0734242X211003969

Chen, X., Kroell, N., Wickel, J., & Feil, A. (2021). Determining the composition of post-consumer flexible multilayer plastic packaging with near-infrared spectroscopy. *Waste Management*, *123*, 33–41. https://doi.org/10.1016/j.wasman.2021.01.015

Christiani, J. (2017). Stand der Technik und Herausforderungen für einzelne Verpackungsmaterialien. Retrieved August 6, 2023, from https://www.bvse.de/images/pdf/Themen__Ereignisse/2017/1-Christiani_Stand_der_Technik_.pdf

Cimpan, C., Maul, A., Wenzel, H., & Pretz, T. (2016). Techno-economic assessment of central sorting at material recovery facilities – the case of lightweight packaging waste. *Journal of Cleaner Production*, *112*, 4387–4397. https://doi.org/10.1016/j.jclepro.2015.09.011

Circle Economy (Ed.). (2023). The circularity gap report 2023. Retrieved August 6, 2023, from https://www.circularity-gap.world/2023#download

Conversio Market & Strategy GmbH (Ed.). (2022). Stoffstrombild Kunststoffe in Deutschland 2021: Zahlen und Fakten zum Lebensweg von Kunststoffen: Kurzfassung der Conversio Studie. Retrieved August 6, 2023, from https://www.bvse.de/dateien2020/2-PDF/01-Nachrichten/03-Kunststoff/2022/Kurzfassung_Stoffstrombild_2021_13102022_1_.pdf

COREPLA (Ed.). (2022). General terms and conditions for sale by auction. Retrieved August 6, 2023, from https://www.corepla.it/sites/default/files/documenti/generaltermscond_rev._no15_march_2022.pdf

Curtis, A., & Sarc, R. (2021). Real-time monitoring of volume flow, mass flow and shredder power consumption in mixed solid waste processing. *Waste management (New York, N.Y.)*, *131*, 41–49. https://doi.org/10.1016/j.wasman.2021.05.024

Der Grüne Punkt (Ed.). (2016). Allgemeine Vertragsbedingungen der Der Grüne Punkt – Duales System Deutschland GmbH (DSD) für Verwerterverträge (AVBV) - Erlöskunden - Stand 07.2016. Retrieved August 6, 2023, from https://www.gruener-punkt.de/fileadmin/Dateien/Downloads/PDFs/geschaeftsbedingungen/AVBV_Erloeskunden_2016_07_04.pdf

Deutsches Institut für Normung e. V. (2012). DIN ISO 9276-6: Darstellung der Ergebnisse von Partikelgrößenanalysen: Teil 6: Deskriptive und quantitative Darstellung der Form und Morphologie von Partikeln.

Deutsches Institut für Normung e.V. (2021). DIN SPEC 91446: Klassifizierung von Kunststoff-Rezyklaten durch Datenqualitätslevels für die Verwendung und den (internetbasierten) Handel.

Deutsches Institut für Normung e.V. (2022). DIN 54390: Feste Sekundärbrennstoffe – Echtzeit-Bestimmung von Parametern mittels Nahinfrarotspektroskopie.

DIE PAPIERINDUSTRIE e.V. (2023). Leistungsbericht Papier 2023. Retrieved August 6, 2023, from https://www.papierindustrie.de/papierindustrie/statistik

Dirzo, R., Young, H. S., Galetti, M., Ceballos, G., Isaac, N. J. B., & Collen, B. (2014). Defaunation in the Anthropocene. *Science (New York, N.Y.)*, *345*(6195), 401–406. https://doi.org/10.1126/science.1251817

Dornbusch, Santjer, Hannes, & Oelgemöller. (2019). Bestimmung des Verpackungsanteils im getrennt erfassten Altpapiergemisch im Sammelbehälter / Erfassungssystem: Endbericht (Institut für Abfall, Abwasser und Infrastruktur-Management GmbH, Ed.). Retrieved August 6, 2023, from https://www.vku.de/fileadmin/user_upload/Verbandsseite/Themen/Infrastruktur_und_Dienstleistungen/INFA-Gutachten_Endbericht_bundesweite_PPK-Analyse.pdf?sword_list%5B%5D=reiche&no_cache=1

European Commission (Ed.). (2019). The European Green Deal. Retrieved August 6, 2023, from https://eur-lex.europa.eu/resource.html?uri=cellar:b828d165-1c22-11ea-8c1f-01aa75ed71a1.0002.02/DOC_1&format=PDF

European Commission. (2020). A new Circular Economy Action Plan. Retrieved August 6, 2023, from https://eur-lex.europa.eu/legal-content/EN/TXT/?qid=1583933814386&uri=COM:2020:98:FIN

European Committee for Standardization. (2005). ÖNORM EN 14899: Charakterisierung von Abfällen - Probenahme von Abfällen - Rahmen für die Erstellung und Anwendung eines Probenahmeplans.

European Committee for Standardization. (2006). CEN/TR 15310-1: Characterisation of waste—sampling of waste materials—part 1: guidance on selection and application of criteria for sampling under various conditions.

European Container Glass Federation (Ed.). (2023). Glass collection for recycling in Europe statistics for 2021. Retrieved August 6, 2023, from https://closetheglassloop.eu/publications-overview/

European Parliament and Council. (2018). DIRECTIVE (EU) 2018/851 on waste. Retrieved August 6, 2023, from https://eur-lex.europa.eu/legal-content/EN/TXT/PDF/?uri=CELEX:32018L0851

Eurostat (Ed.). (2023). Circular economy - material flows - Statistics Explained. Retrieved August 6, 2023, from https://ec.europa.eu/eurostat/statistics-explained/index.php?title=Circular_economy_-_material_flows

Feil, A., Kroell, N., Pretz, T., & Greiff, K. (2021). Anforderungen an eine effiziente technologische Behandlung von Post-Consumer Verpackungsmaterialien in Sortieranlagen: Möglichkeiten und Grenzen. *Müll und Abfall*, *21*(7), 362–370. https://doi.org/10.37307/j.1863-9763.2021.07.04

Feil, A., & Pretz, T. (2020). Mechanical recycling of packaging waste. In T. M. Letcher (Ed.), *Plastic Waste and Recycling* (pp. 283–319). Elsevier. https://doi.org/10.1016/B978-0-12-817880-5.00011-6

Feil, A., Pretz, T., Julius, J., Go, N., Bosling, M., & Johnen, K. (2019). Metal Waste. In T. M. Letcher & D. A. Vallero (Eds.), *Waste* (pp. 211–223). Elsevier. https://doi.org/10.1016/B978-0-12-815060-3.00010-4

Flamme, S., & Krämer, P. (2015). Erhöhung der Ressourceneffizienz durch Echtzeitanalytik. In K. J. Thomé-Kozmiensky (Ed.), *Recycling und Rohstoffe*. TK-Verl.

Forbes (Ed.). (2016). Cleaning Big Data: Most Time-Consuming, Least Enjoyable Data Science Task, Survey Says. Retrieved August 6, 2023, from https://www.forbes.com/sites/gilpress/2016/03/23/data-preparation-most-time-consuming-least-enjoyable-data-science-task-survey-says/?sh=24c9c4e56f63

Forbrig, S., Fischer, T., & Heinz, B. (2020). Bedarf, Konsum, Wiederverwendung und Verwertung von Bekleidung und Textilien in Deutschland (Fachverband Textilrecycling, Bundesverband Sekundärrohstoffe und Entsorgung e. V., Ed.). Retrieved August 6, 2023, from https://www.bvse.de/dateien2020/1-Bilder/03-Themen_Ereignisse/06-Textil/2020/studie2020/bvse%20Alttextilstudie%202020.pdf

GBP Quality GmbH (Ed.). (2023). Sortieranalysen: Aufgabe und Lösung. Retrieved August 6, 2023, from https://www.gbp-quality.eu/ablauf-arbeitsweise-gbp-sortieranalysen/

Greiff, K., Wotruba, H., Feil, A., Kroell, N., Chen, X., Gürsel, D., & Merz, V. (Eds.). (2022). *9th Sensor-Based Sorting & Control 2022*. Shaker. https://doi.org/10.2370/9783844085457

Greyparrot AI (Ed.). (2023). The AI-powered waste analytics system for the circular economy. Retrieved August 6, 2023, from https://www.greyparrot.ai/

Gundupalli, S. P., Hait, S., & Thakur, A. (2017). A review on automated sorting of source-separated municipal solid waste for recycling. *Waste management (New York, N.Y.)*, 56–74. https://doi.org/10.1016/j.wasman.2016.09.015

Horton, A. A., Walton, A., Spurgeon, D. J., Lahive, E., & Svendsen, C. (2017). Microplastics in freshwater and terrestrial environments: Evaluating the current understanding to identify the knowledge gaps and future research priorities. *The Science of the total environment*, *586*, 127–141. https://doi.org/10.1016/j.scitotenv.2017.01.190

Initiative Mülltrennung wirkt. (2021). Ein Jahr Initiative „Mülltrennung wirkt“: Von den Herausforderungen zum Erfolg: Duale Systeme bilden eine starke Allianz für mehr Aufklärung. *Müll und Abfall*, (7), 352–360. https://doi.org/10.37307/j.1863-9763.2021.07.03

Institut cyclos-HTP GmbH (Ed.). (2023). CHiRA: CHI Recyclability Assessment. Retrieved August 6, 2023, from https://www.cyclos-htp.de/leistungen/pr%C3%BCfung-testierung/

Institut für Abfall, Abwasser und Infrastruktur-Management GmbH (Ed.). (2014). Begleitung eines Modellversuchs zur Einführung einer Wertstofftonne im Kreis Paderborn: Endbericht. Retrieved August 6, 2023, from https://www.ave-kreis-paderborn.de/wp-content/uploads/infa-ergebnisbericht2014.pdf

IPCC (Ed.). (2023). *Climate Change 2022 – Impacts, Adaptation and Vulnerability*. Cambridge University Press. https://doi.org/10.1017/9781009325844

IRP (Ed.). (2017). Assessing Global Resource Use: A systems approach to resource efficiency and pollution reduction. Retrieved August 6, 2023, from https://www.resourcepanel.org/reports/assessing-global-resource-use

IRP (Ed.). (2019). Global Resources Outlook 2019: Natural Resources for the Future We Want. A Report of the International Resource Panel. United Nations Environment Programme. Retrieved August 6, 2023, from https://www.resourcepanel.org/reports/global-resources-outlook

Itseez. (2015). Open source computer vision library. https://github.com/opencv/opencv

Jambeck, J. R., Geyer, R., Wilcox, C., Siegler, T. R., Perryman, M., Andrady, A., Narayan, R., & Law, K. L. (2015). Marine pollution. Plastic waste inputs from land into the ocean. *Science (New York, N.Y.)*, *347*(6223), 768–771. https://doi.org/10.1126/science.1260352

Johnen, K., & Kroell, N. (2020). Quantitative Klemmkornbestimmung mittels Bildauswertung am Beispiel der Siebung von Abfallfeinfraktionen. In Deutsche Gesellschaft für Abfallwirtschaft e.V. (Ed.), *10. DGAW-Wissenschaftskongress Abfall- und Ressourcenwirtschaft*. innsbruck university press.

Johnen, K., Kroell, N., & Feil, A. (2020). Entwicklung einer Methodik zur Wertstoffgehaltsbestimmung von feinkörnigen Abfällen. In R. Pomberger, J. Adam, A. Aldrian, M. Altendorfer, A. Curtis, T. Dobra, K. Friedrich, L. Kandlbauer, K. E. Lorber, S. Möllnitz, T. Nigl, R. Sarc, T. Sattler, S. Viczek, D. Vollprecht, T. Weißenbach, & M. Wellacher (Eds.), *Recy & DepoTech 2020*. Abfallverwertungstechnik & Abfallwirtschaft Eigenverlag.

Kaufeld, S., Feil, A., & Pretz, T. (2014). Zeitlich differenzierte Einzelkornerfassung bei der Siebklassierung mittels Radiofrequenz- Identifikation. *Chemie Ingenieur Technik*, *86*(6), 891–898. https://doi.org/10.1002/cite.201300171

Kehres, B. (2018). Problem Fremdstoffe / Kunststoffe in Bioabfall und Kompost. In *Bioabfallforum 2018*. Retrieved August 6, 2023, from https://www.kompost.de/fileadmin/user_upload/Dateien/Themen/Methoden/Kehres_Textbeitrag_Bioabfallforum_2018.pdf

Khodier, K., Viczek, S. A., Curtis, A., Aldrian, A., O'Leary, P., Lehner, M., & Sarc, R. (2020). Sampling and analysis of coarsely shredded mixed commercial waste. Part I: procedure, particle size and sorting analysis. *International Journal of Environmental Science and Technology*, *17*(2), 959–972. https://doi.org/10.1007/s13762-019-02526-w

Kirchherr, J., Reike, D., & Hekkert, M. (2017). Conceptualizing the circular economy: An analysis of 114 definitions. *Resources, Conservation and Recycling*, *127*, 221–232. https://doi.org/10.1016/j.resconrec.2017.09.005

Kirchherr, J., Yang, N.-H. N., Schulze-Spüntrup, F., Heerink, M. J., & Hartley, K. (2023). Conceptualizing the Circular Economy (Revisited): An Analysis of 221 Definitions. *Resources, Conservation and Recycling*, *194*, 107001. https://doi.org/10.1016/j.resconrec.2023.107001

Knappe, F., Reinhardt, J., Kauertz, B., Oetjen-Dehne, R., Buschow, N., Ritthoff, M., Wilts, H., & Lehmann, M. (2021). Technische Potenzialanalyse zur Steigerung des Kunststoffrecyclings und des Rezyklateinsatzes (Umweltbundesamt, Ed.). Retrieved August 6, 2023, from https://www.umweltbundesamt.de/sites/default/files/medien/1410/publikationen/2021-12-10_texte_92-2021_potenzialanalyse-kunststoffrecycling.pdf

Korolkow, J., Pretz, T., & Raulf, K. (2015). Konsum, Bedarf und Wiederverwendung von Bekleidung und Textilien in Deutschland (Fachverband Textilrecycling, Bundesverband Sekundärrohstoffe und Entsorgung e. V., Ed.). Retrieved August 6, 2023, from https://www.bvse.de/images/pdf/Leitfaeden-Broschueren/150914_Textilstudie_2015.pdf

Krebs, T., Putz, H.-J., & Schabel, S. (2019). Neue Methoden zur Erfassung der Altpapierqualität hinsichtlich der Kriterien der Neufassung der DIN EN 643 zur Charakterisierung der Altpapiersorten (Fachgebiet Papierfabrikation und Mechanische Verfahrenstechnik, Ed.). https://doi.org/10.25534/tuprints-00009294

Krenn, A., & Wellacher, M. (2018). Störstoffe und originalverpackte Lebensmittel in Bioabfällen. In R. Pomberger, J. Adam, A. Aldrian, L. Kranzinger, K. Lorber, S. Neuhold, T. Nigl, K. Pfandl, R. Sarc, T. Schwarz, P. Sedlazeck, M. Wellacher, A. Curtis, K. Friedrich, B. Küppers,

S. Möllnitz, B. Rutrecht, T. M. Sattler, S. A. Viczek, … T. Weißenbach (Eds.), *Recy & DepoTech 2018* (pp. 183–188). Abfallverwertungstechnik & Abfallwirtschaft Eigenverlag.

Kroell, N. (2021). imea: A Python package for extracting 2D and 3D shape measurements from images. *Journal of Open Source Software*, *6*(60), 3091. https://doi.org/10.21105/joss.03091

Kroell, N., Chen, X., Feil, A., & Greiff, K. (2023). Sensortechnik in der Sortierung und Aufbereitung von Kunststoffverpackungen - Potenziale und Grenzen. In S. Flamme (Ed.), *18. Kreislaufwirtschaftstage*.

Kroell, N., Chen, X., Greiff, K., & Feil, A. (2022). Optical sensors and machine learning algorithms in sensor-based material flow characterization for mechanical recycling processes: A systematic literature review. *Waste Management*, *149*, 259–290. https://doi.org/10.1016/j.wasman.2022.05.015

Kroell, N., Chen, X., Küppers, B., Lorenzo, J., Maghmoumi, A., Schlaak, M., Thor, E., Nordmann, C., & Greiff, K. (2023). Near-infrared-based determination of mass-based material flow compositions in mechanical recycling of post-consumer plastics: Technical feasibility enables novel applications. *Resources, Conservation and Recycling*, *191*, 106873. https://doi.org/10.1016/j.resconrec.2023.106873

Kroell, N., Chen, X., Küppers, B., Schlögl, S., Feil, A., & Greiff, K. (2024). Near-infrared-based quality control of plastic pre-concentrates in lightweight-packaging waste sorting plants. *Resources, Conservation and Recycling*, *201*, 107256. https://doi.org/10.1016/j.resconrec.2023.107256

Kroell, N., Chen, X., Maghmoumi, A., Koenig, M., Feil, A., & Greiff, K. (2021). Sensor-based particle mass prediction of lightweight packaging waste using machine learning algorithms. *Waste Management*, *136*, 253–265. https://doi.org/10.1016/j.wasman.2021.10.017

Kroell, N., Chen, X., Maghmoumi, A., Lorenzo, J., Schlaak, M., Nordmann, C., Küppers, B., Thor, E., & Greiff, K. (2023). NIR-MFCO dataset: Near-infrared-based false-color images of post-consumer plastics at different material flow compositions and material flow presentations. *Data in brief*, *48*, 109054. https://doi.org/10.1016/j.dib.2023.109054

Kroell, N., Chen, X., Nordmann, C., Pfund, E., Lorenzo, J., Dietl, T., Maghmoumi, A., Küppers, B., Feil, A., & Greiff, K. (2022). Optimierte Sortierung von Leichtverpackungsabfällen durch ein intelligentes Stoffstrommanagement. In R. Pomberger, J. Adam, M. Altendorfer, T. Bouvier-Schwarz, P. Haslauer, L. Kandlbauer, K. Khodier, G. Koinig, N. Kuhn, T. Lasch, N. Mhaddolkar, T. Nigl, B. Rutrecht, R. Sarc, T. Sattler, S. Schlögl, H. Stipanovic, A. Tischberger-Aldrian, & S. Viczek (Eds.), *Vorträge-Konferenzband zur 16. Recy & DepoTech-Konferenz* (pp. 347–352). Abfallverwertungstechnik & Abfallwirtschaft Eigenverlag.

Kroell, N., Dietl, T., Maghmoumi, A., Chen, X., Küppers, B., Feil, A., & Greiff, K. (2022). Assessment of sensor-based sorting performance for lightweight packaging waste through sensor-based material flow monitoring: Concept and preliminary results. In K. Greiff,

H. Wotruba, A. Feil, N. Kroell, X. Chen, D. Gürsel, & V. Merz (Eds.), *9th Sensor-Based Sorting & Control 2022*. Shaker.

Kroell, N., Johnen, K., Chen, X., & Feil, A. (2021). Fine metal-rich waste stream characterization based on RGB data: Comparison between feature-based and deep learning classification methods. In J. Beyerer & T. Längle (Eds.), *OCM 2021 - Optical Characterization of Materials: Conference Proceedings*. KIT Scientific Publishing.

Kroell, N., Maghmoumi, A., Dietl, T., Chen, X., Küppers, B., Scherling, T., Feil, A., & Greiff, K. (2024). Towards digital twins of waste sorting plants: Developing data-driven process models of industrial-scale sensor-based sorting units by combining machine learning with near-infrared-based process monitoring. *Resources, Conservation and Recycling*, *200*, 107257. https://doi.org/10.1016/j.resconrec.2023.107257

Kroell, N., Schönfelder, P., Chen, X., Johnen, K., Feil, A., & Greiff, K. (2022). Sensorbasierte Vorhersage von Korngrößenverteilungen durch Machine Learning Modelle auf Basis von 3D-Lasertriangulationsmessungen. In Deutsche Gesellschaft für Abfallwirtschaft e.V. (Ed.), *11. DGAW-Wissenschaftskongress Abfall- und Ressourcenwirtschaft*. innsbruck university press.

Kuchta, K., & Picuno, C. (2020). Kreislauffähigkeit von Post-Consumer Kunststoffverpackungen. *Müll und Abfall*, *20*(3), 118–124. https://doi.org/10.37307/j.1863-9763.2020.03.04

Küppers, B., Schlögl, S., Kroell, N., & Radkohl, V. (2022). Relevance and challenges of plant control in the pre-processing stage for enhanced sorting performance. In K. Greiff, H. Wotruba, A. Feil, N. Kroell, X. Chen, D. Gürsel, & V. Merz (Eds.), *9th Sensor-Based Sorting & Control 2022* (pp. 17–33). Shaker.

Länderarbeitsgemeinschaft Abfall. (2001). Richtlinie für das Vorgehen bei physikalischen und chemischen Untersuchungen im Zusammenhang mit der Verwertung/Beseitigung von Abfällen.

Landesanstalt für Umwelt Baden-Württemberg (Ed.). (2018). Sortenreinheit von Bioabfällen: Datenerhebung am Beispiel zweier öffentlich-rechtlicher Entsorgungsträger Baden-Württemberg. Retrieved August 6, 2023, from https://lb.boa-bw.de/frontdoor/deliver/index/docId/10028/file/sortenreinheit_von_bioabfaellen17bd.pdf

Lin, D., Wambersie, L., & Wackernagel, M. (2023). Estimating the Date of Earth Overshoot Day 2023. Retrieved August 6, 2023, from https://www.overshootday.org/content/uploads/2023/06/Earth-Overshoot-Day-2023-Nowcast-Report.pdf

Löhle, S., Schmiedel, U., & Bartnik, S. (2020). Analyse der Datenerhebungen nach ElektroG und UStatG über das Berichtsjahr 2018 zur Vorbereitung der EU-Berichtspflichten 2020: Teilbericht (Umweltbundesamt, Ed.). Retrieved August 6, 2023, from https://www.umweltbundesamt.de/sites/default/files/medien/1410/publikationen/2020-07-15_texte_135-2020_eag-daten2018.pdf

Mittermayr, R., & Klüsner, S. (2019). Smart Waste – Wie Digitalisierung und IoT die Welt des Abfalls verändern. In S. Thiel, O. Holm, E. Thomé-Kozmiensky, D. Goldmann, & B. Friedrich (Eds.), *Recycling und Rohstoffe* (pp. 15–24). TK Thomé-Kozmiensky Verlag. Retrieved August 6, 2023, from https://books.vivis.de/wp-content/uploads/2023/01/2019_rur_015-024_mittermayr.pdf

Montag, C. (2017). *Minimierung des Störstoffanteils im Bioabfall in der Stadt Brandenburg an der Havel* (Master thesis). Hochschule Magdeburg-Stendal. Stendal. Retrieved August 6, 2023, from https://repo.bibliothek.uni-halle.de/bitstream/1981185920/13297/1/MA_Montag_Christina_20122071_%20Ingenieur%C3%B6kologie.pdf

Nigl, T., Baldauf, M., Hohenberger, M., & Pomberger, R. (2021). Lithium-Ion Batteries as Ignition Sources in Waste Treatment Processes—A Semi-Quantitate Risk Analysis and Assessment of Battery-Caused Waste Fires. *Processes*, *9*(1), 49. https://doi.org/10.3390/pr9010049

O'Neill, D. W., Fanning, A. L., Lamb, W. F., & Steinberger, J. K. (2018). A good life for all within planetary boundaries. *Nature Sustainability*, *1*(2), 88–95. https://doi.org/10.1038/s41893-018-0021-4

Österreichisches Normungsinstitut. (2011-11-01). Grundlegende Charakterisierung von Abfallhaufen oder von festen Abfällen aus Behältnissen und Transportfahrzeugen.

Pabst, W., & Gregorova, E. (2007). *Characterization of particles and particle systems*.

Pahl, M., Schädel, G., & Rumpf, H. (1973a). Zusammenstellung von Teilchenformbeschreibungsmethoden: 1. Teil. *Aufbereitungstechnik*, *14*(5), 257–264.

Pahl, M., Schädel, G., & Rumpf, H. (1973b). Zusammenstellung von Teilchenformbeschreibungsmethoden: 2. Teil. *Aufbereitungstechnik*, *14*(10), 672–683.

Pahl, M., Schädel, G., & Rumpf, H. (1973c). Zusammenstellung von Teilchenformbeschreibungsmethoden: 3. Teil. *Aufbereitungstechnik*, *14*(11), 759–764.

Parrodi, J. C. H., Kroell, N., Chen, X., Dietl, T., Pfund, E., Küppers, B., & Nordmann, C. (2021). Nahinfrarot-basierte Stoffstromüberwachung von Bau- und Abbruchabfällen. In S. Thiel, E. Thomé-Kozmiensky, D. Senk, H. Wotruba, H. Antrekowitsch, & R. Pomberger (Eds.), *Mineralische Nebenprodukte und Abfälle* (pp. 92–111). Thomé-Kozmiensky Verlag GmbH.

Pedregosa, F., Varoquaux, G., Gramfort, A., Michel, V., Thirion, B., Grisel, O., Blondel, M., Prettenhofer, P., Weiss, R., Dubourg, V., Vanderplas, J., Passos, A., Cournapeau, D., Brucher, M., Perrot, M., & Duchesnay, E. (2011). Scikit-learn: Machine Learning in Python. *Journal of Open Source Software*, *12*, 2825–2830.

Picuno, C., Alassali, A., Chong, Z. K., & Kuchta, K. (2021). Flows of post-consumer plastic packaging in Germany: An MFA-aided case study. *Resources, Conservation and Recycling*, *169*, 105515. https://doi.org/10.1016/j.resconrec.2021.105515

PolyPerception (Ed.). (2023). Change your perception about waste. Retrieved August 6, 2023, from https://www.polyperception.com/

Pomberger, R. (2021). Über theoretische und reale Recyclingfähigkeit. *Österreichische Wasser- und Abfallwirtschaft*, *73*(1-2), 24–35. https://doi.org/10.1007/s00506-020-00721-5

Prata, J. C., Da Costa, J. P., Lopes, I., Duarte, A. C., & Rocha-Santos, T. (2020). Environmental exposure to microplastics: An overview on possible human health effects. *The Science of the total environment*, *702*, 134455. https://doi.org/10.1016/j.scitotenv.2019.134455

Pretz, T., Feil, A., & Greiff, K. (2022). Recyclingquoten für Siedlungsabfälle – eine hohe Hürde. In R. Pomberger, J. Adam, M. Altendorfer, T. Bouvier-Schwarz, P. Haslauer, L. Kandlbauer, K. Khodier, G. Koinig, N. Kuhn, T. Lasch, N. Mhaddolkar, T. Nigl, B. Rutrecht, R. Sarc, T. Sattler, S. Schlögl, H. Stipanovic, A. Tischberger-Aldrian, & S. Viczek (Eds.), *Vorträge-Konferenzband zur 16. Recy & DepoTech-Konferenz* (pp. 101–110). Abfallverwertungstechnik & Abfallwirtschaft Eigenverlag.

Pretz, T., Raulf, K., & Quicker, P. (2020). Waste, 4. Recycling. In *Ullmann's Encyclopedia of Industrial Chemistry* (pp. 1–39). Wiley-VCH Verlag GmbH & Co. KGaA. https://doi.org/10.1002/14356007.o28{\textunderscore}o05.pub2

RecycleMe GmbH (Ed.). (2023). Evaluate recyclability online with circulate. Retrieved August 6, 2023, from https://recycleme.eco/de/en/services/design-for-recycling/evaluate-recyclability-online/

Recyda GmbH (Ed.). (2023). recyda: Packaging Management All in one. Retrieved August 6, 2023, from https://www.recyda.com/

Rizvan, A., Khodier, K., & Sarc, R. (2023). RFID - Tool zur Partikelverfolgung in der Abfallwirtschaft. In Deutsche Gesellschaft für Abfallwirtschaft e.V. (Ed.), *12. Wissenschaftskongress Abfall- und Ressourcenwirtschaft*. innsbruck university press.

Rockström, J., Gupta, J., Qin, D., Lade, S. J., Abrams, J. F., Andersen, L. S., Armstrong McKay, D. I., Bai, X., Bala, G., Bunn, S. E., Ciobanu, D., DeClerck, F., Ebi, K., Gifford, L., Gordon, C., Hasan, S., Kanie, N., Lenton, T. M., Loriani, S., … Zhang, X. (2023). Safe and just Earth system boundaries. *Nature*, *619*(7968), 102–111. https://doi.org/10.1038/s41586-023-06083-8

Rockström, J., Steffen, W., Noone, K., Persson, A., Chapin, F. S., Lambin, E. F., Lenton, T. M., Scheffer, M., Folke, C., Schellnhuber, H. J., Nykvist, B., de Wit, C. A., Hughes, T., van der Leeuw, S., Rodhe, H., Sörlin, S., Snyder, P. K., Costanza, R., Svedin, U., … Foley, J. A. (2009). A safe operating space for humanity. *Nature*, *461*(7263), 472–475. https://doi.org/10.1038/461472a

Sabrowski, R. (2020). Bioabfallanalyse 2019/2020 (Stadtreinigung Leipzig, Ed.). Retrieved August 6, 2023, from https://stadtreinigung-leipzig.de/upload/files/2021/bioabfallanalyse-2019-2020.pdf

Sabrowski, R., Löffler, R., & Wirschin, I. (2018). Hausmüll- und Bioabfallanalyse in der Stadt Brandenburg an der Havel. *Müll und Abfall*, (11). https://doi.org/10.37307/j.1863-9763.2018.11.06

Sailer, M., Hense, J., Mandl, H., & Klevers, M. (2013). Psychological Perspectives on Motivation through Gamification. *Interaction Design and Architecture(s) Journal*, *19*(19), 28–37. https://doi.org/10.55612/s-5002-019-002

Schlögl, S., Kamleitner, J., Kroell, N., & Chen, X. (2022). Implementierung von Sensor-based Material flow Monitoring in einer Kunststoffsortieranlage. In R. Pomberger, J. Adam, M. Altendorfer, T. Bouvier-Schwarz, P. Haslauer, L. Kandlbauer, K. Khodier, G. Koinig, N. Kuhn, T. Lasch, N. Mhaddolkar, T. Nigl, B. Rutrecht, R. Sarc, T. Sattler, S. Schlögl, H. Stipanovic, A. Tischberger-Aldrian, & S. Viczek (Eds.), *Vorträge-Konferenzband zur 16. Recy & DepoTech-Konferenz*. Abfallverwertungstechnik & Abfallwirtschaft Eigenverlag.

Schlögl, S., Kamleitner, J., Kroell, N., Chen, X., & Aldrian, A. (2023). Developing a Prediction Model in a Lightweight Packaging Waste Sorting Plant using Sensor-based Sorting Data combined with Data of External Near-infrared and LiDAR Sensors [under review]. *Waste management & research*.

Schwarz, A. E., Ligthart, T. N., Godoi Bizarro, D., de Wild, P., Vreugdenhil, B., & van Harmelen, T. (2021). Plastic recycling in a circular economy; determining environmental performance through an LCA matrix model approach. *Waste management (New York, N.Y.)*, *121*, 331–342. https://doi.org/10.1016/j.wasman.2020.12.020

Siepenkothen, H.-J., & Neumann, F. (2017). Bio- und Restabfallanalyse im Kreis Schleswig-Flensburg (Aballwirtschaft Schleswig-Flensburg GmbH, Ed.). Retrieved August 6, 2023, from https://www.asf-online.de/fileadmin/media/Downloads/Rest-und_Bioabfallanalyse_ASF_2016_17.pdf

Spies, A., Kroell, N., Ludes, A., Küppers, B., Raulf, K., & Greiff, K. (2023). Paper and board potential in lightweight packaging waste - Manual and sensor-based material flow analysis [in submission]. *Waste Management*.

Steffen, W., Richardson, K., Rockström, J., Cornell, S. E., Fetzer, I., Bennett, E. M., Biggs, R., Carpenter, S. R., de Vries, W., de Wit, C. A., Folke, C., Gerten, D., Heinke, J., Mace, G. M., Persson, L. M., Ramanathan, V., Reyers, B., & Sörlin, S. (2015). Sustainability. Planetary boundaries: guiding human development on a changing planet. *Science (New York, N.Y.)*, *347*(6223), 1259855. https://doi.org/10.1126/science.1259855

Steger, S., Ritthoff, M., Bulach, W., Schüler, D., Kosińska, I., Degreif, S., Dehoust, G., Bergmann, T., Krause, P., & Oetjen-Dehne, R. (2019). Stoffstromorientierte Ermittlung des Beitrags der Sekundärrohstoffwirtschaft zur Schonung von Primärrohstoffen und Steigerung der Ressourcenproduktivität: Abschlussbericht (Umweltbundesamt, Ed.). Retrieved August 6, 2023, from https://www.umweltbundesamt.de/sites/default/files/medien/1410/publikationen/2019-03-27_texte_34-2019_sekundaerrohstoffwirtschaft.pdf

STEINERT GmbH (Ed.). (2023). Combined sensor sorting systems. Retrieved August 6, 2023, from https://steinertglobal.com/magnets-sensor-sorting-units/sensor-sorting/combined-sensor-sorting-systems/

Steuer, M. (2010). Serial classification. *AT Mineral Processing English Edition*, *51*(1).

TOMRA Systems ASA (Ed.). (2023). AUTOSORT™. Retrieved August 6, 2023, from https://www.tomra.com/waste-metal-recycling/products/machines/autosort

UN General Assembly (Ed.). (2015). Transforming our world : the 2030 Agenda for Sustainable Development. Retrieved August 6, 2023, from https://www.refworld.org/docid/57b6e3e44.html

van der Walt, S., Schönberger, J. L., Nunez-Iglesias, J., Boulogne, F., Warner, J. D., Yager, N., Gouillart, E., & Yu, T. (2014). scikit-image: image processing in Python. *PeerJ*, *2*, e453. https://doi.org/10.7717/peerj.453

WeSort.AI GmbH (Ed.). (2023). Abfallanalyse und Sortierung der nächsten Generation durch künstliche Intelligenz. Retrieved August 6, 2023, from https://www.wesort.ai/

Wieczorek, M. (2017). Möglichkeiten und Grenzen moderner LVP-Sortieranlagen.

Wu, X., Kroell, N., & Greiff, K. (2023). Deep learning-based instance segmentation on 3D laser triangulation data for inline monitoring of particle size distributions in construction and demolition waste recycling [under review]. *Resources, Conservation and Recycling*.

WWF (Ed.). (2020). Living Planet Report 2020 - Bending the curve of biodiversity loss.

Zhang, C., Hu, M., van der Meide, M., Di Maio, F., Yang, X., Gao, X., Li, K., Zhao, H., & Li, C. (2023). Life cycle assessment of material footprint in recycling: A case of concrete recycling. *Waste management (New York, N.Y.)*, *155*, 311–319. https://doi.org/10.1016/j.wasman.2022.10.035

Appendix

A Supplementary materials Publication D

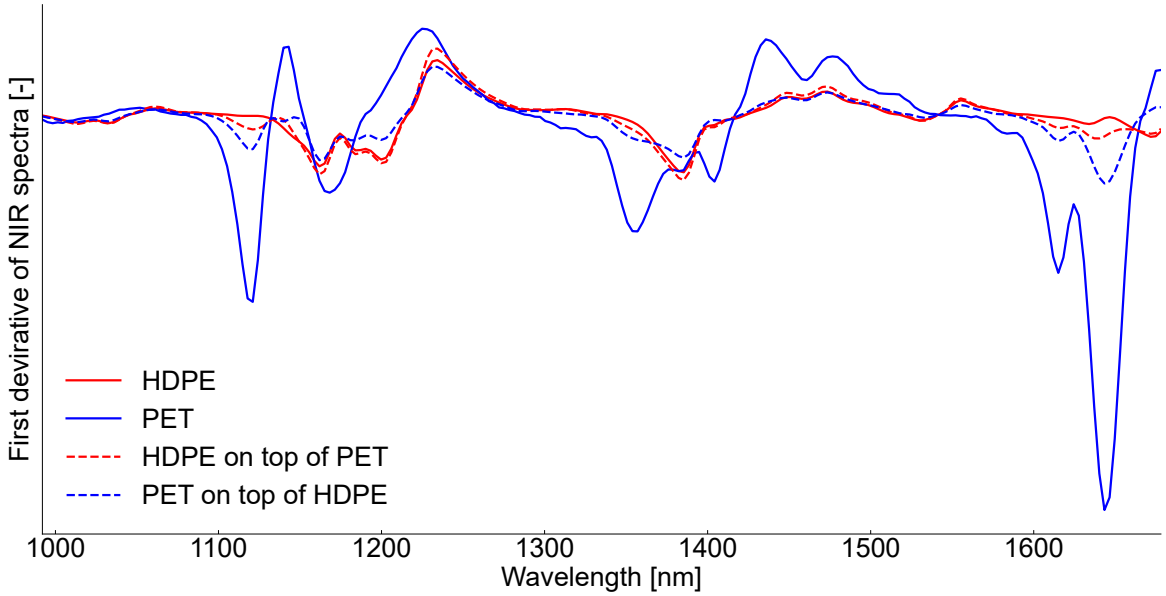

Figure A.1. NIR reference spectra for test series T1 (HDPE and PET flakes).

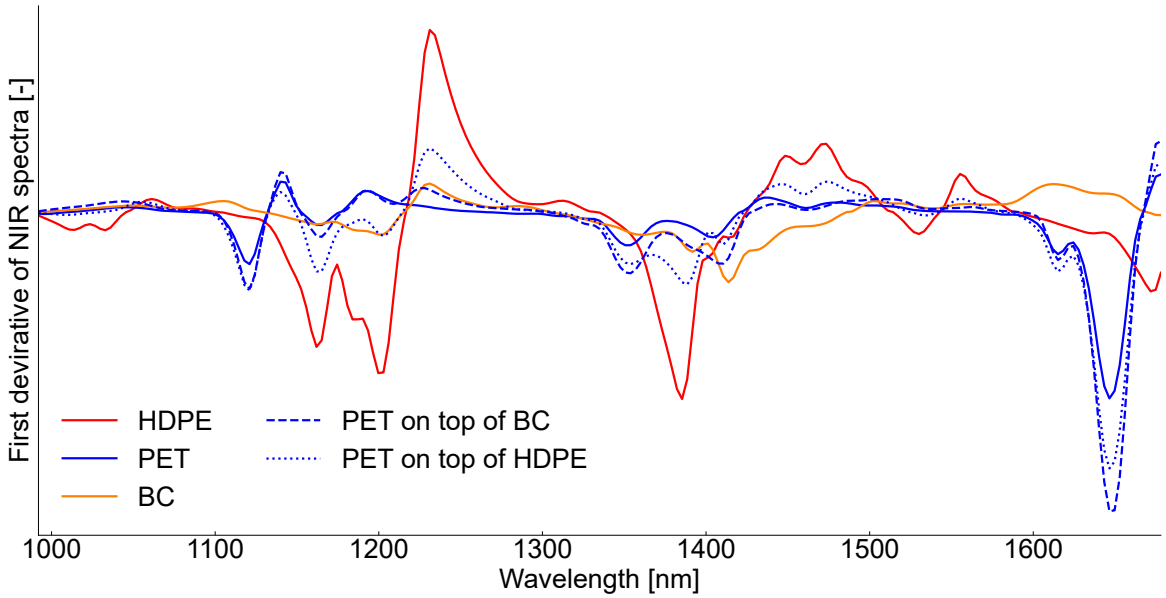

Figure A.2. NIR reference spectra for test series T2 (post-consumer HDPE packaging, PET bottles, and beverage cartons).

Table A.1. Technical data of the used rotary shear for primary comminution.

Parameter	Value
Manufacturer	MOCO Maschinen- und Apparatebau GmbH & Co. KG
Manufacturer location	Viernheim, Germany
Model	AZ 7
Peripheral speed	0.5 m/s
Cutting disc width	28 mm
Drive power	7.5 kW

Table A.2. Technical data of the used cutting mill for secondary comminution.

Parameter	Value
Manufacturer	RETO RECYCLINGTECHNIK GmbH
Manufacturer location	Bergkamen, Germany
Model	GA 37/450
Peripheral speed	9 m/s
Rotor diameter	350 mm
Rotor length	450 mm
Output mesh size	30 mm
Drive power	37 kW

Table A.3. Technical data of the used analytical sieve.

Parameter	Value
Manufacturer	Siebtechnik GmbH
Manufacturer location	Mühlheim (Ruhr), Germany
Model	Analytical sieve machine
Revolution	1,400 rpm
Used mesh sizes	10 mm, 20 mm
Mesh shape	Round
Sieving duration	90 s
Dimensions of screen linings	500 mm x 500 mm
Input power	0.75 kW

B Supplementary materials Publication F

Sample masses

PET tray characteristics

As a necessary prerequisite for calculating the minimum sample masses for a 600 kg PET tray bale, the material flow characteristics summarized in Table B.1 have been determined.

Table B.1. PET tray characteristics for calculated minimum sample masses.

Characteristic	Value	Description	Method
d_{95}	205 mm	95th percentile particle size	Particle measurement of sampled particles
d_5	20 mm	5th percentile particle size	Particle measurement of sampled particles
ρ_{bulk}	40 kg/m³	Bulk density	Bulk density determination using a 90 L sampling container, mean over 5 repetitions
p	82.6 wt%	Average PET tray mass share	Manual sorting analysis, sum over all taken samples

Minimum sample masses for a 600 kg PET tray bale

CEN/TR 15310

The minimum sample mass according CEN/TR 15310 is calculated based on Equation (B.1), where ρ_{bulk} is the bulk density of the material, g is a correction factor for the particle size distribution (Equation (B.2)), which is set to 0.25 in this study. CV is the desired coefficient of variation caused by the fundamental error and p is fraction of the particles with a specific characteristic (PET tray articles in our case). A well-accepted value for CV is 0.1 (Khodier et al., 2020), which is also used in this study. Applying Equation (B.1) to a 600 kg PET tray bale results in a total sample mass of 0.95 kg per bale.

$$m_{\text{sample,CEN/TR 15310[g]}} \geq \frac{1}{6} \cdot \pi \cdot \left(d_{95[\text{cm}]}\right)^3 \cdot \rho_{\left[\frac{\text{g}}{\text{cm}}\right]} \cdot g_{[-]} \cdot \frac{\left(1 - p_{[\text{m/m}]}\right)}{CV^2_{[-]} \cdot p_{[\text{m/m}]}} \tag{B.1}$$

$$g = \begin{cases} 0.25 & \text{if } 4 < d_{95}/d_5 \\ 0.50 & \text{if } 2 < d_{95}/d_5 \leq 4 \\ 0.75 & \text{if } 1 < d_{95}/d_5 \leq 2 \\ 1 & \text{if } d_{95}/d_5 = 1 \end{cases} \tag{B.2}$$

LAGA PN 98

The LAGA PN 98 defines that until a total volume of 60 m^3 $n = 8$ increments must be sampled. The minimum sample volume for particle with a particle size above 120 mm is $V_{inc} = 10$ L. The minimum sample mass for a PET tray bale with 600 kg weight (approx. 15 m^3 uncompacted volume) is then 3.2 kg (cf. Equation (B.3)). (Länderarbeitsgemeinschaft Abfall, 2001)

$$m_{\text{sample,LAGA PN98}} = 8 \cdot V_{\text{increment}} \cdot \rho_{\text{bulk}} \tag{B.3}$$

ÖNORM S 2127

The (ÖNORM S 2127, 2011) defines the minimum increment mass m_{inc}, ÖNROM S 2127 based on 95th percentile particle size (d_{95}) according to Equation (B.4). A total sample (m_{sample}, ÖNORM S 2127) must contain at least 10 increments (Equation (B.5)). Until 200 Mg of waste, one sample is required, resulting in a total sample mass of 123 kg per bale. (Österreichisches Normungsinstitut, 2011-11-01)

$$m_{\text{inc, ÖNORM S 2127[kg]}} \geq 0.06 \cdot d_{95\text{[mm]}} \tag{B.4}$$

$$m_{\text{sample, ÖNORM S 2127}} \geq 10 \cdot m_{\text{inc}} \tag{B.5}$$

GBP Quality GmbH

The GBP Quality GmbH defines the minimum sample mass per bale to 40 kg (Borowski, 2018; GBP Quality GmbH, 2023).

COREPLA

COREPLA defines the minimum sample mass per bale to 50 kg (COREPLA, 2022).

Der Grüne Punkt

Der Grüne Punkt defines the minimum sample mass per bale to 80 kg - 100 kg (Der Grüne Punkt, 2016).

Near-infrared reference spectra

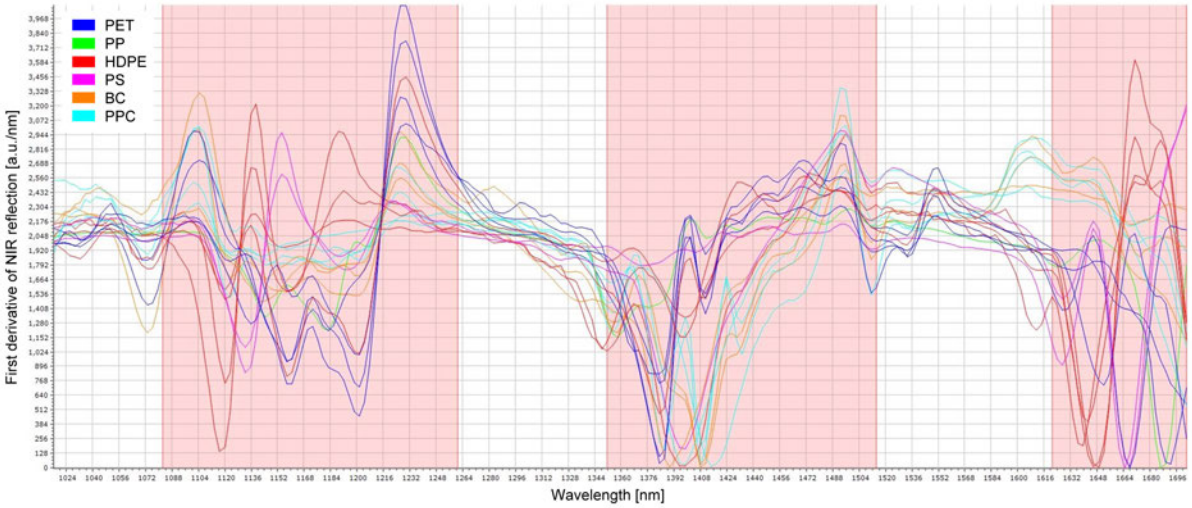

Figure B.1. NIR reference spectra for sensor position 1; PET: polyethylene terephthalate, PP: polypropylene; PE: polyethylene, PS: polystyrene, BC: beverage carton, PPC: paper, paperboard & cardboard; red regions: selected wavelength ranges for classification.

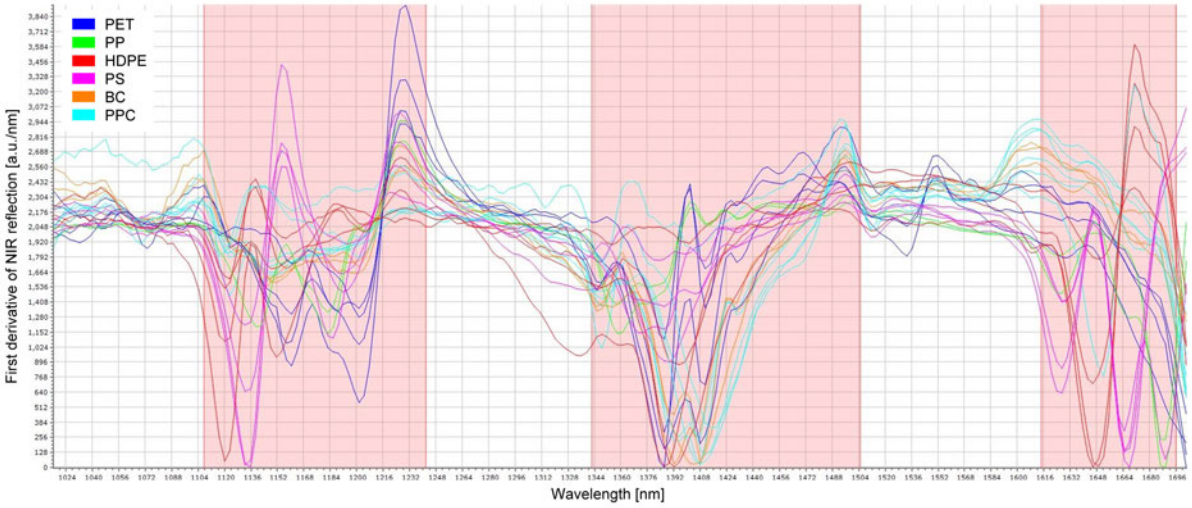

Figure B.2. NIR reference spectra for sensor position 2; PET: polyethylene terephthalate, PP: polypropylene; PE: polyethylene, PS: polystyrene, BC: beverage carton, PPC: paper, paperboard & cardboard; red regions: selected wavelength ranges for classification.

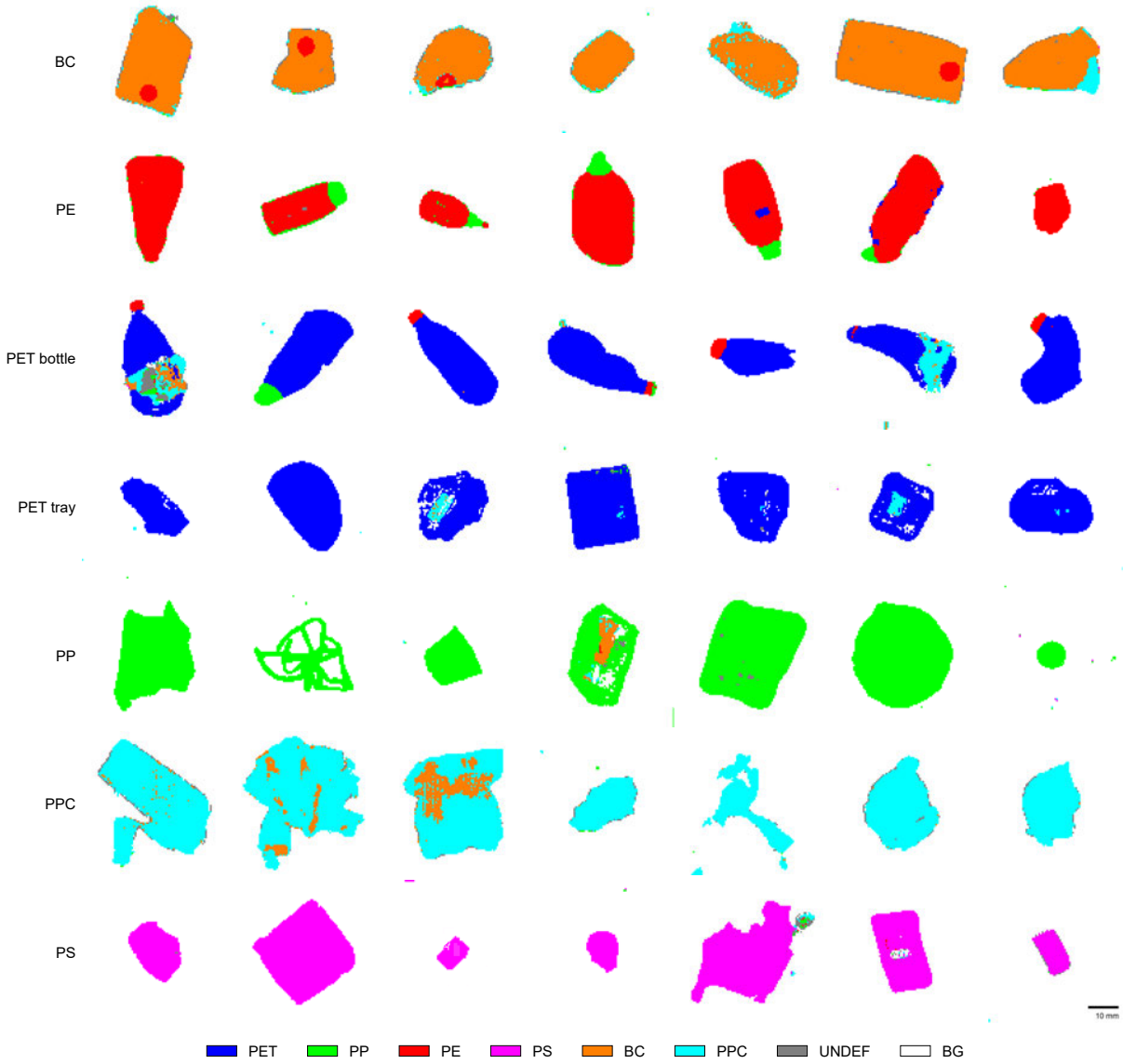

Figure B.3. Exemplary NIR classification results (false-color images) of randomly selected packaging items; PET: polyethylene terephthalate, PP: polypropylene; PE: polyethylene, PS: polystyrene, BC: beverage carton, PPC: paper, paperboard & cardboard, UNDEF: undefined, BG: background.

C Supplementary materials Publication G

Figure C.1. Sample material with a target (PET) material share of 5 wt%.

Table C.1. Article-based material composition of the non-target (non-PET) fraction.

Material class	Non-target material share [wt%]
PP	59.9
PE	30.0
PS	6.2
BC	1.8
PPC	2.2

Table C.2. Investigated machine learning models using the implementation from sklearn (Pedregosa et al., 2011). PR: polynomial regression, RF: random forest, ANN: artificial neural network.

ML Model	Investigated hyperparameters
PR	Custom based on `sklearn.linear_model` and `sklearn.preprocessing.PolynomialFeatures()` (see Table C.1)
RF	`sklearn.ensemble.RandomForestRegressor()`
ANN	`sklearn.neural_network.MLPRegressor()`

Table C.3. Investigated hyperparameters for hyperparameter optimization. [a]imported from sklearn.linear_model (Pedregosa et al., 2011), [b]generation of polynomial features with sklearn.preprocessing.PolynomialFeatures() (Pedregosa et al., 2011), [c]the hyperparameter hidden_layer_sizes is calculated based on n_hidden_layers layers with n_neurons_per_layer neurons each. PR: polynomial regression, RF: random forest, ANN: artificial neural network.

ML Model	Investigated hyperparameters
PR	• `model_types` = {`LinearRegression()`, `RidgeCV()`, `SGDRegressor()`}[a] • `polynomial_degree` = {1, 2, 3}[b]
RF	• `max_samples` = {0.1, 0.2, 0.3, 0.4, 0.5, 0.6, 0.7, 0.8, 0.9} • `max_depths` = {3, 5, 7, 9, 11} • `n_estimators` = {50, 100, 200, 400}
ANN	• activation = {'tanh', 'relu'} • learning_rate = {0.0001, 0.001, 0.01, 0.1} • n_neurons_per_layer = {50, 100, 150, 200}[c] • n_hidden_layers = {1, 3, 5, 7}[c]

Table C.4. ML model configuration of simulated SBS units. PosS: positive sorting (SBS trials with 5 wt%, 30 wt% and 50 wt% PET share), NegS: negative sorting (SBS trials with 70 wt% and 90 wt% PET share).

	Rougher + Scavenger		Cleaner	
Material	**Eject**	**Drop**	**Eject**	**Drop**
PET	PET_PosS	PP_PosS	PP_NegS	PET_NegS
PP	PET_PosS	PP_PosS	PP_NegS	PET_NegS
PE	PET_PosS	PE_PosS	PE_NegS	PET_NegS
PS	PET_PosS	PS_PosS	PS_NegS	PET_NegS
BC	PET_PosS	BC_PosS	BC_NegS	PET_NegS
PPC	PET_PosS	PPC_PosS	PPC_NegS	PET_NegS
UNDEF	PET_PosS	UNDEF_PosS	UNDEF_NegS	PET_NegS